Informatics Control Measurement
in Economy and Environment Protection

2/2023

Informatyka Automatyka Pomiary

w gospodarce i ochronie środowiska

www.e-IAPGOS.pl

ISSN 2083-0157

Kwartalnik Naukowo-Technicznу

1953 - 2023

70 lat POLITECHNIKI LUBELSKIEJ

fot. arch. PL

2/2023

kwiecień – czerwiec

Wydanie pod redakcją naukową
prof. dr hab. inż. Waldemara Wójcika

INFORMATYKA AUTOMATYKA POMIARY

W GOSPODARCE i OCHRONIE ŚRODOWISKA

Informatics Control Measurement in Economy and Environment Protection

p-ISSN 2083-0157, e-ISSN 2391-6761, www.e-iapgos.pl

PRINTING HOUSE – DRUKARNIA

PPH Remigraf Sp. z o.o.
ul. Dźwigowa 61, 01-376 Warszawa
https://remigraf.pl/

nakład: 100 egzemplarzy

OTHER INFORMATION – INNE INFORMACJE

Czasopismo jest indeksowane w bazach:

DOAJ	doaj.org
BazTech	baztech.icm.edu.pl
IC Journals Master List	www.journals.indexcopernicus.com
Google Scholar	scholar.google.pl
POL-index	pbn.nauka.gov.pl
Sherpa RoMEO	www.sherpa.ac.uk
OAJI	oaji.net
SCOPUS	www.scopus.com
EBSCO	www.ebsco.com

Czasopismo *Informatyka, Automatyka, Pomiary w Gospodarce i Ochronie Środowiska* zostało objęte finansowaniem przez Ministerstwo Nauki i Szkolnictwa Wyższego w ramach programu *Wsparcie dla czasopism naukowych* w latach 2019-2020.

Czasopismo znajduje się w wykazie czasopism naukowych opublikowanym w Komunikacie Ministra Edukacji i Nauki z dnia 1 grudnia 2021 r., Unikatowy Identyfikator Czasopisma: 200167 – z przypisaną liczbą punktów przyznawanych za publikację artykułu równą 20.

Zasady publikowania artykułów, przygotowania tekstów, zasady etyczne, procedura recenzowania, wykazy recenzentów oraz pełne teksty artykułów dostępne są na stronie internetowej czasopisma:

www.e-iapgos.pl

W celu zwiększenia oddziaływania czasopisma w środowisku naukowym redakcja zaleca:

- w artykułach publikowanych w IAPGOS cytować artykuły z renomowanych czasopism międzynarodowych (szczególnie indeksowanych w bazach Web of Science oraz Scopus) używając oficjalnych skrótów nazw czasopism,
- w artykułach publikowanych w innych czasopismach (zwłaszcza indeksowanych w bazach Web of Science oraz Scopus) cytować prace publikowane w IAPGOS – zwłaszcza posługując się numerami DOI, np.:
  Kluszczyński K. *Modelowanie – umiejętność czy sztuka?* Informatyka, Automatyka, Pomiary w Gospodarce i Ochronie Środowiska – IAPGOS, 1/2016, 4–15, https://doi.org/10.5604/20830157.1193833.

CONTENTS – SPIS TREŚCI

1. **Łukasz Maciura, Dariusz Wójcik, Tomasz Rymarczyk, Krzysztof Król**
Novel hybrid algorithm using convolutional autoencoder with SVM for electrical impedance tomography and ultrasound computed tomography
Nowy algorytm hybrydowy wykorzystujący autoenkoder konwolucyjny z SVM dla elektrycznej tomografii impedancyjnej i tomografii ultradźwiękowej 4

2. **Igor Palamarchuk, Vladyslav Palamarchuk, Vadim Paziuk, Ruslan Hulevych, Aliya Kalizhanova, Magzhan Sarsembayev**
Analysis of power and energy parameters of the conveyor infrared dryer of oil-containing raw materials
Analiza mocy i parametrów energetycznych przenośnikowej, działającej na podczerwień suszarni surowców zawierających olej 10

3. **Dmytro Milenin, Mykola Lysychenko, Andriy Milenin, Leonid Koval, Saltanat Amirgaliyeva, Maxatbek Satymbekov, Saltanat Adikanova**
Optimization of resource allocation, exposure time and rotary speed of incubative eggs
Optymalizacja alokacji zasobów, czasu ekspozycji i prędkości obrotowej jaj inkubacyjnych 15

4. **Gulnar Balakayeva, Gaukhar Kalmenova, Dauren Darkenbayev, Chris Phillips**
Development of an application for the thermal processing of oil slime in the industrial oil and gas sector
Opracowanie aplikacji do termicznego przetwarzania szlamów olejowych w przemysłowym sektorze naftowym i gazu 20

5. **Gregory S. Tymchyk, Volodymyr I. Skytsiouk, Tatiana R. Klotchko, Leonid K. Polishchuk, Anatolii V. Hrytsak, Saule J. Rakhmetullina, Beibut Amirgaliyev**
Automated definition of the discrete elements interactions in workspace of equipment
Automatyczne określanie interakcji elementów dyskretnych w przestrzeni pracy urządzeń 27

6. **Gregory S. Tymchyk, Volodymyr I. Skytsiouk, Tatiana R. Klotchko, Roman B. Akselrod, Valerii Yo. Shenfeld, Aliya Kalizhanova, Didar Yedilkhan, Gaukhar Borankulova**
TONTOR zones model for automative object monitoring
Model stref TONTOR do automatycznego monitorowania obiektów 36

7. **Viacheslav Titov, Oleksandr Mozghovyi, Ruslan Borys, Mykola Bogomolov, Yedilkhan Amirgaliyev, Zhalau Aitkulov**
Theoretical and experimental substantiation of the extraction process with thinning bimetallic tubular elements of dissimilar metals and alloys
Teoretyczne i eksperymentalne uzasadnienie procesu ciągnienia z przerzedzaniem bimetalicznych elementów rurowych z różnych metali i stopów ... 44

8. **Achraf Benba, Mouna Akki, Sara Sandabad**
The application of machine learning on the sensors of smartphones to detect falls in real-time
Zastosowanie uczenia maszynowego na czujnikach smartfonów do wykrywania upadków w czasie rzeczywistym 50

9. **Yosyp Bilynsky, Aleksandr Nikolskyy, Viktor Revenok, Vasyl Pogorilyi, Saule Smailova, Oksana Voloshina, Saule Kumargazhanova**
Convolutional neural networks for early computer diagnosis of child dysplasia
Konwolucyjne sieci neuronowe do wczesnej diagnostyki komputerowej dysplazji u dzieci 56

10. **Olena Kolesnikova, Olena Vysotska, Anna Potapenko, Anastasia Radchenko, Anna Trunova, Nataliya Virstyuk, Liudmyla Vasylevska-Skupa, Aliya Kalizhanova, Nazerka Mukanova**
Cardiometabolic risk prediction in patients with non-alcoholic fatty liver disease combined with subclinical hypothyroidism
Przewidywanie ryzyka kardiometabolicznego u pacjentów z niealkoholową stłuszczeniową chorobą wątroby w połączeniu z subkliniczną niedoczynnością tarczycy 64

11. **Leonid Timchenko, Natalia Kokriatskaya, Volodymyr Tverdomed, Natalia Kalashnik, Iryna Shvarts, Vladyslav Plisenko, Dmytro Zhuk, Saule Kumargazhanova**
Local difference threshold learning in filtering normal white noise
Proces uczenia względem lokalnego progu różnicy w filtrowaniu normalnego szumu białego 69

12. **Zakir Nasib Huseynov, Mahil Isa Mammadov, Togrul Atabay Ismayilov**
Modeling and analysis of the characteristics of multichannel and multi-node computer networks with priority service
Modelowanie i analiza charakterystyk wielokanałowych i wielowęzłowych sieci komputerowych z usługą priorytetową 74

13. **Vira Petruk, Olena Prozor, Yuliia Sabadosh, Iryna Baranovska, Maksim Palii, Yevheniia Moroz, Saule Kumargazhanova, Dinara Mussayeva**
Statistical methods for evaluating experimental data on the use of mathematical competencies in study for a resilient economy
Statystyczne metody oceny danych eksperymentalnych dotyczących wykorzystania kompetencji matematycznych w badaniach na rzecz odpornej gospodarki 78

14. **Olena Liutak, Olena Baula, Anatolii Tkachuk**
Simulation of the influence of investment and innovation activities on ensuring the international competitiveness of countries
Symulacja wpływu działań inwestycyjnych i innowacyjnych na zapewnienie międzynarodowej konkurencyjności krajów 86

http://doi.org/10.35784/iapgos.3377 *received: 19.12.2022 | revised: 25.01.2023 | accepted: 05.02.2023 | available online: 30.06.2023*

NOVEL HYBRID ALGORITHM USING CONVOLUTIONAL AUTOENCODER WITH SVM FOR ELECTRICAL IMPEDANCE TOMOGRAPHY AND ULTRASOUND COMPUTED TOMOGRAPHY

Łukasz Maciura[1], Dariusz Wójcik[1,2], Tomasz Rymarczyk[1,2], Krzysztof Król[1,2]
[1]Research and Development Center, Netrix S.A,. Lublin, Poland, [2]WSEI University, Lublin, Poland

Abstract: *This paper presents a new hybrid algorithm using multiple support vector machines models with a convolutional autoencoder for electrical impedance tomography, and ultrasound computed tomography image reconstruction. The ultimate hybrid solution uses multiple SVM models to convert input measurements to individual autoencoder codes representing a given scene then the decoder part of the autoencoder can reconstruct the scene.*

Keywords: convolutional autoencoder, SVM, electrical impedance tomography, ultrasound transmission tomography

NOWY ALGORYTM HYBRYDOWY WYKORZYSTUJĄCY AUTOENKODER KONWOLUCYJNY Z SVM DLA ELEKTRYCZNEJ TOMOGRAFII IMPEDANCYJNEJ I TOMOGRAFII ULTRADŹWIĘKOWEJ

Streszczenie. *Artykuł przedstawia nowy hybrydowy algorytm który używa modeli maszyn wektorów nośnych wraz z autoenkoderem konwolucyjnym do rekonstrukcji obrazu z elektrycznej tomografii impedancyjnej oraz ultrasonograficznej tomografii transmisyjnej. Ostateczne rozwiązanie hybrydowe używa wielu modeli SVM do konwersji pomiarów wejściowych do pojedynczych kodów autoenkodera reprezentujących daną scenę a wtedy dekoder wycięty z autoenkodera może zrekonstruować daną scenę.*

Słowa kluczowe: autoencoder konwolucyjny, SVM, elektryczna tomografia impedancyjna, ultradźwiękowa tomografia transmisyjna

Introduction

Ultrasound Transmission Tomography [11, 12, 27] is the process which enables, among others, reconstruction of the scene based on ultrasonic signal measurements. Another [7] paper on ultrasound tomography presents an image reconstruction algorithm based on a conventional neural network (CNN) for two-phase imaging materials. It has also been verified with experimental data. Finally, the paper [4] describes research into applying a dual-domain network for ultrasound tomography.

The EIT reconstruction [16] is based on reconstructing the conductivity from measurements vectors obtained from measurements using electrically conductive electrodes. However, the best results can be obtained using neural networks (especially deep networks). Several works have extensively described the EIT method, among which we can mention works [2, 6, 8, 9, 13, 20, 21, 25].

Several machine-learning methods for EIT reconstruction have been discussed in the literature. In the article [18], the authors explored logistic regression using an elastic net. The paper [16] used neural networks for EIT image reconstruction, where N neural networks trained separately for each output pixel were used to reconstruct image pixel values. Finally, the paper [15] applies convolutional neural network structure in EIT reconstruction.

The multiple ANN reconstruction methods are based on deep and convolutional autoencoders. Paper [10] describes a solution based on EIT reconstruction obtained using a deterministic algorithm (D-Bar) and applies the UNet convolutional model to correct these initial reconstructions.

Another method based on deep convolutional autoencoders is described in [24]. This algorithm uses a deep autoencoder to reconstruct a lung object based on EIT. The method consists of several steps:

1. Minimizing the cost function of the autoencoder with lung images.
2. The fully connected networks are trained on the measurements and outputs of the encoder.
3. Finally, the two networks are combined, where the network from step 2 processes the measurements, and the decoder of the developed autoencoder outputs reconstruction.

There are several numerical methods [5, 14, 17, 19, 22, 23, 24]. The authors have developed an innovative hybrid algorithm for image reconstruction of impedance and ultrasonic transmission tomography. The solution uses the encoder part from the convolutional autoencoder and multiple Support Vector Machines [3, 26] models to convert EIT or UTT measurements into individual autoencoder codes. In the case of EIT, the synthetic data was used only, containing generated scenes and EIT simulations. Therefore, the autoencoder is trained using generated scenes, and the encoder part is used to encode these scenes. In the final solution, the multiple SVM models are used to convert potential difference vectors from EIT simulations into AE codes representing the corresponding scenes. In the case of UTT, the convolutional autoencoder is trained using augmented real-scene images, and then, the encoder part is used for real-scene encoding; next, multiple SVM models are trained to convert real UTT measurements into codes representing real scenes. The ultimate hybrid algorithm in both cases is constructed using multiple SVM models at the input whose outputs are sent to the decoder part of AE, which reconstructs the image of the scene. Such a hybrid algorithm is particularly useful, especially when there is too small of training data (i.e., where training data comes from real measurements), so impossible to use a pure deep learning solution as in our UTT experiments.

1. EIT synthetic data

The model for the synthetic data in Electrical Impedance Tomography was prepared with 16 electrodes placed outside the area. A finite element mesh was prepared in the model, built with 4717 elements. The EIT training dataset used in this experiment consists of synthetic data. The data generation algorithm generated 50,000 cases containing inclusions (one or two inclusions of elliptical or rectangular shape). An EIT simulation was performed for each case to generate 192 measurements between electrodes.

To generate data, we used an EIT simulation algorithm based on the finite element method with square geometry to obtain potential vectors based on the cases generated with the ellipse and rectangle inclusions. The parameters of the simulation algorithm for generating the training dataset used in the experiments were adjusted to make the synthetic data as close as possible to the real data. Finally, the resulting potential vectors were used to calculate the difference between potential – voltage:

$$X_i = x_i - x0_i$$

where x_i – is potential vector for the case with syntethic inclusions, $x0_i$ – is potential vector for the case empty tank, X_i – is the voltage vector, i – is the index of potential vectors and voltage elements.

The 50,000 samples generated from reference images (Y) and potential difference vectors (X) were divided into a training dataset (40,000 samples) and a test dataset (10,000 samples).

2. UTT Input data

The data used in this research was obtained in the laboratory under specific conditions. At the bottom of the polypropylene pail, 76 items numbered 1–77 were marked (no. 18 was omitted). The bucket was filled with chlorinated water. Round phantoms in plastic tubes filled with air were placed in marked positions.

An application was written to facilitate data collection. The application was intended to give the positions of the phantoms. The positions of the phantoms were stored in a defined list. In addition, the application controlled the measurements as follows. When the phantom was placed at the indicated position, and the MEASURE button was pressed, the application saved the last measured measurement frame to memory. After the measurement, the application pointed to the next position where the phantom had to be set. This way, the list (measurement matrix) – (position numbers with phantoms) was completed.

Then, thanks to a hand-prepared set of photos (Fig. 2 and based on position numbers, the phantoms' actual positions were reconstructed in binary images. Each image marked with a single inclusion was segmented into a binary image with a circle in that phantom position. The image of the phantom positions in the individual setting variants of several phantoms was obtained by summing up the appropriate segmented position patterns. The resulting image was scaled down to a resolution of 64x64 pixels in the "nearest" interpolation mode.

The active probe of the ultrasonic tomograph performs measurements with a single piezo transducer using the absorption method. This transducer can operate as a transmitter and receiver of the ultrasonic wave. Its resonant frequency is 40 kHz. The PCB allows connecting an external transducer via an SMB socket. The probe has an integrated signal processing circuit and a microcontroller with an integrated A/D converter. Each probe can adjust the gain of the received signal using a programmable digital potentiometer. Measuring the transit time of an ultrasonic wave from one probe to another is achieved by connecting all probes to an additional communication line. When a low state occurs on this line, all probes except the transmitting probe start timing and stop timing when the ultrasound wave is received. Each receiving probe then sends the measurement result to the tomograph controller. Based on the information of which probe was the transmitter and which probe sent the result, the measurement value is stored in the corresponding cell of the measurement matrix. The probes were made to be placed very close to each other. The power supply lines, the communication bus and the interruption lines necessary for correct timing from sending to receiving on the other probes were carried out using RJ12.

Fig. 1. UST active probes on the measuring tank

There were 21 sensors with a frequency of 40 kHz in the bucket area (Fig. 1). The 21×21 size M measurement matrix contains the ToF (Time of Fly) values of the ultrasonic wave between all sensor pairs in microseconds. The diagonal is filled with zeros only to ensure that the value of $M_{i,j}$ stands for the value measured between the *i*-th and *j*-th sensors and has no effect on the measurements, i.e., the sensor transmitting the wave does not measure the time.

After obtaining the data was split into training (2617 samples) and test (656 samples) datasets.

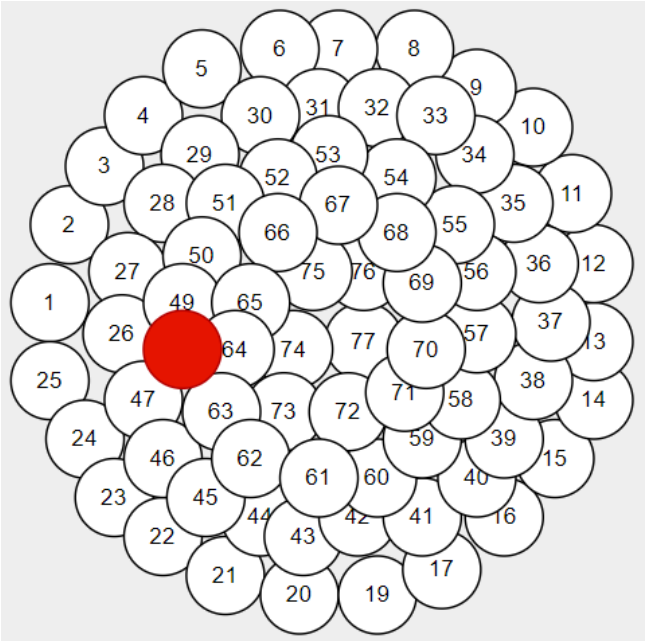

Fig. 2. Sample phantom position during measurements

3. Augmentation of images represented scenes from multimodal tomography (UTT)

Because the collected data from transmission tomography contains a small number of samples (a few thousand), it is too small to train a convolutional autoencoder, so the scene images dataset should be augmented. The image data augmentation is simpler than the augmentation of data tomography measurements. The augmentation of scene images was realized by three transforms performed on images (rotation, scaling and translation) using random parameters. During the augmentation, 25000 images were generated. As a result, 20% of images are empty, and other (80%) images were generated by random affine transformation with maximal rotation change equal to 15 degrees, maximal scale changes equaling 20% and maximal translation equaling 10 pixels. After augmentation, the data was split into a training dataset (containing 20000 images) and a test dataset (containing 5000 images).

4. Training of convolutional autoencoder for EIT data

The convolutional autoencoder for EIT data was trained using synthetic scenes. In table 1, the used convolutional autoencoder model structure details are presented.

The reshape layer (row number 18) in this model makes the reshape operation of input from the previous layer into shape 5×5×1024 to achieve the proper input shape for the next layer.

The training process was performed using 30 training epochs during six stages, each containing five epochs with different optimizers and settings, presented in table 2.

Table 1. Details of the autoencoder model

id	layer name	neurons number	kernel size	activation
1	Conv2D	64	3×3	relu
2	Conv2D	64	3×3	relu
3	MaxPooling2D	-	2×2	-
4	Conv2D	128	3×3	relu
5	Conv2D	128	3×3	relu
6	MaxPooling2D	-	2×2	-
7	Conv2D	256	3×3	relu
8	Conv2D	256	3×3	relu
9	MaxPooling2D	-	2×2	-
10	Conv2D	512	3×3	relu
11	Conv2D	512	3×3	relu
12	MaxPooling2D	-	2×2	-
13	Conv2D	1024	3×3	relu
14	Conv2D	1024	3×3	relu
15	Flatten	-	-	-
16	Dense	512	-	relu
17	Dense	25600	-	relu
18	Reshape	-	-	-
19	UpSampling2D	-	2×2	-
20	Conv2D	512	3×3	relu
21	Conv2D	512	3×3	relu
22	UpSampling2D	-	2×2	-
23	Conv2D	256	3×3	relu
24	Conv2D	256	3×3	relu
25	UpSampling2D	-	2×2	-
26	Conv2D	128	3×3	relu
27	Conv2D	128	3×3	relu
28	UpSampling2D	-	2×2	-
29	Conv2D	64	3×3	relu
30	Conv2D	64	3×3	relu
31	Conv2D	1	3×3	relu

Table 2. Training stages of autoencoder model

stage	optimizer	learning rate
1	Adam	10^{-4}
2	Adam	10^{-4}
3	Adam	10^{-5}
4	Adam	10^{-5}
5	Adam	10^{-6}
6	Adam	10^{-7}

The 12 samples of pairs containing original scenes (reference images) and scenes images restorations made by autoencoder are presented in figure 3.

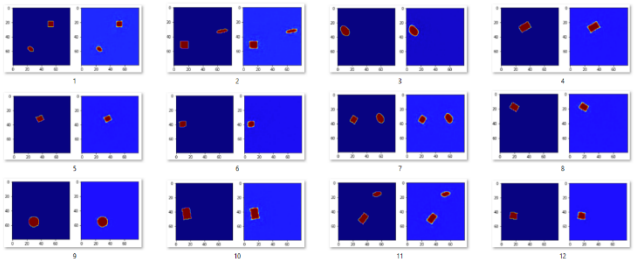

Fig. 3. Sample results of the convolutional autoencoder. In the 12 pairs of samples, there are input scene images (on the left in the pair) and reconstructed input scenes by autoencoder (on the right)

For numerical assessment of results in the form of images, the DICE coefficient [27] was used:

$$DSC = \frac{2TP}{2TP + FP + FN}$$

where:
TP – is the number of true positives (correctly reconstructed pixels, *FP* – is a number of false positives (pixels reconstructed in wrong places), *FN* – is some false negatives pixels not reconstructed in the place where the object exists in the real image

The numerical results of pure EIT scenes autoencoder working were the following. After training the autoencoder, the MAE equal 0.0054 and DICE equal 97.7 were achieved on the training dataset, while the MAE equal 0.0058 and DICE equal 96.5 were achieved on the test dataset.

It should be noted that the results presented above are not reconstruction results but are a measure of the autoencoder's ability to reproduce the input image. Nevertheless, this result assures us that the encoding part of the autoencoder can encode the images correctly.

5. Training of convolutional autoencoder for UTT data

The convolutional autoencoder for UTT data was trained on an augmented scene images dataset similar to real scene images. The used model architecture is similar to EIT's, but the Dense layer with an id equal to 17 has 16384 neurons instead of the 25600 ones used for EIT. In addition, the used Reshape layer (id equal 18) has a destination shape equal to 4×4×1024 instead of 5×5×1024 in the previous version of the autoencoder.

The autoencoder was trained using 35 training epochs (7 stages, each containing five epochs) which was presented in table 3.

Table 3. Training stages of autoencoder model

stage	optimizer	learning rate	weight decay
1	Adam	10^{-4}	-
2	Adam	10^{-4}	-
3	Adam	10^{-4}	-
4	Adam	10^{-5}	-
5	Adam	10^{-5}	-
6	AdamWD	10^{-5}	10^{-8}
7	AdamWD	10^{-5}	10^{-8}

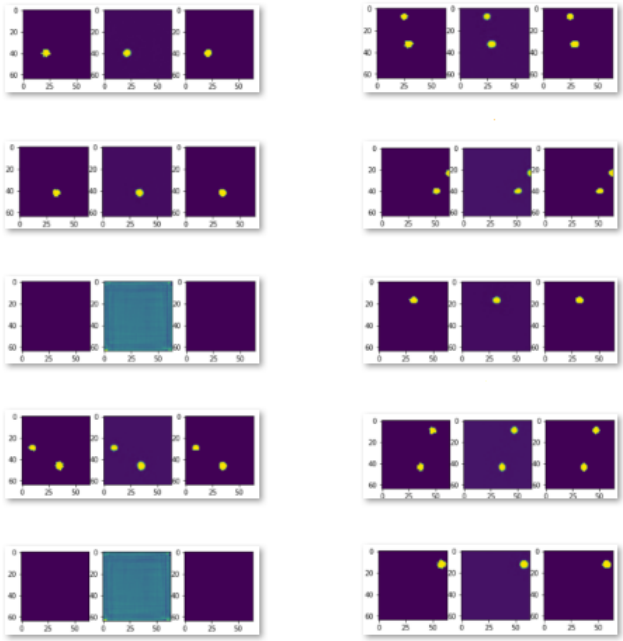

Fig. 4. Samples results of encoding UTT reference images by convolutional autoencoder. In each triplet, on the left is a reference image, in the centre is autoencoder output, and on the right is thresholded autoencoder output

After training, the Mean Absolute Error equal to 0.000826 and DICE equal to 95.37% were achieved on the training dataset, while the MAE equal to 0.0011 and the DICE metric equal to 93.12% were achieved on the test dataset. Then, the encoder part was extracted from the autoencoder pre-trained in the previous step. After extraction, the image scenes from the real dataset were encoded. Finally, the vectors of codes, each containing 512 elements, were generated using the encoder and will be used in the SVM training process.

Figure 3 shows the 10 sample results of EIT reference scene image restoration. Each sample contains a reference image, restored reference image and thresholded restoration result. These samples are generated on the test dataset. The thresholding of outputs is used because empty scenes exist in the dataset, so thresholding was necessary to visualize the output properly.

6. Training of multiple SVM models for EIT and UTT codes represents scenes regression

The final training stage of the ultimate solution uses Support Vector Machines for the regression of codes of scene images based on input from Electrical Impedance Tomography differential potential vectors. The same training stage is performed for Ultrasound Transmission Tomography measurements.

For each *i*-th code from all 512 available, the separate SVM models are trained for regression one of the code based on input measurements.

In Fig. 5 to Fig. 8, four stages of the algorithm were presented. The input and output of this autoencoder are the same reference image. During training, the autoencoder's reproduction of reference images in the latent space produces a compressed vector representation of the images as a side effect. This representation can be regressed more easily than the original image.

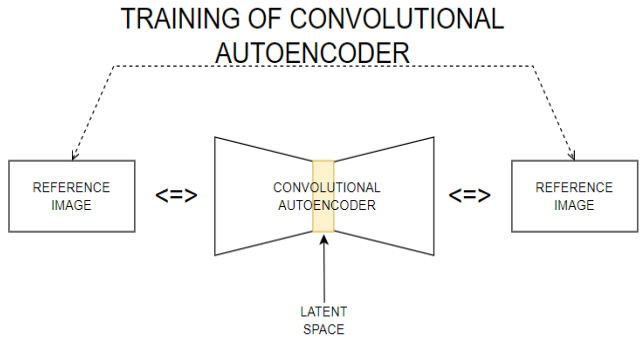

Fig. 5. Training process of the convolutional autoencoder

In Fig. 6, the encoding process of all reference images using the encoder part extracted from the full convolutional autoencoder was presented.

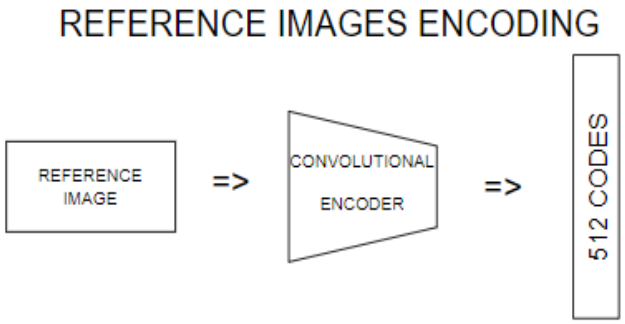

Fig. 6. Reference images encoding (conversion of all reference images into vector

In Fig. 7, the training process of 512 SVM models, each representing one of 512 codes of autoencoder based on input vector with measures (EIT or UTT), was presented.

In Fig. 8, the reconstruction process was presented. In the beginning, the input vector with measures is used as the same input for each 512 SVM model. Then, each i-th SVM model predicts one i-th value from the autoencoder code vector. Finally, the vector of codes is used as input to extracted decoder part of the convolutional autoencoder to predict the output image (final reconstruction).

During the creation of the solution, the sigma value in the SVM model (SVM parameter) was optimized, and the best result was obtained for an epsilon value equal to 0.01 (in the case of EIT data) and 0.01 (in the case of UTT data). Epsilon is an SVM hyperparameter which is a special margin useful for regression. The model's training tries to fit as many samples as possible in one "street" with as few margin violations. The smaller epsilon values were not tested because of the long training process and bigger memory usage.

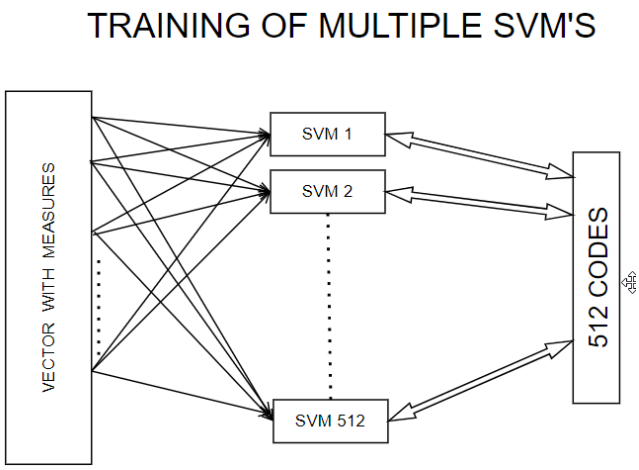

Fig. 7. Training of multiple SVM models to regress 512 codes of vector generated by the encoder

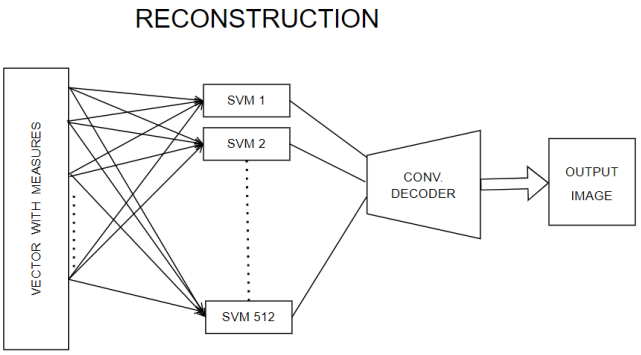

Fig. 8. Whole reconstruction (EIT or UTT) process pipeline

7. Using a decoder with SVM models for transmission tomography image reconstruction for EIT and UTT

The solution for scene image reconstruction has the same form as EIT and UTT. After the pretraining of the autoencoder, the decoder part is extracted. The reconstruction process for EIT and UTT has the following form:

1. In the beginning, the multiple SVM models (trained earlier) are used for individual codes of autoencoder regression based on input measurement (EIT or UTT) where each i – th SVM model can make regression of i – th code in the autoencoder latent space.
2. Obtained vector of codes generated by SVM models is used as an input to the extracted decoder from the pretrained autoencoder, and then the decoder can reconstruct a scene image (for EIT or UTT).
3. The settings of the epsilon parameter are described in paragraphs 9 and 10. The other settings of a single SVM model are the following:
   a) Input is the vector from EIT or UTT measures.
   b) Output is one of regressed value represents one of autoencoder code.
   c) The used kernel type is RBF.
   d) The gamma parameter is calculated using the following formula:

$$\gamma = \frac{1}{n_f * \sigma_X^2}$$

   where:
   n_f – is a number of features,
   σ_X^2 – is an input data variance
   e) The tolerance parameter is set to a value of 0.001.
   f) The C parameter is set to 1.
   g) There is no iteration limit.

8. EIT reconstruction results

The numerical results for the EIT reconstruction final solution are presented in table 4.

Table 4. Final results assessments using different SMV models in full hybrid solution (with different epsilon values)

models no.	epsilon	DICE train	DICE test
1	0.2	84.3894%	83.6964%
2	0.1	85.8310%	84.9856%
3	0.05	86.3073%	85.4069%
4	0.01	86.4789%	85.5485%

In figure 9, the 12 pairs of results represent original scenes and reconstructed scenes are presented using the best SVM models (no. 4 in table 2). Next, the table presents the results of four models, identified by the "models no." column. The second column, "epsilon," represents a hyperparameter used in the models. Finally, the "DICE train" and "DICE test" columns show the DICE coefficient, a metric used to evaluate the performance of image reconstruction models for the training and test sets, respectively.

As the epsilon value decreases (i.e. goes from 0.2 to 0.01), the DICE coefficient for both the training and test sets increases. It suggests that as the epsilon value becomes smaller, the model becomes more precise in its reconstruction.

Model 1, with an epsilon of 0.2, has a DICE coefficient of 84.3894% on the training set and 83.6964% on the test set. Model 2, with an epsilon of 0.1, has a DICE coefficient of 85.8310% on the training set and 84.9856% on the test set. Similarly, Model 3, with an epsilon of 0.05 has a DICE coefficient of 86.3073% on the training set and 85.4069% on the test set. Finally, Model 4, with an epsilon of 0.01 has a DICE coefficient of 86.4789% on the training set and 85.5485% on the test set.

It suggests that as the epsilon value decreases, the models become more precise, and the model's performance increases on both training and test sets.

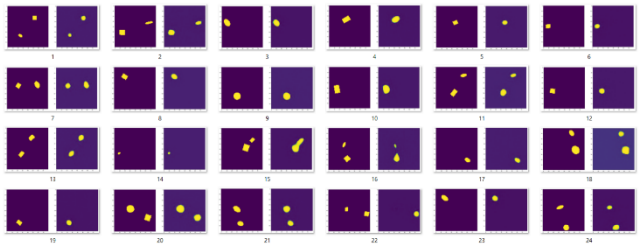

Fig. 9. Sample results of EIT scene reconstructions based on a created hybrid solution. The 12 pairs of results represent original scenes (left images in pairs) and reconstructed scenes (right images in pairs)

9. UTT reconstruction results

The numerical results for the UTT reconstruction final solution were also computed using SVM models trained with epsilon equal to 0.01. The MSE, MAE and DICE metrics are presented in table 5. The table presents the results of a model trained and tested on two different datasets, identified by the "dataset" column. The "MSE" column shows the mean squared error, a metric used to evaluate the performance of regression models, for each dataset. The "MAE" column shows the mean absolute error, another metric used to evaluate the performance of regression models, for each dataset. Finally, the "DICE" column shows the DICE coefficient, a metric used to evaluate the performance of image reconstruction models for each dataset.

The results generally show that the model performed better on the training dataset than on the test dataset. The MSE, MAE and DICE values are generally lower for the training dataset than for the test dataset.

On the training dataset, the MSE is 0.01337, the MAE is 0.01582, and the DICE coefficient is 51.536%. On the test dataset, the MSE is 0.01404, the MAE is 0.01647, and the DICE coefficient is 47.556%.

Table 5. Numerical results of the hybrid model used on UTT data

dataset	MSE	MAE	DICE
training	0.01337	0.01582	51.536%
test	0.01404	0.01647	47.556%

In figure 10, the 8 samples of results of Transmission Tomography reconstruction are presented. Columns 1 and 4 represent the original scene image, columns 2 and 5 represent the reconstructed scene, and columns 3 and 3 represent thresholded results.

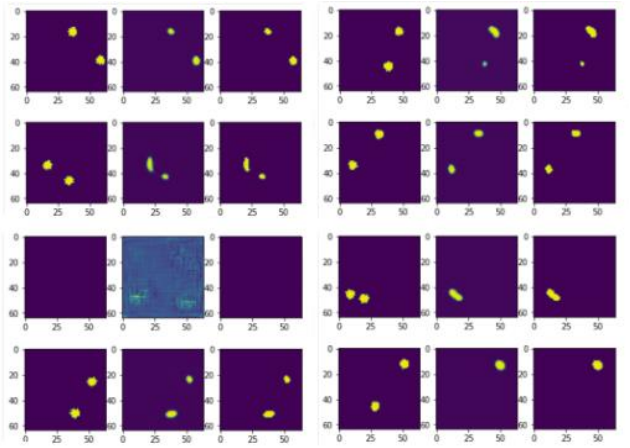

Fig. 10. Sample results of Ultrasound Transmission Tomography reconstruction (columns represent original scenes, reconstructed scenes, thresholded reconstructed scenes)

10. Conclusion

This paper presents a new hybrid algorithm for EIT and UTT scene reconstruction (with all models trained separately). This algorithm consists of multiple SVM models that reconstruct separate codes from the convolutional autoencoder based on EIT or UTT measurements using proper models. Since used convolutional autoencoder could be trained using augmented image data, this hybrid algorithm is very useful for real datasets where data is often limited (as was in our UTT experiments).

Notice that this is our initial research on EIT and UTT scene reconstruction, so the used experimental setup is relatively simple. However, we are planning to use this hybrid method for medical applications. Since convolutional autoencoders have strong possibilities of complex shape reconstruction, we trust that this hybrid solution will also be useful for realistic medical application setups.

The models were implemented in Python with a GPU version of Tensorflow (for convolutional autoencoder) and Scikit – Learn (for SVM libraries).

References

[1] Aziz Taha A., Hanbury A.: Metrics for evaluating 3D medical image segmentation: analysis, selection, and tool. BMC Medical Imaging 15(29), 2015, 1–28.
[2] Chen B. et al.: Extended Joint Sparsity Reconstruction for Spatial and Temporal ERT Imaging. Sensors 18, 2018, 4014.
[3] Chen P. H. et al.: A tutorial on ν-support vector machines. Applied Stochastic Models in Business and Industry 21, 2005, 111–136.
[4] Chen Z. et al.: Application of Deep Neural Network to the Reconstruction of Two-Phase Material Imaging by Capacitively Coupled Electrical Resistance Tomography. Electronics 10, 2021, 1058.
[5] Duraj A., Korzeniewska E., Krawczyk A.: Classification algorithms to identify changes in resistance. Przegląd Elektrotechniczny 91(12), 2015, 82–84.
[6] Dusek J., Mikulka J.: Measurement-Based Domain Parameter Optimization in Electrical Impedance Tomography Imaging. Sensors 21, 2021, 2507.

[7] Fan Y. et al.: DDN: dual domain network architecture for non-linear ultrasound transmission tomography reconstruction. Proc. SPIE 11602, 2021, 1160209 [http://doi.org/10.1117/12.2580911].
[8] Fan Y., Ying L.: Solving electrical impedance tomography with deep learning. Journal of Computational Physics 404, 2020, 109119.
[9] Fernandez-Fuentes X. et al.: Towards a Fast and Accurate EIT Inverse Problem Solver: A Machine Learning Approach. Electronics 7(12), 2018, 422.
[10] Hamilton S. J., Hauptmann A.: Deep D – bar: Real time Electrical Impedance Tomography Imaging with Deep Neural Networks. IEEE Trans. Med. Imaging 37(10), 2018, 2367–2377.
[11] Józefczak A. et al.: Ultrasound transmission tomography-guided heating with nanoparticles. Measurement 197, 2022, [http://doi.org/10.1016/j.measurement.2022.111345].
[12] Kania K. et al.: Image reconstruction in ultrasound transmission tomography using the Fermat's Principle. Przegląd Elektrotechniczny 96(1), 2020, 186–189.
[13] Khan T. A., Ling S.H.: Review on Electrical Impedance Tomography: Artificial Intelligence Methods and its Applications. Algorithms 12(5), 2019, 1–18.
[14] Kłosowski G. et al.: Comparison of Machine Learning Methods for Image Reconstruction Using the LSTM Classifier in Industrial Electrical Tomography. Energies 14(21), 2021, 7269.
[15] Kłosowski G. et al.: Maintenance of industrial reactors supported by deep learning driven ultrasound tomography. Przegląd Elektrotechniczny 98(4), 2022, 138–147.
[16] Kłosowski G. et al.: Neural hybrid tomograph for monitoring industrial reactors, Przegląd Elektrotechniczny 96(12), 2020, 190–193.
[17] Kłosowski G. et al.: Quality Assessment of the Neural Algorithms on the Example of EIT-UST Hybrid Tomography. Sensors 20(11), 2020, 3324.
[18] Kozłowski E. et al.: Logistic regression in image reconstruction in electrical impedance tomography, Przegląd Elektrotechniczny 96(5), 2020, 95–98.
[19] Krawczyk A., Korzeniewska E.: Magnetophosphenes–history and contemporary implications. Przegląd Elektrotechniczny 94(1), 2018, 61–64.
[20] Li X. et al.: An image reconstruction framework based on deep neural network for electrical impedance tomography. IEEE International Conference on Image Processing, Beijing, China, 2017.
[21] Li X. et. al.: A novel deep neural network method for electrical impedance tomography. Transactions of the Institute of Measurement and Control 41(14), 2019, 4035–4049.
[22] Łukiański M., Wajman R.: The diagnostic of two-phase separation process using digital image segmentation algorithms. Informatyka, Automatyka, Pomiary w Gospodarce i Ochronie Środowiska 10(3), 2020, 5–8.
[23] Mosorov V. et al.: Plug Regime Flow Velocity Measurement Problem Based on Correlability Notion and Twin Plane Electrical Capacitance Tomography: Use Case. Sensors 21(6), 2021, 2189 [http://doi.org/10.3390/s21062189].
[24] Seo J. K. et al.: A Learning – Based Method for Solving III – Posed Nonlinear Inverse Problems: A Simulation Study of Lung EIT, SIAM. Journal on Imaging Sciences 12(3), 2019.
[25] Szczesny A., Korzeniewska E.: Selection of the method for the earthing resistance measurement. Przegląd Elektrotechniczny 94, 2018, 178–181.
[26] Yu H., Kim S.: SVM Tutorial: Classification, Regression, and Ranking. Handbook of Natural computing, 2012.
[27] Zhao W. et al.: Ultrasound transmission tomography image reconstruction with a fully convolutional neural network. Phys Med Biol. 65(23), 2020, 235021, [http://doi.org/10.1088/1361-6560/abb5c3. PMID: 33245050].

Ph.D Eng. Łukasz Maciura
e-mail: lukasz.maciura@netrix.com.pl

Since 2019 he has been working in the industry as a software designer/developer on projects related to computer vision / image processing / deep learning / electrical impedance tomography (currently at Research and Development Center, Netrix S.A.)
His research interests include computer vision (especially 3D reconstruction), machine learning (particularly deep learning and time-series recognition), medical informatics and robotics.

http://orcid.org/0000-0001-8657-3472

Ph.D. Dariusz Wójcik
e-mail: dariusz.wojcik@netrix.com.pl

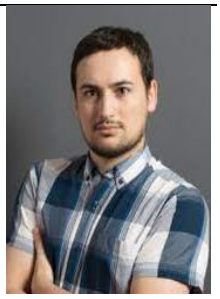

R&D Manager of Algorithmic Systems in Research and Development Center Netrix S.A. The author of the two-fluid numerical code JOANNA focused on the research of the Solar corona. Currently, he is interested in machine learning, neural networks and computer vision and its application to industrial and medical tomography.

http://orcid.org/0000-0002-4200-3432

D.Sc. Tomasz Rymarczyk
e-mail: tomasz.rymarczyk@netrix.com.pl

Director in Research and Development Center Netrix S.A. His research focuses on applying non-invasive imaging techniques, electrical tomography, image reconstruction, numerical modelling, image processing and analysis, process tomography, software engineering, knowledge engineering, artificial intelligence and computer measurement systems.

http://orcid.org/0000-0002-3524-9151

M.Sc. Eng. Krzysztof Król
e-mail: krzysztof.krol@netrix.com.pl

He is an employee of the Research and Development Department at the Research and Development Centre of Netrix S.A. and an assistant at the Higher School of Economics and Innovation in Lublin. He has been associated with computer science for over 14 years. He conducts scientific research in process tomography, IoT and sensor networks. He conducts scientific research in process tomography, IoT and sensor networks.

http://orcid.org/0000-0002-0114-2794

http://doi.org/10.35784/iapgos.3487 *received: 12.02.2023 | revised: 13.03.2023 | accepted: 24.05.2023 | available online: 30.06.2023*

ANALYSIS OF POWER AND ENERGY PARAMETERS OF THE CONVEYOR INFRARED DRYER OF OIL-CONTAINING RAW MATERIALS

Igor Palamarchuk[1], Vladyslav Palamarchuk[2], Vadim Paziuk[3], Ruslan Hulevych[4], Aliya Kalizhanova[5], Magzhan Sarsembayev[6]

[1]National University of Life and Environmental Sciences of Ukraine, Kyiv, Ukraine, [2]Vinnytsia Institute of Trade and Economics of State University of Trade and Economics, Vinnytsia, Ukraine, [3]Institute of Engineering Thermophysics, Kyiv, Ukraine, [4] Vinnytsia National Technical University, Vinnytsia, Ukraine, [5]University of Power Engineering, Almaty, Kazakhstan, [6]Al-Farabi Kazakh National University, Almaty, Kazakhstan

Abstract. *Infrared drying of bulk agricultural products is becoming increasingly widespread in processing and food industries due to energy efficiency, compactness of technological equipment, and ease of operation. The purpose of the presented research is to determine the influence of the technological parameters of the process of infrared drying of the moving layer of oil-containing raw materials. An experimental model of a vibro-conveyor dryer and a set of measuring equipment were developed to solve the problems. The scientific novelty of the work is the confirmation that in the conditions of a vibro-liquefied layer of products, unique conditions are created for the constant renewal of heat exchange surfaces and, accordingly, the leveling of the negative thermal radiation effect on the products, the possibility of advancing the product layer along the working zone, reducing the forces of internal friction in the technological mass, which leads to a decrease in energy consumption on the process Laws have been established regarding the effect of the number of thermoradiation blocks, the load on the flexible belt of the wave conveyor, the speed of product advancement on the belt on the dynamics of infrared drying of soybeans and rapeseed. The practical value of the work was the substantiation of the operating modes of thermoradiation drying with the help of a vibrating wave conveyor installation based on the energy saving of the technological impact, high intensification of the process and minimization of the negative effect on the properties of the processed products.*

Keywords: thermoradiation drying, infrared conveyor dryer, oil-containing raw materials, vibrofluidized bed, energy and power parameters, low-frequency oscillations

ANALIZA MOCY I PARAMETRÓW ENERGETYCZNYCH PRZENOŚNIKOWEJ, DZIAŁAJĄCEJ NA PODCZERWIEŃ SUSZARNI SUROWCÓW ZAWIERAJĄCYCH OLEJ

Streszczenie. *Suszenie podczerwienią produktów rolnych luzem staje się coraz bardziej powszechne w przemyśle przetwórczym i spożywczym ze względu na energooszczędność, kompaktowość urządzeń technologicznych i łatwość obsługi. Celem prezentowanych badań jest określenie wpływu parametrów technologicznych procesu suszenia podczerwienią ruchomej warstwy surowców zawierających olej. W celu rozwiązania problemów opracowano eksperymentalny model suszarki z przenośnikiem wibracyjnym oraz zestaw urządzeń pomiarowych. Naukową nowością pracy jest potwierdzenie, że w warunkach skraplania wibracyjnego warstwy produktów powstają unikalne warunki do ciągłego odnawiania powierzchni wymiany ciepła, a tym samym niwelowania negatywnego wpływu promieniowania cieplnego na produkty, możliwość przesuwania warstwy produktu wzdłuż strefy roboczej, Zmniejszenie sił tarcia wewnętrznego w masie technologicznej, co prowadzi do zmniejszenia zużycia energii w procesie. Zdefiniowano prawa dotyczące wpływu liczby bloków termoradiacyjnych, obciążenia elastycznej taśmy przenośnika falowego, prędkości przesuwania produktu na taśmie na dynamikę suszenia soi i rzepaku w podczerwieni. Praktyczną wartością pracy było uzasadnienie trybów pracy suszenia termoradiacyjnego za pomocą instalacji przenośnika wibracyjno-falowego w oparciu o oszczędność energii oddziaływania technologicznego, wysoką intensyfikację procesu i minimalizację negatywnego wpływu na właściwości przetwarzanych produktów.*

Słowa kluczowe: suszenie termiczne, suszarka przenośnikowa na podczerwień, surowce zawierające olej, złoże wibrofluidyzowane, parametry energii i mocy, oscylacje o niskiej częstotliwości

Introduction

The drying process is one of the most complex mass transfer processes, which is a complex complex of interconnected elements that includes heat transfer during the transfer of heat to products through the boundary layer; evaporation during phase transformation; heat and mass transfer during the transfer of moisture and heat inside the material; heat and mass transfer during the transfer of moisture and heat from the surface of the material to the environment through the boundary layer by diffusion or molecular transfer; filtration or molar transfer under convection conditions; thermodiffusion, that is, the transfer of moisture under the influence of a temperature gradient, for which the direction of the thermodiffusion density of the substance mass flow corresponds to the direction of the heat flow density. When justifying the structural and technological scheme of the equipment for the implementation of the presented stages of heat and mass transfer, it is necessary to conduct an analysis of energy costs to ensure their implementation, to assess the technical and economic feasibility of the process and its impact on the change in the physical and chemical properties of the processed raw materials. It is the power and energy characteristics of the process that ensure the dynamics of the development of these factors [5, 9, 12, 19, 25].

Among the main factors of intensification of the drying process of bulk material, it is possible to note the transfer of heat of the product from the source of radiant energy and the creation of a fluidized layer of products to increase the heat and mass exchange surface. In the process of heat exchange, the radiant flow partially penetrates into the capillary-porous bodies to a depth of 0.1...2 mm and is almost completely absorbed due to a series of reflections from the walls [1, 10, 12, 21, 25, 27]. At the same time, the heat exchange coefficient has a significant value and the duration of the drying process is reduced by 30...100 times compared to the convective or conductive method [1, 8, 21, 22]. The vibration of the executive bodies of the dryer ensures the movement of the particles of the loose medium at a constant speed or at a slowly changing speed. This leads to drift – displacement of the equilibrium positions of such particles and to the appearance of one or more discrete positions of their quasi-equilibrium; as a result of which there is an almost 10-fold decrease in the effective coefficient of friction in the product mass, which increases the coefficient of thermal contact with the product to 100%, significantly reduces the time of technological action and indirectly leads to a 3-5-fold decrease in energy consumption for the process [8, 23, 11, 17, 26, 18].

To carry out the investigated process in modern technologies, vibrating transport and technological machines are used. The main disadvantages of vibro-conveyor systems with an undeformed conveying body remain high metal consumption and energy consumption, structural imbalance and, accordingly, high dynamic loads on support nodes [8, 4, 20, 24, 16]. The presence of a transport device in the form of a flexible conveyor in dryers allows to eliminate the indicated shortcomings and to create energy-saving product processing schemes with prospects for the implementation of automated modes [2, 3, 7, 28, 6]. However, it is the presence of a flexible transport element that greatly complicates the design of the machine, makes it difficult, and in some cases, eliminates the possibility of adjusting the operating modes of the vibrating installation.

Thus, the power and energy characteristics of the researched process determine both the possibilities and the efficiency

of its implementation, the degree of influence on the surface of the loose product and the corresponding provision of the required properties, which determines the relevance of these studies in the design of infrared technological equipment.

1. Object of investigation

The developed drying unit contains a flexible load-bearing body 1 (Fig. 1), on which a running or standing wave is created during the operation of mechanical vibrators 2, 3 [13–15]. Such a wave spreads along the belt 1, occurs as the transportation of products coming from the feeder 7, with a speed that is regulated by the amplitude-frequency characteristics of the vibrators, which leads to the emergence of a fluidized state of the processing material and its intensive mixing. translational movement. This ensures constant renewal of the surface of products with a thermal energy carrier and accordingly reduces the heat intensity on the surface layer while maintaining a sufficiently high flow rate. Oscillation of rollers 5, 6 ensures the advancement of loose material at a speed necessary to maintain the kinetics of the process under study.

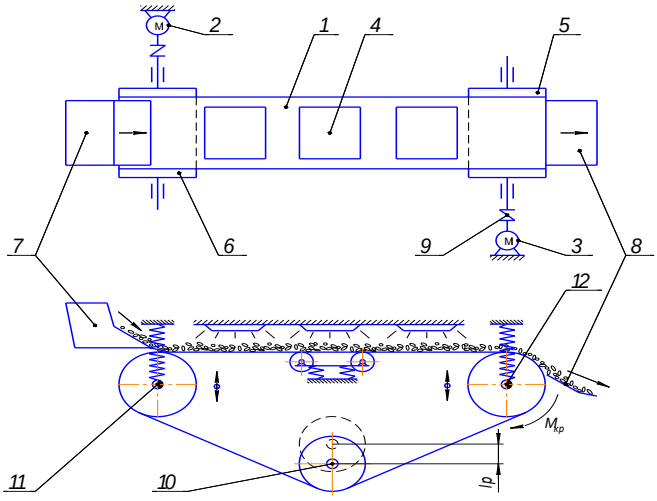

a)

b)

Fig. 1. Schematic diagram of the conveyor vibrating wave infrared dryer (a) and its experimental and industrial model (b): 1 – belt; 2, 3 – motors of vibration exciters; 4 – infrared emitters; 5,6 – rollers; 7 – feeder; 8 – receiving hopper; 9 – flexible coupling; 10 – tension roller; 11, 12 – unbalanced vibrators

The aggregated mechanical vibration exciter in the support rollers 5, 6 of the dryer compactly and organically fits into the scheme of the wave conveyor, allows to reduce the oscillating mass of the drive and provides for the leveling of parasitic vibrations with the help of elastic elements 9. Such a scheme of the drive body, together with the presence of a wave conveyor with a deformable transport element, allows significantly improve the balancing system of the dryer. In addition, it is possible, together with the reduction of the metal and energy consumption of the device compared to existing designs of vibro-infrared dryers of the type "Uragan", "USK", UTZ-4 "M-500", "SVIK" [13], to provide conditions for regulated intensification of the removal process free and physically bound moisture from the processing material. The last factor is implemented by changing the power and energy characteristics of the "vibration field" due to the selection of the corresponding amplitude and frequency of oscillations of the support rollers 5 and 6.

2. Evaluation of the parameters of the investigated infrared drying process

In order to evaluate the desired parameters of the process of infrared irradiation of oily material (Fig. 2), the selection of equipment was carried out according to the following factors: ensuring the necessary level of activity of substances and humidity; implementation of constructive solutions for the organization of infrared irradiation to ensure the necessary energy and technological efficiency of the process; the choice of the method of mechanical action to ensure the transportation and mixing of the material [7, 8, 17, 22].

The process of infrared drying of oil-containing products was carried out in two stages: first, processing of the product at the maximum temperature of the source of infrared radiation until the formation of a browning crust on the surface of the product; then bringing the product to full readiness at a reduced constant temperature of the generators. The temperature decrease in the second stage occurred with the help of reducing the electric power or increasing the distance of the product to the source of infrared radiation. Design solutions for the layout of the infrared lamp block and the generators themselves ensured the achievement of uniform irradiation according to the requirements of this treatment for the corresponding oil-containing material [2, 3], including the content of anti-nutrients [28].

When conducting experimental studies, a certain amount of whole grain of rapeseed or soybeans was received on the tape, obtaining values of specific loading equal to 2.5, respectively; 3.5; 5 kg/m^2. After that, they ensured the promotion of products on tape 2 (Fig. 2) at a speed of 0.13; 0.33 or 0.54 cm/s. At the same time, under the influence of infrared emitters 4, which were turned on individually and together, the product perceives radiation with a power of 100, 200, 300 W. The power of the emitters was adjusted by changing the current strength with the help of current clamps.

Fig. 2. Scheme of the experimental conveyor installation for infrared drying: 1 – drive roller; 2 – ribbon; 3 – tension roller; 4 – infrared irradiated; 5 – production

The temperature of the product layer was determined using a pyrometer through the windows in the casing of the installation, which are located after each of the emitters along the movement of the products on the belt.

3. Determination of the investigated parameters of infrared drying for the moving layer of products

On the basis of the conducted experiments, we obtained numerical data of the desired characteristics of infrared drying of rapeseed and soybeans in a moving layer of products, and built the dependencies presented in Figures 3, 4, 5.

When the speed of the conveyor belt increases from 0.0015 to 0.0285 m/s, the intensity of humidity changes for a fixed processing time decreases by 3 times (Fig. 3). With a 5-fold increase in the power of irradiation, the intensity of humidity changes increases by 8 times (Fig. 4a). When the load of products in the working area changes from 0.2 to 0.5 kg/m^2, the intensity of humidity changes increases by 3.5 times (Fig. 4b).

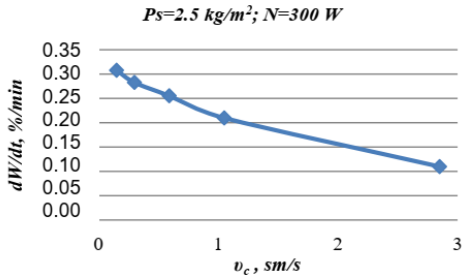

Fig. 3. Dependences of humidity reduction for rapeseed when changing the speed of the belt

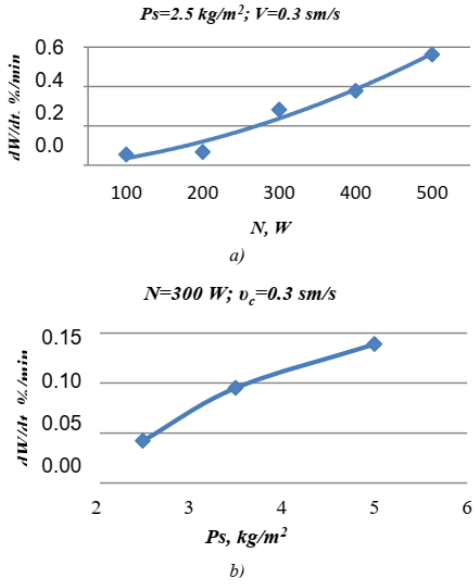

Fig. 4. Dependencies of humidity reduction for rapeseed grain when changing power (a) and when changing specific load (b)

The dynamics of changes in the speed of infrared drying of rapeseed and soybeans depending on the number of radiating modules, with a change in the radiation power N_{op}, loading in the working area P_s, and the speed of the conveyor belt υ_{st} are presented, respectively, in figures 5, 6.

According to the results of the experiments, the most optimal values of the speed of transportation of products were determined in the range from 0.15 to 0.3 cm/s, under the conditions of the power of infrared emitters of 400 – 500 W. It turned out that a specific loading of more than 3.5 kg/m^2 is impractical to use due to the fact that a large layer of products does not allow infrared rays to carry out uniform processing of grains, especially at sufficiently high speeds of the belt movement. It was determined that it is more expedient to carry out the drying process with three successively located infrared emitters, to increase the amount of moisture removed, it is effective to reduce the power of the emitters from 500 to 300 W.

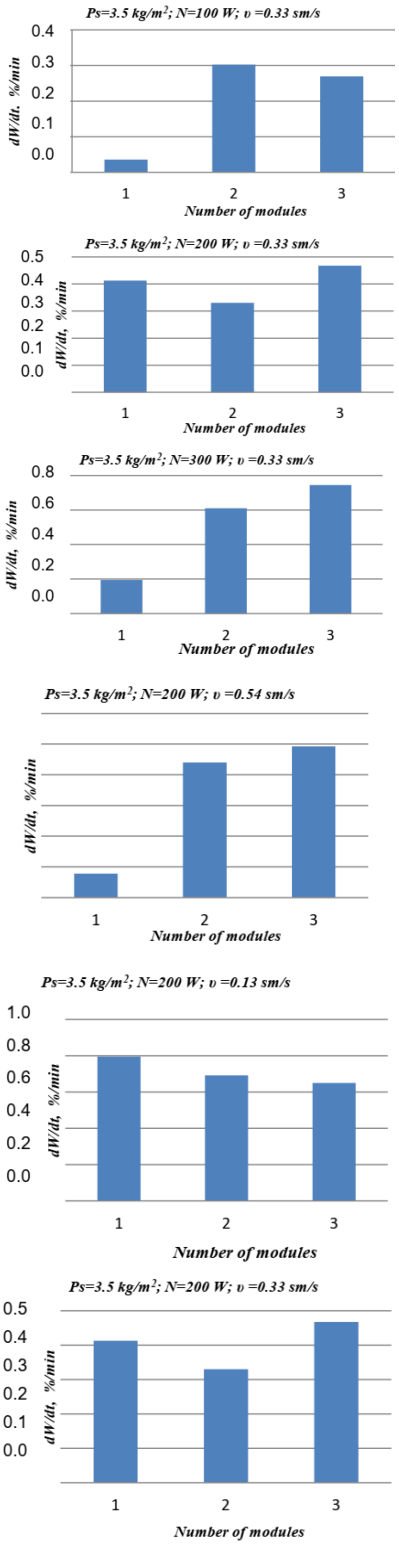

Fig. 5. Change in the speed of infrared drying of soybeans dW/dt (in %/min) in the moving layer of products when the conditions of technological processing vary

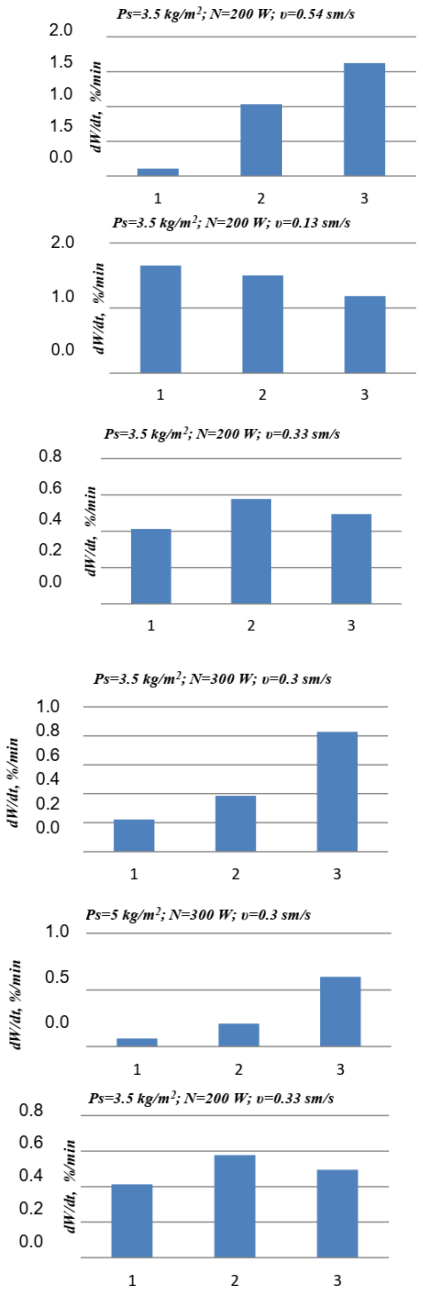

Fig. 6. Change in the rate of infrared drying of rapeseed dW/dt (in %/min) in the moving layer of products when the conditions of technological processing vary

4. Conclusions

1) Experimental studies of the technological parameters of thermoradiation drying for a moving layer of raw materials made it possible to obtain graphs of the drying speed depending on different irradiation modes, different loading of the working area and the speed of the conveyor belt for rapeseed and soybean, which made it possible to obtain the necessary experimental database for substantiating the working parameters infrared vibro-conveyor dryer under the conditions of minimizing energy consumption and thermal damage of oil-containing products, namely, rapeseed and soybeans.
2) The intensity of humidity change for a fixed processing time decreases 3 times when the speed of the conveyor belt increases from 0.0015 to 0.0285 m/s, 8 times – when the irradiation power increases by 5 times; 3.5 times – when the load of products in the working area changes from 0.2 to 0.5 kg/m^2.
3) With the simultaneous operation of two vibration exciters, stable transportation of products by a wave conveyor while ensuring the necessary productivity and quality of processing is observed under the following operating modes of processing: speed of transportation of products in the range from 0.15 to 0.3 cm/s; power of infrared emitters in the range of 400 – 500 W; the specific loading of the load-bearing body should not exceed 3.5 kg/m^2.
4) Carrying out the drying process with three successively located infrared emitters while reducing the power of the emitters from 500 to 300 W made it possible to increase the amount of moisture removed per unit of time.

References

[1] Abbaspour-Gilandeh Y. et al.: Evaluation of the Changes in Thermal, Qualitative and Antioxidant Properties of Terebinth (Pistacia atlantica) Fruit under Different Drying Methods. Agronomy 10, 2020, 20–24.
[2] Bandura V. et al.: Investigation of properties of sunflower and rapeseed oils obtained by the soxhlet and microwave extraction methods. Agraarteadus 33(1), 2022, 48–58.
[3] Bandura V. et al.: Case study: Dynamics of sunflower seed movement in the vibrating tray of the infrared dryer and its influence on the drying process. Agraarteadus 32(2), 2021, 204–213.
[4] Basok B. I. et al.: Radiative-Convective Heat Exchange of a Building with the Environment on Exposure to Solar Radiation. Journal of Engineering Physics and Thermophysics 93(1), 2020, 45–53.
[5] Bahlul N. et al.: Coupling of Microwave Radiations to Convective Drying for Improving Fruit Quality. IDS'2018: 21st International Drying Symposium, 2018, 699.
[6] Bezbah, I. et al.: Designing the structure and determining the mode characteristics of the grain dryer based on thermosiphons – Eastern-European Journal of Enterprise Technologies 2(8-116), 2022, 54–61.
[7] Burdo O. G. et al.: Energetics and Kinetics of Plant Raw Material Dehydration Processes – Energetică și cinetică a proceselor de dezhidratare a proceselor de dezhidratare a materiei prime vegetale. Problems of the Regional Energetics 2, 2022, 111–129.
[8] Burdo O. et al.: Studying the operation of innovative equipment for thermomechanical treatment and dehydration of food raw materials. Eastern-European Journal of Enterprise Technologies 5(11-101), 2019, 24–32.
[9] De Faria R. Q., dos Santos A. R. P., Gariepy Y., da Silva E. A. A., Sartori M. M. P., Raghavan V.: Optimization of the Process of Drying of Corn Seeds with the Use of Microwaves – Drying Technology 38(5-6)/2019, 676–684.
[10] Horuz E. et al.: Effects of Hybrid (Microwave-Convectional) and Convectional Drying on Drying Kinetics, Total Phenolics, Antioxidant Capacity, Vitamin C, Color and Rehydration Capacity of Sour Cherries. Food Chemistry 230, 2017, 295–305.
[11] Kuznietsova I. et al.: Application of the differential scanning calorimetry method in the study of the tomato fruits drying process. Agraarteadus 31(2), 2020, 173–180.
[12] Liu H. et al.: Microwave Drying Characteristics and Drying Quality Analysis of Corn in China. Processes 9(9), 2021.
[13] Palamarchuk I. et al.: The intensification of dehydration process of pectin-containing raw materials. Potravinarstvo Slovak Journal of Food Sciences 16, 2022, 15–26.
[14] Palamarchuk I. et al.: Analysis of main process characteristics of infrared drying in the moving layer of grain produce. Modern Development Paths of Agricultural Production: Trends and Innovations. Part 1 – Springer International Publishing 1, 2019, 317–322
[15] Palamarchuk I. et al.: Optimization of the Parameters 2 for the Process of Grain Cooling. Modern Development Paths of Agricultural Production: Trends and Innovations. Part 2. Springer International Publishing 2, 2019, 981– 988
[16] Paziuk V. et al.: Special aspects of soybean drying with high seedling vigor. UPB Scientific Bulletin, Series D. Mechanical Engineering 83(2), 2021, 327–336.
[17] Petrova Z. A., Slobodyanyuk E. S.: Energy-Efficient Modes of Drying of Colloidal Capillary-Porous Materials. Journal of Engineering Physics and Thermophysics 92(5), 2019, 1231–1238.
[18] Polishchuk L., Bilyy O., Kharchenko Y.: Prediction of the propagation of crack-like defects in profile elements of the boom of stack discharge conveyor. Eastern-European Journal of Enterprise Technologies 6(1), 2016, 44–52
[19] Qu F. et al.: Effect of Different Drying Methods on the Sensory Quality and Chemical Components of Black Tea. Lebensmittel-Wissenschaft + Technologie 99, 2019, 112–118.
[20] Semko T., Palamarchuk, V., Sukhenko, V. Application of ultra-high-temperature processing of raw milk to improve cheese quality. Potravinarstvo Slovak Journal of Food Sciences 13(1), 2019, 840–845.
[21] Snezhkin Y. F., Shapar R. A., Gusarova E. V.: Theoretical and Experimental Studies of Convective Dehydration of Spicy-Aromatic Raw Materials. Journal of Engineering Physics and Thermophysics 95(6), 2022, 1366–1373.
[22] Snezhkin Y. F. et al.: Determination of the energy efficient modes for barley seeds drying. INMATEH – Agricultural Engineering 61(2), 2020, 183–192.
[23] Sorokova N., Didur V., Variny M.: Mathematical Modeling of Heat and Mass Transfer during Moisture–Heat Treatment of Castor Beans to Improve the Quality of Vegetable Oil. Agriculture 12(9), 2022, 1356.

[24] Sorokova N. N. et al.: Mathematical Simulation and Optimization of the Continuous Drying of Thermolabile Materials. Journal of Engineering Physics and Thermophysics 92(5), 2019, 1180–1190.
[25] Wei Q. et al.: Effects of Different Combined Drying Methods on Drying Uniformity and Quality of Dried Taro Slices – Drying Technology 37(3), 2019, 322–330.
[26] Yaropud V. et al.: Experimental studies of design-and-technological parameters of heat exchanger. Badania eksperymentalne parametrów konstrukcyjno-technologicznych wymiennika ciepła. Przeglad Elektrotechniczny 98(10), 2022, 57–60.
[27] Yildiz G., Izli G.: Influence of Microwave and Microwave-Convective Drying on the Drying Kinetics and Quality Characteristics of Pomelo – Journal of Food Processing and Preservation 6(3), 2019 [http://doi.org/10.1111/jfpp.13812].
[28] Zavialov V. et al.: Development of mathematical models of external mass exchange under conditions of vibroextraction from vegetable raw materials. Chemistry & Chemical Technology 3(9), 2015, 367–374.

D.Sc. Igor Palamarchuk
e-mail: vibroprocessing@gmail.com

Doctor of Technical Sciences, professor, National University of Life and Environmental Sciences of Ukraine. Department Processes and Equipment of Agricultural Production Processing, Kyiv, Ukraine.
Research Interests: design and development of mechanical and heat-mass exchange processes and equipment of processing and food industries with vibromechanical intensification of raw material processing.

http://orcid.org/0000-0002-0441-6586

D.Sc.Vadim Paziuk
e-mail: vibroprocessing@gmail.com

Doctor of Technical Sciences, docent, Institute of Engineering Thermophysics, Kyiv, Ukraine.
Research Interests: technical thermal physics and industrial thermal energy.

http://orcid.org/0000-0002-4955-1941

M. Sc. Vladyslav Palamarchuk
e-mail: kupc1989@gmail.com

Canditate of Technical Sciences, Vinnytsia Institute of Trade and Economics of State University of Trade and Economics. Department of Commodity Studies, Expertise and Trade Entrepreneurship, Vinnitsia, Ukraine.
Research Interests: research on issues of intensification of the process of drying oily raw materials.

http://orcid.org/0000-0002-7478-9521

M.Sc. Ruslan Hulevych
e-mail: goruslan98@gmail.com

Vinnytsia National Technical University, postgraduate student, mechanical engineering, Vinnitsia, Ukraine.
Research Interests: research of technological and dynamic processes of equipment for grinding wood and building materials.

http://orcid.org/0000-0003-1359-4146

Ph.D. Aliya Kalizhanova
e-mail: kalizhanova_aliya@mail.ru
Candidate of physical and math. sciences, professor, University of Power Engineering and Telecom–munications, the chief researcher of the Institute of Information and Computational Technologies of the Ministry of Education and Science CS of the Republic of Kazakhstan.
Scientific interests of the models of transport systems network analysis, optimization methods, technologies for developing sensor systems for signals receive – transmit, mathematical modeling of Bragg fiber gratings.

http://orcid.org/0000-0002-5979-9756

Ph.D. Magzhan Sarsembayev
e-mail: magatrone@mail.ru

Senior lecturer of the Department of Computer Science of Al-Farabi Kazakh National University.
Author of more than 10 scientific works published in leading journals of Kazakhstan Republic and the abroad.
Research area: high performance computing, intelligent systems of control, software engineering, 3D modeling and design.

http://orcid.org/0000-0003-2139-2456

http://doi.org/10.35784/iapgos.3494 received: 13.02.2023 | revised: 16.03.2023 | accepted: 24.05.2023 | available online: 30.06.2023

OPTIMIZATION OF RESOURCE ALLOCATION, EXPOSURE TIME AND ROTARY SPEED OF INCUBATIVE EGGS

Dmytro Milenin[1], Mykola Lysychenko[1], Andriy Milenin[1], Leonid Koval[2], Saltanat Amirgaliyeva[3], Maxatbek Satymbekov[4], Saltanat Adikanova[5]

[1]State Biotechnological University, Kharkiv, Ukraine, [2]Vinnytsia National Technical University, Vinnytsia, Ukraine, [3]Academy of Logistics and Transport, Almaty, Kazakhstan, [4]Al-Farabi Kazakh National University, Almaty, Kazakhstan, [5]Sarsen Amanzholov East Kazakhstan University, Ust-Kamenogorsk, Kazakhstan

Abstract. *Recently, the laser technology of influencing biological objects in biology, medicine, and veterinary medicine has become widespread in order to activate certain biochemical and physiological processes in the organism. Any influence of electromagnetic radiation (in particular optical emission) requires the exact adherence to the recommended illumination dose to obtain a positive effect on the biological object. The article presents the results of a theoretical study concerning provision of uniform illumination of the egg's surface, taking into account the location of the laser radiation source and rotating time of the egg.*

Keywords: laser emission, radiation dose, incubating egg

OPTYMALIZACJA ALOKACJI ZASOBÓW, CZASU EKSPOZYCJI I PRĘDKOŚCI OBROTOWEJ JAJ INKUBACYJNYCH

Streszczenie. *Ostatnio technologia laserowego oddziaływania na obiekty biologiczne w biologii, medycynie i weterynarii stała się powszechna w celu aktywacji pewnych procesów biochemicznych i fizjologicznych w organizmie. Każdy wpływ promieniowania elektromagnetycznego (w szczególności emisji optycznej) wymaga dokładnego przestrzegania zalecanej dawki oświetlenia w celu uzyskania pozytywnego wpływu na obiekt biologiczny. W artykule przedstawiono wyniki badań teoretycznych dotyczących zapewnienia równomiernego oświetlenia powierzchni jaja, biorąc pod uwagę lokalizację źródła promieniowania laserowego i czas obrotu jaja.*

Słowa kluczowe: emisja lasera, dawka promieniowania, inkubowane jajo

Introduction

In the process of laser illumination of the shell surface of the incubating egg it is necessary to provide a uniform dose of radiation all over surface under the stipulation that egg rotates around its large axle. A graphs have been drawn under the stipulation that the value of the angular velocity of egg rotation is at the level $\omega = 0.5s^{-1}$ for which the dose value $E_D(z,\theta)$ is obtained. The present and average radiation dose, depending on the position of two lasers against to the egg's surface have ascertained by the way of ccalculations. As a result of theoretical studies, the graphs were obtained: of the changes of average radiation dose, depending on the angle of sight of the laser beam on the egg's surface; excess of the radiation dose above the average values at nodal points; change of the laser radiation dose on the egg's surface with optimal placement of lasers. As a result, it is shown that the position of the lasers against the egg substantially affects the uniformity of the illumination of the egg's surface. The optimum conditions for placing lasers against the egg's surface is the minimum excess of the radiation dose over its average value. The calculations have showed that with high probability ($P = 0.9973$) an increase in the dose of irradiation of the egg's surface, in comparison with the average does, not exceed 5.46%, and the corresponding decrease is 5.92%.

1. Setting the task

The current level of industrial poultry farming requires the use of modern technologies aimed at intensifying the production process, which are base on the results of recent scientific achievements in biophysics and medicine, in particular studies connected with the usage of laser emission [3, 28].

The pointed laser technologies are capable of providing the highest level of productive indicators of poultry at all stages of poultry production, including at the stage of incubation [1, 4, 22]. In addition, the regulating effect of the laser emission of the red wavelength range on the activity of some enzymatic systems [16], the metabolism of proteins, nucleic acids, and lipids [25] has been ascertained. Stimulation of proliferative activity of cells under the influence of laser emission [9, 18], marked hemostimulating [24] and immunomodulating action [7] of laser emission have been shown [17, 24].

A number of studies are devoted to the ascertainment of a probable mechanism of laser emission on biological objects of different levels of organization from cells to a holistic organism [23, 27]. Moreover, all researchers point out that the effectiveness of laser emission, with the wavelength and emission power, significantly depends on the dose of emission $D = J \cdot t$ and the general effect may have both activating and inhibiting effects on biological structures [8, 28].

Therefore, in the application of laser technologies in biology, medicine and agriculture, it is important to observe the required radiation dose [10, 11, 16].

2. Purpose study

Investigation of the conditions of placing the source of laser radiation in relation to the biological object on the example of irradiation of the shell surface of the incubation egg to provide the required radiation dose.

3. Reseach results

Consider the case where the left and right sources are located, respectively, at the points Q' and P' (Fig. 1a). Then the rays from both sources will come to the point D of the cross-section of the ellipsoid at an angle $\gamma = 90°$, leaving the middle part of it to remain non-irradiation. Ideally, in this case, the edges of the ellipsoid will be irradiated (Fig. 1b).

With the given dimensions $c = 0.0293\ m$, $b = 0.0227\ m$ of the half-axles, the angles $\theta = 165°$, $\Theta = 9°$, correspond to the described situations. Obviously, an increase of the angle θ above 165º and a decrease of the angle Θ below $9°$ will only worsen the exposure. If the emission source are at points Q'' and P'' ($\theta = 89°$, $\Theta = 69°$), then a similar situation will arise on the edges O and M of the ellipsoid, which will not be illumined, and the greatest part of the illumination will be obtained by the middle part of the ellipsoid (Fig. 1g). To reduce the angle θ (increase Θ) is impractical for the same reason. Therefore, a qualitative (uniform) illumination should be expected in the range of angles: $89° < \theta < 165°$, $9° < \Theta < 69°$.

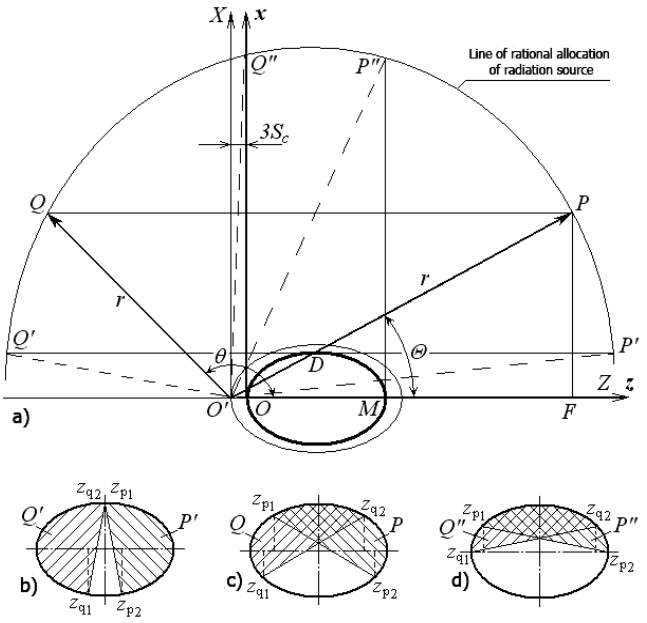

Fig. 1. Estimated pattern of irradiation of the ellipsoid by two sources

As we see, with $\theta = 89°$ the central part of the ellipsoid is the most illuminated, and with the approach to its ends the radiation dose decreases to zero. This corresponds to the scheme in Fig. 1a. If $\theta = 165°$ we have the opposite effect: the radiation dose decreases to zero in the central part of the ellipsoid and the maximum at its ends (Fig. 1b).

And in this case, there is the largest dose rate (from 0 to 50 Ws/m^2). This is explained by the fact that in this position of the sources the ellipsoid are deployed to them with a narrow part and it is closer to the sources than in the case of smaller corners θ. Fig. 1 also shows that the average value of the dose, with change of the sources position, varies slightly, but the deviation of the dose from the average significantly depends on the angle θ [5, 6].

In Fig. 2., on the basis of formula (1), (2) evaluation, the more exacerbated graphs of the current dose of radiation (together with the average value) are at five points of sources placement from the given range of angles. The positions (a), (e) of the figure correspond to the extreme points of the range [2, 13, 26].

The dose of irradiation for the length of the ellipsoid by two symmetrically located sources is equal to

$$E_D(z,\theta) = \frac{2J_i}{\omega}\left[EQ(z,\theta) + EP(z,\theta)\right] \qquad (1)$$

Determine the average value of the radiation dose of the ellipsoid surface:

$$E_D(\theta) = \frac{1}{c}\int_0^c E_D(z,\theta)\,dz = \frac{2J_i}{\omega\, c}\int_0^c \left[EQ(z,\theta) + EP(z,\theta)\right] dz \qquad (2)$$

As it was shown above (Fig. 2), the irradiation dose excess over the average values substantially depends on the angle θ, which determines the allocation of both sources relative to the exposure object. Below we will show that the configuration of the radiation line of the ellipsoid along the axis Oz with suboptimum angular values θ is rather complicated. The program of automatic search of the largest and smallest values irradiation dose in the presence of several (up to seven) local extremes is greatly complicated, and its application is difficult due to a sharp increase in search time. In these conditions, it seems advisable to use the function "Trace" - the system tracing "Mathcad", which allows with sufficient accuracy (up to three characters after a comma) to get the desired quantity according to the function graph [15, 21].

Let's note one more important feature. Graphs of the dose of irradiation in Fig. 1 were being constructed when the value of the circular frequency of the ellipsoid rotation equal to $\omega = 0.5\ s^{-1}$. The optimal value of this frequency is unknown to us yet. But to determine the dose of irradiation, we use formula (3), in which the circular frequency - ω and the radiation source of the source – J_i are included as a constant multiplier – 2 J_i/ω with a variable part *–[EQ(z,θ)+EP(z,θ)]* [12, 14, 28].

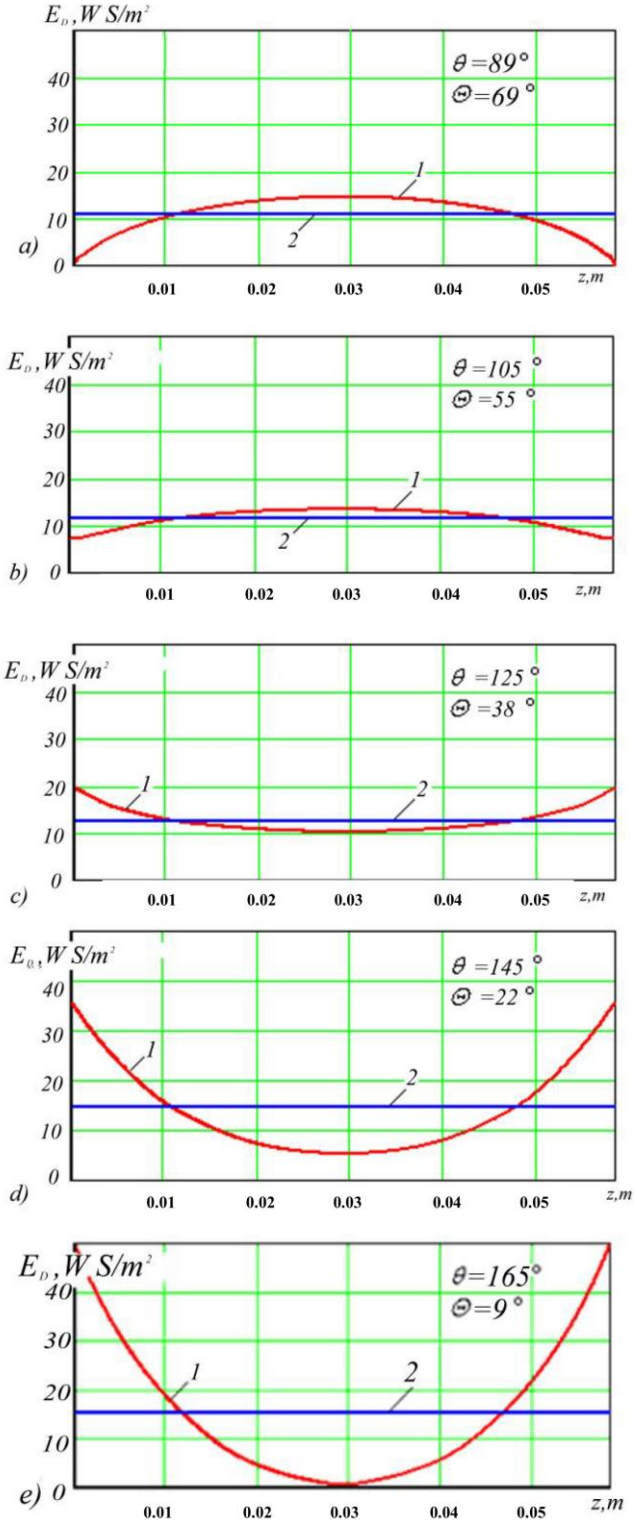

Fig. 2. Current (1) and average (2) doses of radiation depending on the position of sources when c = 0.0229 m; S_c = 0.0014 m; ε = 0.634; ψ = 22°; J_i = 0.05 BT; ω = 0.5 s^{-1}

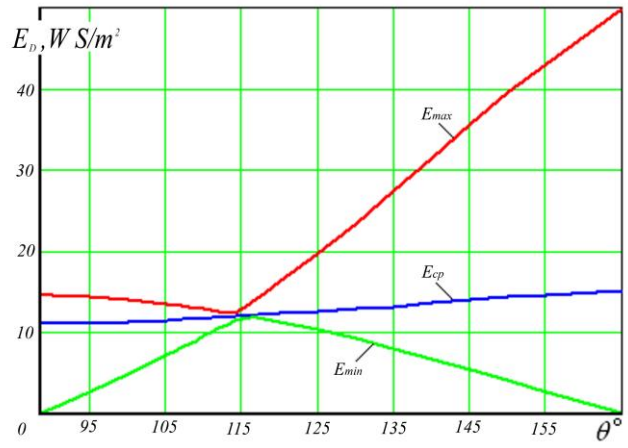

Fig. 3. The average dose rate of radiation and its correlation against the location of the radiation source

Thus, the radiation dose for the length of the ellipsoid by two symmetrically located sources is:

$$E_D(z,\theta) = \frac{2J_i}{\omega}\left[EQ(z,\theta) + EP(z,\theta)\right] \tag{3}$$

Therefore, neither frequency – ω nor power – J_i effect the optimum position. We further, for preserving the physical meaning of the measured value of the dose (radiation dose), will save the multiplier 2 J_i.ω in formula (3) with the indicated above the previous value of the frequency ω. And after determining the optimal allocation of sources of irradiation, this value we are going to specify [13, 17, 19].

On the basis of the obtained equality it is possible to determine the average value of the radiation dose of the ellipsoid surface:

$$E_D(\theta) = \frac{1}{c}\int_0^c E_D(z,\theta)\,dz = \frac{2J_i}{\omega c}\int_0^c \left[EQ(z,\theta) + EP(z,\theta)\right]dz \tag{4}$$

The average (4) and current (3) axis dose values *Oz, z ϵ [0;2c]* were determined to reveal the optimal angle value *θ*. By the method of tracing the current dose its maximum and minimum values were founded. The table of these variables is calculated with a corner angle *θ* in 5º, and in the area of the expected optimum – with step in *1°* (appendix X2). Output data for the calculation are the same as in Fig. 1. Based on the results of calculations, the graphs are drowned (Fig. 3), which allow to reveal (by the same method of tracing) a narrow range of angle *θ* (*113°...114°*). There is a minimum excess of the dose of irradiation above the mean value. The graphs also show that the maximum of the minimum dose and the minimum of the maximum are near, and thus, with a minimum excess of the radiation dose above the mean value, the lower deviation will also be small. In the specified range, the dose exceeded $\Delta E = 100(E_{max}-E_{cp})/E_{cp}$ by step *0.1°*. The results of the calculation are represented by two vectors [14, 27]:

$$Teta := (113.5\ \ 113.6\ \ 113.7\ \ 113.8\ \ 113.9\ \ 114.0\ \ 114.1\ \ 114.2)^T$$

$$DelE := (3.680\ \ 3.506\ \ 3.330\ \ 3.140\ \ 2.979\ \ 3.044\ \ 3.265\ \ 3.729)^T$$

where "T" denotes transposition operation. For the given values, a smooth curve is constructed by the method of cubic interpolation, which in the environment of "Mathcad" is follows:

$$\Delta E(\theta) := \text{interp}\left(\text{cspline}\left(Teta, DelE\right), Teta, DelE, \theta\right)$$

The graph of the obtained dependence is presented in Fig. 4.

The optimal angle value *θ* is obtained using the built-in "Mathcad" function - "Minimize":

$$\theta := 113 \qquad \theta_{opt} := \text{Minimize}\left(\Delta E, \theta\right) \qquad \theta_{opt} = 113.92 \tag{5}$$

The same value can be obtained by tracing the graph in the picture below. The value 113.92° corresponds to 1.988 rad.

The second source corresponds to the optimal angle:

$$\Theta_{opt} = \Theta\left(\theta_{opt}\right) = \Theta(1.988) = 46.7^\circ = 0.815rad \tag{6}$$

But, since the radiation sources are symmetric, the necessary optimal parameters can be obtained from a single source.

Height of laser stand holder:

$$H = X\left(\theta_{opt}\right) = X(1.988) = 0.134m \tag{7}$$

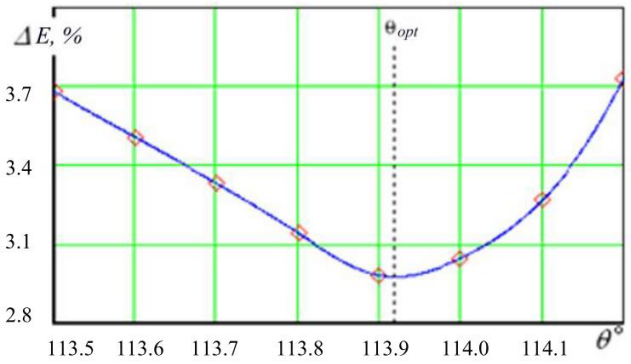

Fig. 4. Excess dose above average together with nodal points

Distance from the rack to the center of the ellipsoid:

$$L = c - Z\left(\theta_{opt}\right) = c - Z(1.988) = 0.093m \tag{8}$$

The circle frequency of the ellipsoid can be founded from formula (4) to determine the average dose of irradiation. Substituting there instead of the angle *θ* its optimal value θ_{opt}, and instead of the average dose value $E_D(\theta)$ – normative $[E_D^N]$, we obtain:

$$\omega = \frac{2J_i}{c[E_D^N]}\int_0^c \left[EQ(z,\theta_{opt}) + EP\left(z,\theta_{opt}\right)\right]dz = 0.46s^{-1} \tag{9}$$

The time of irradiation and the frequency of rotation of the ellipsoid can be found by the way of using the known dependencies:

$$T = \frac{2\pi}{\omega} = 13.6s\,,\ n_{ob} = \frac{60}{T} = 4.4rpm \tag{10}$$

Frequency n_{ob} can be multiply increased without losing the effect of irradiation (eg.: $n_{ob} = 8.8$ revolutions per minute, $n_{ob} = 13.2$ revolutions per minute etc.), under the condition if the time *T* is saved [18, 19].

Now, when the magnitude becomes known, it is necessary to clarify the value of the deviations of the irradiation dose of the ellipsoid from the mean value, which is equal to the normative – $[E_D^N]$. For clarity, we are going to present a schedule for changing the dose along the length of the ellipsoid, which corresponds to the optimal allocation of radiation sources ($\theta = 1.988$; $\Theta = 0.815$).

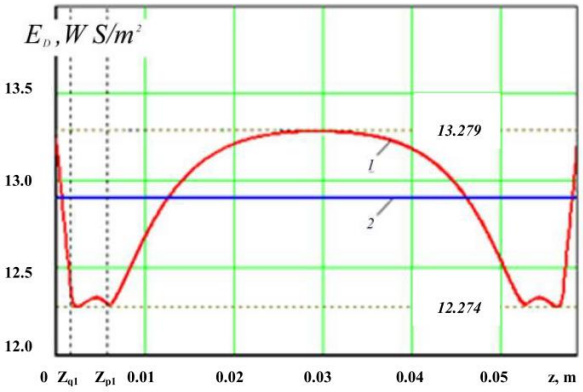

Fig. 5. The irradiation dose change along the length of the ellipsoid under the condition of optimal placement of sources

In the interval $z\epsilon[0;z_{q1}]$, the endpoint of the ellipsoid at first receives an irradiation dose above the mean, and then, to the end of the segment, it drops to almost the minimum value due to the distance from the source Q (increase of coordinate z). At the site $z\ \epsilon[z_{q1};\ z_{p1}]$, with increasing coordinate z, the angle of incidence of rays γ on the surface of the ellipsoid decreases, resulting in a dose increasing. But, at the same time, the irradiated surface continues to move away from the source, and the coverage angle $\phi(z)$ of the irradiation spot decreases. As a result, it reduces the radiation dose to the end of the segment. In the absence of the second source P, the dose reduction would continue to zero at a point $z = z_{q2}$, any longer of which the rays of the first source Q do not reach the surface of the ellipsoid. However, starting from the point $z = z_{p1}$ the influence of source P appears. As a result of radiation imposition of both sources, the radiation dose increases to the maximum value in the middle part of the ellipsoid. The second half of the graph $z = [c,2c]$ is symmetrical to the first and has the same explanation of the "behavior" of the curve [12, 27, 28].

According to the schedule, the upper and lower deviations of the radiation dose from the average value, which, respectively, are equal to: $\Delta E = 2.94\%$; and $\Delta E_H = 4.85\%$ are determined simply. These figures occur for an ellipsoid with medium-sized c, b of half-axes. As has been mentioned more than once, the indicated sizes in the process of radiation range: $c \pm 3S_c$; $b \pm 3Sc\sqrt{1-\varepsilon^2}$. For ellipsoids with the maximum and minimum dimensions of the half-axis, the deviation from the average dose $[E_D^N]$ may not coincide with the same values which were obtained for the average size. Therefore, for the specified limits, additional calculations have been made. From the three pairs of the founded values, including the above, the maximum values of the required indicators are selected [12, 20]:

$$\Delta E = 5.46\%;\ \Delta E_H = 5.92\% \qquad (11)$$

Thus, on the basis of the rule of "three sigmas", it can be argued that with an optimal allocation of sources with a probability of 0.9973, the increase of the irradiation dose of the ellipsoid will not exceed 5.46% compared to the average value, and the reduction does not exceed 5.92%.

All calculations related to the irradiation of the ellipsoid by two sources, conducted in the environment of "Mathcad" on the developed program, which is presented in Annex X3 [28].

4. Conclusions and future work

Ellipsoid irradiation is considered with two identical sources which are installed symmetrically on the line of rational placement. Expressions for determining the current and average doses of the ellipsoid irradiation by each source were obtained. The resulting dose of irradiation was the imposition of radiation doses received from each source.

The dependence of maximum, average and minimum doses of irradiation in the case of synchronous motion of sources along the rational placement is constructed. They showed a significant dependence of the irradiation uniformity on the position of the sources on the specified line. The optimal approach was such sources positioning in which excess radiation dose above the mean value was minimally possible. Calculations conducted in the interval of the ellipsoid size "three sigma" from the average showed that with the probability of 0.9973 increase in the dose of the ellipsoid compared with the average does will not exceed 5.46%, and decrease – will not exceed 5.92%.

References

[1] Avila R. E. et al. : Effects of He-Ne Laser Irradiation on Chicr Embryo Mesonephros. Journal of Clinical Lastr Vtdicint Sergery 10(4), 1992, 287–290.

[2] Avrunin O. G. et al.: Application of 3D printing technologies in building patient-specific training systems for computing planning in rhinology. Information Technology in Medical Diagnostics II. CRC Press 2019, 1–8.

[3] Dubolazov O. V. et al.: Laser Müller matrix diagnostics of changes in the optical anisotropy of biological tissues. Information Technology in Medical Diagnostics II. CRC Press 2019, 195–203.

[4] Dubolazov O. V., Ushenko A. G.: The complex degree of coherence of the laser images of blood plasma and the diagnostics of oncological changes of human tissues. Information Technology in Medical Diagnostics II. CRC Press, Balkema book, Taylor & Francis Group, London, UK, 2019, 185–194.

[5] Grossman N. et al.: 780 nm low power dide laser irradiation stimulates proliferation of kerationocyte cultures: invoivement of reactive oxygen species. Lastr Surg. Med. 22(4), 1998, 212–218.

[6] Kholin V. V., Gamaleia N. F. et al.: Photodynamic therapy with laser scanning mode of tumor irradiation. Proc. SPIE 9816, 2015, 98161F.

[7] Kondratiuk S. et al.: Information technology for security system based on cross platform software. NATO Science for Peace and Security Series A: Chemistry and Biology, 2018, 331–339.

[8] Kondratiu S., Krak I.: Dactyl Alphabet Modeling and Recognition Using Cross Platform Software. 2nd International Conference on Data Stream Mining and Processing – DSMP, 2018, 8478417, 420–423.

[9] Kozlovska T. I., Pavlov S. V.: Optoelectronic Means of Diagnosing Human Pathologies Associated with Peripheral Blood Circulation. LAP LAMBERT Academic Publishing, Beau Bassin 2019.

[10] Krak I. V. et al.: Applied aspects of the synthesis and analysis of voice information. Cybernetics and Systems Analysis 49(4), 2013, 589–596.

[11] Krak I., Kondratiuk S.: Cross-platform software for the development of sign communication system: Dactyl language modelling. 12th International Scientific and Technical Conference on Computer Sciences and Information Technologies – CSIT, 2017, 8098760, 167–170.

[12] Kryvonos I. G. et al.: Predictive Text Typing System for the Ukrainian Language. Cybernetics and Systems Analysis 53(4), 2017, 495–502.

[13] Kvyetnyy R. et al.: Method of image texture segmentation using Laws' energy measures. Proc. SPIE 10445, 2017, 1044561.

[14] Kvyetnyy R. et al.: Modification of fractal coding algorithm by a combination of modern technologies and parallel computations. Proc. SPIE 9816, 2015, 98161R.

[15] Kvyetnyy R. et al.: Blur recognition using second fundamental form of image surface. Proc. SPIE 9816, 2015, 98161A.

[16] Kukharchuk V. V. et al.: Information Conversion in Measuring Channels with Optoelectronic Sensors. Sensors 22(1), 2022, 271 [http://doi.org/10.3390/s22010271].

[17] Milenin D., Lysychenko M., Pankova O. et al.: Research of the ellipsoid area geometry illuminated by a point laser source., Optical Fibers and Their Applications. Proc. SPIE 11456, 2020, 114560M.

[18] Milenin D. M., Lysychenko M. L.: Efektyvnist'lazernoyi obrobky inkubatsiynykh yayets'. Visnyk KHNTUSH 129, 2012, 84–87.

[19] Milenin D., Lysychenko M.: Irradiation conditions still ellipsoid point sources. Pratsi TDAU 15, T.2, 2015, 266–273.

[20] Pavlov S. V. et al.: Methods and computer tools for identifying diabetes-induced fundus pathology. Information Technology in Medical Diagnostics II. CRC Press, Balkema book, 2019, 87–99.

[21] Povoroznjuk A. et al.: Minimization risk doctor-mistake when designing computer decision support system in medicine. 13th International Conference: The Experience of Designing and Application of CAD Systems in Microelectronics – CADSM, 2015.

[22] Rovira R., Tuzhanskyy S.: Polarimetric characterisation of histological section of skin with pathological changes. Proc. SPIE 10031, 2016, 100313E.

[23] Samar M. E. et al.: Histological Changes Produced by He-Ne Laser on Diferent Tissues from Chick Embryo. Journal of Clinical Laser Medicine & Surgery 11(2), 1993, 87–89.

[24] Selivanova K.G. et al.: Virtual training system for tremor prevention. Information Technology in Medical Diagnostics II. CRC Press, Balkema book, 2019, 9–14.

[25] Wójcik W., Pavlov S.: Highly linear Microelectronic Sensors Signal Converters Based on Push-Pull Amplifier Circuits. Komitet Inżynierii Środowiska PAN, 181, Lublin 2022.

[26] Wójcik W. et al.: Information Technology in Medical Diagnostics II. CRC Press, Balkema book, 2019.

[27] Zhemchuzhkina T. V. et al.: Some technical propositions for electromyographical human interface device. Information Technology in Medical Diagnostics II. CRC Press, 2019, 15–21.

Ph.D. Dmytro Milenin
e-mail dm.milenin@gmail.com

Senior lecturer of Department of Electromechanics, Robotics, Biomedical and Electrical Engineering State Biotechnological University. Scientific interests include the development of technical solutions and the study of the processes of efficient use of energy by electrical equipment. The main direction of scientific activity is the study of the effect of electromagnetic radiation in the optical range on hatching eggs and young birds. Published about 45 scientific papers.

http://orcid.org/0000-0003-3058-2243

D.Sc.Eng. Mykola Lysychenko
e-mail: 1prlysychenko@ukr.net

Professor of Department of Electromechanics, Robotics, Biomedical and Electrical Engineering State Biotechnological University.
Scientific interests include the development of technical solutions and the study of the processes of efficient use of energy by electrical equipment.
The main direction of scientific activity is the study of the impact of electromagnetic radiation in the optical range on biological objects, nanotechnology in biomedical engineering.

http://orcid.org/0000-0003-1611-6705

Ph.D. Andriy Milenin
e-mail a-milenin@ukr.net

Associate professor of the Department of Equipment and Engineering of Food and Processing Industries. Published about 30 scientific papers.
The main direction of research "Energy saving in the transportation of various agricultural goods"

http://orcid.org/0000-0003-3521-1652

Ph.D. Leonid Koval
e-mail: koval.l@vntu.edu.ua

Candidate of Technical Sciences, associate professor, Head of the Department of Biomedical Engineering and Optical-Electronic Systems, Vinnytsia National Technical University. Scientific direction – information technology in biomedical applications, information systems for professional selection, automated control systems for remotely controlled devices.

http://orcid.org/0000-0001-9887-2605

Prof. Saltanat Amirgaliyeva
e-mail: saltanat_amirgal@mail.ru

Doctor of Physical and Mathematical Sciences, professor, Academy of Logistics and Transport of the Republic of Kazakhstan. Research interests: Development of methods for optimal stabilization of macroeconomic models taking into account scientific and technological progress, conflict and uncertainties of dispersed controlled dynamic systems, semantic search systems of new generation texts

http://orcid.org/0000-0001-5311-7227

Ph.D. Maxatbek Satymbekov
e-mail: m.n.satymbekov@gmail.com

Assistant professor of the Department of Computer Science of Al-Farabi Kazakh National University. Author of more than 25 scientific works published in leading journals of Kazakhstan Republic and the abroad. Research area: High performance computing, intelligent systems of control, software engineering, artificial intelligence, soft computing.

http://orcid.org/0000-0002-4621-6646

Ph.D. Saltanat Adikanova
e-mail: adikanovas@gmail.com

S. Adikanova is currently the dean of the Higher school of Information Technologies and natural science of S. Amanzholov. She is a co-author of more than 50 articles in journals and conference proceedings. Her professional interests are studying the problems of atmospheric pollution, STEAM training, development of web sites and e-learning resources.

http://orcid.org/0000-0003-0085-8384

http://doi.org/10.35784/iapgos.3463 *received: 26.01.2023 | revised: 10.05.2023 | accepted: 24.05.2023 | available online: 30.06.2023*

DEVELOPMENT OF AN APPLICATION FOR THE THERMAL PROCESSING OF OIL SLIME IN THE INDUSTRIAL OIL AND GAS SECTOR

Gulnar Balakayeva[1], Gaukhar Kalmenova[1], Dauren Darkenbayev[1], Christofer Phillips[2]
[1]Al-Farabi Kazakh National University, Almaty, Kazakhstan, [2]Newcastle University, Newcastle, United Kingdom

Abstract*. The production activities of oil refineries and oil and gas-producing enterprises inevitably have an anthropogenic impact on the environment, so environmental issues and the rational use of natural resources are important. The most dangerous pollutants of all components in the natural environment are oil waste, and one of the most effective methods of processing is heat treatment. The task was set to neutralize oil waste by thermal processing of oil slime to an environmentally safe level. The studies are carried out by methods of mathematical and numerical simulation of thermal processing, the results of which describe changes in temperature and mass of the stream over time. Extensive calculations with varying current operating and other parameters allow us to optimize the flow of heat and mass transfer during the thermal processing of oil slime. Numerical modeling is implemented using the method of alternating directions in an implicit iterative scheme until a convergence condition is met. The purpose of this work is to create an application for solving research and practical problems of oil waste processing. The application used allows the solution of the problems of oil slime processing. With the help of color-animated illustrations and a graphical interface, it supports the visualization of the results obtained, and provides the possibility of interactive interaction with the user, while providing instant control of the results obtained for timely decision-making to prevent environmental pollution in the industrial oil gas sector.*

Keywords: oil slime, software, heat treatment, applied application, ADI, mathematical model

OPRACOWANIE APLIKACJI DO TERMICZNEGO PRZETWARZANIA SZLAMÓW OLEJOWYCH W PRZEMYSŁOWYM SEKTORZE NAFTOWYM I GAZU

Streszczenie*. Działalność produkcyjna rafinerii ropy naftowej oraz przedsiębiorstw wydobywających ropę i gaz nieuchronnie ma antropogeniczny wpływ na środowisko, dlatego tak ważne są kwestie środowiskowe i racjonalne wykorzystanie zasobów naturalnych. Najbardziej niebezpiecznymi zanieczyszczeniami wszystkich składników środowiska naturalnego są odpady olejowe, a jedną z najbardziej efektywnych metod ich przetwarzania jest obróbka cieplna. Zadanie polegało na neutralizacji odpadów olejowych poprzez termiczną obróbkę szlamu olejowego do poziomu bezpiecznego dla środowiska. Badania prowadzone są metodami matematycznej i numerycznej symulacji obróbki cieplnej, której wyniki opisują zmiany temperatury i masy strugi w czasie. Rozbudowane obliczenia przy zmiennym prądzie roboczym i innych parametrach pozwalają nam optymalizować przepływ ciepła i wymiany masy podczas termicznej obróbki szlamów olejowych. Modelowanie numeryczne realizowane jest metodą naprzemiennych kierunków w niejawnym schemacie iteracyjnym, aż do spełnienia warunku zbieżności. Celem pracy jest stworzenie aplikacji do rozwiązywania problemów badawczych i praktycznych przetwarzania odpadów olejowych. Zastosowana aplikacja pozwala na rozwiązanie problemów związanych z przetwarzaniem szlamów olejowych. Za pomocą kolorowych animowanych ilustracji i interfejsu graficznego wspiera wizualizację uzyskanych wyników oraz zapewnia możliwość interaktywnej interakcji z użytkownikiem, zapewniając jednocześnie natychmiastową kontrolę uzyskanych wyników w celu szybkiego podejmowania decyzji zapobiegających zanieczyszczeniu środowiska w sektorze gazu przemysłowego.*

Słowa kluczowe: szlam olejowy, oprogramowanie, obróbka cieplna, zastosowana aplikacja, ADI, model matematyczny

Introduction

The ecological state of our planet has been causing concern for a long time. The anthropogenic impact on the environment causes irreparable harm to it and is one of the serious sources of environmental pollution in the oil, and oil refining, industry. The modern world economy requires a colossal amount of energy resources, the main source of which is oil, and ecology is often relegated to the background. Modern volumes of produced hydrocarbons and the capacity of their processing enterprises bring environmental protection problems to the fore.

The oil industry occupies one of the first places among the leading industries in terms of the level of environmental impact due to the formation of a large amount of heterogeneous waste. One of these is oil slime – a colloidal system of high-molecular compounds of oil, mineral particles of various compositions, and reservoir water. This is the largest waste of the oil production and refining industries, characterized by the complexity of the chemical composition, and is in the process of constant transformation. Sludge is formed during the construction of oil and gas wells, during the field operation of oil refining fields, wastewater disposal, as well as during the cleaning of tanks and other equipment. Various types of oil slime are also common waste for the objects of the energy complex, transport, machine-building, chemical, and metallurgical enterprises. The nature of their formation in these industries is predominantly similar to the waste-forming processes in the oil industry. The most significant amounts of oil-containing waste are formed during the cleaning of tank farms of thermal power plants, airports, railway stations, and metallurgical plants. Steaming stations of railway tank cars and treatment facilities are also sources of large-capacity hydrocarbon-containing slurries of various phase and chemical compositions. Special attention should be paid to such a type of oil-containing waste as smeared soils are formed during emergency oil spills. The main difference between them and oil slime is a lower concentration of hydrocarbons. The reduced viscosity of the spilled oil leads to the fact that it forms a monomolecular film layer on the surface of the relief. If its thickness does not exceed 10 mm, then the penetration of oxygen is delayed by about 5–10%, which does not significantly affect the vital activity of microorganisms. In the case when the ability of oxygen absorption by the oil layer is 80–90%, the process of photosynthesis is hindered, which leads to a decrease in the concentration of oxygen in the soil and contributes to the suppression of the vital activity of organisms until their ultimate death.

Processing and disposal of oil slime is an important environmental and economic task. One of the most effective methods of processing oil slime is heat treatment. Thermal methods of oil slime processing are based on the processes of thermal decomposition of petroleum products [1]. As a result of the complete thermal decomposition of oil products, the final degradation products – CO_2 and H_2O – are formed. It also significantly reduces the volume of inorganic substances, such as metals and salts, and allows the effective elimination of waste.

1. Releated works

In this section, we discuss related research papers that are most relevant to our topic. To discussion on an analysis of the scientific and technical literature on the thermal processing of oil slime we collected, analyzed, and coded author-assigned keywords of papers. In the works the method of solving the heat equation (ADI) is well considered. Considering the works, programming in the high-level language Python was performed for use in the thermal treatment of oil slime [17, 20, 24].

2. The aim and objectives of the study

The aim of the study is to develop a software package for the analysis and intensification of oil slime processing, starting from the study of the characteristics of oil slime and the physical and chemical foundations of the process and ending with the issuance of practical recommendations for the disposal of oil slime to minimize the anthropogenic impact on the environment. The task was set to neutralize oil waste by thermal processing of oil slime to an environmentally friendly level.

- A model has been developed for processing oil slime using convective heating, which makes it possible to evaluate the efficiency and uniformity of heating depending on the temperature and velocity of the flow that heats the oil waste.
- A software implementation of the algorithm for the numerical solution of a non-stationary, inhomogeneous heat conduction problem was implemented using the method of alternating directions according to an implicit iterative scheme until the convergence condition is met.

3. Mathematical and numerical modeling

Modeling is one of the main tools for conducting research in the modern world. It allows you to conduct theoretical experiments quickly and cost-effectively, most reliably displaying the objects under study.

The increase in the capabilities of computer technology opens up more and more prospects and opportunities for studying processes and phenomena.

A mathematical model and computer simulation of the heat conduction process and the implementation of the program code that graphically displays the results of the model, that is, the construction of a digital model of the process, for subsequent use as a module, is described here including processing of the graphical representation of data [7]. To achieve this goal, the following tasks are solved:

- Analysis of the subject area using various information sources of scientific content (books, articles, research papers, etc.).
- Construction of a mathematical model of heat propagation in two-dimensional space over time with variable coefficients.
- Development of a software product that simulates the process of temperature change over time and displays the results in graphical form.

When developing a mathematical model for the thermal processing of oil residues, we consider the heating of the product layer. The mathematical model of the process is characterized by heat and mass equations and forms systems of second-order nonlinear differential equations. Primary and boundary conditions include the Dirichlet and Neumann conditions. The solution is implemented using the method of alternating directions according to a non-obvious difference scheme until a convergence condition is met [4].

Numerical heat transfer is a broad term denoting the procedures for the solution, on a computer, of a set of algebraic equations that approximate the differential (and, occasionally, integral) equations describing conduction, convection, and/or radiation heat transfer. The usual objective in any heat transfer calculation is the determination of the rate of heat transfer to or from some surface or object. In conduction problems, this requires finding the temperature gradient in the material at its surface.

When solving a multidimensional problem, the amount of computation with the required accuracy is of great importance. The solution to the posed differential equation includes a combination of several methods and schemes, which, after transformations, allow us to arrive at a numerical solution to the problem.

Explicit and implicit schemes have the same order of precision. The number of actions at all nodes for an explicit scheme on a new layer is proportional to the number $(N-1)^2$ of grid nodes:

$$Q_{explicit} = O\left(\frac{1}{h^2}\right)$$

In the case of an implicit scheme, it is necessary to solve a system of $(N-1)^2$ equations. This requires significantly more steps than with an explicit scheme:

$$Q_{explicit} = O\left(\frac{1}{h^4}\right)$$

In terms of stability, the implicit scheme is stable for any values of t and h, while the explicit scheme is only stable when $\tau \le \frac{1}{4}h^2$

Economical difference schemes, including the scheme alternating directions, combine the advantages of implicit and explicit schemes [10]. Economical schemes for several the most complex problems in physics and technology allow finding a solution to the numerical model [9]. The main idea of such methods is the sequential solution of one-dimensional problems along rows and along columns.

The longitudinal-transverse scheme (implicit method of alternating directions) expresses this idea most clearly.

To solve multidimensional problems that lead to partial differential equations, the method of alternating directions is most often used. This method is an iterative method for solving systems of linear or nonlinear equations in the approximate solution of boundary value problems for partial differential equations in difference or projection-difference methods.

The method is well described in the mathematical literature but attempts to implement it often turn out to be incorrect or inaccurate. Inaccuracy manifests itself when, considering the boundary conditions, their specification at intermediate time steps is neglected. This neglect can cause instabilities even if the scheme used itself is unconditionally stable in terms of spectral characteristics.

There are various methods for solving boundary problems for the thermal equation, including the variable direction method. In the scheme of the method of the variable direction, as shown in all Division methods, the number of independent spatial variables (two in the two-dimensional case) divides the time period τ. In each particle-time layer, one of the spatial differential operators is approximated by an implicit (scalar pursuit in the direction of the corresponding coordinate is performed), and the others are implicit. In the subsequent fractional step, the next in turn of the differential operator is executed not explicitly, and the others are executed explicitly [25]. This scheme is often referred to as the Peaceman-Reachford scheme (the name of the authors who first proposed it). T (x, t) together with the main values of the lattice function, i.e. the value of T can be considered when $t = t_{n+\frac{1}{2}} = t_n + \frac{\tau}{2}$, $T = T^n$ and the intermediate value $T = T^{n+\frac{1}{2}}$ is entered in the middle of $T = T^{n+1}$). Where the transition from layer n to layer n + 1 is carried out in two steps $\tau/2$. In the two-dimensional case, it can be shown that the scheme of the variable direction method is absolute constant [18].

To solve the heat equation with constant coefficients, an implicit difference scheme can be used, which is constructed by approximating the differential operator with a difference operator on the (n + 1) time layer. The difference scheme approximates the equation with the order $O\left(\Delta\tau + h^2\right)$. We let $\Delta\tau/h^2 = r$ and rewrite it in the form (1):

$$A_k T_{k+1} + B_k T_k + C_k T_{k-1} = F_k \quad (1)$$

To check the stability of the circuit according to the maximum principle, we have:

$$A_k = r > 0, C_k = r > 0, -B_k = 1 + 2r > A_k + C_k$$

The last inequality is always fulfilled. This means that the implicit scheme is absolutely stable.

The advantage of the variable direction method is high accuracy since the method has a second order of accuracy in time. The disadvantage can be attributed to the conditional stability when the number of spatial variables is more than two. In addition, the variable direction method is absolutely constant. The mathematical model obtained as a result of heat treatment of oil waste describes the change in temperature and mass of the flow over time and allows its control [16].

Due to the lack of experimental data for development, (as a temporary replacement) modeling of the heat conduction process is used. The heat equation is a second-order partial differential equation that describes the temperature distribution in a given region of space and its change in time.

In mathematical physics, many different problems of heat conduction can be found, differing in the conditions of the process, but to study the work with computer models, the equation of a two-dimensional heat conduction equation with variable coefficients has been chosen.

To solve this equation, the following input parameters will be used, which are required for calculations:

- τ is the time step;
- h – grid step;
- x1, x2, y1, y2 – values that describe the limits of the region on lines along the OX and OY axes;
- t is the estimated time;
- Nx, Ny – the number of nodes in the grid.

Based on the input parameters, the temperature value is distributed on a coarse mesh uniformly with step h and bounded by the boundaries x1, x2, y1, and y2 along both spatial axes. There are many reasons that affect the values of the thermal conductivity parameters, both internal and external [8]. External causes may include pressure, ambient temperature, magnetic field, etc. Internal causes include the nature of the material, its structure, moisture, density, porosity, and others.

When solving the equation, the following parameters should be obtained:

- (x, y) – coordinates on the plane.
- T (x, y, t) is the temperature value at point (x, y) at time t.

Based on the found parameter values, a graphic display can be produced for further analysis and use by the user.

The studies are carried out by methods of mathematical and numerical simulation of thermal processing, the results of which describe changes in temperature and mass of the stream over time. Extensive calculations with varying parameters allow the optimization of the flow of heat and mass transfer during the thermal processing of oil slime.

4. Development of the mathematical part of the problem

When analyzing the subject area and researching solution methods, the following algorithm for the numerical solution of the equation was identified. Figure 1 describes the sequence of steps for calculating heat and mass transfer values in two-dimensional space.

- The values of the initial conditions are entered.
- Using a local one-dimensional scheme and formulas, calculations are performed using the sweep method and the variable direction method.
- The result of the calculations is the values T (x, y, t) and the corresponding coordinates (x, y) on a given plane at the calculated time t.
- The results of calculating the required function are displayed in tabular and graphical forms.

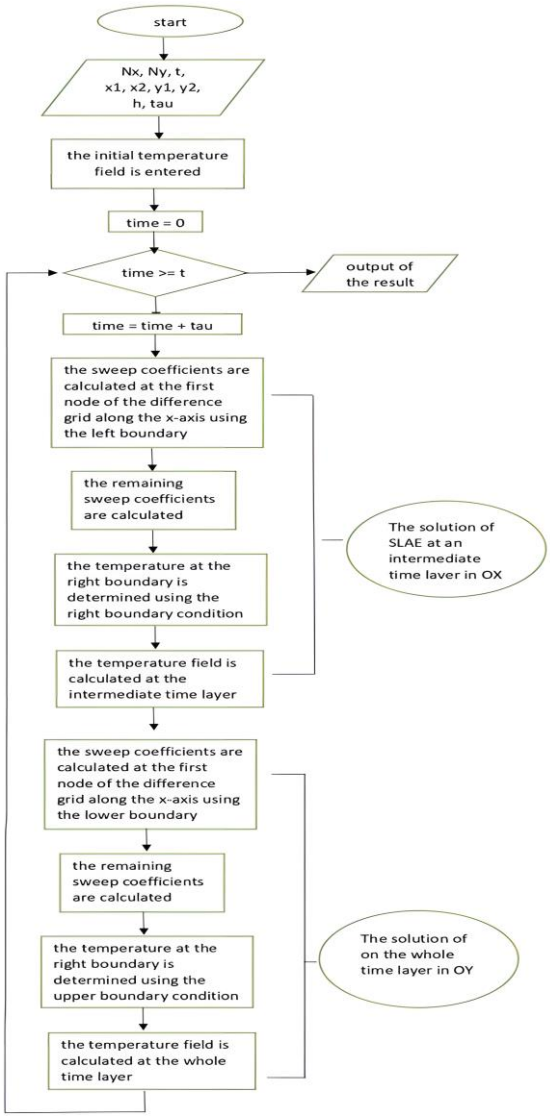

Fig. 1. The block diagram of the calculation algorithm

5. Description of the application

The constant increase in the capabilities of computing opens up great prospects for the study of processes and phenomena of the surrounding world. Computer simulation is, in fact, simulation implemented using computer technology.

The construction of a computer model is based on abstraction from the object under study. The more significant properties are identified and used in a computer model, the more capabilities a system using this model can have. Computer modeling consists of carrying out a series of computational experiments on a computer, the purpose of which is to analyze, interpret and compare the results with the real behavior of the object and then refine the model, if necessary.

Computer simulation provides a number of possibilities and advantages:

- Study of a wide range of objects, including phenomena past and future, objects that cannot be reproduced in real conditions, non-repeating phenomena, etc.;
- Visualization of abstract objects and objects of nature;
- Conducting multiple tests of the model;
- Conducting experiments without the risk of negative consequences for humans or the environment;
- Finding the optimal design of the object, without making test samples.

The developed software package for solving the problems of oil slime processing has the structure shown in figure 2.

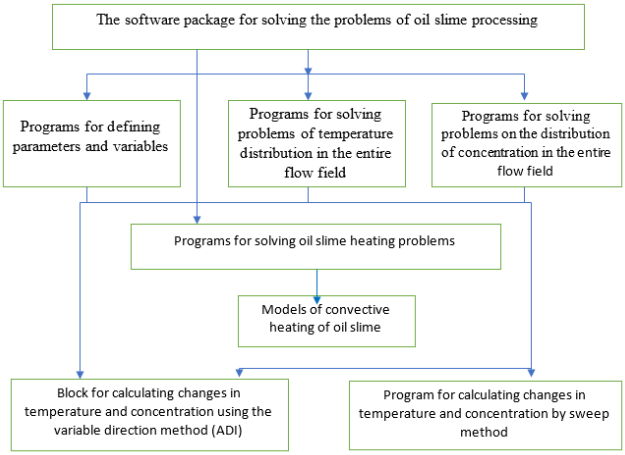

Fig. 2. The structure of the applied application

The main stages of computer modeling of the task are as follows [6]:

1) Statement of the problem and its analysis (the purpose of creation, identification of initial data);
2) Building an information model (determining the parameters and their relationship, describing the mathematical relationship between the parameters);
3) Development of a method and algorithm for the implementation of computer models (selection of a method for obtaining initial data, drawing up an effective algorithm, and checking the correctness of the algorithm);
4) Development of a computer model (selection of software tools, development);
5) Conducting an experiment (developing a research plan, experiment, and analysis of the results).

During the experiment, it may become clear that it is necessary to make changes, refinements, or improvements to the computer model. In this case, it is necessary to return to the stage, that in the first queue affects the identified problem or task.

The program consists of three main parts:

- databases on the composition of oil slime;
- software, including equations and algorithms for calculating flows and temperatures under stationary conditions and their dynamic changes under various influences;
- a user interface that allows the entry of conditions and seeing the results of calculations.

The following describes the functionality and behavior of the application.

The software is implemented in the Python object-oriented programming environment. When creating the program the following are used: heat transfer theory, numerical methods for solving ordinary differential equations, the method of variable directions, etc.

The web application architecture represents relationships and interactions between components such as user interfaces, transaction processing monitors, databases, and others (Fig. 4).

The developed application allows for computer modeling of heat and mass transfer in soils and grounds, the spread of pollutants in the environment in order to further minimize environmental risks.

We've tackled interacting with databases using Flask-SQLAlchemy with advanced Authentication using Flask-Login (Figure 5).

It used necessary libraries: sqlalchemy, flask-sqlalchemy, flask-login, werkzeug, and configparser.

The file app.py contains the code for the Dash application and will be composed of several different layouts to accommodate creating the user account, logging in, and displaying the graphed data.

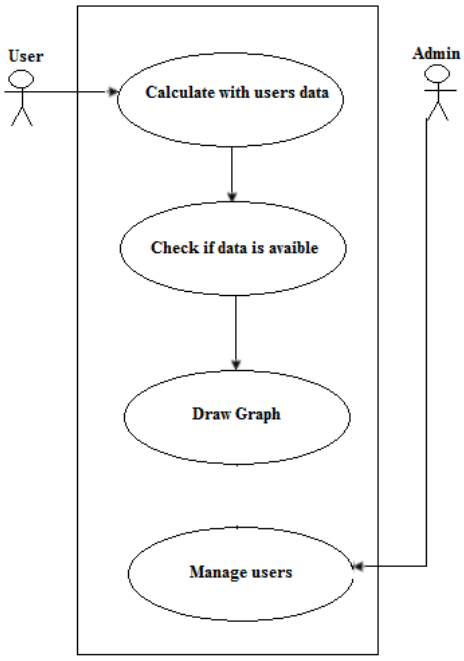

Fig. 3. The description of functionality and behavior of the application

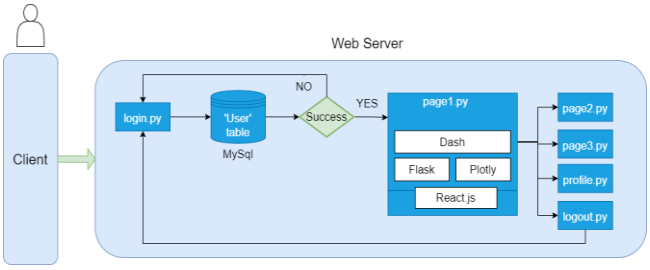

Fig. 4. The architecture of the web application

The users_mgt.py file is the database and stores the username, password, and email address in the Users table. To protect user passwords, the password will be hashed using the werkzeug library. Werkzeug is an advanced web server gateway interface (WSGI) utilities library. Configuring for Flask-Login is kept in the config.py file.

Fig. 5. Web application login

6. Results

Information visualization is the process of presenting abstract data in the form of images that can help in understanding the meaning of the data. Data visualization helps one to present large and complex datasets in a simple and visual way. At the end of the project, it is important to be able to report on its results so that even for non-professionals who do not have the technical knowledge, everything becomes clear and understandable [23].

Data visualization is an integral part of the application. It describes the data visualization framework in Python-Dash, which permits working not only with interactive graphs but also to display them on a website. Dash application code is declarative

and responsive, making it easy to create complex applications that contain many interactive elements [3]. The user interface library Dash will be useful for those who use Python for data analysis, exploration, visualization, modeling, and reporting [11].

Dash makes it much easier to create GUIs (Graphical User Interfaces) for data analysis.

There was no need to write any JavaScript or HTML code when a Dash application is running in a web browser. Dash provides a rich set of interactive web components. Dash provides a simple reactive decorator to bind data analysis code to the Dash UI. When an input element changes (for example, when an item is selected in a dropdown list or when a slider is moved), the Dash decorator provides Python code with a new input value.

Below is the code of the Python application using Dash:

```
import dash
import dash_bootstrap_components as dbc
import dash_core_components as dcc
import dash_html_components as html
from dash.dependencies import Input, Output
import plotly.graph_objects as go
app = dash.Dash()
app.layout = html.Div([
```

The following are specified in the code:

The application is initialized via dash.Dash, where specified the app name.

The layout attribute defines what will be on the web page, and only the Div header will be displayed on the page. All HTML components are in the dash_html_components module and describe high-level components that are interactive and generated using JavaScript, HTML, and CSS via the library React.js.

The application is started via run server. debug =True was set to be able to debug the code. If the application is ready to run on the server, then, for security reasons, the flag should be set to False.

The application is started via the run server. debug=True was set to be able to debug the code. If the application is ready to run on the server, then, for security reasons, the flag should be set to False.

The imported libraries that are needed for the dash system to work, and the python library for creating administrative systems, are based on React. Dash applications running under Flask and the external Dash interface display components using React.js, which are Javascript user interface libraries. The style for the menu and content was defined as follows:

```
# the style arguments for the sidebar
SIDEBAR_STYLE = {
    "position": "fixed",
    "top": 0,
    "left": 0,
    "bottom": 0,
    "width": "16rem",
    "padding": "2rem 1rem",
    "background-color": "#f8f9fa",
}

# the styles for the main content position it to the right of the sideb
ar and
# add some padding.
CONTENT_STYLE = {
    "margin-left": "18rem",
    "margin-right": "2rem",
    "padding": "2rem 1rem",
}
```

To make the time-series graph interactive, it is necessary to create a callback function for the drop-down menu and the output space. However, the hyphen does not allow callbacks for components that are not present in the layout.

To make apps interactive so that things actually happen when the user clicks on them, it needs two callbacks, one to return the different pages of the app, and the other to update the graph.

To do this, it was declared @app.callback. Inside @app. callback, we pass the Output function that is imported at the top of the file. Output parameters:

1. ID of the component that is being updated.
2. The parameter of the component that is being updated.

Then it was passed the Input function to app.callback.

```
@app.callback(
    [Output(f"page-{i}-link", "active") for i in range(1, 4)],
    [Input("url", "pathname")],
)
def toggle_active_links(pathname):
    if pathname == "/":
        # Treat page 1 as the homepage / index
        return True, False, False
    return [pathname == f"/page-{i}" for i in range(1, 4)]
```

Implemented a Dash callback to display graphs that describe changes in temperature and mass flow over time. There is also a slider on the page where you can choose from the composition of the oil slime. This is the essence of reactive programming via callbacks – when the input changes, so do the output.

To update the graph according to the dropdown selection, it is necessary to establish a link between the input data and the output (graph). This will be achieved by adding a callback function.

The following is a callback for a time-series graph.

```
@app.callback([ Output('graph', 'figure'),
    Output('graph1', 'figure')],[Input('input1', 'value'),Input('input2', '
value'),Input('input3', 'value'),Input('input4', 'value'),Input('input5',
'value'),Input('input6', 'value'),Input('input7', 'value')])
```

A Dash application can also have multiple Outputs, i.e. display multiple updatable components on a web page. It is just necessary to put a list of Outputs in the callback decorator, which will be updated depending on the Inputs. The function to be decorated must return as many Output values as specified in the decorator.

```
    [Output(f"page-{i}-link", "active") for i in range(1, 4)],
    [Input("url", "pathname")],
)
def toggle_active_links(pathname):
    if pathname == "/":
        # Treat page 1 as the homepage / index
        return True, False, False
    return [pathname == f"/page-{i}" for i in range(1, 4)]
```

The Dash code itself is declarative and reactive, so creating complex applications that include many interactive elements is easier. In addition, Dash provides a simple reactive decorator that allows the binding of data analysis code to the Dash user interface. If the input element changes, the Dash decorator provides the Python code with a new input value. So a Python function can perform different actions with the new input value and it can see the results in figure 6.

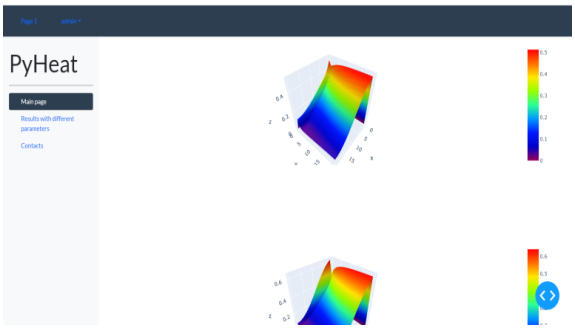

Fig. 6. View of the interactive web application

Dash application properties are stored in the interface (in the browser). This allows the use of applications written using Dash in multi-user mode: several independent sessions can be opened, in which the actions of one user will not affect the data

of other users. Dash application code is functional: it can read values from Python global properties, but cannot modify them. This functional approach can be easily justified and tested – it is just inputs and outputs without any side effects or properties.

The main part of the developed code is based on the above flowchart and uses the methods mentioned above. Solution of the heat and mass distribution equation is performed via the python Def Calculate function.

```
@ def Calculate(l,h,n,m,ti,u0i,vi,T0i)
....
....
fig =
go.Figure(data=[go.Surface(z=T,colorscale='Rainbow')])
   return fig
```

The function def Calculate (l, n, ti, u0i, vi, T0i, C0i) is used to process data, it receives a value as input, processes it, and returns the result to the program.

The function variables are:

T – temperature;
t – time;
u – the projection of the velocity vector on the Ox axis;
v – the projection of the velocity vector on the Oy axis;
l – length of oil slime;
h – width of oil slime ;
N – number of points by coordinates.

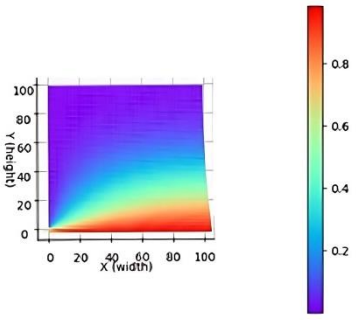

Fig. 7. The graph of oil slime temperature change at temperatures of 250°C at a velocity of 0.83 m/s

Using the statement *return* from the function, it returns the value fig. In the course of the program, calculations are made for the problem of thermal processing of oil slime under consideration. The results of the program are displayed in graphical (Fig. 7–9) forms. In the work of the program used τ = 0.1, h = l = 0.5 m, t = 30, Nx * Ny = 100 * 100.

The main way to present the results is to graph and color the entire area depending on the value of the calculation results.

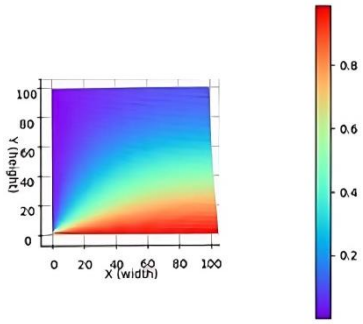

Fig. 8. The graph of oil slime temperature change at temperatures of 250°C at a velocity of 1.6 m/s

To construct graphic elements, the Dash image generation library was used. Also, the written program has the ability to save the construction results in the .png raster image format, download plot as a png, zoom, pan, orbital rotation, turntable rotation, reset the camera to default, reset the camera to last save, toggle show the closest data on hover. These ways of presenting the results help to evaluate better the course of the modeled process: its speed and area of propagation under given conditions.

The graphs are built in the plotly.graph_objects module where there are special objects called graph objects. These objects can also be used to represent shapes, and they have some advantages over dictionaries:

Graphical objects provide accurate data validation. If an invalid property name or value is specified, an exception will be thrown with a clear description of the problem;

Using the statement *return* from the function, it returns the value fig. Graphical objects have Python documentation with complete API reference. Therefore, it is easy to find out about the available properties right in the development environment.

The properties of graphical objects can be accessed either by searching by a key in the dictionary (fig) or by using a point call (fig.layout);

Graphics objects support higher-level helper functions for updating already drawn shapes (.update_layout (), .add_trace (), etc.);

The mass loss histories depicted in Figures 7–9 were plotted for conditions where a common air stream temperature and slab size were kept constant in each. Thus, the graphs show the stream velocity effect on the process of mass transfer. In the course of convective heating, the faster-moving fluid improves, obviously, the heat transfer characteristics in the system, which consequently, enhances the vaporization and diffusion drives within the heated oil slimes.

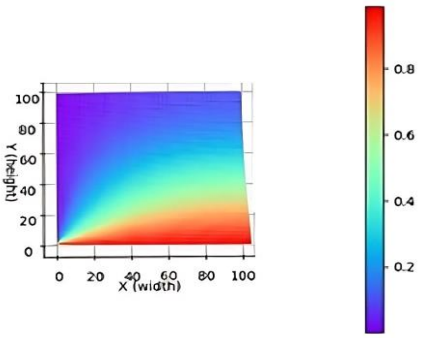

Fig. 9. The graph of oil slime temperature change at temperatures of 250°C at a velocity of 2.7 m/s

Also, the higher velocity fluids at the heated slab, the surface entrains more vapors with their higher momentum. This led to the relatively higher rates of volatilization obtained with higher stream velocities. The ultimate limits of mass loss are expected to be unaffected by the stream velocity, since these limits are controlled solely by the maximum temperatures ultimately achieved within the system. However, the slight effect noticeable in the three graphs could be, at least in part, attributed to the improved heat transfer conditions associated with the higher stream velocities, which might have resulted in slightly higher temperatures within the heated slabs due to the expected thinner boundary layers developed on the slab surface.

Covered in the present study to check this matter further, oil slimes were exposed to air streams at temperatures of 150, 250, 350, and 450°C and stream velocities 0.83, 1.6, and 2.7 m/s.

7. Conclusion

The study presented a detailed analysis of the methods and technologies for processing oil slime, based on which a thermal method was chosen for processing oil slime in order to minimize the impact of waste on the environment. A mathematical model has been built that describes the processes of heat and mass transfer during the evaporation of harmful substances from the oil slime reservoir. Mathematical calculations of the given differential equation were implemented with its reduction to a numerical solution in the form of a system of equations using solution methods.

The developed computer model includes not only the calculation of heat propagation in two-dimensional space over time, but also the construction of a graphical representation of the results obtained in the form of tables and graphs. This allows the user to look at the resulting model in several ways and makes it possible to analyze the results obtained using different approaches.

The developed application implements models and algorithms for management decisions in refining processes for the oil and gas industry and provides a network interface that can be used in the future in the industrial oil and gas sector.

This proposal for the processing of oil slime supports the application of effective technologies to solve environmental problems.

8. Acknowledgments

This research was funded by the Science Committee of the Ministry of Education and Science of the Republic of Kazakhstan (Grant #AP09259208)

References

[1] Abdrabboh M. A.: Studies in Heat and Mass Transfer in Oil Sand Beds. Ph.D. thesis. University of Calgary, Calgary, Alberta, Canada,1983.
[2] Abimbola A., Bright S.: Alternating-Direction Implicit Finite-Difference Method for Transient 2D Heat Transfer in a Metal Bar using Finite Difference Method. International Journal of Scientific & Engineering Research 6(6), 2015.
[3] Altybay A. et al.: Software Application for the Investigation of the Wave Propagation in 1d and 2d Wave Equations with Singular Coefficients. Telematique 21(1), 2022, 7468–7474.
[4] Anderson D. A. et al.: Computational Fluid Mechanics and Heat Transfer. 2nd ed., Taylor & Francis, 1977.
[5] Badrul I.: Petroleum sludge, its treatment and disposal: a review. Int. J. Chem. Sci. 13(4), 2015, 1584–1602.
[6] Balakayeva G. et al: Digitalization of enterprise with ensuring stability and reliability. Informatics, Control, Measurement in Economy and Environmental Protection 13(1), 2023, 54–57 [http://doi.org/10.35784/iapgos.3295].
[7] Balakayeva G., Darkenbayev D.: The solution to the problem of processing big data using the example of assessing the solvency of borrowers. Journal of Theoretical and Applied Information Technology 98(13), 2020, 2659–2670.
[8] Balakayeva G. T. et al.: Numerical modeling of heat and mass transfer in a reactor for continuous movement of oxidation of oil slime. Chemical Bulletin of Kazakh National University 3, 2000, 47–55.
[9] Balakayeva G.T. et all: Using NoSQL for processing unstructured BigData, News of the Republic of Kazakhstan series of Geology and Technical sciences 6(438), 2019, 12–21.
[10] Chang M. J. et al.: Improved alternating-direction implicit method for solving transient three-dimensional heat diffusion problems. Numerical Heat Transfer, Part B: Fundamentals, 1991, 69–84.
[11] Dash User Guide, 2022 [https://dash.plotly.com].
[12] Dong X. et al.: Treatment of layered oily sludge by a thermal steam process. 13th International Conference on Waste Management and Technology (ICWMT 13), Beijing, China, 2018.
[13] Egazaryants S. V. et al.: Oil slime Treatment Processes. Chemistry and Technology of Fuels and Oils 5(51), 2015, 506–515.
[14] Hanafi A. S.: Experimental and Analytical Studies of Volatilization and Burning of Oil Sand Particles. Ph.D. thesis, The University of Calgary, Calgary, Alberta, Canada, 1979.
[15] Hu G. et al.: Recent development in the treatment of oil slime from petroleum industry. Journal of Hazardous Materials 2(61), 2014, 470–490.
[16] Jadidi N. et al.: The Most Recent Researches in Oily Sludge Remediation Process. Am. Journal of Oil and Chemical Technologies 2(10), 2019, 340–348.
[17] Johnson O. A., Affam A. C.: Petroleum sludge treatment and disposal: A review. Environmental Engineering Research 24(2), 2019, 191–201 [http://doi.org/10.4491/eer.2018.134].
[18] Kalmenova G. B., Balakayeva G. T.: Developing a model of oil slime processing. Bulletin of KazNTU. Series Physics and mathematics 3, 2019, 552–555.
[19] Kunlong H. et al.: Status and prospect of oil recovery from oily sludge: A review. Arabian Journal of Chemistry 3(8), 2020, 6523–6543.
[20] Lubanovic B.: Introducing Python: Modern Computing in Simple Packages 2nd Edition. O'Reilly Media, 2019.
[21] Ma Z. et al.: Modeling and Simulation of Oil slime Pyrolysis in a Rotary Kiln with a Solid Heat Carrier: Considering the Particle Motion and Reaction Kinetics. Energy & Fuels 28(9), 2014, 6029–6037 [http://doi:10.1021/ef501263m].
[22] Norzilah A. H., Nursalasawati R.: Alternating Direction Implicit (ADI) Method for Solving Two Dimensional (2-D) Transient Heat Equation. ASM Sci. J., Special for SKSM 26(6), 2019, 28–33.
[23] Python interface to Tcl/Tk, Python Documentation, 2019 [https://docs.python.org/3/library/tkinter.html].
[24] Romano F. et al.: Learn Web Development with Python//Packt Publishing Ltd, 2018.
[25] Shan Z.: A Matched, Alternating Direction Implicit (ADI) Method for Solving the Heat Equation with Interfaces. Journal of Scientific Computing 63(1), 2015, 118–137.
[26] Yao W.: Research and application of oil slime resource utilization technology in the oil field. IOP Conference Series Earth and Environmental Science 170(3), 2018 [http://doi:10.1088/1755-1315/170/3/032026].
[27] Zhang X. et al.: Thermal Desorption Process Simulation and Effect Prediction of Oil-Based Cuttings. ACS Omega 7(25), 2022, 21675–21683 [http://doi:10.1021/acsomega.2c01597].
[28] Ziyi W. et al.: Application and development of pyrolysis technology in petroleum oily sludge treatment. Environmental Engineering Research 26(1), 2021 [http://doi.org/10.4491/eer.2019.460].

Prof. Gulnar Balakayeva
e-mail: gulnardtsa@gmail.com

Doctor of Physical and Mathematical Sciences, professor of the Department of Computer Science, Faculty of Information Technologies, Al-Farabi Kazakh National University, Almaty, Kazakhstan.
Research interests: development of big data processing systems, modeling of physical and chemical processes.

http://orcid.org/0000-0001-9440-2171

M.Sc. Gaukhar Kalmenova
e-mail: kalmenova.g.b@gmail.com

Ph.D. student of the Department of Computer Science, Faculty of Information Technologies, Al-Farabi Kazakh National University, Almaty, Kazakhstan.
Research interests: computer technologies, software engineering, mathematical and computer modeling, numerical computing methods.

http://orcid.org/0000-0002-4124-2423

Ph.D. Dauren Darkenbayev
e-mail: dauren.kadyrovich@gmail.com

Ph.D., associate professor of the Department of Computer Science, Faculty of Information Technologies, Al-Farabi Kazakh National University, Almaty, Kazakhstan.
Research interests: big data processing, mathematical and computer modeling, development of computer systems for the educational process.

http://orcid.org/0000-0002-6491-8043

Prof. Christofer Phillips
e-mail: chris.phillips@newcastle.ac.uk

Ph.D., professor. University of Newcastle upon Tyne, Newcastle, United Kingdom.
Research interests: Big Data processing, mathematical and computer modeling, numerical computing methods.

http://orcid.org/0000-0002-2470-1659

http://doi.org/10.35784/iapgos.3495 *received: 13.02.2023 | revised: 14.03.2023 | accepted: 28.04.2023 | available online: 30.06.2023*

AUTOMATED DEFINITION OF THE DISCRETE ELEMENTS INTERACTIONS IN WORKSPACE OF EQUIPMENT

Gregory S. Tymchyk[1], Volodymyr I. Skytsiouk[1], Tatiana R. Klotchko[1], Leonid K. Polishchuk[2], Anatolii V. Hrytsak[2], Saule Rakhmetullina[3], Beibut Amirgaliyev[4]

[1]National Technical University of Ukraine "Sikorsky Kyiv Polytechnic Institute", Department of Device Production, Kyiv, Ukraine, [2]Vinnytsia National Technical University, Vinnytsia, Ukraine, [3]D.Serikbayev East Kazakhstan Technical University, Ust-Kamenogorsk, Kazakhstan, [4]Astana IT University, Astana, Kazakhstan

Abstract. *Automated monitoring of the presence of such particles present near the main operational means of production or medical equipment with the determination of their trajectories is necessary to improve the efficiency of this equipment and the quality of operations. When performing measurements of the parameters of abstract objects of different origin and properties, for example, at precise parts production, problems of contamination of the surface of the object with discrete particles of another origin are often encountered. It is now known that every abstract entity forms around the area of the presence of solid particles. These solid particles, under the action of interaction forces, have the property to be ordered in space and on the surface of the object.*
This paper is a result of research and modelling of the interaction of such particles during their shredding and their structural self-organization. Severally consideration is given to the formation of dust layers under the action of coupling forces is reviewed. Models of behaviour of these layers for some typical surface forms of control object are created.

Keywords: workspace of equipment, abstract entity, presence zone, space, interaction of elements

AUTOMATYCZNE OKREŚLANIE INTERAKCJI ELEMENTÓW DYSKRETNYCH W PRZESTRZENI PRACY URZĄDZEŃ

Streszczenie. *Zautomatyzowane monitorowanie obecności takich cząstek znajdujących się w pobliżu głównych środków operacyjnych produkcji lub sprzętu medycznego wraz z określaniem ich trajektorii jest niezbędne do poprawy wydajności tego sprzętu i jakości operacji. Podczas wykonywania pomiarów parametrów obiektów abstrakcyjnych o różnym pochodzeniu i właściwościach, na przykład przy wytwarzaniu precyzyjnych części, często napotykane są problemy z zanieczyszczeniem powierzchni obiektu dyskretnymi cząstkami obcego pochodzenia.*
Obecnie wiadomo, że każdy abstrakcyjny obiekt podmiotu tworzy strefę obecności stałych cząstek wokół siebie. Te stałe cząstki pod działaniem sił oddziaływania mają właściwość do uporządkowania w przestrzeni i na powierzchni obiektu. W artykule przedstawiono wyniki badań i symulacji interakcji takich cząstek podczas ich niszczenia i ich strukturalnej samoorganizacji. Osobno rozważa się tworzenie warstw pyłu pod działaniem sił sprzęgających. Modyfikuje się zachowanie tych warstw dla pewnych typowych powierzchniowych obiektów kontrolnych.

Słowa kluczowe: obszar roboczy sprzętu, abstrakcyjny obiekt, strefa obecności, przestrzeń, interakcja elementów

Introduction

The problem of determining the presence of particles of various origins in the space of working equipment is characteristic both for application in industrial production conditions and in the conditions of operation of medical equipment. Therefore, the automated monitoring of the presence of such particles present near the main operational means of production or medical equipment with the determination of their trajectories is necessary to improve the efficiency of this equipment and the quality of operations. At the same time, it is necessary to take into account the possibility of correcting particle trajectories to obtain a certain number of particles and their location coordinates in the working space of the equipment.

Since all research concerns objects of different origins and different applications, however, the problem is the same in view of the importance of determining the nature of the presence and interactions of particles in space, we will define the main object of research as an abstract entity (AE).

On the general background of the abstract entity properties, there are a number of physicochemical effects characteristic of the formation of a zone of presence of individual elements in the space around this entity. These effects form the criteria for determining the parameters of the interaction of elements. One such criterion of signs is the gradual decrease of any parameter of the presence zone of the individual elements and the object itself without determining the critical situation of the function, that is, its derivative does not change the sign within the scope of this law [17, 18].

So, for the time being, we have a series of laws that, in one case or another, gradually decline in their capacity without a hopping derivative. That is, it is a field structure of a steady decrease in power interaction [18]. As a result, we have a case where several independent forces act on the presence zone's discrete segment. For equilibrium and rest in space, the sum of all forces acting on the AE object must be zero. However, this is far from the case, since equilibrium exists only in an imaginary form.

In a real coordinate system, this is simply impossible, because we have the possibility of an imaginary stop for an imaginary coordinate system and we have no possibility of such a stop for the real one. Thus, the situation with regard to the presence zone's segment is illusory and does not correspond to reality. Consequently, as a result, we have drift in space and time as a result of the action of a number of deterministic spatial forces. At present, it has the form of the Brownian movement with a number of diverse varieties [3]. The following parameters are very important for this type of movement: form, speed, mass and size of the Pandan zone [16–18], and the resulting vector of external force.

Thus, in the purpose to research all these parameters, it is necessary to determine with those that have not been considered in one or another researches.

1. Model of the force's interactions in presence zone of abstract object

Thus, it is first necessary to consider the varieties of cases of placement of presence zone's particles in the near-surface layer of media and circle of the AE surface. Currently, such cases are shown in Fig. 1.

Thus, in the study of behaviour of the particles in presence zone of object, we must take into account the following variants of power interaction with environment. The simplest case and the most generalizing are discussed (Fig. 1a). In this variant, we have a generalized situation, which is partly in the near-surface layer of environment relative to the AE surface.

So, we have a classical three-element diagram.

The first component, this is the main force, which attracts the particles to the AE surface. The second component is counterproductive to the previous, that is, it is repulsive. The third component is a tangential force that moves a part along the AE surface.

Consequently, the total vector amount of forces has the form

$$\mathbf{F}_{\Sigma} = \mathbf{F}_{\mathbf{O}} + \mathbf{F}_{\mathbf{B}} + \mathbf{F}_{\tau} \quad (1)$$

where $\mathbf{F}_{\mathbf{O}}$ – component of the precipitate; $\mathbf{F}_{\mathbf{B}}$ – repulsive component; $\mathbf{F}_{\tau}$ – tangential force.

Analyzing the forces that form the equation (1), we have the opportunity to assert the following.

The forces that create values $\mathbf{F}_{\mathbf{O}}$, $\mathbf{F}_{\mathbf{B}}$, $\mathbf{F}_{\tau}$, have the following components:

$\mathbf{F}_{\text{grav.}}$ – gravitational force acting between any AE that has the final shape and mass,

$\mathbf{F}_{\mathbf{e}}$ – electrostatic gravity between objects of AE;

$\mathbf{F}_{\mathbf{m}}$ – component of the magnetic force of attraction in the presence of magnetic properties between objects,

$\mathbf{F}_{\mathbf{ADF}}$ – aero and dynamic forces, which create not only active forces in the direction to the surface, but also different projections from planar parallel to near-surface action.

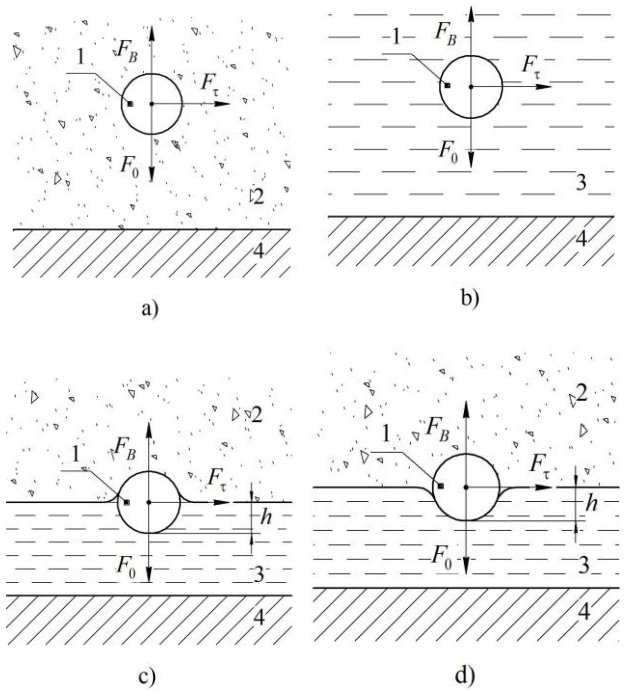

Fig. 1. Cases of location and interaction of presence zone particles on AE surface: a) a general diagram of the forces acting on the presence zone segment in the uncertain environment; b) a diagram of the forces acting on the presence zone portion in a liquid near the surface of the AE; c) a diagram of the forces acting on the presence zone lattice that is wetted when it is located on the surface of the liquid in near-surface layer of AE; d) a diagram of the forces acting on discrete particle that is not damped on the surface of near-surface layer of the liquid AE; 1 – discrete particle, 2 – environment, 3 – liquid, 4 – AE surface

The next component is repulsive $\mathbf{F}_{\mathbf{B}}$, which has a number of components of the following type; $\mathbf{F}_{\mathbf{A}}$ – archimedean force, which is essential in the case when the particle is in the surface environment; $\mathbf{F}_{\mathbf{e}}$ – electrostatic force in the case where the charge particles and the AE surface are opposite; $\mathbf{F}_{\mathbf{CF}}$ – centrifugal force, when the objects are in a state of rotation.

The next component is a tangential force $\mathbf{F}_{\tau}$, that is parallel to the surface and has a number of components of the following type: $\mathbf{F}_{\mathbf{ST}}$ – force of the surface tension, which does not always have a constant value; $\mathbf{F}_{\mathbf{ADF}}$ – aero and hydrodynamic force, which is a consequence of movement of the environment.

Consequently, if we considered to the classical cases of the location of a particle in the near-surface layer of the environment around the AE (Fig. 1a). At the same time, we obtain the situation with respect to the external environment, its density and motion, which causes the displacement of the particles in space. As a result, the spatial vector diagram has the following components.

Firstly, this is what causes the sediment processes in the stratum relative to the surface of the AE.

$$\mathbf{F_0} = \mathbf{F}_{\text{grav.}} + \mathbf{F_e} + \mathbf{F_m} + \mathbf{F_{ADF}} \quad (2)$$

Consequently, the force $\mathbf{F}_{\mathbf{O}}$ leading to the precipitation is always directed towards the AE surface by normal and is main holding part [3].

The first force **($\mathbf{F}_{\text{grav.}}$),** that leads to this movement is the gravitational, directed towards the straight line, carried through the centers of the weight of the object and the lobes. This force is unipolar, that is, in any case, it does not change its polarity

The second force $(\mathbf{F_e})$, that is part of the sediment force is electrostatic. The peculiarity of this force is that it may have different polarity. In this case, with multipolar charges of particles and surfaces, the gravitational force is much larger than gravitational and is higher.

The direction of action is similar to gravitational and is directed to normal to the surface.

The next force acting in the direction of the sediment is magnetic force $(\mathbf{F_м})$. The peculiarity of this force is that it operates in two cases. First, if the lattice and the AE have magnetic properties, they are attracted according to the laws of the magnetic field.

In the second case, if the lattice has electrostatic properties, and AE is magnetic.

In this case, in any third-party motion, the interaction between the particle and the field of the AE arises according to Maxwell's law [1].

The resulting motion is a combination, which gives the corresponding components force $\mathbf{F}_{\mathbf{O}}$ and $\mathbf{F}_{\tau}$.

Another forces worth paying attention to is aero and hydrodynamic, which has the properties of both repulsion and attraction, depending on the direction of the environment flow.

The force that opposes the sediment is the force $\mathbf{F}_{\mathbf{B}}$ of repulsion. This force has the following components. Firstly, it is the Archimedes force, since it acts on any environment density

$$\mathbf{F_B} = \mathbf{F_A} + \mathbf{F_e} + \mathbf{F_{CF}} + \mathbf{F_{ADF}} \quad (3)$$

This force acts in the direction of the minimum pressure of environment.

As already mentioned above, one of the components of the repulsion force can be electrostatic in the case, where the polarity of the particle and the AE is such, that they are repulsed from each other. Another one may be the centrifugal force that arises from the joint rotation of the particle and AE.

The last component of this force can be aero and hydrodynamic ($\mathbf{F_{ADF}}$), which occurs during the movement of the environment relative to the AE surface.

The third force acting on a particle is tangential $(\mathbf{F}_{\tau})$ force, which has an orientation vector, which is perpendicular to the two forces $\mathbf{F}_{\mathbf{O}}$, $\mathbf{F}_{\mathbf{B}}$. This force has the following components that act on the particle of presence zone. The first force is force $\mathbf{F}_{\mathbf{ST}}$ of the surface tension

$$\mathbf{F}_{\tau} = \mathbf{F_{ST}} + \mathbf{F_{ADF}} \quad (4)$$

This force is formed on the interface between two media with different physical properties.

The second component is the aero and hydrodynamic forces, or rather its component, which directed along the surface of environments distribution.

By imaginary presence zone of solid elements modelling, we took a discrete element in the form of a sphere of the correct form with the required diameter for the solution of the problem [1, 11]. However, in the transition to a real situation, this is far from the case. There are currently several classifications. All of them have specific directions and components. According to the

authors, the main classification should be considered natural because it does not have artificial signs.

The second artificial classification has a specific technical application that meets our technological requirements.

So, first let's look at the natural classification of discrete solid presence zone, since it is the oldest and most used.

It currently consists of the following groups:

- wreck breeds, which are fragments of different rocks and minerals;
- clay rocks, which are different types of fine dispersed fractions of amorphous nature;
- chemical rocks, which are residues, having fallen into the precipitate of chemical compounds (gypsum, limestone, etc.) [11, 12];
- organic breeds, which are residues that have fallen into the sediment of dead plants and animals (shellfish, coal, etc.);
- mixed breeds, which represent a mix of all previous components in different proportions.

All these breeds represent the Earth's presence zone [6, 10] and meet us in everyday life at every step. At present, we are interested in wreck breeds, as their destruction leads to the appearance of most others.

The natural classification of the debris of rocks is immediately divided into two main groups: loose (loose) and compact (compacted) [11–13]. Both of these and other groups in turn consist of two subgroups, namely corrugated and rolled. In addition, some of the rock sedimentary rocks refer to both, and to the second subgroup.

Since we are more interested in wrapped up as a product of natural "processing", then we will consider them more reliably. Coated sedimentary rocks are in the shape of the closest to the ball, because in this case the Pandan zone of the debris is exposed to intense pressure. Such a load leads to the destruction of acute protrusions [8]. The general diagram of the action of forces on the fragment leads to the fact that there is a resultant force that rotates a fracture when interacting with others. In the end it leads to a spherical shape.

So, according to this classification, for loose rocks we have the following:

- boulders – rolled up fragments larger than 100 mm;
- pebbles – rolled fragments with a diameter of 10 to 100 mm;
- gravel – rolled fragments with a diameter of 1 to 10 mm;
- sand – rolled and not rolled fragments in diameter from 0.1 to 1 mm;
- aleurite – rolled and not rolled fragments in diameter from 0.01 to 0.1 mm;
- dust – rolled and not rolled fragments with a diameter less than 0.01 mm.

The last three varieties refer to both rolled up and not rolled up. All these varieties, when deposited in a precipitate, form a cemented mass called conglomerate, gravelite, sandstone, and aleurolite. All these factions, consisting in different proportions form the surface accumulation of the globe, creating a number of mineral deposits that are used in the science and technology of industrial production [4]. For engineering, it is very important to mix solid particles and liquids called slurries. Suspensions are conventionally divided into the following kinds:

- coarse suspensions are liquid substances that contain suspended particles with a diameter greater than 100 μm;
- thin suspensions, these are liquid substances filled with particles of solid phase in the size from 0.5 μm to 100 μm. It is at this level of size that the beginning of the Brownian motion begins to occur;
- cloudy are suspensions, where the particle size from 0.5 μm to 0.1 μm has an intense Brownian motion when the particles do not fall precipitated;
- colloidal solutions with particles of a dispersed phase of 0.1 μm or loess to the size of molecules.

Consequently, dust particles are either on the surface of the AE or move in the near-surface area. In addition, the movement is of such a nature that particles of dust are trying to settle on the surface of the object. With all the chaos of this movement, he has some focus on the principle: the smaller object moves towards the greater. Usually this process takes place under the action of gravity, which is always present between bodies that have a finite mass [6]. The collision of particles and deterministic motion is very similar to Brownian motion.

At present, this kind of movement deals a molecular physics, so it is possible with certain restrictions to apply its theoretical foundations. In this case, we have the opportunity to consider the discrete presence zone up to the level of the molecule, because the molecule is also an element of this zone, under such a thesis the application of molecular-kinetic physics is quite justified. The best example here may be sublimation. Consequently, we need to investigate the speed of motion, the trajectory and the degree of its determinism [7, 14, 15].

Let's start with the elementary motion, which occurs in the solid state zone, namely, by the force of gravity. Clearly, the velocity obtained by the lobe during the fall t will be determined as

$$V = g \cdot t \tag{5}$$

where g is the acceleration of gravity.

This equation is valid for a vacuum, but in the presence of liquid or air in the surface space, it does not justify itself. Consequently, when the objects fall in small sizes, less than 1 mm, at a certain speed, they have such resistance to material, that begins to move at a constant rate. The velocity of such a uniform fall is called the rate of precipitation [9]. in the general case, this speed can be determined from the general law of motion resistance of the mass in the environment. The constant rate of precipitation will be reached when gravity becomes equal to strength of the material resistance of environment, which is determined by Newton's law, that is

$$F_0 = \eta \cdot S \cdot d_c \frac{V_0^2}{2g} \tag{6}$$

where η – coefficient of material resistance, S – projection of cross-section of Pandan zone particle, d_c – specific gravity of material.

If we accept the conditions of simulation, that is, the particle has the form of a sphere, then $S = \pi D^2/4$, and equation (6) takes the form

$$F_0 = \eta \frac{\pi D^2}{4} d_c \frac{V_0^2}{2g} \tag{7}$$

In this case, the weight of the spherical particles (except Archimedes forces) will be determined as

$$P = \frac{\pi D^3}{6}\left(d_0 - d_c\right) \tag{8}$$

where d_0 – specific gravity of the particle.

When a constant velocity is reached, that is, the velocity of precipitation, equality is performed

$$F_0 = P \tag{9}$$

and as a result after substitution

$$\eta \frac{\pi D^2}{4} \cdot d_c \frac{V_0^2}{2g} = \frac{\pi D^3}{6}\left(d_0 - d_c\right) \tag{10}$$

we obtain

$$V_0 = \sqrt{\frac{4gD\left(d_0 - d_c\right)}{3\eta d_c}} \tag{11}$$

The material resistance coefficient is a function of the Reynolds number and is determined experimentally, i.e. it depends on the velocity of movement of their size, density and viscosity of the material of object. That is, the coefficient of resistance has a nonlinear dependence on the Reynolds number. If necessary,

this dependence can be divided into three relatively linear parts, especially if you take the form of a particle as a ball. For value of the Reynolds number we get

$$\eta = \frac{24}{R_e} \tag{12}$$

which is called the Stokes' law [3, 19].

When we measure the Reynolds number as $0.2 < R_e < 500$, we obtain an intermediate law in the form

$$\eta = \frac{18.5}{R_e^{0.6}} \tag{13}$$

For a numerical value within $500 < R_e < 150000$ the value of the coefficient there is a constant, that is $\eta = 0.44$, it is the law of Newton. Consequently, if we use these laws, we obtain from equation (11)

$$V_0 = \frac{D^2\left(d_0 - d_c\right)}{18\mu} \tag{14}$$

which a consequence of the Stokes' law is obtained.

If neglected by forces of inertia, orienting only on frictional forces, then the strength of the environment can be defined as

$$F_0 = 3\pi D\mu V_0 \tag{15}$$

Consequently, as can be seen from equation (15), the material resistance of the environment during the movement of small objects is proportional to the first degree of fall velocity.

The use of equation (15) applies only to the upper limit $R_e \le 0.2$. At the same time, the maximum particle size has a limitation. To do this, in equation (14), instead of speed V_0, the substitution of its value according to the Reynolds criterion is $V_0 = R_e\mu g / Dd_c$, i.e. at $R_e = 0.2$ we get it

$$D_{\max} = \sqrt[3]{\frac{3.6\mu^2 g}{d_c\left(d_0 - d_c\right)}} \approx 3.3\cdot\sqrt[3]{\frac{\mu^2}{d_c\left(d_0 - d_c\right)}} \tag{16}$$

For the lower limit of the application of the Stokes' law, the criterion is the deposition conditions, when the size of the particles reaches values equal to the free run of the molecules of the dispersion material.

As a result, the material resistance of the environment in this case will be determined as follows:

$$P_0 = \frac{3\pi D\mu V_0}{1 + A\frac{l_0}{D}} \tag{17}$$

where $l_0 = 10^{-7} m$ – the average mileage of the gas molecule under certain conditions; A is a constant.

Of course, the value is quite conventional and rather strongly dependent on the environment.

The rate of falling particles in the sediment for this case will be determined as

$$V_0 = \frac{D^2\left(d_0 - d_c\right)}{18\mu}\cdot\left(1 + A\cdot\frac{l_0}{D}\right) \tag{18}$$

Thus, for $R_e < 0.2$ the velocity of the particles of the discrete solid presence zone the spherical shape is proportional to the square of their diameter, the difference between the specific gravity of the particles and the environment, and inversely proportional to the viscosity of the environment.

For the values $500 < R_e < 150000$ of the Reynolds number the resistance of the environment is $\eta = 0.44$. If we substitute this value in equation (11), then we obtain the following dependence for the particle motion rate

$$V_0 = 5.48\sqrt{\frac{gD\left(d_0 - d_c\right)}{d_c}} \tag{19}$$

For an intermediate law $\mu = \frac{18.5}{R_e^{0.6}}$, the drop speed will be determined as

$$V_0 = 0.268\sqrt{\frac{gD\left(d_0 - d_c\right)}{d_c}} \tag{20}$$

Thus, having the speed of motion in different cases, we can consider the accumulation of discrete solid presence zone on the AE surface. The basis for solving the problem using equation

$$Q = S\cdot V, \tag{21}$$

where S is the cross-sectional area, V is the velocity of particles moving through this area.

Consequently, if we imagine that it stays at time t and distance, it should have velocity

$$V_\tau = \frac{a}{t} \tag{22}$$

On other, falling of the particles from height h above the AE surface with speed V_0 gives us the same time, that is

$$t = \frac{h}{V_0}. \tag{23}$$

Consequently, substituting (22) and (23) in equation (21), we obtain

$$Q = a\cdot b\cdot\frac{h}{t} = a\cdot b\cdot h\cdot\frac{V_0}{h} = a\cdot b\cdot V_0 \tag{24}$$

where b – length of the incident particles front.

Since the product $a\cdot b$ is area of the AE surface, it is obvious that the amount of deposited mass will be determined as

$$Q = \frac{S_{AC}}{d_u}\cdot V_0\cdot t \tag{25}$$

That is, this slow-moving part of the discrete presence zone is directly dependent on speed and time. Since the velocity chart is chosen in the plane of vectors, we can assume that, according to the aforementioned principle, the entire front of the particles is in siege.

Thus, if our particle is in the environment whose density is different from zero, then the hydrostatic pressure acts on it. To solve problems related to the location of an object in an environment, use the basic equation of hydrostatics [14]. This equation relates the force acting within a unit volume of liquid or gas and measured pressure in a state of balance

$$F_{FA} = grad\ P. \tag{26}$$

For projections on the axis of Cartesian coordinates [10]

$$F_{FA}(x) = \partial P / \partial x,\ F_{FA}(y) = \partial P / \partial y,\ F_{FA}(z) = \partial P / \partial z$$

In this case, the gradient of the scalar P is determined by the Hamiltonian as a potential field.

In the particular case of gravity

$$F_{FA} = d_c g. \tag{27}$$

where d_c – density of the environment, g – acceleration of free fall.

In the general case, equation (26) is a partial case of the Euler equations, which gives a description of the motion of an ideal fluid (environment) in the static case [11], and as a consequence, the simplest law and elementary force that we have a description through of Archimedes law. In general, the law is written as

$$F_A = Q\cdot d_C\cdot g \tag{28}$$

where Q is the volume of the displaced environment.

For a spherical particle with a diameter D this force will be

$$F_0 = \frac{1}{3}\pi h\left(\frac{3}{2}D - h\right) \tag{29}$$

where h is the immersion depth (Fig. 1c).

The pushing force is always directed to the top and passes through the centre of object weight. In addition, there is still a buoyancy centre, as the centre of mass of displaced environment. As a result, we have two centres on which different forces operate. As a result, the stability of the balance of the mass of the AE depends from the distance between these centres. This situation creates the following three cases.

In the first case, the mass of the particle is at balance, if its weight is equal to weight of the environment pushed out by it, and both centres are on the same vertical.

In the second case, if the particle is completely immersed in the environment, then the balance will be, if the centre of mass is below the centre of buoyancy and does not become, if the opposite.

In the third case, for a partial immersion, then the balance will be, if the center of mass is below the metacentre and not constant in the opposite.

Another force that can be directed vertically is Magnus force [2, 8]. The essence of this effect lies in the fact that any object is located, which is in the directed flow of environment begins to rotate. The consequence of such a rotation is the emergence of a dynamic force perpendicular to the direction of motion of the environment. The basis of the effect is that the velocity of the environment on both sides of the ball is different. As a result, there is a dynamic force. Consequently, if our particle is in the incoming of environment's stream. So, in order to simulate the rotation of a particle, we introduce a circulation of velocity around it [1, 9]. Using Bernoulli's law, we can prove that the full force acting on a part in this case will be:

$$F_m = -d_C Circ. \times u \tag{30}$$

where *Circ.* – circulation of the velocity vector around particles, *u* – the flow velocity in infinity.

From (30) it is evident that the total force is perpendicular to the flow, and the direction, depending on the circulation and the flow velocity, has a lifting or lowering character.

At this time, it is possible to determine the magnitude of this force for a globular particle as:

$$F_M = \frac{1}{2} d_C V \cdot S_0 \cdot G \tag{31}$$

where *V* is the velocity of the particles relative to the environment; *G* is the coefficient of lift, which is determined experimentally by Reynolds number and the rotational factor, S_0 is the cross section of sphere.

Since the basis of our model is a sphere, we eventually get it

$$F_m = \frac{1}{8} d_c VDG \tag{32}$$

2. Modelling

At present, the forces discussed above relate to the behavior of the particle without taking into account the interaction with the surface layer of the liquid. However, the surface is not just a coordinates, it is a layer that has certain properties. By its compatibility, it is a layer of molecules combined by intermolecular forces on one side only because it is on the verge of two media. The frequency (sphere) that falls on such a surface behaves in two ways (Fig. 1b, c) since it becomes dependent on the power of intermolecular forces. In the first case, it adheres to the surface (wetting) in the second slip (no wetting). Consequently, the curvature of the surface occurs under the weight of the particles and as a result of additional pressure on the liquid. This additional pressure is dependent on the surface tension (β) and the curvature of the surface.

A superficial tension is called the work performed for isothermal formation of 1 m^2 surface at the boundary with another phase:

$$\sigma = \frac{A}{S}(\overline{E_S - E_V})\frac{N}{S} = (\overline{E_S - E_V})n_1 \tag{33}$$

where $n_1 = \frac{N}{S}$ – number of molecules is 10^{-4} m^2 of the surface layer, $\overline{E_S - E_V}$ is the mean free energy difference and the surface E_S and in the volume E_V, and N is number of molecules in the surface layer.

According to Laplace's law, the surface has the environment curvature

$$H = \frac{1}{2}\left(\frac{1}{R_1} + \frac{1}{R_2}\right) \tag{34}$$

are determined by the main radii of curvature R_1 and R_2.

As a result, the pressure under the broken surface

$$P_K = P_o + \sigma\left(\frac{1}{R_1} + \frac{1}{R_2}\right) \tag{35}$$

where P_o – pressure on the flat surface of the liquid.

At that

$$P_{RK} = \sigma\left(\frac{1}{R_1} + \frac{1}{R_2}\right) = 2\sigma H \tag{36}$$

$P_{RK} > 0$, if the meniscus is convex, $P_{RK} < 0$, if the meniscus is concave.

For a spherical surface

$$P_{RK} = \frac{4\sigma}{D} \tag{37}$$

Thus, we considered a series of forces that are related to the mechanical properties of the environment, is, the viscosity, the Reynolds number, the surface tension, and so on. But in addition to mechanical properties, all physical objects have a number of electrical properties. At the moment, it is an electrostatic and magnetic field that causes a series of phenomena and processes that create active forces. Of course, in the first place is an electric field that is inherent in all AE without exception in one degree or another. In terms of electricity, there is a charge of an object, which for a discrete solid presence zone's segment as q_0 can be determined by the elementary charge of an electron which is defined as a measure of charge, that is,

$$q_0 = ne \tag{38}$$

where *n* – number of electrons, $e = 1.6021892 \times 10^{-19}$ C – charge of electron.

In relation to our situation we are interested in forces acting on the charge near a charged plane. Consequently, the field strength which creates the plane of AE in the surrounding space is defined as

$$E = \frac{1}{2\varepsilon_c \varepsilon_o}\sigma \tag{39}$$

where σ – surface charge density, ε_c – dielectric permeability of environment, ε_o – dielectric constant.

Since the force acting on the charge q_0 is defined as

$$F_0 = q_0 E \tag{40}$$

So, as a result we get

$$F_0 = \frac{q_0 \sigma}{2\varepsilon_c \varepsilon_o} \tag{41}$$

The force of interaction of two particles with a charge q_0 at a distance *r* is determined by the Coulomb's law [1] as

$$F = \frac{1}{4\pi\varepsilon_c \varepsilon_0}\frac{q_0^2}{r^2} \tag{42}$$

Under the action of these forces, a piece in space will move in dependence on the direction of the vectors of the velocity and intensity of electric field.

If we have a homogeneous electric field with parameters $E_x = E,\ E_y = E_z = 0,\ B = 0,\ \ V_x = V_0,\ V_y = V_z = 0$, then the equation of motion can be described as follows

$$m_0 \frac{d^2x}{dt^2} = -q_0 E \tag{43}$$

Solving this equation we obtain a fluid coordinate

$$x(t) = V_0 t - \frac{q_0}{2m_0} Et\ ,\ y(t) = z(t) = 0 \tag{44}$$

at speed

$$V_x(t) = V_0 - \frac{q_0}{m_0} Et\ ,\ V_y(t) = V_z(t) = 0 \tag{45}$$

From equations (40), (41) we obtain the conclusion that the particle will move along the direction of the vector of electric field intensity. In addition, the movement will be either equally accelerated or deceleration, depending on how the vectors one-sidedly or towards one another are directed.

In the case, when the particle moves across the electric field (E_y), we obtain the following result for each coordinate

$$m_0 \frac{d^2x}{dt^2} = 0\ ;\ m_0 \frac{d^2y}{dt^2} = -q_0 E\ ;\ m_0 \frac{d^2z}{dt^2} = 0 \tag{46}$$

Solving all equations (46) we obtain the following dependences for determining the fluctuation of the particle coordinate

$$x(t) = V_0 t; y(t) = -\frac{q_0}{2m_0} Et^2; z(t) = 0 \tag{47}$$

The velocity of motion along the coordinate axes will be

$$V_x(t) = V_0;\ V_y(t) = -\frac{q_0}{m_0} Et\ ;\ V_z(t) = 0 \tag{48}$$

In this case, the trajectory of a particle's motion has a parabolic character

$$y(t) = \frac{q_0}{2m_0} E \frac{x^2}{V_0^2} \tag{49}$$

Thus, the motion of a particle in a transverse electric field is similar to the motion of an object in the conservative field of gravity.

In contrast to the electric field and the generating electric charge, for example, in equation (34), the magnetic field does not have magnetic charges as such. Thus, the theory of magnetism, which is based on the notions of magnetic charges that uses purely external similarity of the interaction of magnets with the interaction of imaginary magnetic charges, is called the formal theory of magnetism.

At present, the formal theory of magnetism is seen in the case when we imagine a long, thin magnet on the extremities concentrated magnetic charges and we have the dependence of the operating force between two magnetic charges in the form of the Coulomb law

$$F = \frac{\mu\mu_0}{4\pi} \frac{q_{m1} q_{m2}}{r^3} r \tag{50}$$

where q_{m1}, q_{m2} – magnitude of charges or quantity of magnetism, $\mu_0 = 4\pi 10^{-7}$ H/m – magnetic force, μ – relative permeability of the environment.

That is, in the case if the discrete presence zone's partical has magnetic properties, then with some assumptions it is possible to use the equation (50). We will now consider how this is considered when using the formalized model. To consider, we take the thesis, that the inner structure of the sphere is the one that creates a homogeneous constant magnetization M_0, which is equal to M_0 in magnitude and directed along the axis Z (by the single vector $\mathbf{e}_3$). Externally, spheres from where at $r > a$ vector can be written, if we take with the negative sign the gradient of scalar magnetic potential satisfying the Laplace equation:

$$B_e = -qrad\Phi_m, \nabla^2\Phi_m = 0 \tag{51}$$

Solving these equations leads to the conclusion that

$$B_0 = B_c e_3\ ,\ H_0 = (B_c - 4\pi M_0)e_3 \tag{52}$$

Hence, as a result, we obtain the result that the field outside the sphere coincides with the field of the dipole and the dipole moment

$$T_0 = \frac{\pi}{6} D^3 M_0 \tag{53}$$

In this case, the internal fields receive the following dependencies

$$B_0 = \frac{8\pi}{3} M_0\ ,\ H_0 = -\frac{4\pi}{3} M_0 \tag{54}$$

In addition, it should be noted that the induction is parallel to the magnetization, while the field, albeit in parallel, but opposite, is directed.

If our particle falls into an external magnetic field, then, based on the linearity of the field equations, we can add external magnetic induction to equations (54). Consequently, as a consequence, the total magnetic induction in the middle of the sphere is defined as

$$B_0 = B_c + \frac{8\pi}{3} M_0\ ,\ H_0 = B_c - \frac{4\pi}{3} M_0 \tag{55}$$

If we imagine that our ball is not a permanent magnet and there is a magnetic or paramagnetic with magnetic permeability of μ, then the magnetization of M occurs in the sphere under the action of the external field, we find the value of M, given μ

$$B_0 = \mu_0 H_0$$

when

$$B_c + \frac{8\pi}{3} M_0 = \mu_0 (B_c - \frac{4\pi}{3} M_0) \tag{56}$$

And as a result we get

$$M_0 = \frac{3}{4\pi} \frac{\mu_0 - 1}{\mu_0 + 2} B_c \tag{57}$$

From equation (57) it can be seen that in the absence of an external field, the magnetization vector disappears. Therefore, this consideration is suitable only for macromolecules and paramagnets, and in any case for ferromagnets. The problem is that even in the absence of an external field, the magnetization of a ferromagnet does not disappear. Nevertheless, if we exclude M from equation (54), we get the relation between H and B

$$B_0 + 2H_0 = 3B_c \tag{58}$$

So, for any external field we have the opportunity to find the corresponding value of the internal field. From the consideration of magnetic properties it can be seen that these properties are either intrinsic to the particles or formed by the external field. In any case, we see that the particle reacts to an external magnetic field. As a result, when any lattice enters the magnetic field, the moment of forces depends on the angle (α) of the difference between the magnetization $\bar{M}_0$ and induction vectors $\bar{B}_c$. The magnitude of the moment is defined as

$$T_0 = \frac{1}{2} \frac{\pi\mu_0 D^3 M_0 B_c}{2\mu_c + \mu_0} \sin\alpha \tag{59}$$

Consequently, the particle gets to the magnetic field with a torque which forces it to rotate. As a consequence of such a rotation, the lens creates around itself the motion of the environment, which leads to the Magnus effect. Thus, if the particle does not even move before it begins to rotate around its magnetic axis, especially if the magnetic field changes its direction. In addition, the magnetized particle reacts with an external magnetic field, there are other cases of interaction. At present, a moving charge (particle) has the property to create around itself a magnetic field which is its presence zone. Thus, we have the case of the interaction of two presence zones as a consequence of motion, that is, it is one example of the power interaction of objects in the presence zone.

According to theoretical electrodynamics, in the general case, the particle with charge q_0, which moves at a velocity in a magnetic field with induction, acts on the force perpendicular to the vectors and is determined by

$$F_m = q_0(V \times B) \tag{60}$$

The module is defined as

$$F_m = q_0 VB \sin\alpha \tag{61}$$

As a consequence, the motion of a charged particle in a magnetic field can be written as an equation of kinetic motion as

$$m_0 \frac{dV}{dt} = q_0(V \times B) \tag{62}$$

So, if the induction *B* is independent of time i.e. $B = B(x, y, z)$, then

$$\frac{m_0 V_0^2}{2} = const \tag{63}$$

That is, the kinetic energy of a particle in a magnetic field does not change. Under this condition, the equation (58) splits into two equivalent ones

$$m_0 \frac{dV_\perp}{dt} = q_0(V_\perp \times B),\ m_0 \frac{dV_{II}}{dt} = q_0(V_{II} \times B) \tag{64}$$

where $V = V_{II} + V_\perp$, V_{II}, $V_\perp$ – components of velocity *V*, parallel and perpendicular to field *B*, $(V_{II} \times B) = 0$.

The acceleration of the particle in this case is steady and absolute in magnitude and is directed perpendicularly to the component of the velocity *V*. Therefore, the particle moves in a circle with velocity. Circle radius with this

$$R = \frac{m_0 V_\perp}{q_0 B} \tag{65}$$

R value is Larmor's radius. The angular frequency ω of rotation is defined as

$$\omega = \frac{2\pi}{T} = \frac{V_\perp}{R} = \frac{q_0 B}{m_0} \tag{66}$$

Consequently, a particle, which enters the magnetic field's moves behind a screw-trajectory with a step $V_{II}T$ radius *R* with a constant angular velocity ώ and a velocity *V*. As a consequence of *V II B*, this particle $V_{II} = V$ moves along the field.

If that $V \perp B$ and $V_\perp = V$, $V_{II} = 0$ the particle moves perpendicular to the field, rotating around the power line at a velocity $V_\perp$ in the circle of radius *R*.

Thus, the magnetic field, along with other external forces, affects the movement of the particles. At present, there are three types of such movement: motion under the influence of extraneous force, movement in an electric field, motion under the action of gravitational field. Consequently, the general equation of motion of a segment in an electromagnetic field can be described in accordance with the second Newton's law by equation

$$P = \frac{d}{dt}(m_0 V) = -q_0 E \ \ -q_0(V \times B) \tag{67}$$

where *P* is a pulse of a charge with q_0.

That is, we have the motion of a q_0 charge in electromagnetic fields. In classical physics, such a movement is called drift with an appropriate magnitude which is defined as

$$V_D = \frac{1}{q_0} \frac{F \times B}{B^2} \tag{68}$$

where *F* is outside force perpendicular to field *B* behind *Z* axis.

If a particle moves under the action of force not perpendicular to the magnetic field, then it performs a complex motion which can be decomposed into three constituents. The first component is the equally accelerated motion along the magnetic force lines under the action of the F_{II} component. The second component is the uniform movement of the larval circle under the action of force

$$F = q_0(V_0 \times B) \tag{69}$$

where $V_0 = V + V_D$ is the velocity of a particle in a coordinate system, which moves with the drift speed

$$V_D = \frac{1}{q_0} \frac{(F_\perp \times B)}{B^2} \tag{70}$$

The third component is the speed of V_D. Electric drift occurs when the external force of excitation is the strength of electric field (40).

In this case, the particle will rotate around the direction of the magnetic field *B* at a rate

$$V_D = \frac{1}{B^2}(E \times B) \tag{71}$$

The velocity V_D is independent of the sign, charge q_0 and of the particle mass. As a result, layers with different charges and masses can't be present in the presence zone

$$V_D = \frac{m_0}{q_0} \frac{(g \times B)}{B^2} \tag{72}$$

If $B \perp g$, that is a scalar

$$V_D = \frac{g m_0}{q_0 B} = \frac{g}{\omega} \tag{73}$$

where ω is the cyclotron frequency. For example, for a proton in the magnetic Earth's field ($B = 7.96 \cdot 10^{-4}$ *T*)

$$V_D \approx 0.98 \cdot 10^{-2} \text{ m/s}$$

In conclusion, considering the secondary presence zone, it is necessary to consider the interaction of particles between themselves. Consequently, a charged electric energy in the course of its motion reacts not only with the electric and magnetic fields, which form the field's presence zone of AE, and between themselves.

The principles of this interaction consist in the fact, that any electric charge during its motion creates around itself in accordance with Maxwell's magnetic field. Consequently, if a charge with q_0 moves uniformly in a space with velocity V_0, then in any part of the space of charges in vector r forms a magnetic field with induction

$$B = \frac{\mu_0 q_0}{r^3}(V_0 \times r)$$

So, if we have two particles with charges q_{01} and q_{02}, which move with speeds V_1 and V_2, then they will interact with each other with forces

$$F_{12} = \frac{\mu_0 q_{01} q_{02}}{r_{12}^3}(V_2 \times (V_1 \times r_{12}))$$

$$F_{21} = \frac{\mu_0 q_{01} q_{02}}{r_{21}^3}(V_1 \times (V_2 \times r_{21}))$$

F_{12} is the force acting on the charge q_{02} from the side of the field B_{01} generated by the charge q_{01} at the point of charge q_{02}; r_{12} is the radius from the charge q_{01} to the charge q_{02}; F_{21} is the force acting on the charge q_{01} from the field B_{02} generated by the charge q_{02}.

In the particular case, if the vectors V_1 and V_2 are parallel with each other and are equally directed, but perpendicular to the vector r_{12}, then

$$F_{12} = F_{21} = \frac{\mu_0 q_{01} q_{02}}{r_{12}^2} V_1 V_2 \tag{74}$$

In this case, the direction of force is dependent on the signs of charges q_{01} and q_{02}, that is, the attraction for the same charge charges of particles and repulsion for the same name.

Consequently, we considered a whole range of forces of different physical origin, which are constituents of the basic equations (5), (6), (7), (8). These forces are the basis of the spatial motion of the particle and are the basis for determining its trajectory.

3. Automated measurement of the features of interaction of particles in the working space of equipment

Measurements are carried out by a measuring integrated sensor of a continuous structure, containing an integrated electromagnetic sensor and an optical sensor for determining the movement of particles. Adjusting the position of the contact on the axis between the flanges of upper and lower parts provides a gap, the change of which allows you to change the position of measuring sensor relative to the axis.

The equipment for determining the interactions of particles provides an opportunity on the basis of digital control to carry out input and functional control of processes in the studied environment with help of measuring tools in a system with common functional characteristics (Fig. 2).

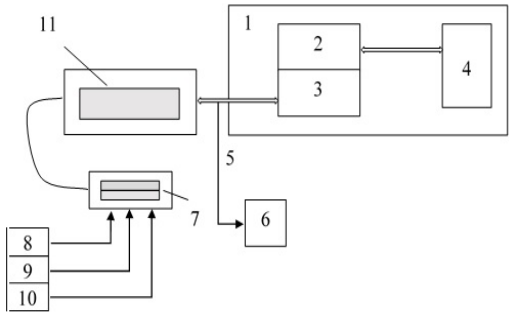

Fig. 2. Functional scheme of the system of correction of the probing trajectory: 1 – digital control unit; 2 – digital control drive; 3 – automatic machine; 4 – block of processing and intermittent sounding; 5 – communication system; 6 – storage of output data; 7 – control panel; 8 – processing and probing programming unit; 9 – block of statistical quality research; 10 – trajectory correction programming module, 11 – visualization unit

The automation system of intermittent sounding is used to control complex trajectories of particle movement at 3D coordinates, it is equipped with software for the formation of trajectory corrections. In addition, the system is designed to measure the dimensions and force interactions of particles in space.

The system allows you to predict tolerance deviations, to investigate the statistical quality of monitoring the presence of environmental pollution [4, 5]. Similar studies provide opportunities to determine the nature of particle interactions, the trajectory of their movement in the working space of the equipment.

4. Conclusions

The article defines the need to solve the problem of determining the presence of particles of various origins in the space of working equipment. The model for determining the presence of such particles and their location coordinates in the working space of the equipment by an automated system that has the ability to correct particle trajectories to obtain a specified number of particles near the main working executive means is shown.

By their natural essence, discrete elements that are located within the space of the presence of an abstract object, always interact with each other.

The basis of these interactions is the forces that create potential forces, inherent in both the AE and each of its individual particles.

Depending on the properties of the substance, of which a discrete particle is formed, there are corresponding force fields that surround each of the particles. The character of these fields is not necessarily the same. The proposed analytical models of the interaction of power fields prove that the particles within the space of the presence zone of the abstract object can't be in a state of rest. As a result of this interaction, the particles try to take such a position, when the allotment of all these field structures at the center of its mass will approach zero. Therefore, for example, the particles that are located on the surface of the AE, try to create a layer of even energy load.

Further directions of scientific research are the creation of analytical models of the grinding process of discrete elements of a solid state zone during power interaction.

Such automated diagnostic equipment for monitoring the state of production or medical equipment is intended to improve the quality of technological operational actions in the conditions of equipment operation.

References

[1] Beer F. P. et al.: Mechanics of Materials. McGraw-Hill Education Private Limited, New Delhi 2017.
[2] Carroll J. S.: Effect of Seam-Height on Curveballs. Senior Theses. 14, 2015 [https://digitalcommons.linfield.edu/physstud_theses/14].
[3] Feynman R.: The character of physical law. A series of lectures recorded by the BBC at Cornell University USA, Cox and Wyman LTD, London 1965.
[4] Globa L. et al.: Approach to building uniform information platform for the national automated ecological information and analytical system. CEUR Workshop Proceedings 3021, 2021, 53–65.
[5] Globa L. et al.: Uniform Platform Development for the Ecology Digital Environment of Ukraine. Progress in Advanced Information and Communication Technology and Systems, 2022, 83–100 [http://doi.org/10.1007/978-3-031-16368-5].
[6] Kittel C.: Introduction to Solid State Physics. Wiley 2004.
[7] Klotchko T. R.: Formalized model of the zone presence of structures of the biological objects. 21st International Crimean Conference "Microwave & Telecommunication Technology", 2011, 1036–1037.
[8] Korn G. A. et al.: Mathematical Handbook for Scientists and Engineers: Definitions, Theorems, and Formulas for Reference and Review (Dover Civil and Mechanical Engineering). Dover Publications, 2000.
[9] Kukharchuk V. et al.: Features of the angular speed dynamic measurements with the use of an encoder. Informatyka, Automatyka, Pomiary w Gospodarce i Ochronie Środowiska 12(3), 2022, 20–26.
[10] Lezhniuk P. et al.: The Sensitivity of the Model of the Process Making the Optimal Decision for Electric Power Systems in Relative Units. IEEE KhPI Week on Advanced Technology, 2020, 247–252.
[11] Lutgens F. K. et al.: Essentials of Geology, 13th Edition. Pearson, 2017.
[12] McPhee J.: Annals of the Former World. Farrar, Straus and Giroux, 1999.
[13] Polishchuk L. et al.: Mechatronic Systems II. Applications in Material Handling Processes and Robotics. Taylor & Francis Group, CRC Press, Balkema book, Boca Raton, London, New York, Leiden 2021.
[14] Semat H., Katz R.: Physics, Chapter 8: Hydrostatics (Fluids at Rest). Rinehart & Company, Inc., New York 1958.
[15] Skytsiouk V. I., Klotchko T. R.: Determination of the coordinates of the pathological zones in the mass of the biological object. 23rd International Crimean Conference "Microwave & Telecommunication Technology", 2013, 1083–1084.
[16] Tymchik G. et al.: Modeling of The Phantom Geometry of Biotechnical Object's Pathological Zone. 41st International Conference on Electronics and Nanotechnology – ELNANO 2022, 363–368.
[17] Tymchyk G. et al.: Forces balance in the coordinate system of object's existence 3D space. Proceedings of SPIE 12476, 2022, 124760U. [http://doi.org/10.1117/12.2659188].
[18] Tymchyk G. et al.: Distortion of Phantom Object's Realizations in Biological Presence Zone. 40th International Conference on Electronics and Nanotechnology – ELNANO 2020, 464–468 [http://doi.org/10.1109/ELNANO50318. 2020.9088896].
[19] Wójcik W. et al.: Mechatronic Systems I. Applications in Transport, Logistics, Diagnostics and Control. Taylor & Francis Group, CRC Press, Balkema book, London, New York 2021.

D.Sc. Eng. Gregory S. Tymchyk
e-mail: deanpb@kpi.ua

Professor, Dean of Instrument Making Faculty, National Technical University of Ukraine "Sikorsky Kyiv Polytechnic Institute". Created a new class of laser spectral-correlation systems based on passive Fabry-Pierre resonators for operational control of quality parameters of parts and the condition of technological equipment in precision instrument manufacturing.

http://orcid.org/0000-0003-1079-998X

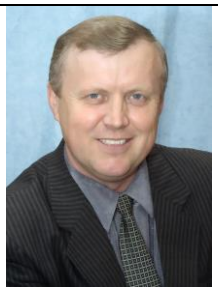

Ph.D. Volodymyr I. Skytsiouk
e-mail: max_sk@bigmir.net

Senior Researcher, Instrument Making Faculty, National Technical University of Ukraine "Sikorsky Kyiv Polytechnic Institute". Scientific directions: These metrological aspects in the automatic mode of operation of object state analysis system determine the properties that increase the accuracy and speed of operations for calculating object movement trajectories in various fields of research

http://orcid.org/0000-0003-1783-3124

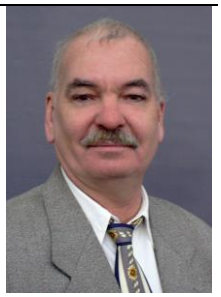

Ph.D. Tatiana R. Klotchko
e-mail: t.klochko@kpi.ua

Senior Researcher, Instrument Making Faculty, National Technical University of Ukraine "Sikorsky Kyiv Polytechnic Institute". Scientific directions: These metrological aspects in the automatic mode of operation of object state analysis system determine the properties that increase the accuracy and speed of operations for calculating object movement trajectories in various fields of research

http://orcid.org/0000-0003-3911-5369

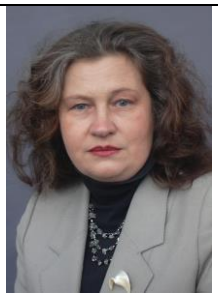

D.Sc. Leonid K. Polishchuk
e-mail: leo.polishchuk@gmail.com

Doctor of Technical Sciences, professor, academician at the Ukraine Academy of Hoisting-and-Transport Sciences. Head of the Department of Industrial Engineering at Vinnytsia National Technical University. The scientific focus is the dynamics of drive systems with devices and control systems with variable operating modes and diagnostics of metal structures of hoisting-and-transport and technological machines.

http://orcid.org/0000-0002-5916-2413

Ph.D. Anatolii V. Hrytsak
e-mail: grytsak.a.v@gmail.com

Candidate of Technical Sciences, associate professor of the Department of Information Systems Management and Security of Vinnytsia National Technical University.
Research interests: security of information systems, software protection, cryptographic protection of information, cyber security.

http://orcid.org/0000-0002-0776-9889

Ph.D. Saule Rakhmetullina
e-mail: Rakhmetullinas@mail.ru

She is currently a Chairman of the Board-rector of the D.Serikbayev East Kazakhstan Technical University. She is a co author over 40 papers in journals, book chapters, and conference proceedings and has 3 copyright certificates for software products. She is a Republican expert on reforming higher education. Her professional interests are mathematical and computer modeling of complex processes.

http://orcid.org/0000-0002-3142-0249

Ph.D. Beibut Amirgaliyev
e-mail: Beibut.amirgaliyev@astanait.edu.kz

Candidate of technical sciences, Professor at Astana IT University. Research interests: machine learning, computer vision, intellectual systems, transportation.

http://orcid.org/0000-0003-0355-5856

http://doi.org/10.35784/iapgos.3518 *received: 23.02.2023 | revised: 14.03.2023 | accepted: 29.04.2023 | available online: 30.06.2023*

TONTOR ZONES MODEL FOR AUTOMATIVE OBJECT MONITORING

Gregory S. Tymchyk[1], Volodymyr I. Skytsiouk[1], Tatiana R. Klotchko[1], Roman B. Akselrod[2], Valerii Yo. Shenfeld[3], Aliya Kalizhanova[4], Didar Yedilkhan[5], Gaukhar Borankulova[6]

[1]National Technical University of Ukraine "Sikorsky Kyiv Polytechnic Institute", Department of Device Production, Kyiv, Ukraine, [2]Kyiv National University of Construction and Architecture, Kyiv, Ukraine, [3]Vinnytsia National Technical University, Vinnytsia, Ukraine, [4]Institute of Information and Computational Technologies CS MHES RK, Almaty, Kazakhstan, [5]Astana IT University, Astana, Kazakhstan, [6]Taraz Regional University M. Kh. Dulaty, Taraz, Kazakhstan

Abstract*. The paper presents the results of analytical modeling of the case of the presence zone of an abstract object characterized by a solid mass. It has several zones of presence based on the foundations of the TONTOR theory. Research determined that the discrete solid-state zone of the presence characterizes the solid part of the AE itself or the particles that form the surrounding space near the abstract entity and is the most powerful zone among the existing zones. The proposed model for determining the parameters of TONTOR zones of an object provides the possibility of analyzing the state of this object during its movements in the working space and metrological measurements of coordinates. These metrological aspects in the automatic mode of operation of object state analysis system determine the properties that increase the accuracy and speed of operations for calculating object movement trajectories in various fields of research.*

Keywords: abstract entity, Pandan zone, automative monitoring

MODEL STREF TONTOR DO AUTOMATYCZNEGO MONITOROWANIA OBIEKTÓW

Streszczenie. *W artykule przedstawiono wyniki modelowania analitycznego przypadku strefy obecności abstrakcyjnego obiektu charakteryzującego się masą stałą. Ma on kilka stref obecności opartych na podstawach teorii TONTOR. Badania wykazały, że dyskretna stała strefa obecności charakteryzuje stałą część samej AE lub cząstki, które tworzą otaczającą przestrzeń w pobliżu abstrakcyjnej jednostki i jest najsilniejszą strefą spośród istniejących stref. Zaproponowany model określania parametrów stref TONTOR obiektu zapewnia możliwość analizy stanu tego obiektu podczas jego ruchów w przestrzeni roboczej i metrologicznych pomiarów współrzędnych. Te aspekty metrologiczne w automatycznym trybie pracy systemu analizy stanu obiektu określają właściwości, które zwiększają dokładność i szybkość operacji obliczania trajektorii ruchu obiektu w różnych dziedzinach badań.*

Słowa kluczowe: abstrakcyjny obiekt, strefa Pandana, automatyczny monitoring

Introduction

An urgent problem in field of control and measuring devices manufacturing, industrial technologies of detail processing, ecology, research of astronomical objects is determination of object's presence, its coordinates of presence in research space. At same time, an important task is to monitor the current state of this object during its movement, which characterizes possible damage and violations of movement trajectory. Therefore, creation of a model for determining parameters by automated technical means provides opportunities to increase the accuracy of measurement, as well as to regulate the speed of these metrological actions.

In authors works [15, 16] main conception from presence zones of abstract entity (AE) are offered. Primary presence TONTOR zone (Pandan zone of AE) is zone, which characterize of mass presence in space. TONTOR Pandan zone as kind of mechanical and physical signal, within consider only power parameters of AE is offered [17].

Around AE, the gravitational zone of presence is performed as a zone in the form of a field structure that characterizes current state of the environment.

At the same time, this zone of presence characterizes the presence and parameters of a discrete solid body and its discrete elements, as well as the parameters of the location in space and the coordinates of the movement of these particles as elements.

So, in a similar way, the particles of the defined solid-state zone and the electric field of the field structure create a zone of presence around the AE and hold their field interactions. The forces of the presence of the zone of intermolecular and atomic interaction were partially considered in [16, 17], but they as the transition of the solid-state zone AE into the atomic-molecular zone are considered.

If we consider a property that can provide the effect of spreading force over a certain distance, then we define the zone of the presence of a solid body as the most powerful relative to other zones in accordance with the foundations of the TONTOR theory. At the same time, force transmission is not observed without a certain deformation of the field structure.

So, the goal of this work is the analytical modeling of basis of determining the parameters of discrete elements that form the zone of AE presence.

1. Proposed model of solid-state zone as AE presence zone

If we analyze the composition and nature of the existence of the AE presence zone, we can determine two phase states that have physical and mechanical properties as a solid discrete zone (SDZ) and a continuous solid zone (CSZ).

It is characteristic of CSZ that it exists inside a solid mass AE or a solid object AE. Such types of AE spaces are characterized by the ability to transmit physical regularities over a distance. SDZ consists of discrete mass, which united by a whole field structure as common block. Such an example can be the force of gravity during the interaction of individual masses of AE.

At same time, it is very important to determine and analyze properties of the constituent elements of AE presence zone, which has finite geometric, mechanical and physical properties.

Taking into account the peculiarities of such delimitation, it can be determined that the elements of zone have nature of existence of AE, which distinguishes finite physical and mechanical properties. Thus, sand located on the Earth's surface, compared to its geometric dimensions, is nothing more than dust, represents a whole structure of an orderly arrangement of discrete elements in space and can be considered as a basic abstract object.

In the case of CSZ, an unbounded solid object is characteristic. The middle of this AE characterizes the process in which the release of energy is observed. So, we have the nature of the field structure of central-metric geometry, for which the distribution patterns of temperature fields, normal, tangential energy loads are determined.

It is normal and tangential loads that can be determined [1, 18], based on relevant laws of theory of material resistance. Characteristic for this case are the analytical dependencies, which in rectangular coordinates determine the equilibrium of the element as

$$\begin{aligned}\frac{\partial\sigma_x}{\partial x}+\frac{\partial\tau_{yx}}{\partial y}+\frac{\partial\tau_{zx}}{\partial z}+\rho X=0,\\ \frac{\partial\tau_{xy}}{\partial x}+\frac{\partial\sigma_y}{\partial y}+\frac{\partial\tau_{zy}}{\partial z}+\rho Y=0,\\ \frac{\partial\tau_{xz}}{\partial x}+\frac{\partial\tau_{yz}}{\partial y}+\frac{\partial\sigma_z}{\partial z}+\rho Z=0,\end{aligned} \quad (1)$$

where ρ is the specific mass of solid object (AE), X, Y, Z are mass of the force in corresponding coordinate, $\tau_{xy},\tau_{yx},\tau_{zx},\tau_{xz},\tau_{yz},\tau_{zy}$ are tangential loads and σ_x, σ_y, σ_z are normal loads by space coordinates *x, y, z*.

These equations (1) characterize internal residual stresses that arise as a result of processes, dislocations in the internal environment of the object. Since we define a solid object as an AE with a large power, the internal stresses begin to weaken, but within a certain time the values level off and disappear at the end of the time interval.

We can determine the dislocation direction and its distance from the excitation coordinate using a strain gauge [2, 18].

Almost all AEs have SDZ, and CSZ compared to SDZ has a very limited application in practice. As a rule, SDZ has a joint movement with the AE surface and the captured part of the medium. Since the particles of SDZ have a finite mass, as a result, they have the shape of any configuration, and for artificial variants of SDZ, the varieties of forms can sometimes take on the appearance of geometric classical shapes, which greatly facilitates calculations and analytical studies of the nature of these elements.

When determining the spectrum of characteristics at a certain distance from the surface of the AE, we get other solutions, for example, the Solar System, where space objects are unevenly distributed at a distance from the Sun in space. Thus, according to Kepler's laws [5, 7], it is possible to determine the spectrum of volume and mass depending on the distance to surface of objects.

So, these are additional spectra in terms of density and the relationship between density and the shape of this object, which allows you to study the properties of surrounding space.

The interaction of SDZ's particles characterizes their mutual contact and its features, when the particles are under the influence of Brownian motion and Saint-Venant principle can be applied for boundary conditions of object's interaction [3, 6]. At the same time, the complex of forces during their action within the surface of the object with a zone can be modeled as a concentrated force.

Since the theory of resistance of materials doesn't study the spatial and temporal parameters of the movement of solid objects mass [9], the study of deformation requires additional informational data.

If the parameters of linear deformation are determined in the general case (Fig. 1), the same methods as [4, 10] are used. The deformation at point A, if we consider this case, will have a different value. As a result of this, it is advisable to specify direction of a single vector and to study the change in gap *AB = ds*, which is obtained as a result of the deformation, while the point *B* is selected on the given straight line.

According to the specified direction, it is appropriate to consider the linear deformation as

$$\varepsilon_s=\frac{A^*B^*-AB}{AB}=\frac{ds^*-ds}{ds} \quad (2)$$

where $A^*B^*=ds$ is length of the point *ds* after deformation according to TONTOR theory.

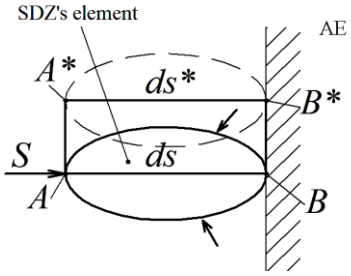

Fig. 1. General model of SDZ's element deformation, where dS is element of object's surface

Value of ε_p determines the true or real deformation as

$$\varepsilon_p\approx\frac{u}{l_0+\frac{1}{2}u}\approx\varepsilon-\frac{1}{2}\varepsilon^2 \quad (3)$$

where parameter u determined AA^* value.

Imagine that there is a coordinate system rigidly built up with the points of attachment of SDZ element (Fig. 2), with some free point having *x, y, z* coordinates. After the deformation, the point will move to the position, and point. In this case, vectors and, respectively, represent the displacement of points and.

If we consider coordinate system that determines the rigid connection of a discrete element of SDF (Fig. 2), in which there is a free point A with spatial coordinates *x, y, z*, then after the existing deformation, the point A will move to other coordinates A^*, and the point $B\to B^*$. So, in this case, the vectors AA^* and respectively represent the displacement of the points A and B^*.

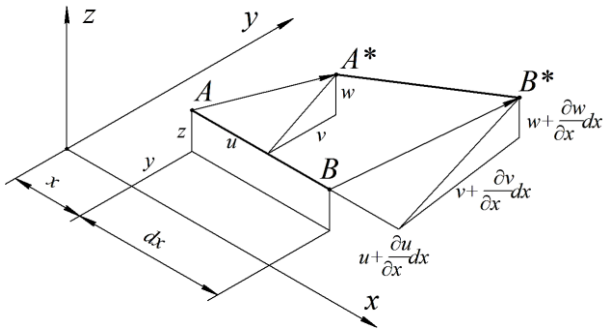

Fig. 2. Model of ε_x deformation value

The component movements of a point *A* along *x, y, z* axes are considered as *u, v, w*.

Then

$$u+\frac{du}{dx}dx,\ v+\frac{\partial v}{\partial x}dx,\ w+\frac{\partial w}{\partial x}dx \quad (4)$$

At same time, it is necessary to consider changing the volume of DSZ element. So, volume of discrete element will be

$$dV = dxdydz \quad (5)$$

After deformation we considered ε_x, ε_y, ε_z.

So, we have to get a new volume, neglecting movement deformations

$$dV = (1+\varepsilon_x)\ (1+\varepsilon_y)\ (1+\varepsilon_z)dxdydz \quad (6)$$

In this case, volume deformation will be

$$\varepsilon_V=\frac{dV-dV_0}{dV_0}=(1+\varepsilon_x)(1+\varepsilon_y)(1+\varepsilon_z)-1 \quad (7)$$

or within limits of small deformations

$$\varepsilon_V=\varepsilon_x+\varepsilon_y+\varepsilon_z \quad (8)$$

The presented analytical model determines the patterns of change in the deformation process of a separate element of SDZ, while the modelling concerns only one element of AE zone.

2. Structure of DSZ macro element's placement in space AE

From the preliminary examination it is very well seen that the AE surface is always under pressure, which leads to its certain destruction. As a result, a layer of solid elements is formed around AE. These only partial elements are in a state of relative calm, and therefore gradually form certain layers. Currently, it is possible to isolate three layers around AE. The first layering is a dense layer on the object surface. In this case, being in close contact with the surface and with each other, they do not have intermolecular adhesion, although they are under pressure. In this case, above physical and mathematical description is quite suitable for a single element, but not for the entire layer as a whole.

The second layer is characterized by fact that DSZ elements are in such close proximity to each other that any outside force can lead to a chain reaction of pushing elements. In this case, the external force that acts on discrete element leads to its movement. As a result, this element does a blow to the neighboring one, which in turn is also neighboring and so on.

The third layer is characterized by the fact that a single element can move to infinity around AE without ever encountering other elements.

All of the foregoing proves that there is a problem of the location of discrete sized elements in different layers of zone. In study of literary sources, it turned out that the spectrum in size is result of the solution of second-order differential equation in aperiodic form [11]. The maximum value of such an aperiodic function is number of elements of a definite size obtained as a result of a certain technological process. In general, the distribution function *n(d)*, depending of the granule *d* diameter, in its construction is very similar to the entire function of solving differential equation, as

$$n(d) = E(A_1 e^{k,d} - A_2 e^{-k_2 d}) \tag{9}$$

where A_1, A_2, k_1, k_2 are amplitudes of quantity and capacity in technological and natural processes.

This equation becomes more understandable if its result is presented as a result of the interaction of two phantoms, namely phantom of the formation of granules and phantom scrap. The general situation with shape of granules (SDZ particles) is currently purely subjective description. It is believed that longer the external forces act on the object, more it approaches the spherical shape, that is, even the diameter d in equation (9) should be taken as the average.

A classic example is a form of sand granules, pebbles, and the like that have been formed for millions of years. Such layers of objects of sphere form a zone of presence of the globe, etc. And if the spectrum of diameters can somehow be guided by the principles of expression (9), then the spectrum of distribution in size, depending on the distance to the surface in general, is extremely difficult to determine. If the planar version of the projections of this zone can still be modeled, then with a 3D solution to this problem, the situation is extremely difficult.

So, let's try to simulate a variant of the flat task simulating SDZ, based of this simulation is following conditions.

First, it is possible to simulate on SDZ plane only in situation when the basic elements are quite easily formed into some definite form of the finite element. At present, we can consider such elements a square, equilateral and equilateral triangle.

Boundary of any AE Pandan zone is a sphere, and projection of a sphere is a circle. Consequently, in each elementary SDZ there is a finite number of projection sphere (Fig. 3).

Our task is to determine the zone that is not involved in the DSZ. This problem has two solutions, namely direct and inverse. For a direct task, we focus on shapes with sides 2a and the angles between the sides of which we have, or. At the same time, these figures should be the simplest, so that they could be composed of layers of DSZ (Fig. 3).

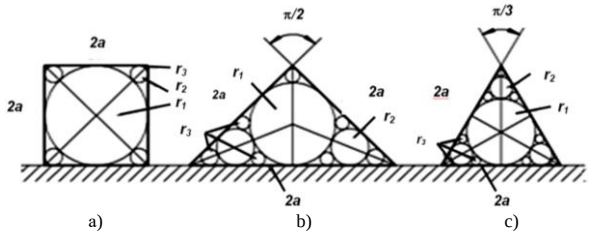

Fig. 3. Simulation of SDZ plane task: a) a square with a side 2a, b) a rectangular equilateral triangle with a side 2a, c) an equilateral triangle with a side 2a

Since boundary of the Pandan zone is a sphere, and its projection onto the circle plane, a definite number of round objects may be located within the limits of the completed geometric figure. In addition, they should occupy the maximum zone. Thus, the inverse problem can be considered determination of the number and size of round objects, which maximally fill a certain zone of the surface. This task is very complicated, because it requires solving equation (9), which has many unknowns. Therefore, we confine ourselves to considering a direct problem based on (Fig. 3a). So, we need to find out the principle of filling the plane of an elementary figure. At present, the following formula can be used to determine such percentage dependence

$$S_e(\%) = \frac{\Delta S}{S_e}100\% = \frac{S_e - S_0}{S_e}100\%$$

where S_e is DSZ of elemental particle, S_0 - zone by circle is covered.

Thus, if the elementary particle has the shape of a square (Fig. 3a), then we obtain the following result. Square $S_k = 4a^2$; square of circle radius r_1: $S_{01} = \pi r_1^2 = \pi a^2$; square of circle radius r_2: $S_{02} = \pi r_2^2 = \pi r_1^2 \left(\frac{1-\sin\frac{\pi}{4}}{1+\sin\frac{\pi}{4}}\right)^2 = \pi a^2 \left(\frac{1-\sin\frac{\pi}{4}}{1+\sin\frac{\pi}{4}}\right)^2$.

Thus, the percentage of uncovered zones will be

$$S_k(\%) = \frac{S_k - S_{01} - 4S_{02}}{S_k}100\% = \left[1 - \frac{\pi}{4} - \pi\left(\frac{1-\sin\frac{\pi}{4}}{1+\sin\frac{\pi}{4}}\right)^2\right]100\% = 12.2\% \tag{10}$$

If we have square of an equilateral rectangular triangle $S_{\Delta 1} = 2a^2$, square of circle radius r_1: $S_{01} = \pi r_1^2 = \pi a^2\left(\frac{4-\sqrt{2}}{4}\right)^2$; square of circle radius r_2: $S_{02} = \pi r_2^2 = \pi a^2\left(\frac{4-\sqrt{2}}{4}\right)^2\left(\frac{1-\sin\frac{\pi}{8}}{1+\sin\frac{\pi}{8}}\right)^2$; square of circle radius r_3: $S_{03} = \pi a^2\left(\frac{4-\sqrt{2}}{4}\right)^2\left(\frac{1-\sin\frac{\pi}{4}}{1+\sin\frac{\pi}{4}}\right)^2$.

Thus, the percentage of uncovered zones will be

$$S_{\Delta 1}(\%) = \frac{S_{\Delta 1} - S_{01} - 2S_{02} - S_{03}}{S_{\Delta 1}}100\% = \left\{1 - \frac{\pi}{2}\left(\frac{4-\sqrt{2}}{4}\right)^2\left[1 + \left(\frac{1-\sin\frac{\pi}{8}}{1+\sin\frac{\pi}{8}}\right)^2 + \left(\frac{1-\sin\frac{\pi}{4}}{1+\sin\frac{\pi}{4}}\right)^2\right]\right\}100\% = 25.9\% \tag{11}$$

In addition to dependencies (10) and (11), where there is a fairly good relationship between the square and the rectangular triangle, there is another one. This dependence shows the relationship between the radiuses of inserted objects at the right angles of a square or a rectangle. Currently, this is a series of circles, whose centers are located on bisector of the corner and which have four tangents. Of these, two touch the sides of the right corner, and two other previous and next circles.

The radius of this circle will be

$$r_n = a\left(\frac{\sqrt{2}-1}{\sqrt{2}+1}\right)^n \tag{12}$$

where n = 0, 1, 2, 3 ... ∞ and is the serial number of circle from center.

At the same time for zero reference first circle is taken.

In this case, the circle's zone will be:

$$S_{0n} = \pi\left[a\left(\frac{\sqrt{2}-1}{\sqrt{2}+1}\right)^n\right]^2 \tag{13}$$

If we have square of an equilateral triangle as $S_{\Delta 2} = a^2\sqrt{3}$; square of circle radius r_1: $S_{01} = \frac{1}{3}\pi a^2$; square of circle radius r_2: $S_{02} = \pi\frac{a^2}{3}\left(\frac{1-\sin\frac{\pi}{6}}{1+\sin\frac{\pi}{6}}\right)^2$, percentage of uncovered zones will be

$$S_{\Delta 2}(\%) = \frac{S_{\Delta 2} - S_{01} - 3S_{02}}{S_{\Delta 2}}100\% = \left\{1-\frac{\pi}{\sqrt{3}}\left[\frac{1}{3}+\left(\frac{1-\sin\frac{\pi}{6}}{1+\sin\frac{\pi}{6}}\right)^2\right]\right\}100\% = 19.4\% \tag{14}$$

Consequently, among all these figures, square and least efficient rectangular triangle are most effectively used, although it would seem that density of use of the square in it should have been greater.

Take one more step. That is, we introduce additional circles in all figures in Fig. 3. They may now have following dimensions.

For a square this can be circles of radius r_3 located at its angles (4 pieces) (Fig. 3a), for a rectangular equilateral triangle it is possible to add circles of radius r_3 in the amount of six pieces (Fig. 3b), for an equilateral triangle we have the ability to add nine circles of radius r_3. In this way, we will have a general covering of zone in the following form:

$$S_k(\%) = \frac{S_k - S_{01} - 4S_{02} - 4S_{03}}{S_k}100\% = 11.9\%$$

$$S_{\Delta 1}(\%) = \frac{S_{\Delta 1} - S_{01} - 2S_{02} - 7S_{03}}{S_{\Delta 1}}100\% = 7.7\%$$

$$S_{\Delta 2}(\%) = \frac{S_{\Delta 2} - S_{01} - 3S_{02} - 9S_{03}}{S_{\Delta 2}}100\% = 12.67\%$$

As can be seen from preliminary consideration of the possibility of covering square, the best square and its halves. It should be noted that the percentage of non-covering of square is maintained regardless of number of SDZ selected elements. From the preceding equations (10), (11), (13) and (14) it is possible to imagine a series of dependencies that give the percentage of uncovered zone as equations (15) gives only an idea of the possible number of circles on SDZ elemental zone:

$$S\% = \left\{1-\pi k^2\left[a^2 + b^2\left(\frac{1-\sin\frac{\pi}{n}}{1+\sin\frac{\pi}{n}}\right)^2 + c^2\left(\frac{1-\sin\frac{\pi}{2n}}{1+\sin\frac{\pi}{2n}}\right)^2 + d^2\left(\frac{1-\sin\frac{\pi}{4n}}{1+\sin\frac{\pi}{4n}}\right)^4 + \ldots + m^2\left(\frac{1-\sin\frac{\pi}{mn}}{1+\sin\frac{\pi}{mn}}\right)^{2m}\right]\right\}100\% \tag{15}$$

Currently, the last member of this series is uniquely relying on value. Again, we remind that all elementary particles of SDZ are in close contact, such as sand or pebbles on the shore of the reservoir. In the case of a violation of this state, this layer is transferred to a new state.

This new layer, as we have already mentioned above, in general classification resembles a well-known suspension of colloidal chemistry [12–14].

At moment it is understood (suspenzo – latching hanging) a certain amount of solid particles of a certain size that move at the same speed in a definite direction. At the same time, all particles do not comply with laws of Brownian motion [9, 16].

The third layer of SDZ is a series of discrete objects that move around AE in some closed orbits. Such objects, as a rule, move in one direction and eventually go to the plane (disk). A good example of this stratum is astronomical phenomena such as, for example, galaxies or solar planetary system. In addition, one can consider such a phenomenon as an electron shell of an atom. Such a shell has a rather specific character [5] because it has a duality of behavior as a layer of SDZ.

Consequently, the atom has a kernel and an electric shell. The core consists of electrically neutral neutrons and positively charged protons. Both protons and neutrons move in middle of the nucleus under influence of nuclear forces. The electron shell consists of electrons moving along the "orbitals" rather than orbits. This phenomenon gives a description of the quantum-mechanical theory of atom construction. According to quantum mechanical theory of atom construction, the electron has a dual nature, that is, on the one hand, it behaves like a solid particle, and on the other, like a wave. At present, mechanical properties of an electron are due to the presence of a mass of rest and associated properties. Nevertheless, during the movement of electron behaves like a wave, that is, it has amplitude, wavelength, frequency of oscillations, etc. But it is not clear why the wave has no mass? Therefore, the quantum-mechanical theory believes that it is impossible to speak of an orbit with some parameter, but only about the probability of finding an electron in one or another point in space. Consequently, under this thesis, under the electron orbit, one should understand not a specific trajectory of motion, but some stratum around the nucleus, where the probability of an electron at a certain moment is greatest.

Thus, the electronic orbit does not characterize the moving of an electron from point to point, but only characterizes the parameters of layer, which determines the distance of its location from nucleus. Therefore, electron does not represent in the form of a material point, but if the electric cloud covering nucleus of an atom, which has its condensation and thawing

of the charge. However, it should be borne in mind that this cloud does not have sharply defined contours, and therefore, at great distances from nucleus, there is a probability of finding an electron. The electronic cloud has no clearly defined boundaries. Explanation at the level of hydrogen atom, which represents failure of a regular sphere. In this ball there is ability to determine the equipotential surfaces on which electron density will have same value.

In the case of hydrogen atom, it is concentric spheres. In the atom of hydrogen on the electron, only the force of attraction of a positively charged nucleus is valid. In the multielectron atom only the force of a positive charged nucleus acts. In addition, in a multi-electron atom, the interaction forces of discrete electrons are interconnected [16], that is, we have one example of the law of aggression [15, 17, 19] in the study of various types of applications. At the same time, a very important aspect is the application of the active surface sensor, which is used in automatic systems for metrological measurements of parameters and monitoring of the coordinates object during its movement in space.

As a result, we have certain stratification, namely, internal layers weaken the action of the field of nucleus most distant layers. In addition, this shielding does not have an isotropic state when interacting with each electric cloud. Therefore, in many-electron atoms, the electron energy depends not only on the principal quantum number, but also on the size of orbital quantum number, which determines the shape of electron cloud.

Unlike the microcosm, we have some other physical phenomena in the macro world. Consequently, starting with a certain particle size that is much larger than an atom, we have the opportunity to explain all the processes of motion in the SDZ on the basis of aero and hydrodynamics and astronomical phenomena. It was mentioned above that all particles of SDZ move around the AE for approximately a circular orbit. In addition, this situation is typical for almost all AE regardless of scaling. For this purpose we turn to theoretical astronomy as a means of explaining such a movement in space. Consequently, the principles of the description of such an orbital motion are based on Kepler's laws [5]. At the moment, most important for us is first law, that is: orbit of the planet in essence of ellipse in one of tricks of which is sun. Thus, if we discard all secondary signs (astronomical), then we must assume that any SDZ moving around the AE has a description for the canonical equation of the ellipse, that is:

$$\frac{x^2}{a^2}+\frac{y^2}{b^2}=1 \tag{16}$$

where a and b are large and small semi-ellipse.

Thus, eccentricity of ellipse

$$e=\frac{c}{a} \tag{17}$$

where c is the distance of ellipse tricks from its center.

On the other

$$c=\sqrt{a^2-b^2} \tag{18}$$

or after transformations

$$b=a\sqrt{1-e^2} \tag{19}$$

Quite often, instead of eccentricity e, angle φ is introduced by

$$\sin\varphi=e \tag{20}$$

As a consequence, the previous equations (17), (18), (19) and (20) have an opportunity to rewrite as

$$\left.\begin{aligned} e&=a\sin\varphi\\ b&=a\cos\varphi\\ \cos\varphi&=\sqrt{1-e^2}\end{aligned}\right\} \tag{21}$$

Quite often the focal equation of an ellipse is used

$$r=\frac{P}{1+e\cos V} \tag{22}$$

where r is the focal radius of vector of ellipse point, P is the ellipse parameter or focal coordinate, V is polar angle of ellipse point.

In addition to Kepler's laws, there are problems in astronomy about two, three and n bodies that interact with each other due to force of gravity [20]. If we discard secondary astronomical signs, then we will have a number of n interacting AE's. Currently, the section devoted to gravity zone of presence, shows most generalized cases of interaction.

Consequently, if we have an AE with mass m moving in orbit in accordance with (21), (22) then on section of size dl on it the force F of gravity, i.e.

$$m\frac{d^2\overline{l}}{dt^2}=F \tag{23}$$

If we take into account that vector of force F has projections on the coordinate axis, then equation (23) can be rewritten in following form:

$$\left.\begin{aligned} m\frac{d^2x}{dt^2}&=\mathbf{F}\cos\alpha\\ m\frac{d^2y}{dt^2}&=\mathbf{F}\cos\beta\\ m\frac{d^2z}{dt^2}&=\mathbf{F}\cos\varphi\end{aligned}\right\} \tag{24}$$

On other, if we have two AE with masses m and m_1 at a distance ρ from each other, then, according to Newton's law, they interact with force

$$F=\gamma\frac{mm_1}{\rho^2}$$

where γ – constant of gravity.

So, if we choose a fixed coordinate system, then coordinates for masses of AE will be: $m\text{-}x, y, z$; $m_1\text{-}x_1, y_1, z_1$. Using these coordinates, we have the opportunity to write down

$$\left.\begin{aligned} r^2&=x^2+y^2+z^2\\ r_1^2&=x_1^2+y_1^2+z_1^2\\ \rho^2&=(x_1-x)^2+(y_1-y)^2+(z_1-z)^2\end{aligned}\right\} \tag{25}$$

where γ, γ_1 – radius-vectors m_1, m_2.

Similarly, from (25) we obtain

$$\left.\begin{aligned} \cos\alpha&=\frac{x_1-x}{\rho}\\ \cos\beta&=\frac{y_1-y}{\rho}\\ \cos\varphi&=\frac{z_1-z}{\rho}\end{aligned}\right\} \tag{26}$$

If we obtain equations (25) and (26) in (24), we obtain equation of motion for the masses m and m_1.

Consequently, the equation for the motion of AE with a mass m will be

$$\left.\begin{aligned} m\frac{d^2x}{dt^2}&=\gamma mm_1\frac{x_1-x}{\rho^3}\\ m\frac{d^2y}{dt^2}&=\gamma mm_1\frac{y_1-y}{\rho^3}\\ m\frac{d^2z}{dt^2}&=\gamma mm_1\frac{z_1-z}{\rho^3}\end{aligned}\right\} \tag{27}$$

The equations of motion for AE with the mass m_1 will look

$$\left.\begin{aligned} m\frac{d^2x}{dt^2} &= -\gamma m m_1 \frac{x_1 - x}{\rho^3} \\ m\frac{d^2y}{dt^2} &= -\gamma m m_1 \frac{y_1 - y}{\rho^3} \\ m\frac{d^2z}{dt^2} &= -\gamma m m_1 \frac{z_1 - z}{\rho^3} \end{aligned}\right\} \quad (28)$$

If we integrate equations (27) and (28), then we will have a solution to the problem of motion of two AE under the action of mutual attraction.

In order to solve this problem we make a number of assumptions, the main of which is the placement of the mass m_1 at the origin, that is $x_1 = y_1 = z_1 = 0$. As a consequence, we obtain

$$\left.\begin{aligned} \frac{d^2x}{dt^2} &= -\gamma(m_1 + m)\frac{x}{r^3} \\ \frac{d^2y}{dt^2} &= -\gamma(m_1 + m)\frac{y}{r^3} \\ \frac{d^2z}{dt^2} &= -\gamma(m_1 + m)\frac{z}{r^3} \end{aligned}\right\} \quad (29)$$

In astronomy [5, 7], equation (29) is called the differential equations of a material point with a mass m around a material point with a mass m_1 (the typical nonsense mass has a size, hence it is a point).

Equations (29) have a special case of solution. The essence of this solution is that if we take the mass of one point in M and position it at the origin, then motion of a point with mass μ around it can be rewritten by equation (29) in following form:

$$\left.\begin{aligned} \mu\frac{d^2x}{dt^2} &= -\gamma\mu M\frac{x}{r^3} \\ \mu\frac{d^2y}{dt^2} &= -\gamma\mu M\frac{y}{r^3} \\ \mu\frac{d^2z}{dt^2} &= -\gamma\mu M\frac{z}{r^3} \end{aligned}\right\} \quad (30)$$

If (30) is reduced to μ, then we obtain

$$\left.\begin{aligned} \frac{d^2x}{dt^2} &= -\gamma M\frac{x}{r^3} \\ \frac{d^2y}{dt^2} &= -\gamma M\frac{y}{r^3} \\ \frac{d^2z}{dt^2} &= -\gamma M\frac{z}{r^3} \end{aligned}\right\} \quad (31)$$

In the case of solving problem of three bodies we accept following input data:

- mass of the AE: m, m_1, m_2;
- coordinates of the masses: x, y, z; x_1, y_1, z_1; x_2, y_2, z_2;
- mutual distances: ρ_{01}, ρ_{12}, ρ_{02}.

By analogy with previous case, we have the following dependencies:

$$\left.\begin{aligned} \rho_{01}^2 &= (x_1 - x)^2 + (y_1 - y)^2 + (z_1 - z)^2 \\ \rho_{02}^2 &= (x_2 - x)^2 + (y_2 - y)^2 + (z_2 - z)^2 \\ \rho_{12}^2 &= (x_2 - x_1)^2 + (y_2 - y_1)^2 + (z_2 - z_1)^2 \end{aligned}\right\} \quad (32)$$

If we solve this problem in a similar way to previous one, we obtain a series of equations for masses m, m_1 and m_2

$$\left.\begin{aligned} m\frac{d^2x}{dt^2} &= k^2 m m_1\frac{x_1 - x}{\rho_{01}^3} + k^2 m m_2\frac{x_2 - x}{\rho_{02}^3} \\ m\frac{d^2y}{dt^2} &= k^2 m m_1\frac{y_1 - y}{\rho_{01}^3} + k^2 m m_2\frac{y_2 - y}{\rho_{02}^3} \\ m\frac{d^2z}{dt^2} &= k^2 m m_1\frac{z_1 - z}{\rho_{01}^3} + k^2 m m_2\frac{z_2 - z}{\rho_{02}^3} \end{aligned}\right\}$$

$$\left.\begin{aligned} m_1\frac{d^2x_1}{dt^2} &= -k^2 m m_1\frac{x_1 - x}{\rho_{01}^3} + k^2 m_1 m_2\frac{x_2 - x_1}{\rho_{12}^3} \\ m_1\frac{d^2y_1}{dt^2} &= -k^2 m m_1\frac{y_1 - y}{\rho_{01}^3} + k^2 m_1 m_2\frac{y_2 - y_1}{\rho_{12}^3} \\ m_1\frac{d^2z_1}{dt^2} &= -k^2 m m_1\frac{z_1 - z}{\rho_{01}^3} + k^2 m_1 m_2\frac{z_2 - z_1}{\rho_{12}^3} \end{aligned}\right\} \quad (33)$$

$$\left.\begin{aligned} m_2\frac{d^2x_2}{dt^2} &= -k^2 m m_2\frac{x_2 - x}{\rho_{02}^3} - k^2 m_1 m_2\frac{x_2 - x_1}{\rho_{12}^3} \\ m_2\frac{d^2y_2}{dt^2} &= -k^2 m m_2\frac{y_2 - y}{\rho_{02}^3} - k^2 m_1 m_2\frac{y_2 - y_1}{\rho_{12}^3} \\ m_2\frac{d^2z_2}{dt^2} &= -k^2 m m_2\frac{z_2 - z}{\rho_{02}^3} - k^2 m_1 m_2\frac{z_2 - z_1}{\rho_{12}^3} \end{aligned}\right\}$$

where k_2 – gravity constant of astronomical signs.

If in the system of equations, to formulate the equations containing x, then three, which contain y, and three z, which containing z.

Then integrate of result twice, then we obtain following system of equations

$$\left.\begin{aligned} m\frac{dx}{dt} + m_1\frac{dx_1}{dt} + m_2\frac{dx_2}{dt} &= \alpha \\ m\frac{dy}{dt} + m_1\frac{dy_1}{dt} + m_2\frac{dy_2}{dt} &= \alpha' \\ m\frac{dz}{dt} + m_1\frac{dz_1}{dt} + m_2\frac{dz_2}{dt} &= \alpha'' \end{aligned}\right\} \quad (34)$$

The following transformations give

$$\left.\begin{aligned} mx + m_1x_1 + m_2x_2 &= \alpha t + \beta \\ my + m_1y_1 + m_2y_2 &= \alpha' t + \beta' \\ mz + m_1z_1 + m_2z_2 &= \alpha'' t + \beta'' \end{aligned}\right\} \quad (35)$$

where $\alpha,\alpha',\alpha'',\beta,\beta',\beta''$ are constant of integration.

Quite often, equation (35) is called integrals of motion of the center of mass.

In this mode of movement, the integral of zone, which is obtained in a similar way, as well as previous equations, is very important

$$\left.\begin{aligned} \sum m\left(y\frac{dz}{dt} - z\frac{dy}{dt}\right) &= c_1 \\ \sum m\left(z\frac{dx}{dt} - x\frac{dz}{dt}\right) &= c_2 \\ \sum m\left(x\frac{dy}{dt} - y\frac{dx}{dt}\right) &= c_3 \end{aligned}\right\} \quad (36)$$

For solve the problem of the interaction of n bodies, the so-called potential function is introduced, which is determined by the equation

$$E_{\Pi} = k^2\left(\frac{mm_1}{\rho_{01}} + \frac{mm_2}{\rho_{02}} + \frac{m_1m_2}{\rho_{12}}\right) \quad (37)$$

In the general case, that is, the problem with n objects in brackets must be members, that is, the number of combinations for two of the all mutually attracted objects. For example, for four objects, the number of members will be, for five objects, for six, and so on. In the future, expressions of derivatives in the function $E_{\text{П}}$ for each coordinate are obtained.

In the final case, we obtain the equation

$$\frac{d}{dt}\sum m\left[\left(\frac{dx}{dt}\right)^2+\left(\frac{dy}{dt}\right)^2+\left(\frac{dz}{dt}\right)^2\right]=2\frac{dE_{\text{П}}}{dt} \tag{38}$$

This equation can be integrated and obtained

$$\sum m\left[\left(\frac{dx}{dt}\right)^2+\left(\frac{dy}{dt}\right)^2+\left(\frac{dz}{dt}\right)^2\right]=2E_{\text{П}}+h \tag{39}$$

where h – constant of integration.

Since the linear velocity V is defined as

$$\left(\frac{dx}{dt}\right)^2+\left(\frac{dy}{dt}\right)^2+\left(\frac{dz}{dt}\right)^2=V^2 \tag{40}$$

then equation (39) can be rewritten in the form

$$\sum mV^2=2E_{\text{П}}+h \tag{41}$$

Equations (39) and (41) are called integrals of a living force or energy integrals. It should be emphasized that exploring the form of orbits in the problem of three bodies is strictly analytically feasible only in some particular cases. Therefore, in all other cases, methods of partial integration are applied.

From the above description of the motion in distant layer of SDZ zone, it can be seen that macro processes have a significant difference from the micro processes. Thus, at the level of construction, SDZ's atom, which is an electronic cloud, has a dual nature of the wave and the corpuscles. At the macro level of SDZ, wave properties are completely left. Objects, that rotate around their centers of mass, move along ellipsoidal orbits. Moreover, in the course of the movement all free-moving elements of SDZ are tuned into one plane with the subsequent process of creating larger objects. The most successful example [8, 20] here is Saturn with its rings (Fig. 4). There is another rather significant difference, namely, that atom's Pandan zone has a spherical shape, and the Pandan zone of the macro object is a mix of sphere and disk.

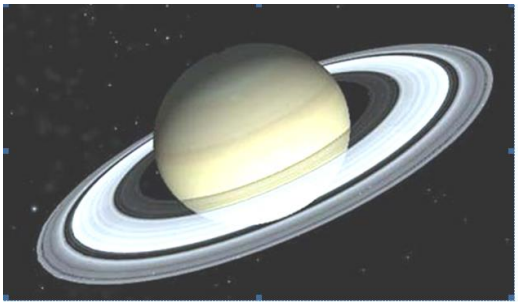

Fig. 4. Rings of Saturn

The approximate mathematical dependence has form:

$$\left.\begin{aligned} y&=\frac{1}{ax+bx+c}\\ y&=\frac{1}{-ax-bx-c}\end{aligned}\right\} \tag{42}$$

which represents two curves that rotate relative to the vertical axis of symmetry with a coordinate at the point and have a maximum in size.

3. Conclusions

Thus, on the basis of the conducted research, it was determined that any abstract object that is in a suitable environment, near its main mass, has its own surrounding space filled by individual solid particles. For the most part, particles comply with physical laws in view of their interaction with the main mass of AE and the surrounding space.

Thus, these particles create a solid-state zone of the presence of an abstract entity, have a different geometric shape, density. The physical essence of the existence of particles around an abstract entity is characterized by the parameters of common electric, magnetic fields, gravity and acoustic fields.

Volume of the abstract entity is determined by the force field of the space close to the surface of the main mass, this space is filled by particles that can enter the near zone from the surrounding space of the environment with force fields or their components, that is, electrostatic, gravitational, acoustic fields of the main abstract object. In other cases, the particles are the products of the decay of the abstract entity itself, which occurs either with time of existence or as a result of violations of the normal modes of its action.

Thus, surface particles located in dense interaction with an abstract object do not have gravity with the main mass due to molecular force fields, but they move along the surface with a certain trajectory.

Therefore, it can be determined that the particles located in the AE space are subject to fields of various origins, for example, electric, magnetic, gravitational fields, when interacting with the aerohydrodynamic environment, which is characteristic of bodies, which located in outer space.

Therefore, the presence of a deterministic zone of the presence of a multidisperse solid body is characteristic of all objects. Similar zones of presence can be considered in a wide range of objects of different sizes and basic masses, that is, they can be used in the study of both galactic bodies and atomic masses using methods similar to analytical results.

Therefore, proposed model for determining the parameters of TONTOR zones of object provides the possibility of analyzing the state of this object during its movements in the working space, metrological measurements of coordinates.

These metrological aspects in the automatic mode of operation of object state analysis system determine the properties that increase the accuracy and speed of operations for calculating object movement trajectories in various fields of research

References

[1] Beer F. P. et al.: Mechanics of Materials. McGraw-Hill Education Private Limited, New Delhi 2017.
[2] Bonnie A. S. et al.: The Dynamics of Small Bodies in the Solar System. A Major Key to Solar Systems Studies. Springer Science & Business Media, 1998.
[3] Globa L. et al.: Approach to building uniform information platform for the national automated ecological information and analytical system. CEUR Workshop Proceedings 3021, 2021, 53–65.
[4] Globa L. et al.: Approach to Uniform Platform Development for the Ecology Digital Environment of Ukraine. Progress in Advanced Information and Communication Technology and Systems, 2022, 83–100, [http://doi.org/10.1007/978-3-031-16368-5].
[5] Karp B., Durban D.: Saint-Venant's Principle in Dynamics of Structures. Appl. Mech. Rev. 64(2), 2011 [http://doi.org/10.1115/1.4004930].
[6] Kittel C.: Introduction to Solid State Physics, 8th Edition. Wiley, 2004.
[7] Korn G. A., Korn T. M..: Mathematical Handbook for Scientists and Engineers: Definitions, Theorems, and Formulas for Reference and Review (Dover Civil and Mechanical Engineering), 2 Revised Edition. Dover Publications 2000.
[8] Kukharchuk V. et al.: Features of the angular speed dynamic measurements with the use of an encoder. Informatyka, Automatyka, Pomiary w Gospodarce i Ochronie Środowiska 12(3), 2022, 20–26.

[9] Levchuk S. A., Khmelnytskyi A. A.: Stress-strain state calculation procedure for compound technical objects using potential theory methods. Strength Mater., 47(5), 2015, 705–710 [http://doi.org/10.1007/s11223-015-9707-2].
[10] Lezhniuk P. et al.: The Sensitivity of the Model of the Process Making the Optimal Decision for Electric Power Systems in Relative Units. IEEE KhPI Week on Advanced Technology, 2020, 247–252.
[11] Misner Ch. W., Thorne K. S., Wheeler J. A.: Gravitation. Freeman, San Francisco 1973.
[12] Polishchuk L. et al.: Mechatronic Systems 2. Applications in Material Handling Processes and Robotics. Taylor & Francis Group, CRC Press, Balkema book, Boca Raton, London, New York, Leiden 2021 [http://doi.org/10.1201/9781003225447].
[13] Polzer G., Meissner F.: Grundlagen zu Reibung und Verschleiss. VEB Deutscher Verlag fur Grundstoffindustrie, Leipzig 1983.
[14] Skoog D. A., Leary J. J.: Principles of Instrumental Analysis, Fourth Edition. Saunders College Publishing, Fort-Worth, Philadelphia, San Diego, New York, Orlando, Austin, San Antonio, Toronto, Montreal, London, Sydney, Tokyo 1992.
[15] Tymchyk G. S. et al.: Distortion of Phantom Object's Realizations in Biological Presence Zone. IEEE 40th International Conference on Electronics and Nanotechnology – ELNANO 2020, 2020, 464–468.
[16] Tymchyk G. S. et al.: Distortion of geometric elements in the transition from the imaginary to the real coordinate system of technological equipment. Proc. SPIE 10808, 2018, 108085C [http://doi.org/10.1117/12.2501624].
[17] Tymchyk G. S. et al.: Forces balance in the coordinate system of object's existence 3D space. Proc. SPIE 12476, 2022, 124760U [http://doi.org/10.1117/12.2659188].
[18] Walker G.: Astronomical Observations: an optical perspective. Cambridge University Press, Cambridge 1987.
[19] Walsh A., Willis J. B.: Atomic Absorption Spectrometry. Standard Methods of Chemical Analysis 3A, 1966.
[20] Wójcik W. et al.: Mechatronic Systems I. Applications in Transport, Logistics, Diagnostics and Control. Taylor & Francis Group, CRC Press, Balkema book, London, New York 2021.

D. Sc. Eng. Gregory S. Tymchyk
e-mail: deanpb@kpi.ua

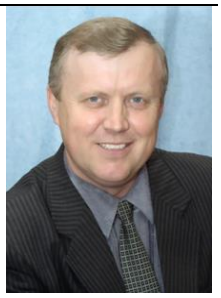

Professor, dean of Instrument Making Faculty, National Technical University of Ukraine "Sikorsky Kyiv Polytechnic Institute". Created a new class of laser spectral-correlation systems based on passive Fabry-Pierre resonators for operational control of quality parameters of parts and the condition of technological equipment in precision instrument manufacturing.

http://orcid.org/0000-0003-1079-998X

Ph.D. Volodymyr I. Skytsiouk
e-mail: max_sk@bigmir.net

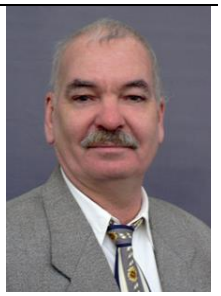

Senior Researcher, Instrument Making Faculty, National Technical University of Ukraine "Sikorsky Kyiv Polytechnic Institute". Scientific directions: These metrological aspects in the automatic mode of operation of object state analysis system determine the properties that increase the accuracy and speed of operations for calculating object movement trajectories in various fields of research.

http://orcid.org/0000-0003-1783-3124

Ph.D. Tatiana R. Klotchko
e-mail: t.klochko@kpi.ua

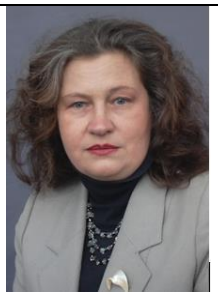

Senior Researcher, Instrument Making Faculty, National Technical University of Ukraine "Sikorsky Kyiv Polytechnic Institute". Scientific directions: These metrological aspects in the automatic mode of operation of object state analysis system determine the properties that increase the accuracy and speed of operations for calculating object movement trajectories in various fields of research.

http://orcid.org/0000-0003-3911-5369

D.Sc. Roman B. Akselrod
e-mail: akselrod.knuba@ukr.net

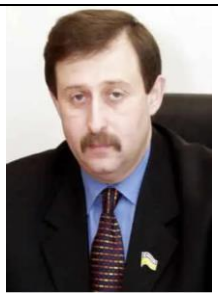

Doctor of Science, Vice-rector for academic work and regional development, Kyiv National University of Construction and Architecture, Kyiv, Ukraine.
Scientific directions are evaluation and forecasting of the efficiency of investments in entrepreneurial projects, in logistics and economic systems of various levels, in human capital. Deals with Financial instruments of international scientific and technical cooperation, modeling of the marketing business-processes under the industrial enterprise's competitiveness reflexive control, and modeling of the dialogue "human-computer" for ergonomic support of e-learning.

http://orcid.org/0000-0001-7643-7194

Ph.D. Valerii Yo. Shenfeld
e-mail: leravntu@gmail.com

Ph.D., Associate Professor, Associate Professor of department of Industrial Engineering of Vinnytsia National Technical University. Research Interests: development and research of new technology samples, in particular for vibration cutting and surface deformation strengthening of machine parts.

http://orcid.org/0000-0002-5548-6971

Ph.D. Aliya Kalizhanova
e-mail: kalizhanova_aliya@mail.ru

Candidate of physical and mathematical sciences, professor, Institute of Information and Computational Technologies CS MHES RK, Almaty, Kazakhstan, the chief researcher of the Institute of Information and Computational Technologies of the Ministry of Education and Science CS of the Republic of Kazakhstan. Scientific interests of the leader: mathematical modeling of systems, models of transport systems network analysis, optimization methods, technologies for developing sensor systems for signals receive - transmit, mathematical modeling of Bragg fiber gratings.

http://orcid.org/0000-0002-5979-9756

Ph.D. Didar Yedilkhan
e-mail: yedilkhan@gmail.com

Ph.D, associate professor at Astana IT University, Department of Computer Engineering. Research interests: Data science, Machine learning, Deep learning, Intelligent systems, optimization.

http://orcid.org/0000-0002-6343-5277

Ph.D. Gaukhar Borankulova
e-mail: b.gau@mail.ru

Candidate of Technical Sciences, Associate Professor, head of Chair department of "Information systems", Taraz Regional University M. Kh. Dulaty. Research area: Information systems, Big data.

http://orcid.org/0000-0001-5701-8074

http://doi.org/10.35784/iapgos.3497 *received: 13.02.2023 | revised: 14.03.2023 | accepted: 28.04.2023 | available online: 30.06.2023*

THEORETICAL AND EXPERIMENTAL SUBSTANTIATION OF THE EXTRACTION PROCESS WITH THINNING BIMETALLIC TUBULAR ELEMENTS OF DISSIMILAR METALS AND ALLOYS

Viacheslav Titov[1], Oleksandr Mozghovyi[2], Ruslan Borys[1], Mykola Bogomolov[1], Yedilkhan Amirgaliyev[3], Zhalau Aitkulov[4]

[1]National Technical University of Ukraine "Igor Sikorsky Kyiv Polytechnic Institute", Kyiv, Ukraine, [2]Vinnytsia Mykhailo Kotsiubynskyi State Pedagogical University, Vinnytsia, Ukraine, [3]Information and Computational Technologies CS MHES RK, Almaty, Kazakhstan, [4]Kazakh National Women's Teacher Training University, Almaty, Kazakhstan

Abstract. *The article proposes a scheme of the process of manufacturing bimetallic tubular elements by extraction a cylindrical cup of two dissimilar metals without thinning and extraction with thinning cup. At the same time, in the process of extraction in the heated state, the layers of dissimilar metals and alloys are connected and the desired shape of the product is obtained. A mathematical model of deformation of the process of joint extraction with thinning of two dissimilar metals with heating in a flat deformed state is developed. The influence of the deformation value on the dispersion of mechanical energy by bimetal was revealed.*

Keywords: deformation, bimetal tubular elements, stretching with thawing, dispersing of mechanical energy

TEORETYCZNE I EKSPERYMENTALNE UZASADNIENIE PROCESU CIĄGNIENIA Z PRZERZEDZANIEM BIMETALICZNYCH ELEMENTÓW RUROWYCH Z RÓŻNYCH METALI I STOPÓW

Streszczenie*. W artykule zaproponowano schemat procesu wytwarzania bimetalicznych elementów rurowych poprzez ciągnienie cylindrycznego kielicha z dwóch różnych metali bez przerzedzania i ciągnienie z przerzedzaniem kielicha. W procesie ciągnienia w stanie nagrzanym warstwy różnych metali i stopów są łączone i uzyskuje się pożądany kształt produktu. Opracowano matematyczny model odkształcenia procesu wspólnego ciągnienia z przerzedzaniem dwóch różnych metali z ogrzewaniem w płaskim stanie odkształconym. Ujawniono wpływ wartości odkształcenia na rozpraszanie energii mechanicznej przez bimetal.*

Słowa kluczowe: odkształcenie, bimetaliczne elementy rurowe, ciągnienie z przerzedzaniem, rozpraszanie energii mechanicznej

Introduction

Modern trends in the development of the engineering industry are characterized by increased requirements for the quality and performance of products while reducing the cost of their production. To ensure the effectiveness of engineering products in their designs are widely used various metals and alloys with high relative strength, as well as specific functional properties.

Bimetallic tubular elements (BTE) are used in the construction of high-tech engineering products for connecting pipelines of various metals such as aluminum, steel, titanium and others.

Methods of production of BTE are introduced in metallurgical and machine-building production and based on methods of molding and plastic deformation. They are focused on mass and large-scale production. They are economically advantageous to use in small-scale and single production. Methods based on high-energy processes of plastic deformation and diffusion welding, which can be implemented in small-scale production, require specific conditions of implementation and increased safety requirements [8, 12, 16].

The sharp competition of mechanical engineering products in the world market requires the mobility of production, and discrete unstable programs of production of products-production of their single copies. The mobility of production can be provided by using the universal equipment of machine-building enterprises, as well as by creating technologies for the manufacture of bimetallic tubular elements from traditional semi-finished products, such as sheet semi-finished metals and alloys, using non-complex die tooling methods of extraction [7, 14, 20].

1. Problem formulation

The aim of the work is to develop a method of control of the main parameters of working out the technological process of extraction with the refinement of dissimilar sheet materials, which ensure the quality of the connection in the conditions of machine-building enterprises.

2. The stress-strain state of the process of co-extrusion

In this paper, the authors solved the actual scientific and practical problem of improving the efficiency of manufacturing BTE in machine-building production by developing a control method at the stage of development of the technological process, which would allow to determine the parameters of the technological process of extraction with thinning, which ensure the quality (strength) of the connection and allows to predict the performance properties.

The basis of the work is the scientific idea of constructing the process of manufacturing bimetallic tubular elements from individual layers of sheet blanks by extraction with thinning in the heated state, which provides conditions for obtaining a given shape of the product and connecting the layers.

Based on the generalization of scientific publications, a typical scheme of the BTE manufacturing process was proposed, which includes pulling two dissimilar metals without thinning, pulling the cup with thinning in the heated state, followed by cutting the bottom part and removing individual layers of metals [1, 21, 22]. The use of pulling the cylindrical cup with thinning in the heated state provides a connection of layers of dissimilar metals and alloys.

For theoretical analysis of the process used by General equations of the theory of plastic flow in continuum mechanics, based on the specified kinematic model in the form of vector components of the speeds of movement of the metal particles in the deformation zone allow to determine the stress-strain state and energy-power parameters of process of deformation of layers of dissimilar metals subject to the conditions of compatibility of deformations in the limiting surface. To account for the interaction of layers of metals and working of the walls of the matrix and punch on the boundary surfaces is set to the value of the coefficient of friction, and the optimization of the velocity field is performed using the extreme principles of the theory of plastic deformations [2, 6, 9].

Structural changes that occur in the material during plastic deformation significantly affect the dispersion of mechanical energy. Various types of defects in metals and damages at the interface in the bimetal composition, arising during the process cycle of manufacturing BTE, correlated with losses of mechanical energy [2]. To study the effect of deformation on the loss of bimetal mechanical energy samples were made in the form of a rectangular plate width of 4 mm, the working length was 45 mm, one part of the sample cantilever clamped, and at the free end transverse vibrations of the audio frequency. Recording and calculations of the obtained parameters of free damped oscillations were carried out using computer programs Sound Forge i Damping [3, 4, 18].

Time dependences of frequency, amplitude and logarithmic decrement of oscillations were obtained. Spectral analysis by Sound Forge allows you to explore the fundamental frequency and overtones that are present in the recording. Spectrum analysis represents sound vibrations in the frequency domain – the number of oscillations of a certain frequency.

Created a special program Damping gives the opportunity: to carry out frequency analysis of a bandpass signal envelope is recorded with the program Sound Forge sweep time of the free mechanical oscillations of the investigated samples; calculate the logarithmic decrement of damping of vibrations according to one of the harmonics. To do this, the signal is sequentially divided into 2048 samples (about 0.05 seconds) and a fast Fourier transform is performed. The coincidence of the final and initial sample count is controlled. The conversion results are used to calculate the parameters of the total envelope of all harmonics of the sound range 20–20000 Hz, envelope of the frequency band of all harmonics specified by the operator: the value of the amplitude of the envelope of one harmonic, the frequency of the maximum harmonic in a given frequency band [11, 15].

The studied samples were subjected to bending deformation and alignment. One bend and alignment - one deformation cycle. Through 5, 10, 15 and 20 such cycles were measured parameters of free oscillations.

Theoretical analysis of extraction process with the thinning of the multilayer of metals is based on the process of pulling monometal [5, 8, 10] and joint deformation in metals is heterogeneous layers in the hearth of deformation. The first step is the analysis of the stress-strain state of the workpiece from monometallic (Fig. 1).

In the theoretical analysis of extraction with thinning, the following assumptions about the deformed state of the deformation center are accepted:

- the inner diameter of the workpiece wall does not change, and the outer at a significant ratio d/S has minor changes. This allows us to assume that the deformation is realized according to the scheme, which is close to the scheme of plane deformation. Therefore, the velocity of the material particles in the circumferential direction is zero [8, 14];
- we believe that in the deformation zone the radial velocities of the material particles depend on the radial coordinate r and do not depend on the cell coordinate θ.

Then, in general, the components of the velocity vector of the material particles have the form:

$$V_r = V_r(r);\ V_\theta = 0;\ V_z = 0 \tag{1}$$

By integrating (1) together with the condition of compatibility of deformations and the boundary condition that $r = R_B$ the velocity component of deformations $V_r = V_0$, where V_0 – the velocity of movement of material particles, which is equal to the velocity of the punch, is obtained:

$$V_r = \frac{V_0 R_B}{r};\ V_\theta = 0;\ V_z = 0 \tag{2}$$

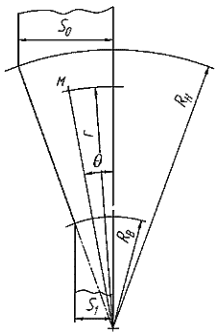

Fig. 1. Calculation scheme of deformation of a monometal in the center of deformations

The speed of deformation is determined by differentiation of the velocity for the respective coordinate:

$$\varepsilon_{rr} = -\frac{V_0 R_B}{r^2};\ \varepsilon_{\theta\theta} = \frac{V_0 R_B}{r^2};$$
$$\varepsilon_{zz} = \varepsilon_{\theta z} = \varepsilon_{zr} = \varepsilon_{r\theta} = 0. \tag{3}$$

To determine the component of the stress tensor used in equation of the relationship between the deviators of stress D_σ and D_ε strain rate:

$$D_\sigma = \frac{2}{3}\frac{\sigma_i}{\varepsilon_i} D_\varepsilon \tag{4}$$

where ε_i and σ_i – accordingly, the intensity of strain rates and stresses.

We believe that the metal workpiece is ideally plastic that the process is performed under hot (isothermal) plastic deformation $\sigma_i = \sigma_s$.

The average voltage II is determined from the equation proposed by Yu.M. Alekseev:

$$grad\sigma = -\frac{2}{3} div\left(\frac{\sigma_i}{\varepsilon_i} T_\varepsilon\right) \tag{5}$$

where T_ε – strain rate tensor.

Taking into account the limiting condition, at $r = R_H$, $\sigma_{rr} = 0$, the stress tensor components have the form:

$$\sigma_{rr} = \frac{2}{\sqrt{3}}\sigma_S \ln\frac{R_H}{r}$$
$$\sigma_{\theta\theta} = -\frac{2}{\sqrt{3}}\sigma_S\left(1 - \ln\frac{R_H}{r}\right) \tag{6}$$
$$\sigma_{zz} = \frac{2}{\sqrt{3}}\sigma_S \ln\frac{R_H}{r} - \frac{\sigma_S}{\sqrt{3}}$$

The obtained results are used for theoretical analysis of two-layer metal extraction.

The kinematic feature of the deformation of a two-layer metal is that at the exit of the deformation center at $r = R_B$ due to the different mechanical properties of the layers, the ratio of the metal thickness changes. This leads to the fact that the limiting surface in the deformation zone is rotated by a certain angle relative to the radial direction (Fig. 2). As a result, the calculated radii of the layers are changed.

When calculating the thickness of the layers after extraction, the physical condition of the joint deformation of the layers in the deformation cell is taken into account-the equality of the tangential stresses normal to the limit surface $\sigma_{\theta\theta_I} = \sigma_{\theta\theta_{II}}$, and also taken into account the relationship of individual layers S_{1B} and S_{2B} at the output of the deformation cell dependence $S_{2B} = S_K - S_{1B}$, where S_K – the total thickness of the workpiece wall after extraction, which is determined by the design of the matrix. The result is an equation for determining the thickness of the first layer [1, 11, 12]:

$$S_{1B} = S_K - e^{A-1} S_{2H}\left(\frac{S_{1B}}{S_{1H}}\right)^A \tag{7}$$

where $A = \sigma_{S_1} / \sigma_{S_2}$ – coefficient of mechanical heterogeneity of two-layer metal.

Velocity fields for both layers:

$$V_{r_i} = \frac{V_0 \dfrac{S_{iB}}{S_{iH} - S_{iB}} (S_{0H} - S_{0k}) ctg\alpha}{r}; \; V_\theta = 0; \; V_z = 0 \tag{8}$$

where i – the index of the layer of metal.

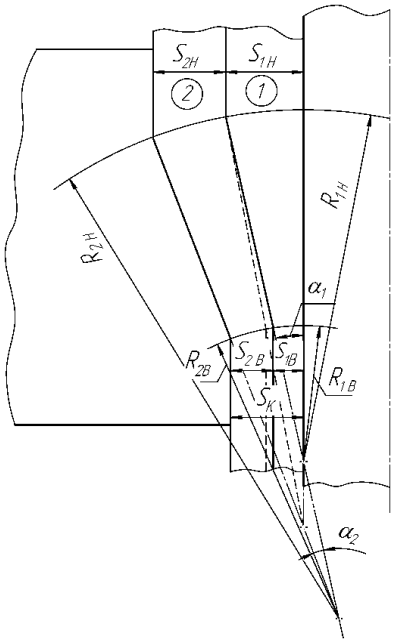

Fig. 2. Scheme of deformation of a two-layer metal in the center of deformations

Components of strain rates in the radial direction for the first and second layers:

$$\varepsilon_{rr_i} = -\frac{V_0 \dfrac{S_{iB}}{S_{iH} - S_{iB}} (S_{0H} - S_{0k}) ctg\alpha}{r^2}$$

$$\varepsilon_{\theta\theta_i} = \frac{V_0 \dfrac{S_{iB}}{S_{iH} - S_{iB}} (S_{0H} - S_{0k}) ctg\alpha}{r^2} \tag{9}$$

$$\varepsilon_{zz} = \varepsilon_{\theta z} = \varepsilon_{zr} = \varepsilon_{r\theta} = 0$$

The components of the stress tensor:

$$\sigma_{rr_i} = \frac{2}{\sqrt{3}} \sigma_{S_i} \ln \frac{\dfrac{S_{iH}}{S_{iH} - S_{iB}} (S_{0H} - S_{0k}) ctg\alpha}{r}$$

$$\sigma_{\theta\theta_i} = -\frac{2}{\sqrt{3}} \sigma_{S_i} \left(1 - \ln \frac{\dfrac{S_{iH}}{S_{iH} - S_{iB}} (S_{0H} - S_{0k}) ctg\alpha}{r} \right) \tag{10}$$

$$\sigma_{zz_i} = \frac{2}{\sqrt{3}} \sigma_{S_i} \ln \frac{\dfrac{S_{iH}}{S_{iH} - S_{iB}} (S_{0H} - S_{0k}) ctg\alpha}{r} - \frac{\sigma_{Si}}{\sqrt{3}}$$

Kinematic dependences (8) make it possible to calculate the distribution of the radial velocity difference ΔV_r at the interface of the layers along the deformation zone, the length of which is determined by the coordinate r. It is shown that:

- the maximum difference in the rates of movement is observed at the entrance of metals to the deformation site;
- layer which has a lower boundary of turnover, ahead of the layer with greater border strength, due to the fact that it thins to a greater extent [13, 14, 15];
- at the output of the deformation cell, the velocity of the layers is aligned [16, 17].

3. Calculation of the parameters of the extraction process with thinning taking into account friction on the boundary surfaces

It is shown that taking into account the friction forces on the boundary surfaces of the layers provides a more accurate solution. For this purpose, the analysis of the energy-power parameters of extraction with with thinning, taking into account the friction forces on the boundary surfaces using the method of power balance.

The power balance equation for the deformation center of each layer has the following form:

$$N_{\sigma_{z_i}} = N_{mp} + N_{mp}^{мс} + N_{\sigma_{ri}} + N_{\sigma_{\theta_i}} + N_{\tau_{r\theta_i}} + N_{R_{iH}}^{зс} + N_{R_{iB}}^{зс} \tag{11}$$

When solving the equation (11), the friction forces are taken into account by the friction coefficient according to the Amonton-Coulomb law on the boundary surfaces of the workpiece with the matrix – μ_3, and a punch – μ_1, and between the layers of the workpiece – μ_2. Then the total deformation power of both layers is determined by the dependence:

$$\begin{aligned} N_{\sigma_z} = {} & \frac{2}{\sqrt{3}} \sigma_{S_1} \alpha_1 V_0 \left[\mu_2 \left(1 - \ln \frac{S_{1H}}{S_{1B}} \right) \frac{(S_{0H} - S_{0k}) ctg\alpha}{S_{1B}} - \right. \\ & - \mu_1 \left(1 - \ln \frac{S_{1H}}{S_{1B}} \right) \frac{(S_{0H} - S_{0k}) ctg\alpha}{S_{1B}} + \\ & \left. + \frac{S_{1B}}{S_{1H}} + \ln \frac{S_{1H}}{S_{1B}} \right] + \frac{2}{\sqrt{3}} \sigma_{S_2} \alpha_2 V_0 \\ & \left[\mu_3 \left(1 - \ln \frac{S_{2H}}{S_k - S_{1B}} \right) \frac{(S_{0H} - S_{0k}) ctg\alpha}{S_k - S_{1B}} - \mu_2 \times \right. \\ & \left. \times \left(1 - \ln \frac{S_{2H}}{S_k - S_{1B}} \right) \frac{(S_{0H} - S_{0k}) ctg\alpha}{S_k - S_{1B}} + \frac{S_{1B}}{S_{1H}} + \ln \frac{S_{2H}}{S_k - S_{1B}} \right] \end{aligned} \tag{12}$$

Equation (12) makes it possible to determine the unknown thickness of the first layer taking into account the extreme energy principles of plastic deformation S_{1B} after extraction. Its determination is made by minimizing the power of the process:

$$\frac{\partial N_{\sigma_z}}{\partial S_{1B}} = 0 \tag{13}$$

Equation (13) is solved by a numerical method of simple iterations. Comparison of the calculation results of the layer thickness with a lower yield point when pulling with the thinning of the workpiece with the initial (S_{0H} = 2.8 mm, S_{1H} = S_{2H} = 1.4 mm) and final S_k = 1.12 mm the thickness of the layers (Fig. 3) shows that when taking into account the forces of friction thinning is manifested to a greater extent than without taking into account the forces of friction. The calculation error does not exceed 10...11%.

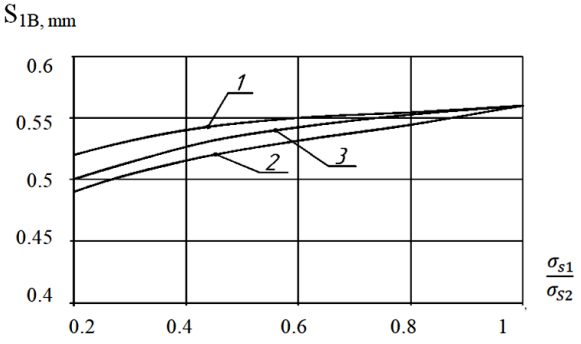

Fig. 3. Comparison of the thickness of the metal layer having a lower yield strength from the coefficient of mechanical heterogeneity: 1 – excluding friction forces; 2 – taking into account friction forces; 3 – experiment

The General solution (13) with the system of equations (8) – (10) allows analyzing the stress-strain state, kinematic and energy-force parameters of the pulling process taking into account the friction forces [18, 19].

The stability of the extraction process with thinning is limited by the destruction of one of the layers of the part due to the achievement of the critical value of the accumulated shear deformation in the deformation zone, which is determined by the use of (9). Taking into account the constancy of the stress state scheme in the established process of stretching, using the V. L. Kolmogorov criterion, a functional is constructed, the minimization of which allowed to determine the maximum degree of wall compression during the process:

$$\Phi = \left| \ln \frac{\sqrt{3}\int_0^i [\varepsilon_i(r,\varphi,z,t)\mu]dt}{\Lambda\ (\Pi_\sigma)} \right| = 0 \qquad (14)$$

4. The effect of amount of deformation on the dissipation of the mechanical energy bimetal

In determining the overall strength of bimetal $\sigma_б$ along the connection plane of the components can be used a simplified representation of the theory of combined action, according to which each component makes an independent contribution to the overall strength:

$$\sigma_б = \sigma_1 V_1 + \sigma_2 V_2, \qquad (15)$$

where σ_1, σ_2 – strength of the first and second components of bimetal, V_1, V_2 – accordingly, their volume content.

With a slight deformation, each component is deformed elastically. The modulus of elasticity of the bimetal ($E_б$) it can be determined according to the law of additivity:

$$E_б = E_1 V_1 + E_2 V_2. \qquad (16)$$

The bond strength at the interface of two metals should be sufficient for their joint deformation.

But the rule of additively does not take into account many factors that can change the properties of bimetal in one direction or another. External load during deformation can cause blocking of dislocations, which increases the strength of the material. The formulas (15) and (16) and the method of their preparation do not take into account the presence of the boundary between the two metals. Bimetal with a developed transition zone can be considered as a three-component and four-component system. In this case, the volume content of the system is represented by the expression:

$$V_1 + V_2 + V_{TZ} = 1 \qquad (17)$$

where V_{TZ} – volume content of the transition zone. Then equation (15) in the first approximation takes the form:

$$\sigma_б = \sigma_1 V_1 + \sigma_2 V_2 + \sigma_{TZ} V_{TZ} \qquad (18)$$

where σ_{TZ} – the strength of the transition zone between the components of bimetal. The use of (15) and (18) makes it possible to theoretically predict the strength of the bimetal.

It is difficult to determine experimentally the size of the transition zone and the strength of the connection of the two components of bimetal. The use of the structure-sensitive non-destructive method of internal friction in the work allowed establishing the nature of changes in the physical and mechanical characteristics of the transition zone, the components of the bimetal and the strength of their connection under the influence of external influences. Analysis of the magnitude of the defect at the border of the two metals in size and nature of the dispersion of mechanical energy system is promising in determining the optimal technological modes of manufacture of finished parts [16, 21].

Given the integral nature of internal friction, for complex structures it can be written that $Q^{-1} = \sum_{i=1}^{n} Q_i^{-1} + Q_{LZ}^{-1}$, where Q^{-1} – losses of mechanical energy by the structure as a whole, Q_i^{-1} – loss of mechanical energy in each metal that is part of the structure; Q_{LZ}^{-1}- loss of mechanical energy in the transition zone. For bimetal compounds between metals may have a different number of defects: from contact, when metals have a very small number of defects at the junction, to a simple clamp to each other with the possibility of slippage. However, such a structure loses its physical and mechanical properties as bimetal.

During the study, the losses of mechanical energy on the samples that were not deformed and on the samples subjected to different numbers of deformation cycles were determined. The obtained graphs of damped oscillations are presented in Fig. 4.

The analysis of the results shows that in the process of deformation in the material there are damages in the form of vacancies and dislocations, and on the border of the two metals may appear makrocracks. The existing damage had little effect on the graphs of damped oscillations and slight changes in the spectral analysis were observed. Harmonics with frequencies 756 Hz, 4642 Hz, 6340 Hz are observed on all charts. With an increase in the number of harmonic deformation cycles with frequencies of 1820 Hz and 2740 Hz are observed, respectively, at lower frequencies of 1676 Hz and 2658 Hz. After 15 deformation cycles, harmonics appeared at frequencies of 3360 Hz. On the graph without deformations observed harmonic frequency 10349 Hz and increasing the number of deformation cycles frequency (up to 10922 Hz) and its intensity increases (table 1).

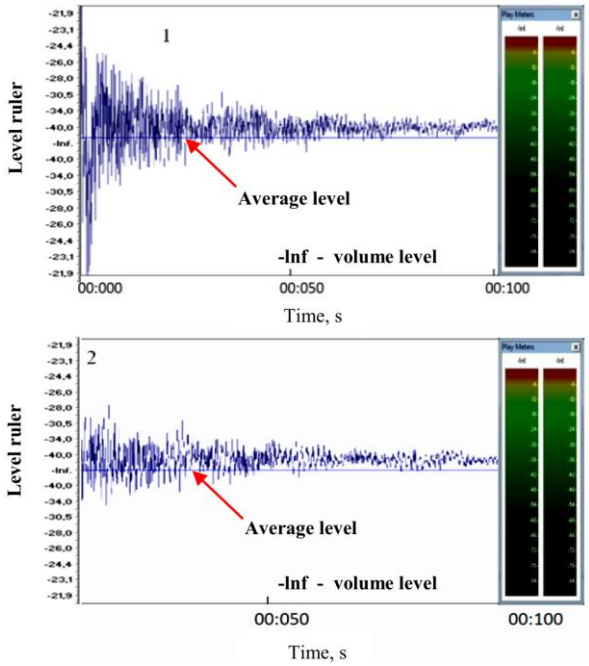

Fig. 4. Experimental studies of bimetal: graphs of free damped oscillations of cantilever clamped samples: 1 – without deformation; 2 – deformation of 50 deformation cycles; spectral analysis of free damped oscillations of samples

Table 1. Changing the frequency of harmonics with increasing number of deformation cycles of the bimetallic strip

Frequency, Hz	0 cycles	5 cycles	15 cycles	30 cycles	50 cycles
0 ÷ 1000	756	756	756	756	756
1000 ÷ 2000	1820	1799	1676		1676
2000 ÷ 3000	2740	2617	2679	2658	2556
3000 ÷ 4000			3292	3364	3313
4000 ÷ 5000	4867	4642	4642	4642	4642
5000 ÷ 6000		5460		5215	5236
6000 ÷ 7000	6565	6361	6340	6340	6299
10000 ÷ 11000	10349	10595		10902	10922

The Damping program made it possible to determine the logarithmic decrement of attenuation, oscillation frequency and amplitude change in the process of vibration damping. The nature of the amplitude decrease from the beginning of attenuation is the same (Fig. 5), but different decay rate. Rapid attenuation of vibrations occurs at the greatest deformation.

Fig. 5 shows that the damping of the oscillations occur with oscillations, on the parameters which affects the amount of deformation cycles.

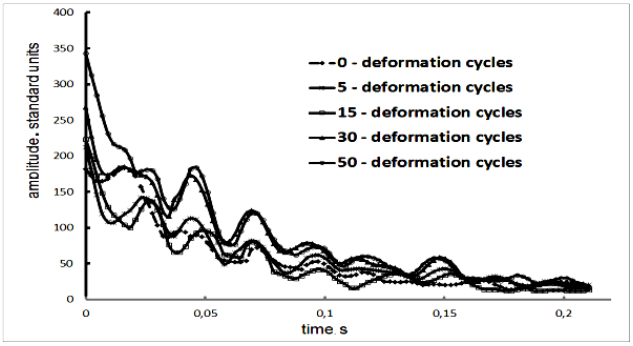

Fig. 5. Graphs of changes in the amplitude of free oscillations of a deformed aluminum-steel bimetal with different amounts of deformation

5. Conclusions

1. The actual scientific and practical task of increase of efficiency of production of bimetallic tubular elements in machine-building production is proved and solved – for the first time on the basis of generalization of results of the analysis of scientific publications the idea is offered, the machine-building concept of process of production of bimetallic tubular elements from separate sheet dissimilar metals is developed, theoretically and experimentally proved with a thinning in the heated state which is based on the existing theories of diffusion connection of dissimilar metals by realization of conditions of joint deformation, pressure, heating on their boundary surfaces.

2. A complex method of theoretical and experimental study of the process of pulling with thinning of a two-layer billet of dissimilar metals is developed. Evaluation of the stress-strain state and energy-force parameters of the process in the deformation zone is performed using the theory of plastic flow in deformation and the basics of the theory of composite materials in the interaction of layers of dissimilar metals on the limiting surface, as well as extreme energy principles of plastic deformation taking into account the friction forces. The substantiation of analytical results and results of numerical modeling is carried out with the help of full-scale experiment with the use of standardized methods on the certified equipment.

3. Using the theory of plastic flow, a mathematical model of deformation of the process of joint pulling with thinning of two dissimilar metals with heating under conditions of flat deformed state was developed, which allowed to establish the relationship between the parameters of the stress-strain state on the limiting surface and the degree of deformation of thin layers with the initial geometric parameters of the workpiece, the mechanical properties of individual layers and the geometry of the working surface of the matrix. It is shown that the error does not exceed 10 for calculating the thickness of layers with an ideal plastic model of metals...14% in relation to experimental data. The use of extreme energy principles of deformation, taking into account the friction forces on the boundary surfaces, has improved the accuracy of determining the thickness of the layers after deformation to 10...11%.

4. As a result of numerical simulation of the process in the CAD / CAE ANSYS and DEFORM-3D system, it is found that for pulling with a degree of deformation, the thinning is 50% for the bimetal of the aluminum+titanium system with a minimum coefficient of friction (μ=0,01) the maximum values of the pulling force do not differ significantly, and when μ= 0.3 there is an increase in the force as well as the work of pulling while reducing the taper angle of the matrix from 10º to 4º by 45...47%. The value of radial stresses on the limiting surface of the layers increases in proportion to the degree of compression, and their maximum value corresponds to the zone close to the output of the matrix and increases with decreasing taper angle of the matrix. In this case, the thinning of the layers depends on the coefficient of mechanical heterogeneity of metals. It is shown that the main obtained regularities of deformation qualitatively and quantitatively with a sufficient degree of accuracy coincide with the results of the calculation of two-layer billets with other mechanical properties, for example, aluminum+brass, aluminum+stainless steel systems and others.

5. Based on the analysis of the stress-strain state and the kinematic interaction, it is found that conditions are created in the deformation zone of the layers that contribute to the diffusion connection of the layers:

- maximum compressive stress on the limiting surface of the layers reaches the boundary of the metal layer flow with less mechanical properties;
- the difference between the axial deformations of the layers, as well as the presence of shear deformations in the interaction of layers on the limiting surface provide the destruction of oxide films, which contributes to the interaction of layers;
- in the zone close to the exit of the matrix, the difference between the movement of the material layers on the limiting surface is reduced to zero;
- the presence of heating layers to the activation temperature contributes to their interaction.

6. On the basis of analytical and numerical results, a constructive and technical solution for the use of an additional angle is proposed β = 1º…2º at the exit of the cone matrix with the base angle α = 7º, this provided a more effective effect of radial compressive stresses on the limiting surface due to the uniformity of their application and increasing the interaction time of the layers. It is also shown that the time of finding the layers in the deformation zone can be effectively guided by the rate of extraction and the length of the deformation zone.

7. The main scientific results obtained by analytical and numerical calculations are experimentally confirmed. It is shown that the maximum error of calculation of power parameters does not exceed 7...10%, the advance of the layer with a lower yield strength does not exceed 9...11%, the deformation layer thickness after extraction with thinning does not exceed 10...14% for the different coefficients of mechanical anisotropy of metals.

In experimental conditions typical BTE were obtained, metallographic analysis of which showed the interaction of layers. Evaluation of the strength of the layers showed that it reaches 80...85% of the shear stress for the alloy with lower yield stress.

8. The influence of the damage value of the material on the dispersion of mechanical energy is revealed: the nature of the course and the type of curves of free damped oscillations in the sound range are changed; the frequency of low-frequency harmonics is changed and does not change for high frequencies; the decay rate is changed.

References

[1] Aliieva L., Zhbankov Y. Radial-direct extrusion with a movable mandrel. Metallurgical and Mining Industry 11, 2015, 175–183.
[2] Alekseev Yu. N.: Questions of plastic flow of metals. Publishing house of the KhSU, Kharkov 1958.
[3] Borys R., Titov V.: Ensuring the quality of the connection of layers from different metals in the manufacture of bietallic tubular elements by drawing. Mechanics and Advanced Technologies 1(85), 2019, 63–70 [http://doi.org/10.20535/2521-1943.2019.85.162508].
[4] Hedayatia O., Koreia N., Adelia M., Etminanbakhshb M.: Microstructural evolution and interfacial diffusion during heat treatment of Hastelloy/stainless steel bimetals. Journal of Alloys and Compounds 712, 2017, 172–178.
[5] Inoue J., Nambu S., Ishimoto Y., Koseki T.: Fracture elongation of brittle/ductile multilayered steel composites with a strong interface. Scripta Materialia 59, 2008, 1055–1058.
[6] Kalyuzhnyi V. L., Aliieva L. I., Kartamyshev D. A., Savchinskii I. G.: Simulation of Cold Extrusion of Hollow Parts. Metallurgist 61, 2017, 359–365.

[7] Lebedev A. O.: Methods and results of the processes of accumulation of damage in metallic materials under different load conditions. Bulletin of NTUU "KPI". Mechanical engineering 44, 2003, 42–57.
[8] Limberg, E. A. Selivanov G. D.: Determination of the specific pressure of filling the fillet radii in the tool for forging of. Metal forming in engineering 17, 1981, 22–27.
[9] Polishchuk L., Mamyrbayev O., Gromaszek K.: Mechatronic Systems II. Applications in Material Handling Processes and Robotics. Taylor & Francis Group, CRC Press, Balkema book, Boca Raton, London, New York, Leiden 2021.
[10] Tallafuss P., Johnston J.: Defects, causes and prevention controls in the continuous bronze/steel bimetal strip sintering process. Engineering Failure Analysis 92, 2018, 34–43.
[11] Shulga M., Krivov G., Fedorenko Yu., Titov V., Akimov V.: Modeling and calculation of structural elements made of heterogeneous materials. Technology, 1996.
[12] Springer H., Kostka A., Payton E. J., Raabe D., Kaysser-Pyzalla A., Eggeler G.: Onthe formation and growth of intermetallic phases during interdiffusion between lowcarbon steel and aluminum alloys. Acta Mater. 59, 2011.
[13] Springer H., Szczepaniak A., Raabe D.: On the role of zinc on the formation and growth of intermetallic phases during interdiffusion between steel and aluminium alloys. Acta Mater. 96, 2015.
[14] Titov V. A.: The influence of diamond smoothing the surface of the steels on the mechanical energy dissipation. Ttov V. A., Mozgovy O. V.: Bulletin of National Technical University of Ukraine "Kyiv Polytechnic Institute". Engineering 54, 2008.
[15] Viala J. C., Peronnet M., Barbeau F., Bosselet F., Bouix J.: Interface chemistry in aluminium alloy castings reinforced with iron base inserts. Composites Part A: Applied Science and Manufacturing 33(10), 2002, 1417–1420 [http://doi.org/10.1016/S1359-835X(02)00158-6].
[16] Wójcik W., Pavlov S., Kalimoldayev M.: Mechatronic Systems I. Applications in Transport, Logistics, Diagnostics and Control. Taylor & Francis Group, CRC Press, Balkema book, London, New York 2021.
[17] Wang T. M., Liang C. H., Chen Z. N., Zheng Y. P., Kang H. J., Wang W.: Development of an 8090/3003 bimetal slab using a modified. J. Mater. Process. Technol. 214, 2014, 347–352.
[18] Wenming Jiang, Guangyu Li, Yao Wu, Xinwang Liu: Zitian Fan Effect of heat treatment on bonding strength of aluminum/steel bimetal produced by a compound casting. Journal of Materials Processing Technology 258, 2018 [http://doi.org/10.1016/j.jmatprotec.2018.04.006].
[19] Xu W. C., Zhang Z. P., Huang K., Shan D. B.: Effect of heat treatment and initial thickness ratio on spin bonding of 3A21/5A03 composite tube. J. Mater. Process. Technol. 247, 2017, 143–157.
[20] Zhbankov I., Perig A., Aliieva L.: Calculation of recovery plasticity in multistage hot forging under isothermal conditions. Springer Plus 69, 2016, 174–180.
[21] Zhbankov I. G., Perig A. V., Aliieva L. I.: New schemes of forging plates, shafts and discs. Int. J. of Advanced Manufacturing Technology 82, 2015, 287–301 [http://doi.org/10.1007/s00170-015-7377-7].
[22] Zhou Li et al.: Analysis of bending characteristics of bimetal steel composite. International Journal of Mechanical Sciences 148, 2018 [http://doi.org/10.1016/j.ijmecsci.2018.08.032].

Prof. Viacheslav Titov
e-mail: vat.kpi@gmail.com

D.Sc., professor of the Department of Aircraft Production Technology, National Technical University of Ukraine «Igor Sikorsky Kyiv Polytechnic Institute», Kyiv, Ukraine.
Resource-saving technologies for diagnosing the technical condition, ensuring the resource and operational reliability of mechanical engineering products by technological methods.

http://orcid.org/0000-0002-4234-6961

Ph.D. Olexandr Mozghovyi
e-mail: mavimfto@gmail.com

Ph.D., associate professor of the Department of the Physics and methods of teaching physics, astronomy Vinnytsia Mykhailo Kotsiubynskyi State Pedagogical University.
Research Interests: surface engineering, mechanical spectroscopy, composite materials with metal and polymer matrices.

http://orcid.org/0000-0002-0797-8779

Ph.D. Ruslan Borys
e-mail: boris_ryslan@ukr.net

Ph.D., associate professor of the Department of Aircraft Production Technology, National Technical University of Ukraine «Igor Sikorsky Kyiv Polytechnic Institute», Kyiv, Ukraine.
Scientific interests: manufacturing technologies of composite materials, extraction of bimetallic tubular elements from dissimilar metals and alloys.

http://orcid.org/0000-0002-4098-1013

Ph.D. Mykola Bogomolov
e-mail: nbogom@yahoo.com

Candidate of Technical Sciences, Associate Professor of the Department of Biomedical Engineering of National Technical University of Ukraine "Ihor Sikorsky Kyiv Polytechnic Institute".
Head of the Scientific and Educational Laboratory of Laser Medicine.
Research interests: laser medicine, fiber-optic sensors, laser diagnostic equipment, optoelectronic rehabilitation equipment.

http://orcid.org/0000-0002-4351-527X

Prof. Yedilkhan Amirgaliyev
e-mail: amir_ed@mail.ru

Doctor of technical sciences, professor, head of the Laboratory of Mathematical and Computer Modeling of the Institute of Information and Computational Technologies CS MHES RK. The Institute is the leading organization in the field of information technology in the country.

The main directions of the research laboratory is an intelligent decision-making systems, robotics, wireless sensor technology, computer modeling of technological processes, etc.

http://orcid.org/0000-0002-6528-0619

M.Sc. Zhalau Aitkulov
e-mail: zh.aitkulov@alt.edu.kz

Doktorant Ph.D. on a specialty "Information Systems", a programmer at the Information and Computational Technologies CS MHES RK, Kazakh National Women's Teacher Training University.
Research interests: mathematical modeling of discrete systems, evacuation tasks, operations research, technology design of complex systems.

http://orcid.org/0000-0002-5928-3258

http://doi.org/10.35784/iapgos.3459 *received: 23.01.2023 | revised: 27.02.2023 | accepted: 12.03.2023 | available online: 30.06.2023*

THE APPLICATION OF MACHINE LEARNING ON THE SENSORS OF SMARTPHONES TO DETECT FALLS IN REAL-TIME

Achraf Benba[1], Mouna Akki[1], Sara Sandabad[2]
[1]Mohammed V University in Rabat, Ecole Nationale Supérieure d'Arts et Métiers, Electronic Systems Sensors and Nanobiotechnologies, Rabat, Morocco, [2]Hassan II University of Casablanca, Ecole Normale Supérieure de l'Enseignement Technique de Mohammadia, Electrical Engineering and Intelligent Systems, Casablanca, Morocco

Abstract. *With the increasing prevalence of smartphones, they now come equipped with a multitude of sensors such as GPS, microphones, cameras, magnetometers, accelerators, and more, which can simplify our daily lives. When it comes to healthcare, smartphones can become indispensable. The detection of geriatric falls is crucial as even the slightest injury can have fatal consequences. Therefore, we proposed the use of accelerometers in our research to detect falls in the elderly. Our project involved the development of an automated, continuous, and reliable monitoring system that would generate a list of elderly people at risk of falling and present it on a webpage for emergency services. This approach aimed to minimize the long-term impacts and save lives promptly. We started by developing a mobile application and used MATLAB to classify the falls as either "fall" or "not fall." Finally, we created a webpage that would facilitate communication between the mobile application and MATLAB.*

Keywords: fall detection, smartphone accelerometers, SVM, KNN, machine learning

ZASTOSOWANIE UCZENIA MASZYNOWEGO NA CZUJNIKACH SMARTFONÓW DO WYKRYWANIA UPADKÓW W CZASIE RZECZYWISTYM

Streszczenie. *Wraz z rosnącą popularnością smartfonów są one wyposażone w wiele czujników, takich jak GPS, mikrofony, kamery, magnetometry, akceleratory i inne, które mogą uprościć nasze codzienne życie. Jeśli chodzi o opiekę zdrowotną, smartfony mogą stać się niezastąpione. Wykrywanie upadków geriatrycznych ma kluczowe znaczenie, ponieważ nawet najmniejszy uraz może mieć śmiertelne konsekwencje. Dlatego zaproponowano wykorzystanie w naszych badaniach akcelerometrów do wykrywania upadków osób starszych. Nasz projekt polegał na opracowaniu zautomatyzowanego, ciągłego i niezawodnego systemu monitoringu, który generowałby listę osób starszych zagrożonych upadkiem i prezentował ją na stronie internetowej służb ratowniczych. Podejście to miało na celu zminimalizowanie długoterminowych skutków i szybkie ratowanie życia. Rozpoczęto od opracowania aplikacji mobilnej i za pomocą MATLABa sklasyfikowano upadki jako „upadek" lub „nie upadek". Ostatecznie stworzono stronę internetową, która ułatwiłaby komunikację między aplikacją mobilną a MATLABem.*

Słowa kluczowe: detekcja upadku, akcelerometry smartfonów, SVM, KNN, uczenie maszynowe

Introduction

The World Health Organization's "OMS" reports that falls are a significant global public health issue. Falls are the second biggest cause of accidental fatality after injuries from motor accidents, with an estimated 684,000 fatalities per year. Over 80% of fatal falls have place in developing and middle-income nations. Around the world, those over 60 have the highest death rates. Even when they are not fatal, over 37.3 million falls annually are severe enough to necessitate medical attention [16].

One of the most significant risk factors for falls is age. The danger of dying or receiving serious injuries from falls increases with age for older adults. For instance, 20–30% of senior individuals who fall in the United States get moderate to serious injuries, such as contusions, hip fractures, or head damage. This level of risk might be affected by age-related physical, sensory, and cognitive changes as well as environments that are not designed for an aging population. Seniors who fall frequently get disoriented and unable to stand up or walk independently [12]. Falls can happen indoors or outside. Here, prolonged lying after a fall can result in serious injuries and is the main cause of post-accident death and chronic disorders. To stop chronic effects from occurring after a fall and to save the elderly in a timely manner, a monitoring system that is automated, continuous, and dependable is required. Therefore, it's essential to provide fall detection and remote monitoring rescue alternatives.

The most significant risk factors were a history of falls, balance and gait issues, and a number of medications. Older age, being a woman, having eye issues, diminishing cognitive function, particularly issues with attention and execution, and environmental effects are additional risk factors [8]. Smartphones have grown in importance in contemporary society as a result of their cutting-edge features, cutting-edge technology, and a variety of sensors that may be applied to the healthcare industry. Smartphones are a really portable computer that anybody can own and carry with them wherever. Anyone who falls will frequently land on the ground or another lower surface. Occasionally, a body part strikes something and arrests the fall. They stand a genuine risk of falling when they live alone or in specialized facilities, which is regrettable given how much a fall may impair a senior's freedom. The leading cause of death for elderly individuals is falling. Over the age of 65, falls account for 80% of incidents in daily life, according to the 2016 issue of the Permanent Survey of Accidents in Everyday Life (EPAC) [1]. Our concept employs smartphone accelerometer sensors to quickly react when an elderly person falls in order to save the elderly person who lives alone in residential or hospital units.

1. Database acquisition

Any issue requiring remote monitoring of fall occurrences is covered by the provided approach [3, 9, 11]. Numerous recordings of interested subjects participating in various activity types are needed for the robust development and testing of fall detection algorithms. The SisFall dataset is selected in this instance since it provides data from 38 people (15 elderly and 23 youth). It contains diverse activity data from 19 commonplace tasks and 15 unique fall tasks, all of which were performed repeatedly during intervals of 12 to 100 seconds. SisFall data were recorded using two accelerometers, a gyroscope, and a 200 Hz sampling rate [14, 15]. In this investigation, only data from one accelerometer was used. Real-time remote monitoring of falls was done in two different scenarios: fall (F – Falls) and non fall (D – Activities of daily living ADL). We focus on the prevalence of falls among the elderly rather than the minutiae of daily routines or fall types in our work.

2. Methodology

Wearable technology is the most suitable, efficient, and aesthetically appealing solution for continuous monitoring, regardless of where the individual is or how they are positioned. Additionally, compared to ambient or camera-based systems, wearable technology is less expensive, more efficient, and less intrusive. Each person's smartphone serves as the wearable device in our approach, thus there is no additional cost.

Our project will be finished in three stages.

The three-axis accelerometer on the elderly person's smartphone is being utilized to gather information. This software sends user data and accelerometer parameters to a web page.

We created a website that would record user information and provide files for each user that contained the accelerometer's x, y, and z properties in real-time.

The website calculates the various qualities.

MATLAB emails the user repeatedly asking for these derived characteristics in order to categorize the data.

The instances (fall and not fall) are put together into a database that will be used and processed to classify the subjects based on their attributes, leading to a decision that will be delivered by MATLAB to the web page. In order to act quickly and save older people in the case of a fall, the latter compiles a registry of older people who have fallen. This stage has been completed at the level of a portable computer. The aim of this work is to investigate and create a system that can quickly detect the presence of a fall using machine learning methods. The information is continuously captured using a smartphone with a triaxial accelerometer. Our project's classes are described (fall and not fall). The organizational structure of the algorithm used in our system is shown in figures 1 and 2.

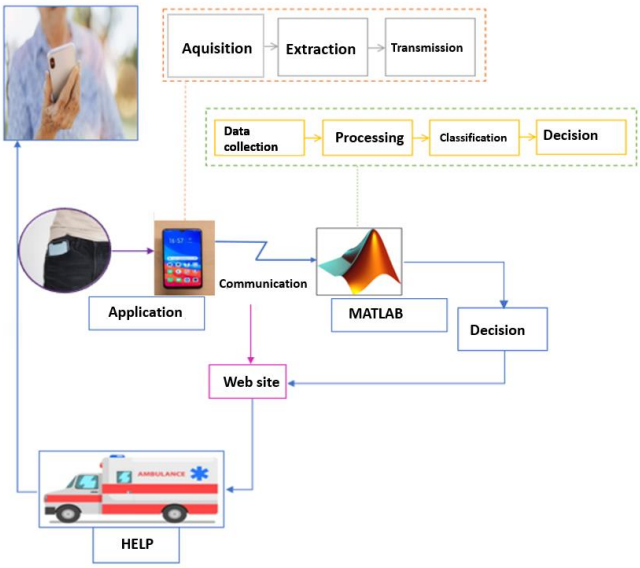

Fig. 1. Falls Remote Monitoring System Architecture

You might consider pattern recognition as a categorization technique. Their ultimate goal is to improve the extraction pattern and separate one class from another depending on certain criteria [6]. It offers the option to interpret each fresh observation in light of a body of facts or information amassed (or form). Existing observations are divided into classes in order to find new ones. It is therefore a tool for learning.

Pattern recognition is one of the many elements of artificial intelligence [10]. It makes it possible to employ a group of information or previously acquired understanding to justify each new observation (or shape). To find new observations, existing ones are grouped into classes (prototypes). It serves as a teaching tool as a result. An observation of a process is documented on a form. It is described by a collection of d parameters and represented by a point in the representation space, a space of dimension d that is specified by the different parameters (or characters).

The form vector's properties, when seen in the context of the diagnosis, represent the system under study. To associate an observed form with a recognized standard form is the issue of recognition. Typical forms (or prototypes) are representative points of this space. A fresh observation will seldom be the same as one of the prototypes due to perturbations (measurement noise, sensor precision, etc.). As a result, classes (ω_1, ω_2, …, ω_C, ω_M) correspond to areas in space, grouping together similar forms in order to translate the impact of noise. The premise of recognition is to choose which class [Xi = xi1, xi2,..., xid] seen should belong to out of M known classes. Classes relate to recognized modalities of operation in terms of diagnosis. They make up the Xa learning set, which is our initial batch of data. Finding one of these modes is the first step in classifying a new observation.

Three stages are involved in the creation of a diagnostic system by RdF: perception, analysis, and operational.

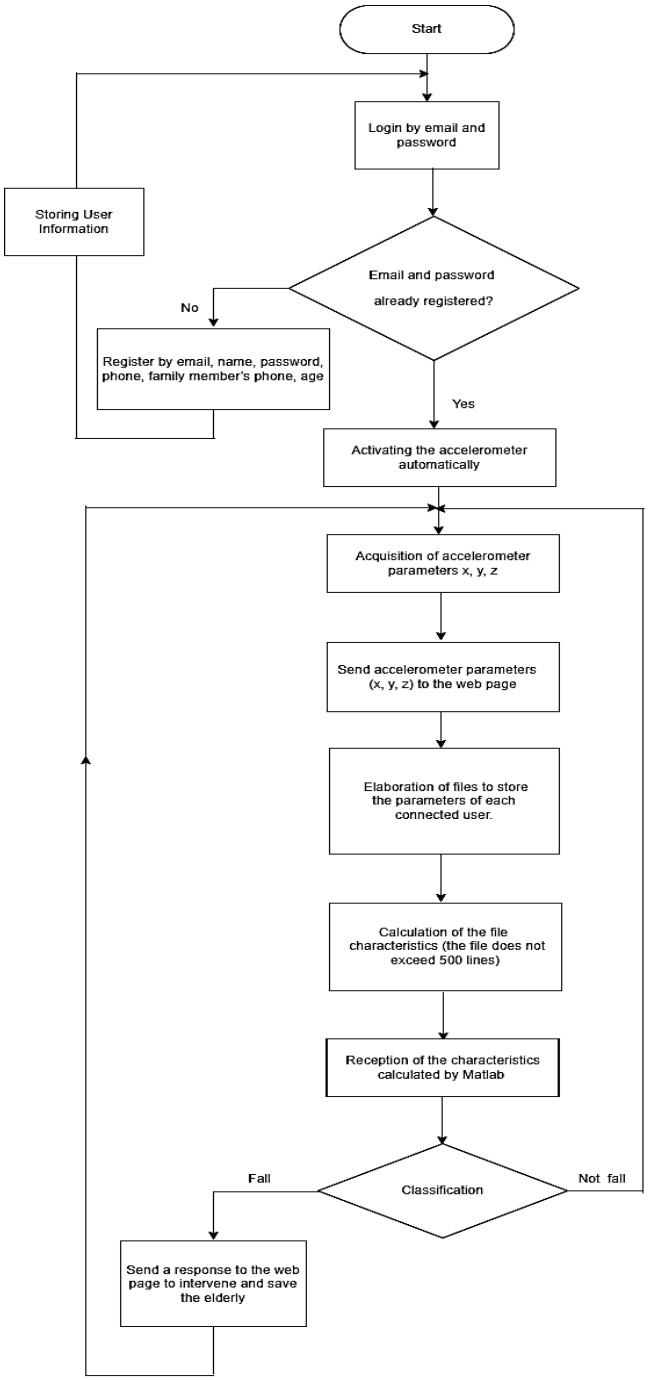

Fig. 2. Organigram of the used algorithm

The primary source of system information comes from the data collection phase. There are two steps to it. a phase in the data collecting procedure where the hardware setup necessary for signal collection on the under-review system is chosen (such as the kind, number, and sample time of the sensors to be used). The captured signals must provide pertinent data that may be used to assess the system's operational status. After this first stage, there follows a preliminary stage of signal preprocessing (filtering, de-routing, etc.). The data produced by the installed sensors in the system are examined during the analysis phase. It is essential to extract numerical features (or parameters) from the data if the information is provided as signals. These variables, which make up the form vector as well, must be able to characterize the system's behavior. At this stage of the study,

the classes that will represent the various modes of operation must be carefully defined. The following phase involves classifying a group of N observations (X1, X2,..., Xn) into M categories. This serves as the study guide. The prototypes of a class are then represented by its observations.

To divide the learning set into the several categories, a classification method is then applied. This procedure will lay out the guidelines for selecting which of the predefined classes to add a new observation to during the operational phase. In order to determine the right settings and apply the necessary changes, the analysis procedure typically entails using all of the system's data. By using the related decision rule, the operational phase (decision phase) enables the identification of an unnamed new observation X acquired on the system to one of the classes established during the classification phase. The importance of the form vector and the performance of the decision rule depend on the efficiency of the decision-making system. Before moving on to the choice, the next sections give a thorough explanation of the many stages required to create the diagnostic using pattern recognition.

At this stage, measurements of the physical system are used to produce the form vector.

The process of creating parameters from the acquired data involves applying signal processing techniques in the final phase, which is referred to as parameter generation. The best mode of operation distinction requires careful selection of these qualities.

As a result, an array of N vector forms with d parameter values, or a numerical table of size (N*d), is produced from the observations. The learning package is made up of the N forms (X1, XN) gathered on the system.

The vector initial form's calculated parameters might not all be suitable for the investigated operating modes. Thus, it is crucial to employ parameter reduction techniques in order to maintain just the most representative parameters.

Selecting a subset of parameters that preserves the division of classes from the original learning set is the first step in reducing the form vector. Either parameter extraction methods or parameter selection methods can be used to reduce the representation space.

The unsupervised methods and supervised methods subcategories of categorization approaches are the two main groups.

When it is possible to determine the beginning class of each observation or vector form, the decision space is completely known and supervised learning is practical. The next step is to specify the allocation rules for a hypothetical form x to one of the M classes.

On the other hand, the categorization must be done in an unsupervised way if there is no information provided regarding the architecture of the classroom learning set (the observations are not tagged). When the system is not understood and it is not apparent if the measurements apply to different classes, this scenario may occur.

In this case, the observations have been used to generate classes. It entails grouping observations into classes based on shared criteria. For the rest of this study, we will only offer the supervised type categorization.

2.1. Supervised learning

The learning package was divided into several spaces at the conclusion of the analysis process. The specification of the form vector ensures that the observations that are grouped together are completely understood. Every observation in the data is labeled to indicate that it belongs to one of the recognized M classes: whatever Xi, I = 1,..., N, there is j; j = 1,..., M as Xi belongs to _j. Let Xa represent the learning set (X1, X2,..., XN) and (ω_1, ω_2, …, ω_C, ω_M). recognized M courses (or modes of operation in diagnostics). The next step is to decide which class to allocate a fresh X observation that was acquired at a specific time on the system. To do this, decision boundaries between classes must be constructed together with a decision procedure. The decision methods that were used define a categorization rule for new observations to the various classes of the learning set. The decision rule might be created by the use of statistical or analytical techniques.

2.1.1. Using statistical analysis: KNN

A data categorization technique known as the k-Nearest Neighbor (KNN) algorithm calculates the likelihood that a data point will belong to one group or another depending on the group to which the data point nearest to it belongs [7, 17]. Following are the stages involved in classification using KNN.

Select the K whose categorization will work best.

The best prediction rate is achieved when K is between 5 and 18; above this amount, we can witness the phenomena of "overfitting", which happens when a model becomes very familiar with the specifics and noise of training data to the point that it degrades model performance on fresh data. Following are the stages involved in classification using KNN.

The Euclidean distance between two points in Euclidean space is the length of the right segment that connects them. The Pythagorean theorem may be used to calculate it from the points' Cartesian coordinates, thus the name Pythagorean distance.

2.1.2. SVM as the analytical method

This approach looks for the mathematical representations of the boundaries that best define classes using data from the learning set. Which boundary is most suited depends on the complexity of the decision boundary, or more precisely, on whether or not classes are properly split from the learning set. The goal of the SVM approach is to locate a hyperplane in an N-dimensional space (N = number of features) that classifies data points in a certain manner [2]. These two types of data points can be split using a variety of possible hyperplanes. We are seeking for the greatest gap between two different data point types at level H, which has the broadest margin. The advantage from increasing edge distance helps subsequent data points be identified more accurately. The data points at the slab's edge that are closest to the separation hyperplane are known as support vectors. These definitions are shown in the accompanying picture, where the + denotes Type 1 data points and the - denotes Type -1 data points.

3. Results

When we examine at the first three columns of the database's accelerometer 1, which are seen in figure 3, we see that there are many entries for each individual.

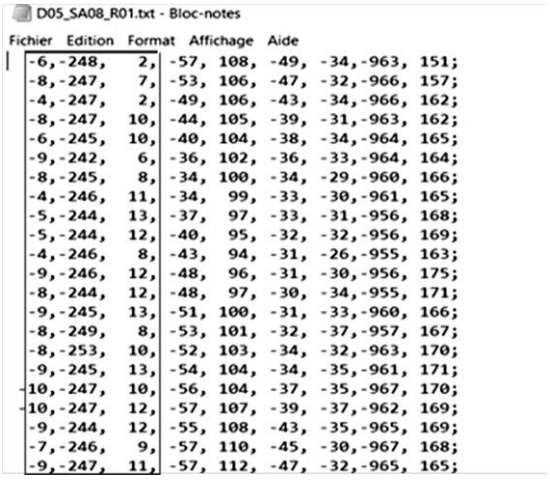
D05_SA08_R01.txt - Bloc-notes

Fichier Edition Format Affichage Aide

-6,-248,	2,	-57,	108,	-49,	-34,-963, 151;
-8,-247,	7,	-53,	106,	-47,	-32,-966, 157;
-4,-247,	2,	-49,	106,	-43,	-34,-966, 162;
-8,-247,	10,	-44,	105,	-39,	-31,-963, 162;
-6,-245,	10,	-40,	104,	-38,	-34,-964, 165;
-9,-242,	6,	-36,	102,	-36,	-33,-964, 164;
-8,-245,	8,	-34,	100,	-34,	-29,-960, 166;
-4,-246,	11,	-34,	99,	-33,	-30,-961, 165;
-5,-244,	13,	-37,	97,	-33,	-31,-956, 168;
-5,-244,	12,	-40,	95,	-32,	-32,-956, 169;
-4,-246,	8,	-43,	94,	-31,	-26,-955, 163;
-9,-246,	12,	-48,	96,	-31,	-30,-956, 175;
-8,-244,	12,	-48,	97,	-30,	-34,-955, 171;
-9,-245,	13,	-51,	100,	-31,	-33,-960, 166;
-8,-249,	8,	-53,	101,	-32,	-37,-957, 167;
-8,-253,	10,	-52,	103,	-34,	-32,-963, 170;
-9,-245,	13,	-54,	104,	-34,	-35,-961, 171;
-10,-247,	10,	-56,	104,	-37,	-35,-967, 170;
-10,-247,	12,	-57,	107,	-39,	-37,-962, 169;
-9,-244,	12,	-55,	108,	-43,	-35,-965, 169;
-7,-246,	9,	-57,	110,	-45,	-30,-967, 168;
-9,-247,	11,	-57,	112,	-47,	-32,-965, 165;

Fig. 3. Signals of first accelerometer from database

These values are then normalized by the following equation:

$$Num = \left(\frac{2 \times Range}{2 \times Resolution}\right) \times Num \quad (1)$$

with: Range = 16; Resolution = 13.

The following parameters were calculated from each axis of the first accelerometer and from each record in the next step:

Maximum peak to peak amplitude, Maximum, Variance, Standard Deviation, and Minimum.

A confusion matrix resembles a list of forecasts for a certain categorization issue. It contrasts the target variable's actual data with the model's predictions for that variable.

There are 4500 items in our database, including 2702 from the activities of daily living (ADL) class and 1798 from the falling scenario class. The strategy of holdout validation was used. A total of 3375 records, or 75% of the database, were used in the training phase. 1349 recordings were made in a falling scenario, while 2026 recordings were made in an ADL scenario. For the validation phase, we used a total of 1125 recordings, which accounts for the remaining 25%. 676 recordings from the ADL situation and 449 recordings from the fall semester.

In order to compute performances of our algorithms, several methods were used:

$$Accuracy = \frac{T_P+T_N}{T_P+T_N+F_P+F_N} \times 100 \quad (2)$$

$$Sensitivity = \frac{T_P}{T_P+F_N} \times 100 \quad (3)$$

$$Precision = \frac{T_P}{T_P+F_P} \times 100 \quad (4)$$

$$Specificity = \frac{T_N}{T_N+F_P} \times 100 \quad (5)$$

$$F1-Score = \frac{2\times Précision\times Sensibilité}{Précision+Sensibilité} \quad (6)$$

As seen in figure 4, the confusion matrix shows what happens when the best kernel SVM model is used. As we can see, only 435 out of the fall instances were accurately categorized, whereas 14 of them were. Out of 667 recordings that were accurately identified for the ADL scenarios, only 9 recordings were misclassified.

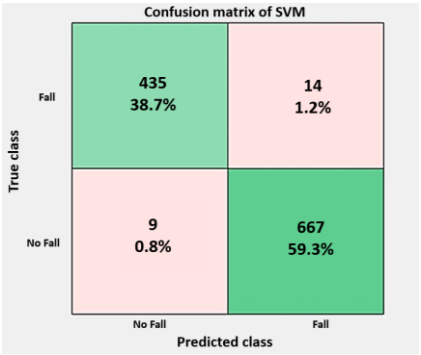

Fig. 4. SVM confusion matrix

The confusion matrix in figure 5 displays the results obtained using the KNN model with the best closest neighbor. As we can see, just 3 fall scenario classifications were inaccurate, leaving 446 properly classified. Out of 675 recordings that were successfully categorized for the ADL scenarios, just one was misclassified.

Table 1 lists the outcomes from the SVM and KNN models. As seen in table 2, both models' accuracy is highly outstanding, however the KNN model's accuracy score is significantly greater at over 99.6%. The KNN model also performs better in terms of sensitivity, accuracy, specificity, and the F1-score. Tables 3 and 4, which summarized the findings, show that KNN and SVM models were flawless in their ability to anticipate every situation.

Table 1. Obtained results using hold out validation scheme for KNN and SVM models

Methods	SVM	KNN
True Positive TP	435	446
True Negative TN	667	675
False Positive FP	9	1
False Negative FN	14	3

4. Discussions

For the fall situations and ADL scenarios in the aforementioned results, there were several recordings for each individual. We calculated the averages of the retrieved variables for each participant in order to obtain only one recording for each one. There are already 62 recordings in our new database, along with 24 falls situations and 38 ADL scenarios. We utilized 75% of the database for training and 25% for testing. Figure 6 shows the confusion matrix for the SVM model and Figure 7 shows the confusion matrix for the KNN model.

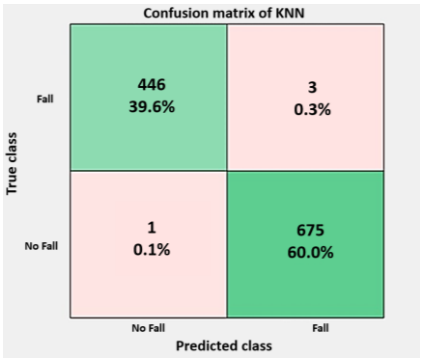

Fig. 5. KNN confusion matrix

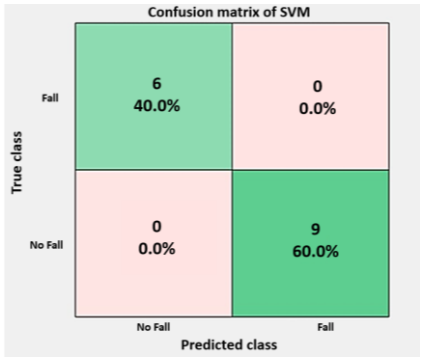

Fig. 6. SVM confusion matrix after computing the average

Table 2. Performance comparison between SVM and KNN

Parameter	SVM	KNN
Accuracy	97.9%	99.6%
Sensitivity	96.8%	99.3%
Precision	97.9%	99.7%
Specificity	98.6%	99.8%
F1-Score	97.34%	99.49%

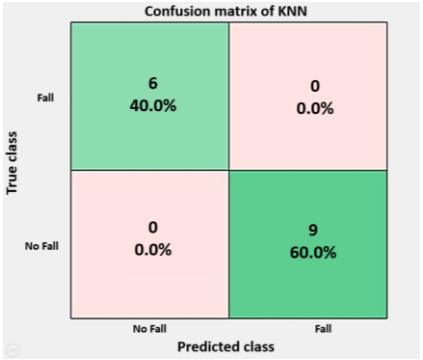

Fig. 7. KNN confusion matrix after computing the average

We used the Google-first, Massachusetts Institute of Technology-run MIT App Inventor [13], an online tool for developing Android apps for smartphones and tablets (MIT).

Three windows are available for development:

- One for designing the user interface for a machine; this is how your software will appear.
- One for self-programming, which enables the construction of application behavior out of building pieces.

Provides a testing environment for the software. The emulator makes it possible to verify the proper execution of the application rather than using the terminal.

Table 3. Obtained results using hold out validation scheme for KNN and SVM models after computing the average

Methods	SVM	KNN
True Positive TP	6	6
True Negative TN	9	9
False Positive FP	0	0
False Negative FN	0	0

Table 4. Performance comparison between SVM and KNN after computing the average

Parameter	SVM	KNN
Accuracy	100%	100%
Sensitivity	100%	100%
Precision	100%	100%
Specificity	100%	100%
F1-Score	100%	100%

We can download the application and test it out by connecting to a real Android smartphone. The application will work the same way whether this terminal is a phone or a tablet.

We'll develop a program that captures user motion, collects information from the accelerometer's x, y, and z axes, and transmits that information to a website we have developed to look for signs of a fall.

To create the interface, we picked each component, moved it into the phone's screen, and adjusted its options:

- Screen 1 is the application's main screen; it is shown for 5 seconds before switching to screen 2.
- Using the technique shown in figure 8, the user may sign up or log in using screen 2 (email and password).
- Screen 3 enables user registration (email, name, passwords, phone number, phone number of a family member and age).
- If the criteria is not verified, screen 4 enables you to immediately activate the accelerometer, display the accelerometer parameters in the program interface, and communicate these information to the webpage in real time.

For this job, we developed a dynamic website. A database, which is a collection of structured data that enables research, maintenance, and updating [4], may be handled by our website utilizing MySQL and PhpMyAdmin. Data is arranged in rows, columns, and tables in databases. They are indexed so that using computer software, the required information may be found fast. Data is updated and erasable when further information is supplied.

The smartphone may be used in any direction; there is no specific position in which to utilize it for precise results. We tested our system in a seemingly random location, and it worked well.

Figures 9, 10, 11, and 12 depict the many steps of communication between the application, website, and MATLAB for each level.

For instance, the user line and the -connect- column box both display 1 when the user (mouna@gmail.com) inputs their email address and password to access the website. The webpage creates a file with the email and accelerometer parameters that is no longer than 500 lines long (if it is, the first 500 lines are erased to maintain the file at 500 lines), then calculates the characteristics. Given that 200 ms is the greatest amount of time needed for an old person who is falling to strike the ground, the rate of accelerometer data receipt should be less than 200 ms [5]. Therefore, even if there is a delay in transmission, it is imperative to continuously send all signal samples, and the entire history should be saved and delivered. Although we analyze 500 lines in our solution, we may run additional studies to account for all delayed samples. The accelerometer activates automatically (Minimum, Maximum, Average, Median, Variance, Standard deviation, Maximum amplitude of peak to peak). MATLAB will repeatedly ask for these characteristics in order to categorize the data and send the classifications to the website.

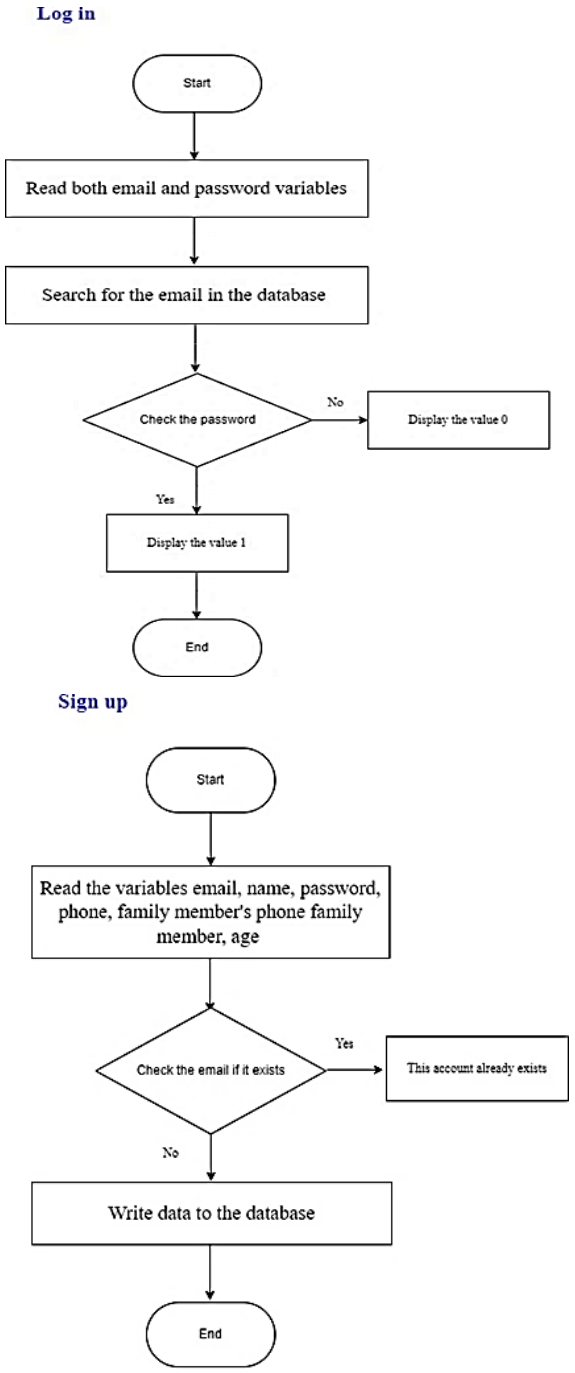

Fig. 8. Flowchart of registration and connection

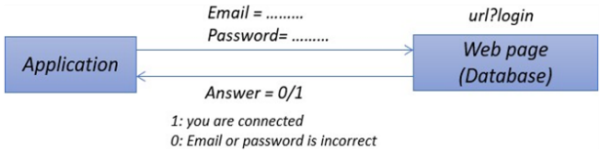

Fig. 9. Login phase

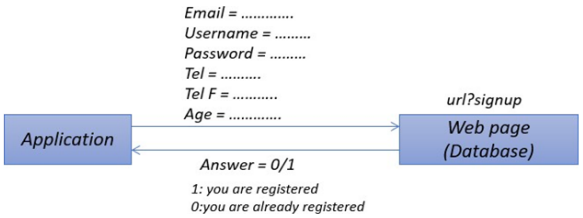

Fig. 10. Sing up phase

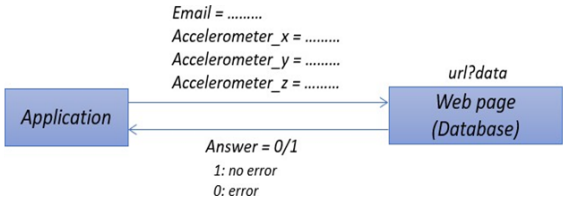

Fig. 11. Data recording phase

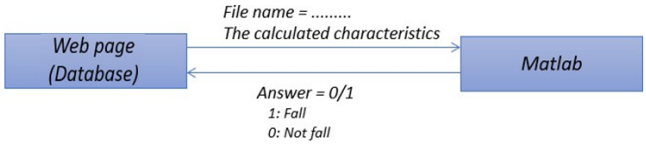

Fig. 12. State assessment phase

In order to examine and save older individuals or anybody else when a fall happens, a web portal that enables the emergency services to link and visualize each person who requires examination is required. We have created a website just for emergency services (username and password must be distinct and recognized by all emergency services).

To provide a summary of the entire project, let's assume that this is the case. When a new user registers and connects, the accelerometer is automatically activated and the parameters are sent to the web page. A file is created for the new user once the website examines the properties. MATLAB repeatedly asks the 4 users (the new user plus the users who are already connected) to do the classification in real time. After ascertaining that the newly connected user and the presently connected users are both falling, MATLAB allocates 1 to the "falling" box of the four users. The website then compiles a list of topics that are losing popularity.

5. Conclusion

Even while a fall could be unpleasant, it could be lethal for someone who has certain conditions. for example, elderly people or those who experience seizures. Therefore, precise and straightforward fall detection is crucial and can help in protecting and assessing these kinds of persons. We choose smartphones since they are actually accessible to everyone, offer commuting interfaces, and include sensors and GPS localization in addition to other features. As we demonstrated, the system we developed distinguishes between fall situations and other scenarios involving everyday tasks more precisely. A web service, a processing node that in our case utilizes MATLAB to make choices, and a mobile app that can be utilized on any device make up our system. The emergency center in charge of assessing these persons is also alerted when a fall happens. Overall, we believe that this approach will be quite helpful, and the results are both hopeful and pleasant. By enabling it to sleep when no activity is being detected and lowering the frequency of data collection, this program's energy-saving features might be improved. In the presence of activity or motion, data collection frequency must rise.

Conflict of interest

No author claims to have any conflicts of interest.

References

[1] Bouilly M., Thélot B.: Les accidents de la vie courante aux urgences en France métropolitaine en 2010 selon l'enquête EPAC. Revue d'Épidémiologie et de Santé Publique 60, 2012, S145.
[2] Cherkassky V., Ma Y.: Practical selection of SVM parameters and noise estimation for SVM regression. Neural networks 17(1), 2004, 113–126 [http://doi.org/10.1016/S0893-6080(03)00169-2].
[3] El Attaoui A. et al.: Machine learning-based edge-computing on a multi-level architecture of WSN and IoT for real-time fall detection. IET Wireless Sensor Systems 10(6), 2020, 320–332 [http://doi.org/10.1049/iet-wss.2020.0091].
[4] Enterprise J.: HTML, PHP, dan MySQL untuk Pemula. Elex Media Komputindo 2018.
[5] Er P. V., Tan K. K.: Non-intrusive fall detection monitoring for the elderly based on fuzzy logic. Measurement 124, 2018, 91–102 [http://doi.org/10.1016/j.measurement.2018.04.009].
[6] Fukunaga K.: Introduction to statistical pattern recognition. Elsevier 2013.
[7] Guo G. et al.: KNN model-based approach in classification. Lecture Notes in Computer Science 2888, 2003 [http://doi.org/10.1007/978-3-540-39964-3_62].
[8] James K.: Falls and Fall Prevention in the Elderly. West Indian Med J. 56(6), 2007, 534.
[9] Le H. L. et al.: A novel feature set extraction based on accelerometer sensor data for improving the fall detection system. Electronics 11(7), 2022, 1030 [http://doi.org/10.3390/electronics11071030].
[10] Li D., Wu M.: Pattern recognition receptors in health and diseases. Signal transduction and targeted therapy 6(1), 2021, 291 [http://doi.org/10.1038/s41392-021-00687-0].
[11] Noury N. et al.: Fall detection-principles and methods. 29th annual international conference of the IEEE engineering in medicine and biology society, 2007, 1663–1666 [http://doi.org/10.1109/IEMBS.2007.4352627].
[12] Pannurat N. et al.: Automatic fall monitoring: A review. Sensors 14(7), 2014, 12900–12936 [http://doi.org/10.3390/s140712900].
[13] Patton E. W.: MIT app inventor: Objectives, design, and development. Computational thinking education, 2019, 31–49 [http://doi.org/10.1007/978-981-13-6528-7].
[14] Rashid F. A.: Simulation of SisFall Dataset for Fall Detection Using MATLAB Classifier Algorithms. 12th International Symposium on Parallel Architectures, Algorithms and Programming – PAAP, 2021, 62–68, [http://doi.org/10.1109/PAAP54281.2021.9720481].
[15] Sucerquia A. et al.: SisFall: A fall and movement dataset. Sensors 17(1), 2017, 198 [http://doi.org/10.3390/s17010198].
[16] World Health Organization: Ageing, Life Course Unit. WHO global report on falls prevention in older age. World Health Organization; 2008.
[17] Zhang S. et al.: Learning k for kNN classification. ACM Transactions on Intelligent Systems and Technology 8(3), 2017, 1–9 [http://doi.org/10.1145/2990508].

Prof. Achraf Benba
e-mail: achraf.benba@ensam.um5.ac.ma

Received the Ph.D. degree in electrical engineering from ENSAM, Mohammed V University, Rabat, Morocco, in 2017. He is a member of E2SN teams at ENSAM, Mohammed V University. His interests are in speech processing for detecting people with neurological disorders and Cardiac abnormalities.

http://orcid.org/0000-0001-7939-0790

Eng. Mouna Akki
e-mail: mouna.akki72@gmail.com

Received the engineering degree in biomedical engineering from ENSAM, Mohammed V University, Rabat, Morocco, in 2022. She is interested in embedded systems applied in health assessment.

http://orcid.org/0009-0001-8532-1158

Prof. Sara Sandabad
e-mail: s.sandabad@isem.ac.ma

Received the B.Sc. and the M.Sc. degrees in Electrical Engineering from ENSET, Mohamed V University of Rabat (Morocco) and the Ph.D. degree from ENSIAS from the Mohamed V University of Rabat, all in Electrical Engineering, in 2010, 2012, and 2016, respectively. Currently, she is a Professor of Electrical Engineering at ISEM, Hassan II University of Casablanca. She is also an academic member of Laboratory of Control and Mechanical Characterization of Materials and Structures, ENSEM, Hassan II University of Casablanca, Morocco.

http://orcid.org/0000-0002-0813-6178

http://doi.org/10.35784/iapgos.3499 *received: 13.02.2023 | revised: 16.03.2023 | accepted: 29.04.2023 | available online: 30.06.2023*

CONVOLUTIONAL NEURAL NETWORKS FOR EARLY COMPUTER DIAGNOSIS OF CHILD DYSPLASIA

Yosyp Bilynsky[1,2], Aleksandr Nikolskyy[3], Viktor Revenok[2,3], Vasyl Pogorilyi[3], Saule Smailova[4], Oksana Voloshina[5], Saule Kumargazhanova[4]

[1]Vinnytsia National Technical University, Vinnytsia, Ukraine, [2]Vinnytsia National Agrarian University, Vinnytsia, Ukraine, [3]National Pirogov Memorial Medical University, Vinnytsya, Ukraine, [4]D.Serikbayev East Kazakhstan State Technical University, Ust-Kamenogorsk, Kazakhstan, [5]Vinnytsia Mykhailo Kotsubynsky State Pedagogical University, Vinnytsya, Ukraine

Abstract. *The problem in ultrasound diagnostics hip dysplasia is the lack of experience of the doctor in case of incorrect orientation of the hip joint and ultrasound head. The aim of this study was to evaluate the ability of the convolutional neural network (CNN) to classify and recognize ultrasound imaging of the hip joint obtained at the correct and incorrect position of the ultrasound sensor head in the computer diagnosis of pediatric dysplasia. CNN's such as GoogleNet, SqueezeNet, and AlexNet were selected for the study. The most optimal for the task is the use of CNN GoogleNet showed. In this CNN used transfer learning. At the same time, fine-tuning of the network and additional training on the database of 97 standards of ultrasonic images of the hip joint were applied. Image type RGB 32 bit, 210 × 300 pixels are used. Fine-tuning has been performed the lower layers of the structure CNN, in which 5 classes are allocated, respectively 4 classes of hip dysplasia types according to the Graf, and the Type ERROR ultrasound image, where position of the ultrasound sensor head and of the hip joint in ultrasound diagnostics are incorrect orientation. It was found that the authenticity of training and testing is the highest for the GoogleNet network: when classified in the training group accuracy is up to 100%, when classified in the test group accuracy – 84.5%.*

Keywords: convolutional neural networks, computer diagnosis, ultrasound image child dysplasia

KONWOLUCYJNE SIECI NEURONOWE DO WCZESNEJ DIAGNOSTYKI KOMPUTEROWEJ DYSPLAZJI U DZIECI

Streszczenie*. Problemem w diagnostyce ultrasonograficznej dysplazji stawu biodrowego jest brak doświadczenia lekarzy w zakresie nieprawidłowej orientacji stawu biodrowego i głowicy ultrasonograficznej. Celem tego badania była ocena zdolności konwolucyjnej sieci neuronowej (CNN) do klasyfikowania i rozpoznawania obrazów ultrasonograficznych stawu biodrowego uzyskanych przy prawidłowym i nieprawidłowym położeniu głowicy ultrasonograficznej we wspomaganej komputerowo diagnostyce dysplazji dziecięcej. Do badania wybrano sieci CNN, takie jak GoogleNet, SqueezeNet i AlexNet. Wykazano, że najbardziej optymalne dla tego zadania jest użycie CNN GoogleNet. Jednocześnie w CNN zastosowano metodologię uczenia transferowego. Zastosowano precyzyjne dostrojenie sieci i dodatkowe szkolenie na podstawie 97 próbek obrazów ultrasonograficznych stawu biodrowego, typ obrazu RGB 32 bity, 210 × 300 pikseli. Przeprowadzono dostrajanie dolnych warstw struktury CNN, w której zidentyfikowano 5 klas, odpowiednio 4 klasy typów dysplazji stawu biodrowego według Grafa oraz obraz ultrasonograficzny typu ERROR, w którym pozycja głowicy ultrasonograficznej i stawu biodrowego w diagnostyce ultrasonograficznej mają nieprawidłową orientację. Stwierdzono, że niezawodność szkolenia i testowania jest najwyższa dla sieci GoogleNet: podczas klasyfikacji w grupie szkoleniowej dokładność wynosi do 100%, podczas klasyfikacji w grupie testowej dokładność wynosi 84,5%.*

Słowa kluczowe: konwolucyjne sieci neuronowe, diagnostyka komputerowa, obrazowanie ultrasonograficzne dysplazji dziecięcej

Introduction

Statistics of hip joint disease are widespread in almost all countries of the world (2–3%), but there are significant ethnic features of its distribution. For example, the incidence of congenital malformations of the hip joint in newborns in the Scandinavian countries reaches 4%, in Germany -2%, in the USA it is higher among the white population than in African Americans, and is 1–2% [1]. Hip dysplasia is a disease characterized by underdevelopment during embryogenesis of all elements involved in the formation of the joint: ligaments, cartilage, bone surfaces, muscles, nerve and vascular structures. Diagnosis of this disease is quite difficult, so in cases of late detection and late treatment of hip dysplasia in children develop severe irreversible morphological and functional changes in the affected limb. It is possible to diagnose malformations of the hip joint in newborns and young children on the basis of the re sults of clinical and ultrasound or X-ray examin ation. However, the radiation load of X-ray examination does not allow to use this method of examination of the hip joints in children under three months. In addition, the radiograph does not show non-ossified structures – elements of the femoral head, the roof of the acetabulum, which make up the majority of these anatomical formations in children of the first year of life. The use of the method of artificial contrast of the joint is quite difficult and dangerous for the child. Today, the ultrasound method of examination of the hip joints is actively developing. Ultrasound (US) in modern medicine is a fairly common method of diagnosis and provides diagnosis of local abnormalities and malformations of the human body degenerative and dystrophic diseases of the ligaments. Therefore, ultrasound is beginning to be actively used to detect developmental hip dysplasia. Ultrasound assessment of the hip joint has the advantage over X-ray examination in that it, along with the image of the hip bone, also reflects cartilaginous structures, and covers the femoral head with the cartilage of the acetabulum. Another advantage of ultrasound diagnosis is that it can be done repeatedly, studying the development of hip dysplasia over time. The main methods of ultrasound assessment of the hip joint are the methods of Graf, Rosendahl, Harcke and Morin, Terjesen, Dahlstrom [8, 10–12, 17–19, 22]. However, they have a low reliability of diagnosis, because the result of diagnosis mainly depends on the qualifications of the doctor, because the study may be incorrect visualization of anatomical landmarks of the hip joint, diagnosed in the wrong position of the child, that is when the ultrasound sensor deviates from the standard position perpendicular to the body. The cartilaginous lip (limbus) is clearly visualized only if the sensor surface is perpendicular to the body. When fixing the ultrasound sensor with an inclination to the hip joint, the image of the limbus becomes blurred due to the effect of anisotropy. Failure to comply with the criteria of the standard ultrasound cut and, accordingly, the oblique direction of the ultrasound beam relative to the hip joint distortion of the image of the joint and make its assessment incorrectly [2, 17]. This makes it impossible to properly measure the angular performance. In addition, a fairly large error is made by visually determining the angles on the noisy speckle noise of the ultrasound image. Thus, the source of errors in determining the condition of the hip joint there is a lack of training of ultrasound specialists working in practical health care institutions, ignorance and misunderstanding that any, even minimal deviation from conventional research technology leads to projective distortion of the image on the sonogram, and therefore to the wrong conclusion. Therefore, one of the main ways to increase the reliability of the study of the hip joints is to create a new method and hardware and software for secondary processing of ultrasound images based on computer

technology. The aim of this study was to evaluate the ability of the convolutional neural network (CNN) to recognize and classify ultrasound imaging of the hip joint as the correct or incorrect at position of the ultrasound sensor head in the computer diagnosis of pediatric dysplasia.

1. Ways of CNN structure reconstruction

The method of studying the condition of the hip joints on the basis of analysis of ultrasound images and classification of hip dysplasia on their basis involves the following steps:

1. Pre-processing computer of ultrasound image of the hip joint.
2. Recognition and classification of ultrasound images of the hip joint when the obtained at the correct or incorrect position of the ultrasound sensor head in the computer diagnosis of pediatric dysplasia.
3. Identification of angles in the coronal plane of the hip joint.
4. Classification of hip dysplasia according to the results of the obtained angular indicators by the Graf's method.

The algorithm can be implemented both software and hardware [3–6]. In this study we will consider in detail the main part of this approach, namely the implementation of testing and rejection of correct ultrasound images of the hip joint, which provides a significant increase in the reliability of its diagnosis as a whole. To solve this problem, we use such a powerful tool as CNN, the task of which is to assign the input image to a certain class. The widespread use of neural networks is made possible by the large number of ready-made solutions for learning deep neural networks, including the use of modern multi-core processors, computing accelerators, and computing clusters with distributed memory. Structure CNN contain several layers, such as Convolution layers, ReLU layers, Pooling layers, and Fully connected (FC) layers. The structure CNN scheme for the tasks of the classification of ultrasound images of hip dysplasia is shown in Fig. 1. The CNN architecture may vary depending on the types and number of layers included. The types and number of layers depend on the specific application of the CNN or the data it works with. Based on the analysis, it was found that the MATLAB software platform is the best option for such studies. MATLAB – Deep Learning Toolbox ™ provides a basis for the development and implementation of deep neural networks. The connection of the layers in the convolutional neural network in script MATLAB® for the tasks of classification of ultrasound images of hip dysplasia can be performed as follows:

```
layers = [imageInputLayer([210 300 1])
convolution2dLayer(5,20)
reluLayer
maxPooling2dLayer(2,'Stride',2)
fullyConnectedLayer(10)
softmaxLayer
classificationLayer];
```

After defining the layers of CNN, it is necessary to specify training options using the 'trainingOptions' function. For example, options = trainingOptions ('sgdm'); Then, CNN is trained in the training sample using the 'trainNetwork' function. Training data, layers, and variants become input to the training function. Example, convnet = trainNetwork(data, layers, options);
To perform the classification of ultrasound images of the hip joints with a size of 210 × 300 pixels by the Graf's method, experimental studies were performed using such CNN's as GoogLeNet [21], SqueezeNet [9], and AlexNet [16]. The CNN's data were chosen not by chance, as they won the ImageNet Large Scale Visual Recognition Challenge (ILSVRC) in different years.

CNNs underwent a process of training on a sample of 97 ultrasound images, divided into classes by the method of Graf [2]: Type I; Type IIa, Type IIb; Type III, IV; and Type EROR. Type EROR includes ultrasound images of the hip joints, in which the cartilaginous lip (limbus) is indistinctly visualized in the case of tilting the position of the sensor surface to the body. In case of ultrasound sensor tilt:

- to the back – the contours of the lower edge of the iliac bone and the acetabulum become blurred, the thickness of the epicartilage increases;
- to the front – a more pronounced bony roof of the acetabulum, the outer bony protrusion becomes pointed;
- down – the lower edge of the iliac bone is not clearly visualized;
- to the top – the bone-cartilage border or its atypical form does not get to an ultrasonic cut, thus only back departments of an acetabulum are visualized.

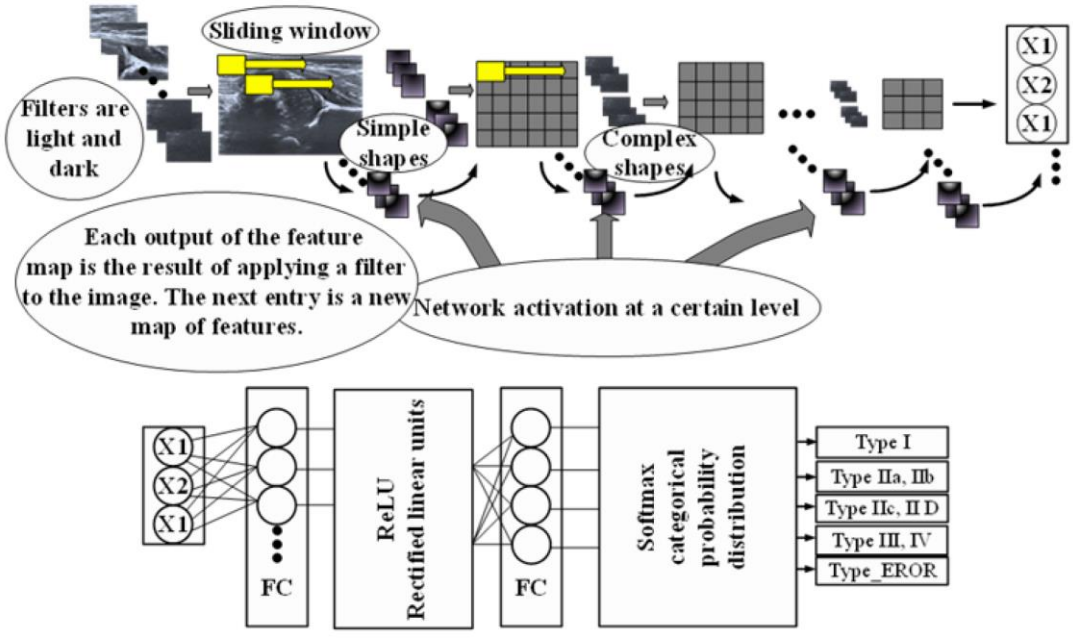

Fig. 1. Detailing of the structure of CNN for the tasks of classification of ultrasound images of hip dysplasia according to the Graf

As a result of the conducted researches the work of CNN used was compared. In Fig. 2 shows the image of the hip joint at the wrong (Fig. 2a) and correct position of the ultrasonic sensor head (Fig. 2b). A sample of 97 ultrasound images is usually insufficient, but for this task can be considered representative. The study presents as an example of GoogLeNet CNN configuration and training, but the same studies were done on SqueezeNet and AlexNet CNN. Due to the large amount of material epy studys, SqueezeNet and AlexNet are not considered in the article, but their final parameters are compared.

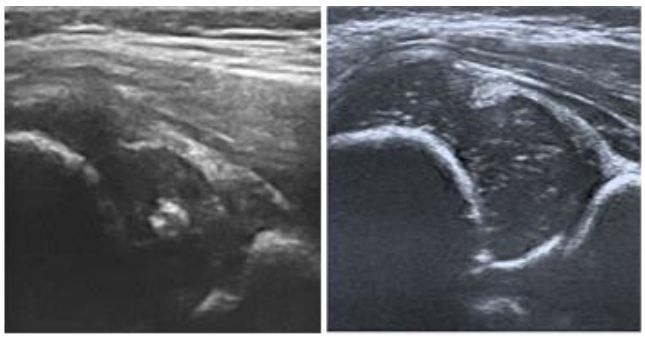

a) b)

Fig. 2. Image of the hip joint: a) the image of the hip joint in the case of the inclined position of the ultrasound sensor head to the rear (incorrect position of the ultrasonic head sensor); b) the image of the hip joint at the correct position of the sensor of the ultrasonic head

2. Fine-tuning and learning of CNN on the example of GoogLeNet

GoogLeNet is a convolutional neutron network that not only shows high accuracy, but also requires relatively low computing power of the PC [21]. It was used to identify abnormalities on chest radiographs. In addition, the network has shown itself well in the task of recognizing breast cancer, which shows its effectiveness in working with medical images [23]. In this study used transfer learning CNN [24], that is, this approach involves the use of CNN GoogLeNet, which earlier was trained on one data, and then reconfigured the network and learning to solve the problems of classification of ultrasound images of hip dysplasia.

It is called fine-tuning of the network while retraining took place on the database of 97 benchmark datasets of the trained sample of ultrasonic images of the hip joint were applied. CNN GoogLeNet has the structure shown in Fig. 4, 5. CNN contains 144 layers (input and output layers) and its at structure fine-tuning for the classification of hip dysplasia images. On her you can view the structure and settings of Convolution, ReLU, MaxPooling, and Inception blocks. In Fig. 3 shows the result of fine-tuning the lower layers of the GoogLeNet CNN structure, in which 5 classes are allocated, respectively (4 classes of hip dysplasia types according to the method Graf, and the Type ERROR class described above).

Fragments of the GoogLeNet CNN structure and Convolution, ReLU, MaxPooling, and Inception settings (input layers and output layers) are shown in Fig. 4 and 5, respectively.

3. Training of CNN GoogLeNet

A benchmark datasets of ultrasound images of the hip joints has been prepared for the CNN training. For this purpose, we used the library of images of the hip joints, which was provided by National Pirogov Memorial Medical University. Ultrasound images of hip dysplasia were selected for the experiments and divided into 5 classes: Type I; Type IIa, IIb; Type IIc, II D; Type III, IV; by Graf, and Type_ERROR. Quantitative indicators of the base of benchmark datasets for training and testing are presented in table 1.

As can be seen from the table, fifteen images were selected from each class for teaching and 3 for testing. During the construction of the base of benchmark datasets, 97 ultrasound images of hip joints 210 × 300 pixels, RGB image type, color depth 32 bits were prepared. The process of learning CNN is shown in Fig. 6.

Before learning, the learning parameters were set, which are shown in the MATLAB script snippet:

```
miniBatchSize=10;
numImages=numel(train.Files);
maxEpochs=30;
lr=0.0004;
opts = trainingOptions ('sgdm', ...
'InitialLearnRate',lr,...
'LearnRateSchedule','piecewise', ...
'LearnRateDropFactor',0.2, ...
'LearnRateDropPeriod',6, ...
'MaxEpochs',maxEpochs, ...
'MiniBatchSize',miniBatchSize, ...
'Plots','training-progress');
net=trainNetwork(train,lgraph_2,opts);
% save('trainedNetIn.mat','net')
% save('test.mat','test')
```

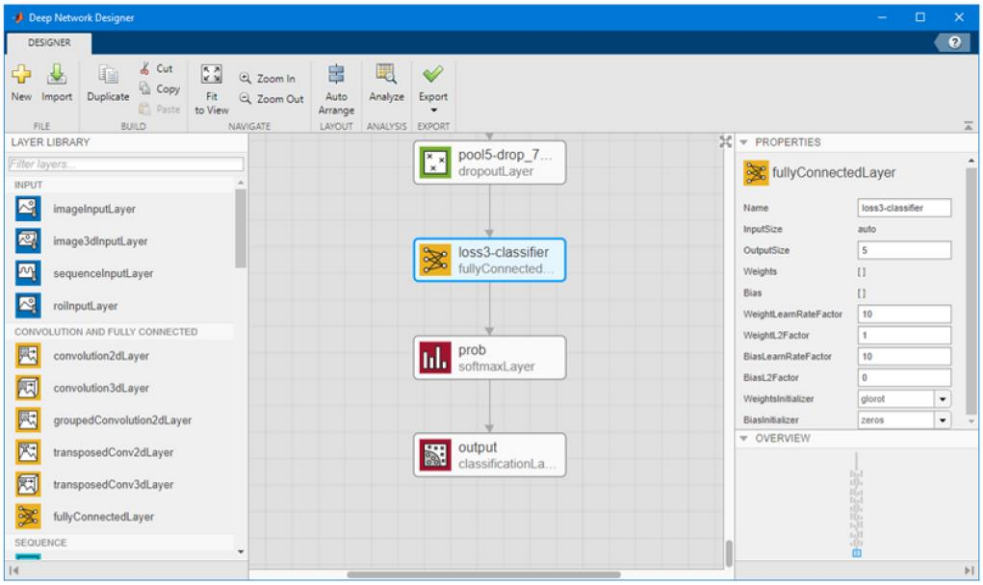

Fig. 3. Fragments of the lower layers of the GoogLeNet CNN structure and the results of fine-tuning

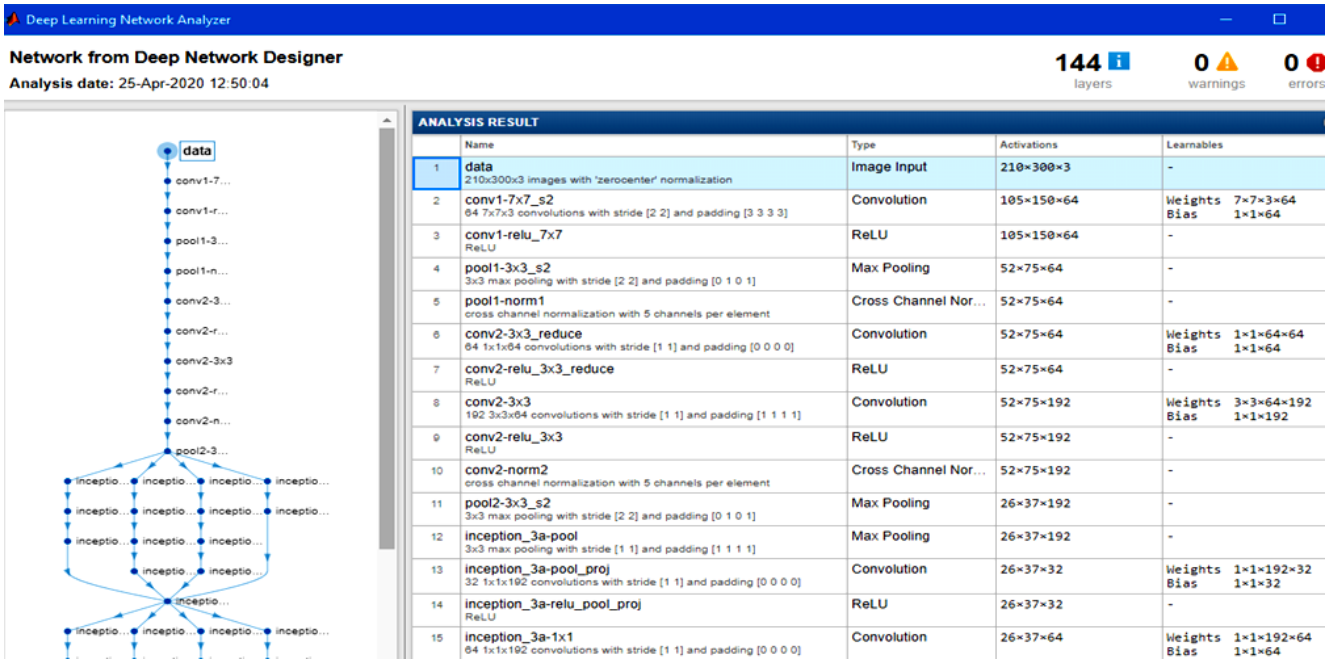

Fig. 4. Fragments of the GoogLeNet CNN structure and Convolution, ReLU, MaxPooling settings (input layers)

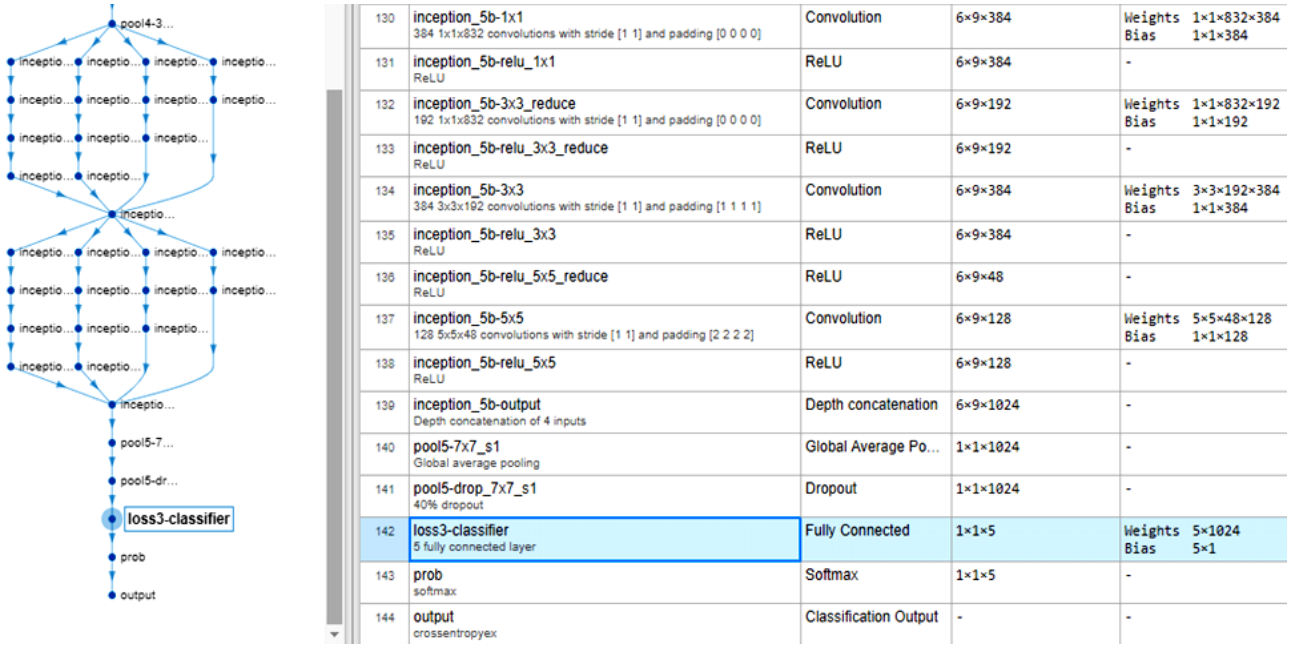

Fig. 5. Fragments of the GoogLeNet CNN structure and Convolution, ReLU, MaxPooling settings (output layers)

Table 1. Quantitative indicators of the base of benchmark datasets for training and testing

tbl = 5×2 table (The presence of benchmark datasets in the training sample)			ans = 5×2 table (Selection of probabilistic benchmark datasets from each class)		
	Label	**Count**		**Label**	**Count**
1	Type I	18	**1**	Type I	18
2	Type III, IV	18	**2**	Type III, IV	18
3	Type IIa, IIb	25	**3**	Type IIa, IIb	18
4	Type IIc, II D	18	**4**	Type IIc, II D	18
5	Type_ ERROR	18	**5**	Type_ ERROR	18

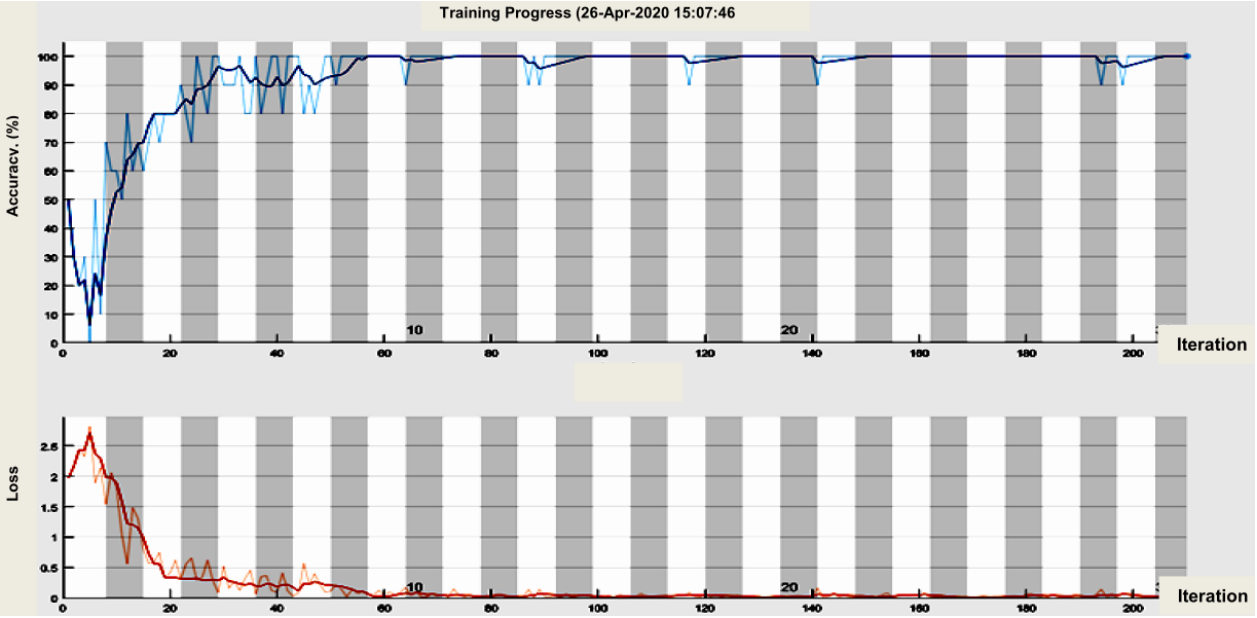


```
Training on single GPU.
Initializing input data normalization.
|=========================================================================================|
|  Epoch  |  Iteration  |  Time Elapsed  |  Mini-batch  |  Mini-batch  |  Base Learning  |
|         |             |   (hh:mm:ss)   |   Accuracy   |     Loss     |      Rate       |
|=========================================================================================|
|       1 |           1 |       00:00:01 |       50.00% |       1.9713 |          0.0004 |
|       8 |          50 |       00:00:57 |      100.00% |       0.1120 |       8.0000e-05 |
|      15 |         100 |       00:01:55 |      100.00% |       0.0255 |       1.6000e-05 |
|      22 |         150 |       00:02:52 |      100.00% |       0.0267 |       3.2000e-06 |
|      29 |         200 |       00:03:50 |      100.00% |       0.0057 |       6.4000e-07 |
|      30 |         210 |       00:04:01 |      100.00% |       0.0260 |       6.4000e-07 |
|=========================================================================================|
```

Fig. 6. CNN GoogLeNet learning process

lr = 0.0004 – the LR (learning speed) hyperparameter can significantly affect the time required for a training model. The speed of learning determines how quickly the weight coefficients of convolutional neural networks are updated. The maximum number of epochs is 30. The minimum package size for analysis is 10. Some specific learning parameters 'LearnRateDropFactor' – 0.2, 'LearnRateDropPeriod' – 6 respectively, the rate of decline in learning speed and the rate of decline of the learning period.

The parameters listed in the table Fig.6 have the following definition:

- Mini-batch accuracy in CNN training. The accuracy of the classification of the mini-batch of training data sets, which is reported during the training of CNN, corresponds to the accuracy of the specific classification of the mini-group of data sets on a given iteration. During training using the Stochastic Gradient Descent with momentum (SGDM) optimization algorithm, the algorithm groups the complete set of data into iterations. The iteration corresponds to the calculation of network gradients for each mini-batch of data sets.
- Epoch – the algorithm of the neural network is iterative; its steps are called epochs or cycles. Epoch – one iteration in the learning process, which includes the presentation of all examples of data sets from the learning set and, possibly, to check the quality of learning on a test sample. The learning process is carried out on a training sample.
- Mini-Batch loss – trends in loss and accuracy when learning on a mini-group of data sets. If the source layer is a Classification Source Level object, then the loss is an entropy cross loss for a multiclassification task with mutually exclusive classes.
- Base Learning rate – Basic learning speed. The software multiplies the norm coefficients of the rate of learning of the layers by this value.

Convolutional neural networks through the use of a special operation – the actual convolution – allows you to simultaneously reduce the amount of information stored in memory, thereby better cope with images of higher resolution. This allows you to highlight reference features of the image, such as edges, contours or borders. At the next level of processing from these edges and faces it is possible to recognize repeating fragments of textures which can further develop into fragments of the image. In essence, each layer of the neural network uses its own transformation. If on the first layers the network operates with such concepts as "edges", "borders", etc., then the concepts "texture", "parts of objects" are used further. As a result of such processing, we can correctly classify the image of a condition of a hip joint of the child. In Fig. 7 shows the so-called tile images of the input image of the hip joint of the child, which forms the first convolutional layer conv1 CNN filters with an amount of 8 × 8, size 7 × 7 × 3.

The script of the MATLAB R2019b package for forming a tile of the state of the child's hip joint, for the first convolutional layer conv1 CNN is written below:

```
net = GoogLeNet;
im = imread(fullfile(matlabroot,'examples','nnet','60-57_300-210.jpg'));
imshow(im)
imgSize = size(im);
imgSize = imgSize(1:2);
act1 = activations(net,im,'conv1');
sz = size(act1);
act1 = reshape(act1,[sz(1) sz(2) 1 sz(3)]);
I = imtile(mat2gray(act1),'GridSize',[8 8]);
imshow(I)
```

CNN GoogLeNet on 144 layers was trained in a training sample of 97 images of hip dysplasia with learning parameters: number of epochs 30, number of iterations 210, training time 4.1 minutes, mini – batch accuracy in classification on the training group up to 100%, mini – batch loss in training on mini-group of data sets – 0.0260, basic learning speed – 6.4×10^{-7}, network weight after training 87,739 MB, table on the Fig. 6.

The personal computer on which the learning process took place had the following computing power:

- CPU: Intel (R) Core (TM) i7-4702MQ CPU @ 2.2GHz… 2.2GHz;
- RAM: 8.00 GB;
- GPU video adapter: GT 750M (GK107 graphics processor is equipped with 384 CUDA cores and operates at a frequency of 967 MHz (turbo mode is supported), and the width of the memory bus is 128 bits).

4. Experimental research and comparison of modeling results

In order to select the best CNN for the task of recognition, classification and selection of correct ultrasound images of the hip joint, machine learning and testing of GoogLeNet, SqueezeNet and AlexNet CNNs were carried out. Characteristics of the considered CNN's are summarized in table 2.

As can be seen from table 2, reliability in training and testing on a sample of 97 images of hip dysplasia the highest for the GoogLeNet network: up to 100% for classification in the training group, 84.5% for classification in the test group. The main objective of this study was to classify ultrasound images hip joint on the correct (Type I; Type IIa, IIb; Type IIc, IID; Type III, IV; by Graf), and incorrect class Type_ERROR, where position of the head of ultrasound sensor in ultrasound diagnostics of the hip joint are incorrect orientation to the body. In Fig. 8 shows a histogram of the comparison of the main characteristics of CNN's SqueezeNet, GoogLeNet, AlexNet.

Table 2 and the histogram show that a number of key characteristics such as the number of layers, the weight of the network after training (MB) – CNN SqueezeNet has better performance, and the accuracy in the classification of the test group (%) approaching GoogleNet. Also, in the study of CNN AlexNet found that the number of layers – 25 is not enough to achieve accuracy in the classification of the test group at least up to 80%. In the future, it is proposed to use software and hardware of artificial intelligence, which are discussed in [13,14,15], which will help improve the proposed approach and increase the speed and reliability of diagnosing ultrasound medical images of hip dysplasia.

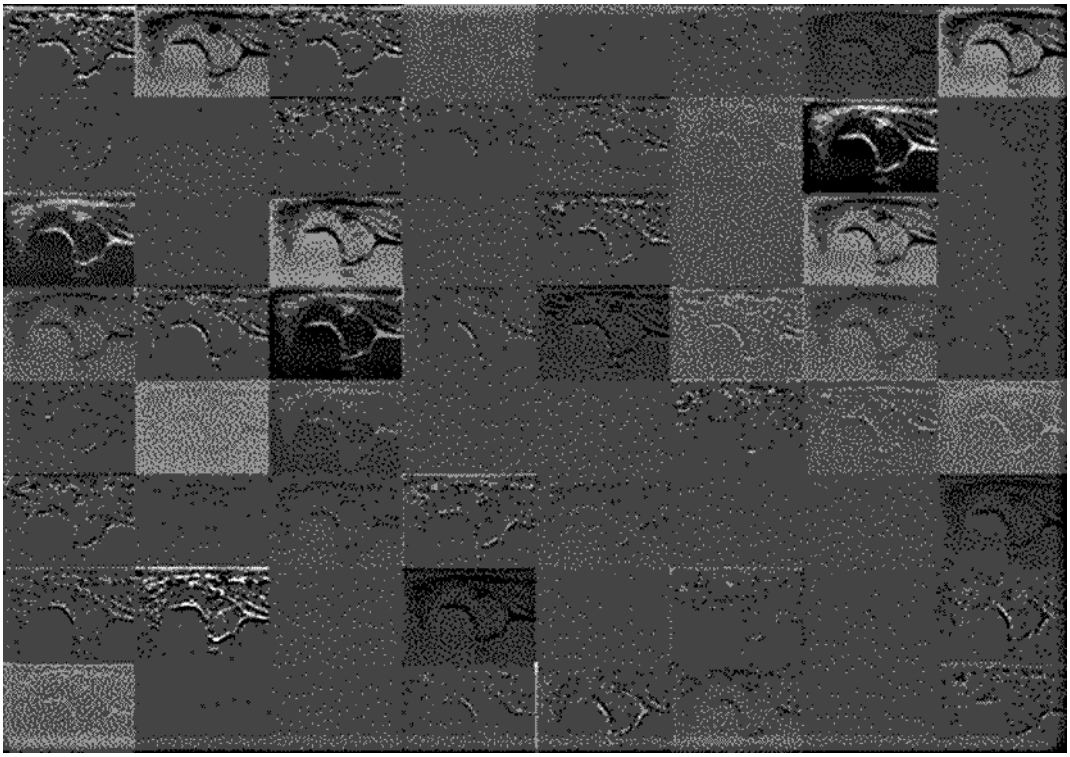

Fig. 7. Tiles of the images of the input image of the hip joint of the child, which forms the first convolutional layer conv1 CNN filters in the amount of 8 × 8, size 7 × 7 × 3

Table 2. Characteristics of CNN's SqueezeNet, GoogLeNet and AlexNet during training and testing on a sample of 97 images of hip dysplasia

	SqueezeNet	GoogLeNet	AlexNet
Number of layers	68	144	25
Number of epochs	30	30	12
Number of iterations	270	210	216
Training time (minutes)	2.16	4.7	0.46
Accuracy in the classification of the training group (%)	up to 100%	up to 100%	up to 75%
Accuracy in the classification of the test group (%)	83	84.5	62.7
Basic learning speed (coefficient)	6.4×10^{-7}	6.4×10^{-7}	8.0×10^{-5}
Network weight after training (MB)	13	87.739	68.4

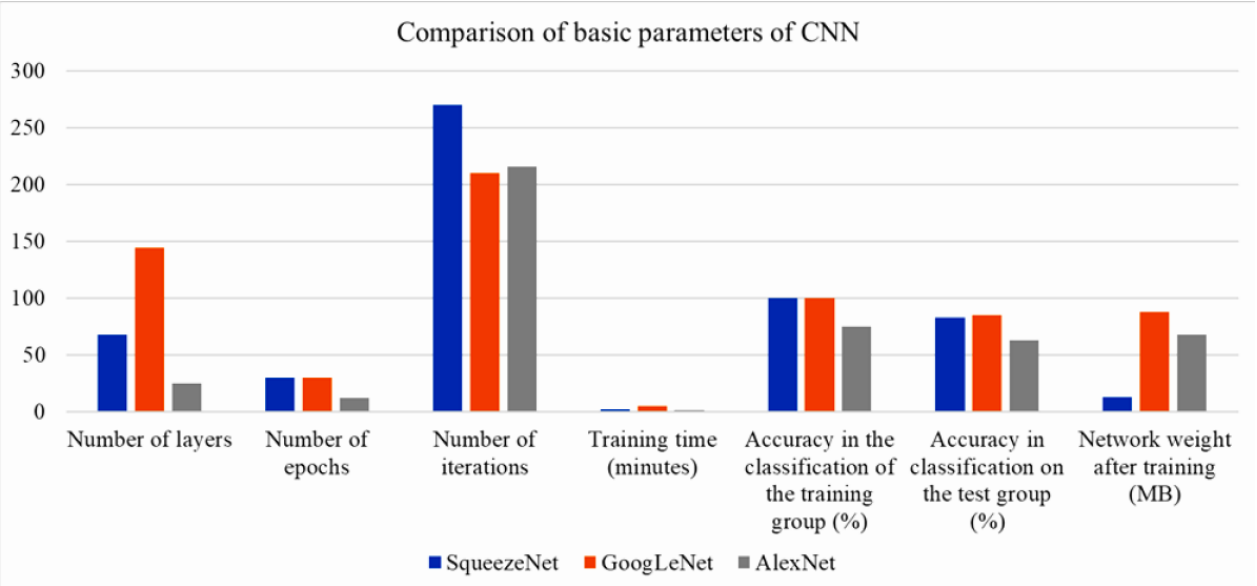

Fig. 8. Comparison of the main characteristics of CNN's SqueezeNet, GoogLeNet, AlexNet

5. Discussion

It is possible to diagnose malformations of the hip joint in newborns and young children on the basis of the re sults of clinical and ultrasound or X-ray examination. Ultrasound assessment of the hip joint has the advantage over X-ray examination in that it, along with the image of the hip bone, also reflects cartilaginous structures, and covers the femoral head with the cartilage of the acetabulum. Another advantage of ultrasound diagnosis is that it can be done repeatedly, studying the development of hip dysplasia over time. The main methods of ultrasound assessment of the hip joint are the methods of Graf, Rosendahl, Harcke and Morin, Terjesen, Dahlstrom [8,10,11,12,17,18,19,22]. However, they have a low reliability of diagnosis, because the result of diagnosis mainly depends on the qualifications of the doctor, because the study may be incorrect visualization of anatomical landmarks of the hip joint, diagnosed in the wrong position of the child, that is when the sensor deviates from the standard position perpendicular to the body. The cartilaginous lip (limbus) is clearly visualized only if the sensor surface is perpendicular to the body. When fixing the sensor with an inclination to the hip joint, the image of the limbus becomes blurred due to the effect of anisotropy. Failure to comply with the criteria of the standard cut and, accordingly, the oblique direction of the ultrasound beams relative to the hip joint distortion of the image of the joint and make its assessment incorrectly [17,2]. Thus, the problem in ultrasound diagnostics hip dysplasia is the lack of experience of the doctor in case of incorrect orientation of the hip joint and ultrasound head. Therefore, the work has taken the first step towards creating an intelligent system that will predict the class of development of hip dysplasia and will filter out ultrasound images of the hip joint with incorrect diagnostics. Similar CNN-based systems are used to recognize and classify diseases in medical images [7, 20]. In the future, it is proposed to add a computer algorithm for quantitative measurement of the angles α and β of the hip joint according to Graf's method.

6. Conclusion

The study proposes a computer method for classification of ultrasound images of hip dysplasia using Graf's classification. The positive possibilities of the convolutional neural network for the classification and recognition of images of the hip joint obtained at the correct or incorrect position of the ultrasound sensor head are shown. The ability of CNN to select correct ultrasound images of the hip joint, thereby improving the accuracy of diagnosing pediatric dysplasia, has been demonstrated. With this purpose it was conduct experimental studies on GoogLeNet, SqueezeNet, and AlexNet CNNs to select the best. The CNN's data were chosen not by chance, as they won the ImageNet Large Scale Visual Recognition Challenge (ILSVRC) in different years. They were fine-tuned and trained using a database of ultrasound images of the hip joint. It was found that the reliability of training and testing on a sample of 97 images of the hip joint is the highest for the GoogLeNet network: when classified in the training group accuracy is up to 100%, when classified in the test group accuracy – 84.5%. According to the others parameters such as the number of layers, the accuracy of classification in the test group, the weight of the network after training, CNN SqueezeNet has marginally better performance. In the study of CNN AlexNet found that the number of layers of 25 is insufficient to achieve accuracy in the classification of the test group at least up to 80%.

References

[1] Bilynsky Y. Y., Urvan O. G., Guralnyk A. B.: Modern methods of perinatal diagnosis of hip dysplasia: global trends. Scientific Proceedings of VNTU 4, 2019, 40–50.
[2] Bilynsky Y. Y. et al.: Overview of methods of ultrasound diagnosis of hip dysplasia and determination of the most appropriate of them for computer prediction of the disease. Medical Informatics and Engineering 3, 2019, 49–58 [http://doi.org/10.11603/mie.1996-1960.2019.3.10432].
[3] Bilynsky Y. Y. et al.: Algorithm of computer diagnostics of 2D ultrasound images of hip dysplasia. Modern problems of information communications, radioelectronics and nanosystems. International scientific and technical conference, Vinnytsia 2019, 150–153.
[4] Bilynsky Y. Y. et al.: Computer analysis of 2D ultrasound images of the hip joint and measurement of its geometry. Information Technologies and Computer Engineering 3(46), 2019, 4–13 [http://doi.org/10.31649/1999-9941-2019-46-3-4-14].
[5] Bilynsky Y. Y. et al.: Contouring of microcapillary images based on sharpening to one pixel of boundary curves. Proc. SPIE 10445, 2017, 104450Y [http://doi.org/10.1117/12.2281005].
[6] Bilynsky Y. et al.: Controlling geometric dimensions of small-size complex-shaped objects. Proc. SPIE 10445, 2017, 104450I [http://doi.org/10.1117/12.2280899].
[7] Breve F. A.: COVID-19 detection on Chest X-ray images: A comparison of CNN architectures and ensembles. Expert Systems With Applications, 2022, [http://doi.org/10.1016/j.eswa.2022.117549].
[8] Dahlström H.: Dynamic ultrasonic evaluation of congenital hip dislocation. University of Umeå, 1989.
[9] Forrest N. I. et al.: SqueezeNet: Alexnet-level accuracy with 50x fewer parameters and <0.5mb model size. arXiv:1602.07360, 2016.
[10] Graf R. et al.: Hip sonography update. Quality-management, catastrophes-tips and tricks. Medical Ultrasonography 15(4), 2013, 299–303.
[11] Graf R.: The diagnosis of congenital hip-joint dislocation by the ultrasonic combound treatment. Arch. Orth. Traum. Surg. 97, 1980, 117–133, [http://doi.org/10.1007/BF00450934].
[12] Harcke H. et al.: Examination of the infant hip with real-time ultrasonography. J. Ultrasound Med. 3, 1984, [http://doi.org/10.7863/jum.1984.3.3.131].

[13] Krasilenko V. et al.: Modeling optical pattern recognition algorithms for object tracking based on nonlinear equivalent models and subtraction of frames. Proc. SPIE 9813, 2015, 981302 [http://doi.org/10.1117/12.2205779].
[14] Krasilenko V. et al.: Design and simulation of programmable relational optoelectronic time-pulse coded processors as base elements for sorting neural networks. Proc. SPIE 7723, 2010, 77231G [http://doi.org/10.1117/12.851574].
[15] Krasilenko V. et al.: Design and simulation of optoelectronic complementary dual neural elements for realizing a family of normalized vector 'equivalence-nonequivalence' operations. Proc. SPIE 7703, 2010, 77030P [http://doi.org/10.1117/12.850871].
[16] Krizhevsky A. et al.: ImageNet classification with deep convolutional neural networks. Communications of the ACM 60(6), 2017, 84–90.
[17] Marochko N. V.: Ultrasound study of hip joints in children of the first year of life: textbook for the system of post-graduate professional education of doctors. Izd. IPKSZ center, Khabarovsk 2008.
[18] Morin C. et al.: The infant hip: real-time US assessment of acetabular development. Radiology 157, 1985, 673–677.
[19] Rosendahl K. et al.: Developmental dysplasia of the hip: prevalence based on ultrasound diagnosis. Pediatr. Radiol. 26(9), 1996, 635–639, [http://doi.org/10.1007/BF01356824].
[20] Shokraei F. et al.: From CNNs to GANs for cross-modality medical image estimation. Computers in Biology and Medicine 146, 2022, 105556.
[21] Szegedy C. et al.: Going deeper with convolutions. ArXiv 2014 [http://arxiv.org/pdf/1409.4842.pdf].
[22] Terjesen T., Bredland T., Berg V.: Ultrasound for hip assessment in the newborn. J Bone Joint Surg Br. 71(5), 1989, 767–773.
[23] Wang D. et al.: Deep Learning for Identifying Metastatic Breast Cancer. ArXiv 2016 [http://arxiv.org/pdf/1606.05718.pdf].
[24] Weiss K., Khoshgoftaar T. M., Wang D.: A Survey of Transfer Learning. Journal of Big Data 3(1), 2016, 1–9 [http://doi.org/10.1186/s40537-016-0043-6].

D.Sc. Eng., Professor Yosyp Bilynsky
e-mail: Yosyp.bilynsky@ gmail.com

Doctor of technical sciences, professor Department of General Physics of Vinnytsia National Technical University, professor Departments of Computer Sciences and Economics of Cybernetics of Vinnytsia National Agrarian University, Vinnytsia, Ukraine. Corresponding member of the Academy of Applied Electronics.
Scientific direction: development of sensors, processing signals and images.

http://orcid.org/0000-0002-9659-7221

Ph.D. Aleksandr Nikolskyy
e-mail: nikolskyy@i.ua

Candidat of Technical Sciences, associate professor of the Biophysics, Informatics and Medical Equipment Department of National Pirogov Memorial Medical University, Vinnytsia, Ukraine.
Scientific direction: Neural Networks, preprocessing of medical images, Optoelectronic Structure.

http://orcid.org/0000-0002-0098-0606

Ph.D. Viktor Revenok
e-mail: vrevenok@ ukr.net

Candidat of Technical Sciences, associate professor of the Biophysics, Informatics and Medical Equipment Department of National Pirogov Memorial Medical University, Vinnytsia, Ukraine, associate professor Departments of Computer Sciences and Economics of Cybernetics of Vinnytsia National Agrarian University, Vinnytsia, Ukraine.
Scientific direction: computer modeling of biophysical systems, preprocessing of medical images, modernization of endoscopic systems.

http://orcid.org/0000-0002-8239-6955

D.Sc. Med. Vasyl Pogorilyi
e-mail: pogoriliy@vnmu.edu.ua

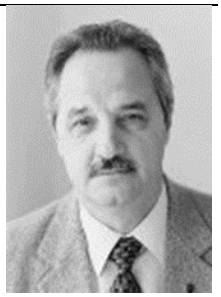

Doctor of Medical Sciences, professor, Vice-rector on Scientific and Pedagogical (Medical) Work, National Pirogov Memorial Medical University, Vinnytsia, Ukraine.
Scientific direction: prevention of children's surgery, surgical intervention technique for peritonitis, intestinal obstruction, congenital malformations, injuries, pinched hernias, treatment of purulent-inflammatory diseases of soft tissues and bones.

http://orcid.org/0000-0001-5317-5216

Ph.D. Saule Smailova
e-mail: Saule_Smailova@mail.ru

Saule Smailova is currently a lecturer at the Department of Information Technology. D.Serikbayev East Kazakhstan State Technical University Ust-Kamenogorsk, Al-Farabi Kazakh National University, Almaty, Kazakhstan.
She is a co-author over 60 papers in journals, book chapters, and confer ence proceedings. Member of Expert Group in the Computer Science specialization of IQAA.
Her professional interests are teaching, artificial intelligence, software engineering, data processing.

http://orcid.org/0000-0002-8411-3584

Ph.D., Associate Professor Oksana Voloshina
e-mail: woloshina5555@gmail.com

Candidate of Pedagogic Sciences, associate professor, Vinnytsia Mykhailo Kotsubynsky State Pedagogical University, Ministry of Education and Science of Ukraine, Vinnitsa. Scientific directions: pedagogy, professional education and management of educational institutions, training of highly qualified specialists.

http://orcid.org/0000-0002-9977-7682

Ph.D. Saule Kumargazhanova
e-mail: SKumargazhanova@gmail.com

She is currently the dean of the Department of Information Technologies and Intelligent Systems of D. Serikbayev East Kazakhstan Technical University. She is a co-author over 50 papers in journals and conference proceedings. Her professional interests are software engineering, data processing and analysis.

http://orcid.org/0000-0002-6744-4023

http://doi.org/10.35784/iapgos.3654 *received: 15.05.2023 | revised: 08.06.2023 | accepted: 12.06.2023 | available online: 30.06.2023*

CARDIOMETABOLIC RISK PREDICTION IN PATIENTS WITH NON-ALCOHOLIC FATTY LIVER DISEASE COMBINED WITH SUBCLINICAL HYPOTHYROIDISM

Olena Kolesnikova[1], Olena Vysotska[2], Anna Potapenko[1], Anastasia Radchenko[1], Anna Trunova[2], Nataliya Virstyuk[3], Liudmyla Vasylevska-Skupa[3], Aliya Kalizhanova4, Nazerka Mukanova[5]

[1]Government Institution "L. T. Malaya Therapy Institute of the National Academy of Medical Science of Ukraine", Kharkiv, Ukraine, [2]National Aerospace University "Kharkiv Aviation Institute", Kharkiv, Ukraine, [3]Ivano-Frankivsk National Medical University, Ivano-Frankivsk, Ukraine, [3]Vinnytsia Mychailo Kotsiubynskyi State Pedagogical University, Vinnytsia, Ukraine, [4]Institute of Information and Computational Technologies, Almaty, Kazakhstan, [5]Gymnasium No. 159 named after Y. Altynsarin, Almaty, Kazakhstan

Abstract. *One of the most common diseases of our time is non-alcoholic fatty liver disease (NAFLD). Recently published research results indicate that patients with NAFLD along with traditional risk factors for cardiovascular diseases (CVD) have "new" risk factors such as endothelial dysfunction (ED), carotid intima-media thickness (CIMT), an increase in the CRP level, as well as risk factors combined into the Framingham scale. It is also known that combination of NAFLD with subclinical hypothyroidism (SH) forms an abnormal metabolic phenotype, which is associated with cardiometabolic risk factors. The study of cardiometabolic predictors and vascular markers in patients with NAFLD in combination with SH will provide an opportunity to improve the strategy of cardiovascular events prevention in such comorbid patients.*

Keywords: cardiometabolic risk, non-alcoholic fatty liver disease, subclinical hypothyroidism, prediction, binary regression logistic analysis, validation of prognostic models

PRZEWIDYWANIE RYZYKA KARDIOMETABOLICZNEGO U PACJENTÓW Z NIEALKOHOLOWĄ STŁUSZCZENIOWĄ CHOROBĄ WĄTROBY W POŁĄCZENIU Z SUBKLINICZNĄ NIEDOCZYNNOŚCIĄ TARCZYCY

Streszczenie. *Niealkoholowe stłuszczenie wątroby (NAFLD) jest jedną z najczęstszych chorób naszych czasów. Ostatnio opublikowane wyniki badań sugerują, że pacjenci z NAFLD, wraz z tradycyjnymi czynnikami ryzyka chorób sercowo-naczyniowych (CVD), mają "nowe" czynniki ryzyka, takie jak dysfunkcja śródbłonka (ED), grubość błony wewnętrznej i środkowej tętnicy szyjnej (CIMT), podwyższony poziom CRP i czynniki ryzyka połączone w skali Framingham. Wiadomo również, że połączenie NAFLD z subkliniczną niedoczynnością tarczycy (SH) tworzy nieprawidłowy fenotyp metaboliczny związany z czynnikami ryzyka kardiometabolicznego. Badanie predyktorów kardiometabolicznych i markerów naczyniowych u pacjentów z NAFLD w połączeniu z SH pozwoli na ulepszenie strategii zapobiegania zdarzeniom sercowo-naczyniowym u takich współistniejących pacjentów.*

Słowa kluczowe: ryzyko kardiometaboliczne, niealkoholowe stłuszczenie wątroby, subkliniczna niedoczynność tarczycy, rokowanie, binarna analiza regresji logistycznej, walidacja modeli prognostycznych

Introduction

In recent years, an increasing number of cardiovascular pathologies worldwide makes it necessary to search for new risk factors that could serve as an indicator and determine the likely prognosis of patients with somatic diseases. Currently, the concept of "cardiometabolic risk" is increasingly used in clinical practice. It involves the risk of developing cardiovascular diseases and/or type 2 diabetes, combining both classical ("traditional") risk factors such as smoking, high levels of low-density lipoprotein cholesterol (LDL-C), arterial hypertension, an increase in glucose level, and factors directly associated with abdominal (especially visceral) obesity – insulin resistance (IR), low high-density lipoprotein cholesterol (HDL-C), hypertriglyceridemia, and an increase in proinflammatory markers [8]. The attention of researchers is attracted by the search for early predictors of cardiometabolic changes and vascular markers – markers of inflammation (C-reactive protein, CRP), dyslipidemia, IR, tumor necrosis factor – α (TNF-α), endothelial dysfunction (ED) indicators such as circulating desquamated endothelial cells (CDECs), vascular endothelial growth factor (VEGF), that could act as a "predictive" [1, 7].

One of the most common diseases of our time is non-alcoholic fatty liver disease (NAFLD) – a chronic liver disease that is considered as a component of some diseases associated with IR, such as metabolic syndrome (MS), obesity, and diabetes. The development of NAFLD is very closely associated not only with abdominal obesity, but also has a significant effect on the formation of cardiometabolic risk factors such as hypertriglyceridemia, a decrease in HDL-C level, hypertension, hyperglycemia, thereby increasing the degree of cardiometabolic risk itself and affecting the prognosis and life expectancy of patients [8, 18].

Recently published research results indicate that patients with NAFLD along with traditional risk factors for cardiovascular diseases (CVD) (obesity, diabetes, MS and others) have "new" risk factors such as endothelial dysfunction (ED), carotid intima-media thickness (CIMT), an increase in the CRP level, as well as risk factors combined into the Framingham scale (age, gender, hypertension, hyperlipidemia, smoking). Also, "traditional" cardiovascular risk factors include: markers of chronic inflammation, hyperhomocysteinemia, impaired blood viscosity, as well as substances that the endothelium secretes (NO, Willebrand factor, P-selectin, adhesion molecule ICAM-1 and VCAM-1, endothelin-1, PAI-1) [7, 8].

According to The Rotterdam Study, 28% of patients with NAFLD have signs of subclinical hypothyroidism (SH) [10, 11]. Targher G. et al. revealed a link between thyroid hormones and serum liver enzyme activity (levels of thyroid stimulating hormone (TSH), alanine aminotransferase (ALT), γ-Glutamyl Transpeptidase (GGTP)) in a study involving a large cohort of patients [1, 8].

Atherogenic dyslipidemia already occurs during SH and the early stages of NAFLD. It is characterized by an increase in the level of very low-density lipoprotein cholesterol (VLDL-C), LDL-C, and may also occur due to the thyroid hormone deficiency, which leads to a decrease in LDL receptors in the liver, as a result of a decrease in hepatic total cholesterol excretion, and then — to an increase in LDL-C and VLDL-C levels. The combination of NAFLD with SH forms an abnormal metabolic phenotype, which is characterized by the presence of dyslipidemia, hyperinsulinemia and IR associated with oxidative stress and endothelial dysfunction [12, 14].

Thus, the study of cardiometabolic predictors and vascular markers in patients with NAFLD in combination with SH will provide an opportunity to broaden understanding of the mechanisms of cardiometabolic risk formation and to individualize the strategy of cardiovascular events prevention in a comorbid patient within this framework.

One of the rapidly progressing trends in clinical medicine is undoubtedly the predicting of diseases using special scales. The SCORE scale (or the electronic version of HeartScore),

popular in Europe, is limited to the age of 45–64 years, while the age range in the PCE scale was much wider – 20–79 years old, but it is recommended to use it in the range of 40–79 years [3, 19].

Solving the problems of medical forecasting often involves the use of regression models. For example, Weibull regression was used in the SCORE scale, Cox regression was used in the second version of the GRACE scale, and the logistic regression was used in the CHA2DS2-VASc scale [2, 20]. One of the principal limitations of the scales is the impossibility of an individual assessment, since scales can only give a probabilistic risk assessment for a group of patients with given levels of risk factors.

Preventive treatment of CVD is largely based on model creation methods for assessing the "absolute risk" of future cardiovascular events in order to substantiate decisions about therapeutic approaches [5].

Neural networks widely used in medical science. Kojuri J. et al. [6] reported on the development of a neural network that predicts acute myocardial infarction for two weeks.

Jasnickij L. and Cherepanov F. [17] showed in their article the possibility of creating neuroexpert medical systems, allowing to perform long-term prognosis of the diseases development to predict the occurrence of new diseases in future periods of the patient's life.

The introduction of machine learning allows increasing the accuracy of prediction of cardiovascular events [15]. However, the use of a large array of heterogeneous data instead of selected patient cohort can reduce the accuracy of risk classification and the proximity of the forecast to the frequency of real events [4, 9, 13, 16].

The subject of the present work is creating a model for predicting cardiometabolic risk in patients with NAFLD in combination with SH.

The paper presents the results of the GI "L.T. Malaya Therapy Institute of the National Academy of Medical Science of Ukraine" scientific research on the topic: "Influence of factors of cardiovascular development on premature aging" (security number 0117U003031).

1. Materials and methods

71 patients were selected to create a prediction model for cardiometabolic risk in patients with NAFLD in combination with SH. All patients were divided into three groups as follows:
Group 1 – low risk patients (6 patients);
Group 2 – patients with moderate risk (43 patients);
Group 3 – high-risk patients (22 patients).

The following factors were used as potential predictors: age, body mass, waist circumference, thigh circumference, CRP, CDECs, CIMT, VEGF level; telomeres in the blood; telomeres in the buccal epithelium, total cholesterol (TC), triglycerides (TG), VLDL-C, HDL-C, atherogenic coefficient, ALT, aspartate aminotransferase (AST), GGTP, alkaline phosphatase (ALP), HbA1C, TSH, free tyroxine (free T4), free triiodothyronine (free T3), anti-thyroid peroxidase antibodies (TPOAb). All indicators were encoded and placed according to the 27-dimensional vector, which takes into account the absence, which displays the value of each metric.

Mathematical processing of the results was carried out using the SPSS19 application package for Windows.

2. Results of binary regression logistics analysis

49 patients of the first and second groups were analyzed to construct an equation of logistic regression, which determines the probability of having a moderate cardiovascular risk (CVR), taking into account the considered indicators.

Comparison of groups 1 and 2 showed that among all the evaluated factors, the length of the telomeres in the buccal epithelium, the levels of CRP, CDECs had the statistically significant effect on the probability of development of moderate cardiometabolic risk in patients with NAFLD in combination with SH. As a result, the regression function was constructed. It included 3 indicators (table 1).

The binary logistic function selected from the training sample looks like:

$$\hat{P} = \left[1 + e^{-(11.024X_1 + 0.533X_2 + 1.256X_3 - 25.352)}\right]^{-1} \quad (1)$$

where $\hat{P}$ is the probability of developing moderate CVR in patients with NAFLD in combination with SH.

Table 1. Factors of moderate cardiometabolic risk

Code	Factor
X_1	Telomere length in the buccal epithelium
X_2	CRP
X_3	CDECs

The calculated coefficients of the regression function and the results of checking their significance are presented in table 2. All variables are significant ($p < 0.05$) and selected correctly according to Wald's statistics.

Table 2. Regression function coefficients

Indicators (X_i)	Coefficients (b_i)	Standard errors (S_i)	Wald's criterion (W_i)	Significance (p_i)
X_1	11.024	5.487	4.037	0.045
X_2	0.533	0.290	3.384	0.046
X_3	1.256	0.662	3.599	0.048
Constant	-25.352	11.348	4.991	0.025

The quality of the regression model approximation was estimated using the similarity function. In our study, G = 11,612 at p = 0.001, that is as a whole the informative indications isolated as independent variables have a significant effect on the development of cardiometabolic risk in patients with NAFLD in combination with SH. The Cox and Schell, and Nagelkerke indices indicate that the dispersion part explained by the developed logistic model stands at 75.8% (table 3).

Table 3. Characteristics of the model of binary logistic regression, created to determine the probability of developing moderate cardiometabolic risk in patients with NAFLD in combination with SH

-2 Log Credibility (G)	R^2 of Cox and Shell	R^2 of Nagelkerke	χ^2	p
11.612	0.397	0.758	24.822	0.001

The figure 1 shows the classification diagram. The distribution point was P = 0.5. The closer the value of the predicted probability is to unit, the higher the probability of developing moderate cardiometabolic risk in patients with NAFLD in combination with SH is.

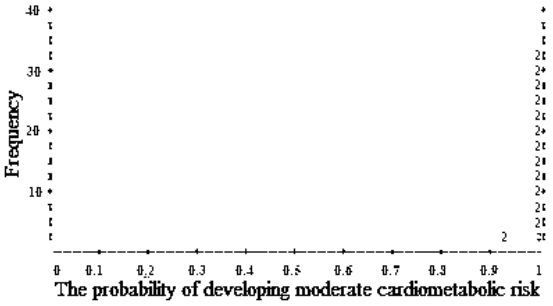

Fig. 1. Chart of classification. Symbols: 1 – low risk patients; 2 – patients with moderate risk

The results of the classification of patients in a training group using the developed prognostic model are given in table 4.

5 patients of the total number of patients with low risk, equal to 6, were correctly and 1 was mistakenly attributed to the moderate risk group.

Of the total number of patients with moderate risk of 43 people, 42 patients were accurately identified and 1 was

erroneously assigned to a group of low-risk patients. In general 47 cases out of 49 were correctly identified, representing 95.9%.

A general assessment of the agreement between the influence of risk factors found in the model and the actual occurrence of an adverse outcome was carried out using the Hosmer-Lemeshow (HL) test.

The resulting low value of HL = 4.391 at a significance level of $p > 0.05$ ($p = 0.820$), indicates the minimum differences between observed and predicted frequencies and the high quality of the selected regression model.

Table 4. Classification results of the model of binary logistic regression, created to determine the probability of moderate CVR in patients with NAFLD in combination with SH

Observed groups		Presumed groups		
		Risk		% correctly predicted
		Low	Moderate	
Risk	Low	5	1	83.3±15.23
	Moderate	1	42	97.7±2.29
Total percentage				95.9±2.83

The ROC analysis of the obtained model (figure 2) confirmed its effectiveness and excellent predictive quality. The area under curve (AUC) was 0.977 at p = 0.001.

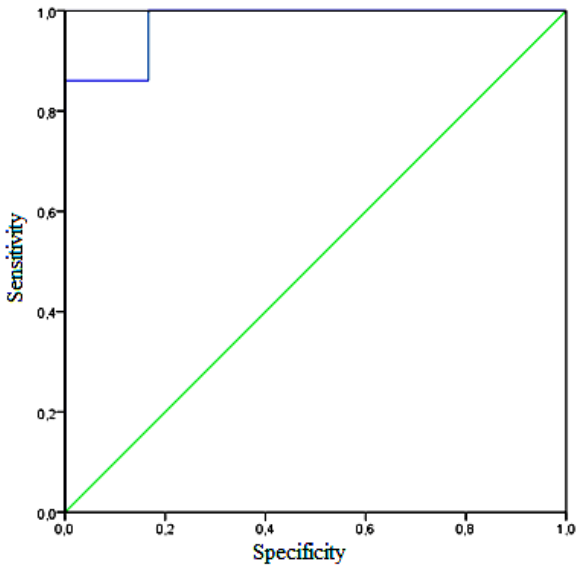

Fig. 2. ROC Curve

Thus, a mathematical model has been developed that includes metabolic risk factors such as the length of telomeres in the buccal epithelium, CRP and CDECs, to determine effectively and qualitatively the probability of forming moderate cardiometabolic risk in patients with NAFLD in combination with SH.

Data from 65 patients in the second and third groups were analyzed for the purpose of constructing a prediction model of cardiometabolic risk of higher gradations in patients with NAFLD in combination with SH. As a result of the binary logistic regression analysis, an equation has been obtained, which determines the likelihood of developing high CVR in patients with NAFLD in combination with SH:

$$\hat{P} = \left[1 + e^{-(4.366X_1 + 0.860X_2 + 0.009X_3 + 0.871X_4 - 19.391)}\right]^{-1} \quad (2)$$

where $\hat{P}$ is the probability of developing high CVR in patients with NAFLD in combination with SH;
X_1 – telomere length in the blood;
X_2 – LDL-C;
X_3 –VEGF;
X_4 – TSH.

Comparison of 2nd and 3rd groups therefore showed that of all of the factors evaluated, telomere length in blood, LDL-C, VEGF and TSH had a statistically significant effect on the likelihood of high cardiometabolic risk developing in patients with NAFLD in combination with SH.

All variables are significant ($p < 0.05$) and selected correctly according to Wald's statistics (table 5).

Table 5. Regression function coefficients

Indicators (X_i)	Coefficients (b_i)	Standard errors (S_i)	Wald's criterion (W_i)	Significance (p_i)
X_1	4.366	1.738	6.311	0.012
X_2	0.860	0.437	3.872	0.049
X_3	0.009	0.004	6.661	0.010
X_4	0.871	0.361	5.820	0.016
Constant	-19.391	4.787	16.407	0.001

In the study, G = 39.297 at p = 0.001 shows that independent variables have a significant contribution to predict the dependent variable in general. The part of the dispersion, explained by logistic regression according to R^2 of Cox and Schell stands at 68% (table 6).

Table 6. Characteristics of the model of binary logistic regression, created to determine the probability of developing high cardiometabolic risk in patients with NAFLD in combination with SH

-2 Log Credibility (G)	R^2 of Cox and Shell	R^2 of Nagelkerke	χ^2	p
39.297	0.680	43.905	0.001	39.297

A chart of classification of patients in the second and third study groups is presented in fig. 3 with the help of the developed mathematical model for predicting high cardiometabolic risk in patients with NAFLD in combination with SH.

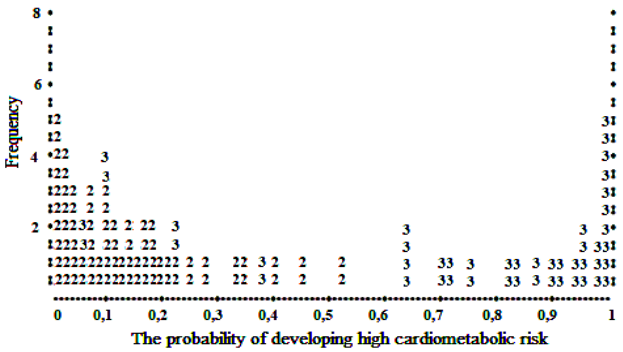

Fig. 3. Chart of classification. Symbols: 2 – moderate risk patients; 3 – high-risk patients

The value of P = 0.5 served as the limiting point of distribution. The closer the value of the predicted probability is to unity, the higher the degree of cardiometabolic risk in patients with NAFLD in combination with SH is. The classification results presented in table 7 indicate that in general 59 cases were correctly identified out of 65 that is 90.8%.

Table 7. Classification results of the model of binary logistic regression, created for the determination of the probability of development of high CVR in patients with NAFLD in combination with SH

Observed groups		Presumed groups		
		Risk		% correctly predicted
		Moderate	High	
Risk	Moderate	41	2	95.3±3.23
	High	4	18	8.8±8.23
Total percentage				95.9±2.83

The resulting low value of HL = 10.905 at a level of significance p = 0.143 indicates the high quality of the selected model. The ROC analysis of the resulting model (figure 4) confirmed the excellent quality of the developed model: the AUC value was 0.919 (p = 0.001).

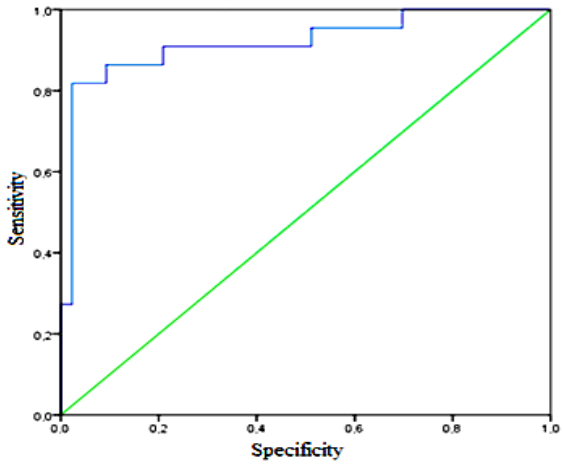

Fig. 4. ROC Curve

Thus, blood serum indices – LDL-C; VEGF; TSH and the length of telomeres in the blood may be factors that determine the probability of forming cardiometabolic risk of higher gradations in patients with NAFLD and SH.

3. Validative review of developed prognostic models

The usefulness of the developed mathematical models has been tested in practice while predicting the development of cardiometabolic risk in patients with NAFLD in combination with SH, who were screened and treated at the Government Institution "L.T. Malaya Therapy Institute of the National Academy of Medical Science of Ukraine". 34 patients were examined and divided into the following groups:
Group 1 – moderate-risk patients (9 patients);
Group 2 – high-risk patients (17 patients).
Group 3 – high-risk patients (8 patients).

The results of testing the model of binary logistic regression, created to determine the probability of moderate CVR development in patients with NAFLD in combination with SH, are presented in table 8.

Table 8. Classification results of the model of binary logistic regression, created to determine the probability of moderate CVD development in patients with NAFLD in combination with SH, on the test sample

Observed groups	Predicted results (n)		% correctly predicted
	Group 1	Group 2	
Group 1	9	0	100,0
Group 2	1	16	94.1±6.03
Total percentage			96.2±3.92

According to the results obtained, the outlook for 25 examined patients was made unmistakably. Thus, it was confirmed in 96.2% of cases.

The results of checking the model of binary logistic regression, created to determine the likelihood of high CVD in patients with NAFLD in combination with SH, are presented in table 9.

Table 9. Classification results of the model of binary logistic regression, created to determine the probability of moderate CVD development in patients with NAFLD in combination with SH, on the test sample

Observed groups	Predicted results (n)		% correctly predicted
	Group 2	Group 3	
Group 2	16	1	94.1±5.71
Group 3	1	7	87.5±11.69
Total percentage			92.0±5.43

The outlook was unmistakably accurate for 24 patients surveyed according to the results. Thus, the forecast was confirmed in 92.0% of cases.

That means, that the application of synthesized logistic models will allow predicting the development of cardiometabolic risk, which will ensure early diagnosis and appointment of treatment and prevention measures in order to avoid the development of cardiometabolic complications of high gradations.

4. Conclusions

The developed mathematical models allow predicting the degree of cardiometabolic risk in patients with NAFLD in combination with SH based on the of cumulative changes in lipid, carbohydrate states, thyroid function compensation, vascular factors and telomere lengths as a marker for vascular aging. The application of the proposed prognostic models in clinical practice allows to achieve an improvement in the quality of the cardiometabolic risk determination in patients with NAFLD in combination with SH due to the identification of factors that influence the progression of cardiometabolic changes in patients with NAFLD precisely in combination with SH, and the improvement of the applied mathematical apparatus, which in turn will help the physician to prescribe adequate treatment and preventive measures and improve the quality of medical services provision for patients with NAFLD in combination with SH.

References

[1] Bano A., Chaker L., Plompen E. P. C., et al.: Thyroid Function and the Risk of Nonalcoholic Fatty Liver Disease: The Rotterdam Study. J Clin Endocrinol Metab. 101(8), 2016, 3204–3211.
[2] Belyalov F. I.: Prognozirovaniye i shkaly v kardiologii 2ye-izd. MEDPRESS-inform, Moscow 2018.
[3] Belialov F. I.: Risk prediction scores of diseases. Complex Issues of Cardiovascular Diseases 7(1), 2018, 84–93 [http://doi.org/10.17802/2306-1278-2018-7-1-84-93].
[4] Georgiyants M., Khvysyuk O., Boguslavskaya N. et al.: Development of a mathematical model for predicting postoperative pain among patients with limb injuries. Eastern-European Journal of Enterprise Technologies 2, N4(86), 2017, 4–9 [http://doi.org/10.15587/1729-4061.2017.95157].
[5] Graham I., Atar D., Borch-Johnsen K. et al.: European guidelines on cardiovascular disease prevention in clinical practice: full text. Eur. J. Cardiovasc. Prev. Rehabil. 14, 2007, S1–S113.
[6] Kojuri J., Boostani R., Dehghani P., Nowroozipour F., Saki N.: Prediction of acute myocardial infarction with artificial neural networks in patients with nondiagnostic electrocardiogram. Journal of Cardiovascular Disease Research. 6(2), 2015, 51–60.
[7] Kolesnikova E. V.: Sovremennyy patsiyent s zabolevaniyem pechenii patologiyey serdechno-sosudistoy sistemy: kakoy vybor sdelat? Contemporary gastroenterology 2(76), 2014, 85–94.
[8] Kolesnikova O. V., Nemtsova V. D.: Effect of preventive measures for major metabolic parameters in patients with non-alcoholic fatty liver disease and cardiovascular risk. The ESC Textbook of Preventive Cardiology. Comprehensive, practical, and the official textbook of the European Association for Cardiovascular Prevention and Rehabilitation. Oxford University press, 2015.
[9] Koval S. M., Snihurska I. O., Vysotska O. et al.: Prognosis of essential hypertension progression in patients with abdominal obesity. Wójcik W., Pavlov S., Kalimoldayev, M. (Eds.): Information Technology in Medical Diagnostics II. Taylor & Francis Group, CRC Press, Balkema book, London 2019.
[10] Krak I. V., Kryvonos I. G., Kulias A. I.: Applied aspects of the synthesis and analysis of voice information. Cybernetics and Systems Analysis 49(4), 2013, 589–596.
[11] Krak I., Kondratiuk S.: Cross-platform software for the development of sign communication system: Dactyl language modelling. 12th International Scientific and Technical Conference on Computer Sciences and Information Technologies – CSIT, 2017, 1,8098760, 167–170
[12] Ludwig U., Holzner D., Denzer C. et al.: Subclinical and clinical hypothyroidism and non-alcoholic fatty liver disease: a cross-sectional study of a random population sample aged 18 to 65 years. BMC Endocr Disord. 15. 2015, 41.
[13] Ross D. S., Burch G. B, Cooper D. S. et al.: American Thyroid Association Guidelines for Diagnosis and Management of Hyperthyroidism and other causes of Thyrotoxicosis. Thyroid 26(10), 2016, 1343–1421.

[14] Sinn D. H., Cho S. J., Gu S. et al.: Persistent Nonalcoholic Fatty Liver Disease Increases Risk for Carotid Atherosclerosis. Gastroenterology 151(3), 2016, 481–488.
[15] Strashnenko A. N., Vysotskaya E. V., Demin Y. A. et al.: A method for prognosis of primary open-angle glaucoma. International Review on Computers and Software 8, 2013, 1943–1949.
[16] Weiwei He, Xiaofei An, Ling Li et al.: Relationship between Hypothyroidism and Non-Alcoholic Fatty Liver Disease: A Systematic Review and Meta-analysis. Front Endocrinol (Lausanne) 8, 2017, 335.
[17] Weng S. F., Reps J., Kai J., Garibaldi J. M., Qureshi N.: Can machinelearning improve cardiovascular risk prediction using routine clinical data? PLOS ONE 12(4), 2017, e0174944 [http://doi.org/10.1371/journal.pone.0174944].
[18] Wójcik W., Pavlov S., Kalimoldayev M.: Information Technology in Medical Diagnostics II. Taylor & Francis Group, CRC Press, Balkema book, London 2019.
[19] Yakubovska S., Vysotska O., Porvan A. et al.: Developing a method for prediction of relapsing myocardial infarction based on interpolation diagnostic polynomial. Eastern-European Journal of Enterprise Technologies 5(9(83)), 2016, 41–49 [http://doi.org/10.15587/1729-4061.2016.81004].
[20] Yasnitsky L. N., Cherepanov F. M.: Neyroekspertnaya sistema diagnostiki, prognozirovaniya i upravleniya riskami serdechno-sosudistykh zabolevaniy. Prikladnaya matematika i voprosy upravleniya 3, 2018, 107–126.

Prof. Olena Kolesnikova
e-mail: kolesnikova1973@gmail.com

Deputy director for Scientific work, head of the Department for the study of aging processes and prevention of metabolic-associated diseases.
Government Institution "L.T. Malaya Therapy Institute of the National Academy of Medical Science of Ukraine".
Scientific interest: information technologies in medicine.

http://orcid.org/0000-0001-5606-6621

Prof. Olena Vysotska
e-mail: o.vysotska@khai.edu

Head of the Department of Radio-Electronic and Biomedical Computerized Means and Technologies.
National Aerospace University "Kharkiv Aviation Institute".
Scientific interest: information technologies in medicine.

http://orcid.org/0000-0003-3723-9771

Ph.D. Anna Potapenko
e-mail: annav1611sh@gmail.com

Researcher at the Department for the study of aging processes and prevention of metabolic-associated diseases, Endocrinologist of the second qualification category.
Government Institution "L.T. Malaya Therapy Institute of the National Academy of Medical Science of Ukraine".
Scientific interest: information technologies in medicine.

http://orcid.org/0000-0002-1658-0156

Anastasia Radchenko
e-mail: anastasha.radchenko@gmail.com

Postgraduate student of the department of studying aging processes and prevention of metabolic-associated diseases.
Government Institution "L.T. Malaya Therapy Institute of the National Academy of Medical Science of Ukraine".

http://orcid.org/0000-0002-9687-8218

Ph.D. Anna I. Trunova
e-mail: a.pecherska@khai.edu

Associate professor of the Department of Radio-Electronic and Biomedical Computerized Means and Technologies National Aerospace University "Kharkiv Aviation Institute".
Scientific interest: information technologies in medicine.

http://orcid.org/0000-0001-7069-0674

Prof. Nataliya Virstyuk
e-mail: if_dermven@ukr.net

Head of the Department of Pharmacology and Internal Medicine No 3 named after M.M. Berezhnytskyi Ivano-Frankivsk National Medical University.
Scientific interest: information technologies in medicine.

http://orcid.org/0000-0002-5794-8754

Ph.D. Liudmyla Vasylevska-Skupa
e-mail: lpvasylevska@gmail.com

Associated professor of Vinnytsia Mychailo Kotsiubynskyi State Pedagogical University.
Scientific interest: information technologies in medicine, pedagogy.

http://orcid.org/0000-0002-1989-7175

Ph.D. Aliya Kalizhanova
e-mail: kalizhanova_aliya@mail.ru

Candidate of physical and mathematical sciences, professor, University of Power Engineering and Telecommunications, the chief researcher of the Institute of Information and Computational Technologies of the Ministry of Education and Science CS of the Republic of Kazakhstan.
Scientific interests: mathematical modeling of systems, models of transport systems network analysis, optimization methods, technologies for developing sensor systems for signals receive – transmit, mathematical modeling of Bragg fiber gratings.

http://orcid.org/0000-0002-5979-9756

M.Sc. Nazerka Mukanova
e-mail: mukanova0124@gmail.com

Master of Pedagogical Sciences, teacher of the highest category of computer science of gymnasium No. 159 named after Y. Altynsarin, a prize-winner of several national and international competitions, her scientific articles have been published in several domestic and international publications, and she is a participant in various international teaching-methodical pedagogical conferences.
Scientific interest: information technologies in medicine.

http://orcid.org/0009-0002-7945-7187

http://doi.org/10.35784/iapgos.3664 received: 20.05.2023 | revised: 6.06.2023 | accepted: 12.06.2023 | available online: 30.06.2023

LOCAL DIFFERENCE THRESHOLD LEARNING IN FILTERING NORMAL WHITE NOISE

Leonid Timchenko[1], Natalia Kokriatskaya[1], Volodymyr Tverdomed[1], Natalia Kalashnik[2], Iryna Shvarts[3], Vladyslav Plisenko[1], Dmytro Zhuk[1], Saule Kumargazhanova[4]

[1]State University of Infrastructure and Technology, Kyiv, Ukraine, [2]National Pirogov Memorial Medical University, Vinnytsia, Ukraine,
[3]Vinnytsia National Technical University, Vinnytsia, Ukraine, [4]D.Serikbayev East Kazakhstan State Technical University Ust-Kamenogorsk, Kazakhstan

Abstract. *The article was aimed at studying the process of learning by the local difference threshold when filtering normal white noise. The existing learning algorithms for image processing were analyzed and their advantages and disadvantages were identified. The influence of normal white noise on the recognition process is considered. A method for organizing the learning process of the correlator with image preprocessing by the GQP method has been developed. The dependence of the average value of readings of the rank CCF (RCCF) of GQPs of the reference and current images, representing realizations of normal white noise, on the probability of formation of readings of zero GQP is determined. Two versions of the learning algorithm according to the described learning method are proposed. A technique for determining the algorithm efficiency estimate is proposed.*

Keywords: training, local difference threshold, filtering normal white noise

PROCES UCZENIA WZGLĘDEM LOKALNEGO PROGU RÓŻNICY W FILTROWANIU NORMALNEGO SZUMU BIAŁEGO

Streszczenie. *Celem pracy było zbadanie procesu uczenia za pomocą lokalnego progu różnicy podczas filtrowania normalnego białego szumu. Przeanalizowano istniejące algorytmy uczenia do przetwarzania obrazu oraz zidentyfikowano ich zalety i wady. Uwzględniono wpływ normalnego białego szumu na proces rozpoznawania. Opracowano metodę organizacji procesu uczenia korelatora z przetwarzaniem wstępnym obrazu przy użyciu metody GQP. Określono zależność średniej wartości próbek rangi CCF (RCCF) GQP obrazów referencyjnego i bieżącego, reprezentujących realizacje normalnego białego szumu, od prawdopodobieństwa utworzenia zerowych próbek GQP. Zaproponowano dwie wersje algorytmu uczenia opartego na opisanej metodologii uczenia. Zaproponowano metodę określania szacunkowej skuteczności algorytmu.*

Słowa kluczowe: uczenie, lokalny próg różnicy, filtrowanie normalnego białego szumu

Introduction

Pattern recognition is a relevant and promising area in the field of information technology, the scope of its application is expanding every year. In turn, recognition [4, 5] has separate tasks that should be solved in order to obtain the most accurate result. This includes the recognition process itself, image pre-processing to detect and eliminate noise, segmentation, real-time recognition, etc.

The choice of the value ψ of the local difference threshold (LDT) in order to maximally suppress the additive normal white noise in the image is relevant for the generalized *Q*-transformation (GQT) of the image or after its partial *Q*-summation (in the latter case, when creating wide-field correlators) [3, 17]. Partially, for the case of correlation detection of a signal of constant amplitude in the presence of the specified type of noise, this issue is covered in [2, 6, 13].

To implement image recognition, a high-precision and fast learning algorithm is required. Existing algorithms have a number of shortcomings, which creates the need to create new teaching methods. Good recognition accuracy is provided by preprocessing using the GQP method. Thus, in the article will be developed a method based on such preprocessing. The method will allow effective system training for recognition under the influence of normal white noise on the image [8, 10, 13].

1. Purpose and tasks of the study

This article describes a method for organizing the learning process of a correlator with image preprocessing using the GQP method, carried out in order to select the value ψ_{opt} of LDT, which minimizes the average value of reports of the rank cross-correlation function (RCCF) $Q_{+\zeta}(\vec{\tau})$ of the reference $G(i`,j`) = \{\zeta_{i,j}\}$ and the current $F(i,j) = \{f_{i,j}\}$ images, which are realizations of normal white noise [7, 14, 16].

2. Materials and research methods

Consider the graph of the probability density $P(u)$ of the white noise amplitude distribution. It is shown on Fig. 1 and is expressed by the formula:

$$P(u) = \frac{1}{\sqrt{2\pi}\cdot\sigma} \cdot e^{-\frac{u^2}{2\cdot\sigma^2}} \quad (1)$$

where σ – standard deviation (SD) of the noise signal amplitude.

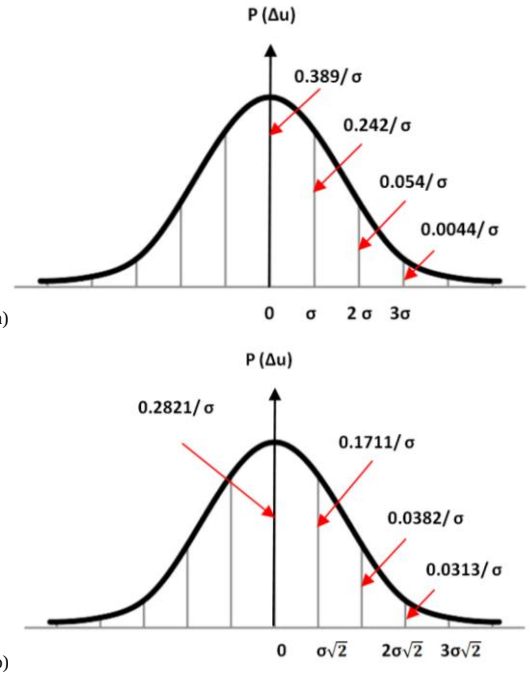

Fig. 1. Graphs of the probability density of the distribution of the amplitude of white noise (a) and the probability density of the distribution of the difference between the white noise samples (b)

Expression (1) is valid for describing the noise of the transmission channel of a television image or the noise of a television photodetector, but cannot be used to describe a unipolar signal from a random background image (background) with a normal distribution of the brightness probability density [8, 15].

The distribution law of the probability density $P(\Delta u)$ of the difference Δu of samples of normal white noise (Fig. 1b) has the following form:

$$P(\Delta u) = \frac{1}{\sigma\sqrt{2}\sqrt{2\pi}} \cdot e^{-\frac{\Delta u^2}{2(\sigma\sqrt{2})^2}} \quad (2)$$

This law is also valid for the difference between the signal samples from a random background with a normal law of distribution of the brightness probability density. Therefore, the conclusions regarding the suppression of the contribution of the additive normal white noise in the RCCF can be extended to the suppression of the contribution of the random background signal to this correlation function [2, 9, 12].

The quantization of the difference signal $\Delta u_{i,j} = u_{i,j} - u_{i+r_x,j+r_y}$, where $(r_x, r_y) = \vec{r}$ is the rank of the generalized Q-preparation, leads to replacing the continuous distribution function $P(\Delta u)$ on m_b of quantization levels, this function is not limited in length, with a lattice function $\rho_p(\Delta u_n)$, where $\Delta u_n = \frac{\Delta u}{\sqrt{2}\cdot\sigma}$, limited (Fig. 2) in length by the number m_b, which is related to the confidence interval $2k_\sigma \cdot \sigma\sqrt{2}$ (k_σ is the coefficient) and the confidence probability $P_{surr\,k_\sigma}$ as follows:

$$m \geq INT\left[\frac{1}{1-P_{surr\,k_\sigma}} + 0.5\right] \quad (3)$$

where INT[ ] – integer part of a number,

$$P_{surr\,k_\sigma} = 2\int_0^{k_\sigma\sqrt{2\sigma}} \rho(\Delta u)d\Delta u = \frac{2}{\sqrt{2\pi}\sigma\sqrt{2}}\int_0^{k_\sigma\sqrt{2\sigma}} e^{-\frac{\Delta u^2}{2(\sigma\sqrt{2})^2}} d\Delta u =$$

$$= \frac{2}{\sqrt{2\pi}}\int_0^{k_\sigma} e^{-\frac{y^2}{2}} dy = 2\Phi_0(k_\sigma) \quad (4)$$

where $\Phi_0(k_\sigma)$ – tabulated probability integral.

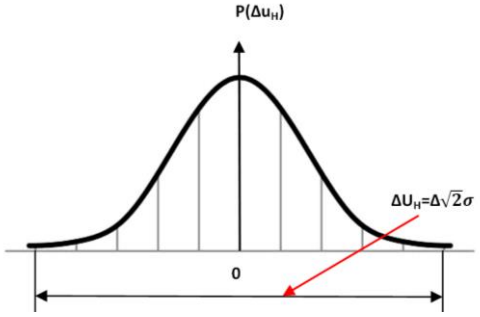

Fig. 2. Lattice function graph

From (3) and (4) follows, that:

$$m_b \geq \frac{1}{(1-2\Phi_0(k_\sigma))} \quad (5)$$

or

$$P_{surr\,k_\sigma} \leq \frac{b}{m_b - 1} \quad (6)$$

Functional dependency $m_b(P_{surr\,k_\sigma})$ in case of equality in (3) is reflected in the table 1. Since preparation usually follows quantization, then (3) has the form:

$$m'_b \geq 2INT\left[\frac{1}{1-P_{surr\,k_\sigma}} + 0.5\right] = 2m_b \quad (7)$$

From (7) it follows that with generalized contour preparation, the bit depth of the analog-to-digital converter (ADC) should be twice as large as with conventional correlation processing.

According to the table 1 it follows that a small difference ($m_b \leq 64$) of high-speed ADCs (for example, type 1107 PVZ) provides processing of the prepared image with a confidence probability $P_{surr} \leq 0.9844$.

Let m_g^r is the length of the GQP if the one-dimensional reference noise image $G(i', j')$:

$$m_g = m_g^r + r \quad (8)$$

For the preparated images, we omit the index r for brevity and instead of the designations m_g and m_f, we mean the designations m_g^r and m_f, respectively.

The number $n_{m0,m+,m-}$ of possible reference images having the same number of samples of zero ($m_{g,0}$), positive ($m_{g,+}$) and negative ($m_{g,-}$) GQPs for a given length m_g, is defined as follows:

$$n_{m0,m+,m-} = \frac{m_g!}{m_{g,0}!m_{g,+}!m_{g,-}!} \quad (9)$$

The probability of each such combination ($m_{g,0}, m_{g,+}, m_{g,-}$):

$$P_{m0,m+,m-} = P_0^{m_{g,0}}\left(\frac{1-P_0}{2}\right)^{m_g - m_{g,0}} \quad (10)$$

here P_0 – sample probability of zero GQP:

$$P_0 = \frac{2}{\sqrt{2\pi}}\int_0^{\Psi_n} e^{-\frac{y^2}{2}} dy = 2\Phi_0(\Psi_n) \quad (11)$$

where $\Psi_n = \frac{\Psi}{\sigma\sqrt{2}}$ – normalized LDT.

The total probability of all possible combinations:

$$P_{\sum m_{g,0},m_{g,+},m_{g,-}} = P_{m_{g,0},m_{g,+},m_{g,-}} \cdot n_{m_{g,0},m_{g,+},m_{g,-}} \quad (12)$$

Maximum (12) takes place at $m_0^g = m_g P_0$.

From the complete symmetry of the left and right parts of this equation, it follows:

$$P_0 = \frac{1-P_0}{2} \quad (13)$$

Let us determine the total probability $P_{cm\Sigma}$ of combinations coinciding in m samples with the combination of the standard $m_g = m_{\dot{y}}^0 + m_{\dot{y}}^+ + m_{\dot{y}}^-$ for the case $P_0 = P_n = P_+ = P_- = \frac{1-P_0}{2} = \frac{1}{3}$.

The initial moment of the first order will be equal to:

$$P_{H1} = \sum_{m=1}^{m_g} m\, P_{cm\Sigma} = \sum_{m=1}^{m_g} m\binom{m_g}{m} 2^{m_g - m} 3^{-m_g} \quad (14)$$

$$\frac{m_g - m}{m} = 2, m_g = 3m, m = \frac{m_g}{3} \quad (15)$$

Distribution $mP_{cm\Sigma}$ is mainly concentrated in the range $[1, \frac{2}{3}m_g]$ of values m, being nearly symmetrical with relatively to $m = \frac{m_g}{3}$.

For this range, the initial moment of the first order is equal to half, i.e. $\frac{m_g}{3}$.

Therefore, neglecting the distribution components contribution $mP_{cm\Sigma}$ in the range $\left[\frac{2m_g}{3}, m_g\right]$, we can make a conclusion, that for the whole range $[0, m_g]$ of values m:

$$P_{H1} \approx \frac{m_g}{3} \quad (16)$$

i.e. coincides with the distribution maximum $mP_{cm\Sigma}$.

The number of all possible combinations with a length m of the GQP standard is

$$N = 3^{m_g} \quad (17)$$

Therefore, we assume that there takes place

$$m_f \geq N = 3^{m_g} P_{cm\Sigma} \quad (18)$$

Table 1. Functional dependency $m_b(P_{surr\,k_\sigma})$

k_σ	1	2						3			4	
$Psurr\,k_\sigma$	0.6827	0.9375	0.9545	0.9688	0.9844	0.9922	0.9961	0.9973	0.9980	0.999	0.9999	0.99994
m_b	4	16	22	32	64	128	256	371	512	1024	10000	15773
m'_b	8	32	44	64	128	256	512	742	1024	248	20000	31546

Let us consider the general case $P_0 \neq P_n = \frac{1-P_0}{2}$, using the fact that maximum P_{H1} when varying the set $(m_{g,0}, m_{g,+}, m_{g,-})$ takes place at $m_{g,0} = m_g P_0 m_g^0$, $m_{g,+} = m_{g,-} = m_g \frac{1-P_0}{2} = m_g^+ = m_g^-$:

$$P_{H1} = \sum_{m=1}^{m_g} m \sum_{m_{1,0}, m_{1,+}, m_{1,-}} \binom{m_{g,0}}{m_{1,0}} \binom{m_{g,+}}{m_{1,+}} \binom{m_{g,-}}{m_{1,-}} P_0^{m_{1,0}} \left(\frac{1-P_0}{2}\right)^{m-m_{1,0}} \times (P_0 + P_n)^{m_{g,-}-m_{1,-}} \quad (19)$$

where $m_g = m_{g,0} + m_{g,+} + m_{g,-}$, $m = m_{1,0} + m_{1,+} + m_{1,-}$, $0 \leq m_{1,0} \leq m_{g,0}$, $m_{1,0} = \overline{0, m_{g,0}}$, likewise $m_{1,+} = \overline{0, m_{g,+}}$, and $m_{1,-} = \overline{0, m_{g,-}}$.

After transformations, we get:

$$P_{H1} = \sum_{m=1}^{m_g} 2^{\frac{m}{m_g}} \sum_{(m_{1,+}, m_{1,-})} \binom{m_{g,+}}{m_{1,+}} \binom{m_{g,-}}{m_{1,-}} \quad (20)$$

The conclusion is explained by the data of table 3 for the case $m_g = 12$ and $P_n = 0.5$. From table 2 it follows that $P_{H1} = \frac{24576}{4096} = 6$.

Let us consider the case $P_0 + 1, P_0 = 1 - \frac{2}{m_g}, P_n = \frac{1}{m_g}$. Wherein $m_{1,0}, m_{1,-} \leq 1$, therefore, in (19) from the combinations $(m_{1,0}, m_{1,+}, m_{1,-}) \in \{(m, 0,0), (m-1,0,1), (m-2,1,1)\}$ we can leave only combinations $(m, 0,0)$, since the rest, as it is easy to show, make a much smaller contribution to P_{H1}.

Dependency $\sum_2, m\sum_2$ when varying the set$(m_{g,0}, m_{g,+}, m_{g,-})$.

In this way, $m_{1,0} = m$. With this in mind:

$$P_{H1} \approx \sum_m \frac{m}{m_g{}^{m_g}} \binom{m_g - 2}{m} (m_g - 2)^m \cdot \cdot (m_g - 1)^{2-(m_{1,+}+m_{1,-})} 2^{m_g-2-m} \approx \approx \frac{2^{m_g-2}(m_g-1)^2}{m_g{}^{m_g}} \sum_m m \binom{m_g-2}{m} (m_g-2)^m 2^{-m} = \quad (21)$$

$$= \frac{\left(\frac{m_g-1}{2}\right)^2}{\left(\frac{m_g}{2}\right)^{m_g}} \sum m \binom{m_g-2}{m} \left(\frac{m_g-2}{2}\right)^m$$

Let us find the value m corresponding to the maximum probability density for the sum (21):

$$\frac{d}{dm}\left[m\binom{m_g-2}{m}\left(\frac{m_g-2}{2}\right)^m\right] = 0 \quad (22)$$

From (22) it follows:

$$\varphi + m\varphi' = 0 \; [\ln \varphi]' = -\frac{1}{m} \quad (23)$$

Using the Stirling formula for the approximate calculation of $z!$, we obtain:

$$[\ln \varphi]' = -\left(\ln m + \frac{m+1/2}{m}\right) + \left[\ln(m_g - 2 - m)\right] + + \frac{(m_g - 2 - m + 1/2)}{m_g - 2 - m} + \ln \frac{m_g - 2}{2} + \frac{m}{2} \frac{2}{m_g - 2} = \ln \frac{m_g-2-m}{2} \frac{m_g-2}{2} + \varphi_1(m, m_g) \quad (24)$$

From (24) at $m_g \to \infty, m \to \infty$ follows $\lim[\ln \varphi]' = 0$. Then:

$$\ln\left[\frac{m_g - 2 - m}{m} \frac{m_g - 2}{2}\right]^{-1/\varphi_1} = 0$$

and $\varphi_1 \neq 0$, i.e. $m \neq m_g - 2$, then:

$$\frac{m_g - 2 - m}{m} \frac{m_g - 2}{2} = 1$$

$$m = \frac{(m_g-2)^2}{m_g} \quad (25)$$

From inequality $\frac{(m_g-2)^2}{m_g} > \frac{m_g}{2}$ at $m_g > 7$ given that the change of the m near $m' = \frac{(m_g-2)^2}{m_g}$ is much less than the change of φ, and also that, as can be shown,

$$\sum_{m \leq m'} m\varphi \leq \sum_{m' < m} m\varphi$$

it follows that:

$$P_{H1} \geq m' = \frac{(m_g-2)^2}{m_g} \quad (26)$$

We accept that $P_{H1} \approx x$.

This conclusion is explained by the data in table 3 for a case $m_g = 10$, $P_0 = 0.8$, $P_n = 0.1$.

By the data of this table:

$$P_{H1} = \sum_{m=1}^{10} \frac{m\sum_2}{10^{10}} = \frac{6.59999 \cdot 10^{10}}{10^{10}} \cong 6.6 \quad (27)$$

Dependency $\frac{\sum_2}{10^8}$, $\frac{m\sum_2}{10^8}$ for a case $m_g = 10$, $P_0 = 0.8$, $P_n = 0.1$.

For a case $P_0 > P_n$:

$$P_{H1} \approx \frac{m_g}{2}\left(1 + \frac{P_0}{m_g}\right) = \frac{m_g}{2}\left(1 + {P_0}^2\right) \quad (28a)$$

$$P_{H1} \approx \frac{m_g}{2}(1 + P_0) \quad (28b)$$

Table 4 shows the data calculated by the exact formulas for the case $m_g = 5, P_0 = 0.2, P_n = 0.4$.

The initial moment P_{H1} (for a case $m_g = 5$, $P_0 = 0.2$, $P_n = 0.4$).

$$P_{H1} \approx \sum_{m=1}^{5} \frac{1}{m_g} m \sum\nolimits_2 = \frac{9801}{5^5} = 3.136$$

Dependency $\sum_2, m\sum_2$ for a this case (table 4).

Using the expansion in the Maclaurin series, we get:

$$2P_0\left(\Psi_{H_{opt}}\right) = P_0 = 0.33 \quad (29)$$

$$\psi_{H_{opt}} \approx \frac{1}{3}\sqrt{\frac{\pi}{2}} \approx 0.418 \approx \widetilde{\Psi_{H_{opt}}}$$

$$\delta\psi_{H_{opt}} \approx \frac{\Psi_{H_{opt}} - \widetilde{\Psi}_{H_{opt}}}{\Psi_{H_{opt}}} 100\% \approx 3.97\ \% \quad (30)$$

Table 2. Functional dependency ($\sum_2, m\sum_2$)

m	1	2	3	4	5	6	7	8	9	10	11	12
$\sum_2$	12	66	220	495	792	924	792	495	220	66	12	1
$m\sum_2$	12	132	660	1980	3960	5544	5544	3960	1980	660	132	12

Table 3. Functional dependency ($\frac{\sum_2}{10^8}, \frac{m\sum_2}{10^8}$)

m	1	2	3	4	5	6	7	8	9	10
$\frac{\sum_2}{10^8}$	0.00668	0.096383	0.76383	38.8219	12.72578	26.46999	32.61071	19.92294	3.35544	0.16777
$\frac{m\sum_2}{10^8}$	0.00668	0.18875	2.2915	15.52876	63.62891	158.8199	228.275	159.3835	30.19899	1.67772

Table 4. Data is calculated for the case $m_g = 5, P_0 = 0.2, P_n = 0.4$

m	1	2	3	4	5
$\sum_2$	945	3168	600	160	16
$m\sum_2$	945	6336	1800	640	80

For the existence of a single extremum A, it is necessary to fulfill the condition (at $P_0 = \frac{1}{3}$):

$$INT(m_g P_0) = m_g P_0$$

this implies:

$$m_g = 3k \tag{31}$$

where $k \in N^+$ (set of natural numbers).

To implement an ideal LDT learning process, it is necessary that, with a minimum change in the threshold ψ_H by one conventional unit (per quantization discrete) in the vicinity of $\psi_{H_{opt}} = 0.435$, there was a change per unit of the numbers $m_{g,0}$, or $m_{g,n}$:

$$\Delta m_{g,0} = m_g{}^0 - m_{g,0} = m_g P_\infty - m_g(P_\infty + \Delta P) = 1$$

when

$$-m_g \Delta P = 1$$
$$\Delta P < P_\infty = 0.33$$

Let us put $k_p \Delta P = P_{00}$ $(k_p \geq 2)$:

$$m_g = \frac{1}{|\Delta P|} = 3k_P \tag{32}$$

$$m_g \leq \frac{lg(\frac{m_f}{P_{\partial o6} k_\sigma})}{lg3} \tag{33}$$

The specific distribution of samples within the rank mask of the reference should be symmetrical. In order to sharpen the peak of the rank autocorrelation function of the GQP standard [10, 11], for example,

$$G^r(i'): +0-\ -0+, \tag{34}$$

where symbols +, 0 – denote the samples of the positive, zero and negative GQPs of the standard, respectively.

The variable value range is $P_0 - \left[\frac{1}{6}, \frac{3}{6}\right]$ with a discrete $\frac{1}{6}$.

The block diagram of the algorithm of the learning process based on the calculation of the RCCF of the GQP of the noise image of the current frame (line) and the generated GQP.

The formation of a generalized contour preparation at the second step of the algorithm is not fundamental. It is possible to use and preprocess according to the method of rank sign delta modulation [10]. However, since in this case $\overset{0}{Q}{}^r_{fg}(\tau) = 0$ (values $\overset{+}{Q}{}^r_{fg}(\tau)$ and $\overset{-}{Q}{}^r_{fg}(\tau)$ are not being changed), the appropriate adjustment of the formulas (32–34) is necessary.

LDT training stops when the specified error is reached $\varepsilon > 0$. If those conditions are met:

$$0 \leq r_x \leq m_{fx} - r_x$$
$$0 \leq r_y \leq m_{fy} - r_y$$
$$m_{fx} \ll m_{gx}$$
$$m_{fy} \ll m_{gy} \tag{35}$$

Despite the advantage of such an algorithm, which consists in the uniformity of the LDT learning process (the difference lies in the reference images), this algorithm is difficult to implement and can be significantly simplified. The simplification is based on the fact that for the current noise image takes place $m_{f,0} = m_f \cdot P_0$:

$$0.5\left(m_{f,+} + m_{f,-}\right) = m_f\left(\frac{1-P_0}{2}\right) = m_f P_n \tag{36}$$

in this case, this formula corresponds to formula (29) for P_{H1}, if we accept that $m_g^r = m_f^r$ is the reference noisy image length.

The main advantage of this algorithm is its extreme simplicity, since it does not require the calculation of the RCCF at all and can be combined with the output and preparation of the frame of the current image.

The learning process of the LDT is reduced to finding the average $\tilde{\Delta} f^r$ module of sample mean values 00 of positive and negative differences in the difference noise or background image and setting the LDT $\psi = \tilde{\Delta} f^r$. At the same time, taking into account the stationarity of the noise in adjacent image frames, to save memory, it is advisable to combine the calculation of the estimates $\tilde{\Delta} f^r$ with the input of the current image frame, and the threshold $\psi = \tilde{\Delta} f^r$ is advisable to be used in preprocessing by the LDT method of the subsequent frames following it (the number of which is determined by the time of the stationarity of noise or background, respectively) [1, 11, 12].

For the confidence probability $0 < P_{surr\,k_\sigma} < 1$ (also works for $P_{surr\,k_\sigma} = 1$) such an estimate will be calculated by the formula:

$$\tilde{\Delta} f^r = \frac{1}{2}\left|\frac{M^+_\Delta f^r + M\left|\bar{\Delta} f^r\right|}{e^{-\frac{K_\sigma^2}{2}} - 1}\right| = \frac{1}{2}\frac{M^+_\Delta f^r + M\left|{}_\Delta f\right|}{1 - e^{-\frac{K_\sigma^2}{2}}} \tag{37}$$

3. Research results

As a result of the study, it was determined that the dependency $P_{H1}(P_0)$ of the average value of the samples of the rank CCF (RCCF) of the GQP of the reference and current images, representing the realizations of normal white noise, on the probability P_0 of the formation of samples of the zero GQP, which, in turn, depends from LDT ψ, has a clearly defined extremum at the point $P_0 = P_{00} = 0.33$. In the extremum region, the dependences $P_{H1}(\psi)$ are close to the asymptotes $P_{H1}(\psi) = 0.5 m_g\left(1 - \psi\sqrt{\frac{2}{\pi}}\right)$ and $P_{H1}(\psi) = m_g\sqrt{\frac{2}{\pi}}$. In this case, the value of ψ_{opt} is $0.33\sqrt{\frac{\pi}{2}}$ – standard deviation of the difference noise image. The extremum of the dependence $P_{H1}(P_0)$ corresponds to the maximum of the total absolute margin of the reference image, which ensures minimization of the amplitude at average of the false peak amplitude of the total CCF of the GQP of the reference and current images when working on arbitrary backgrounds.

Algorithms for the learning process have been developed, they minimize the average value of the RCCF samples of the reference and current noise images preprocessed by the GQP method. One algorithm is based on the calculation of the RCCF and requires small measurements of the performance of the GQP correlator.

Another algorithm is simpler to implement and is based on counting the number of single samples of the current image GQP. There was shown the definition of the estimates $\tilde{\Delta} f^r \approx \psi_{opt}$, which requires minimal calculations and equal to the average modulus of the sample avarage means of the positive and negative differences of the current image.

4. Conclusions

In this article was considered the recognition of discretized images in the conditions of noise on the image, namely, training in the recognition of such images. The corresponding learning algorithms were analyzed and their advantages and disadvantages were presented. A method was developed for organizing the learning process of the correlator with image preprocessing according to the GQP method, which is carried out in order to select the value ψ_{opt} of LDT. The dependency $P_{H1}(P_0)$ has been identified and the extremum of this dependence of the average value of the samples of the rank CCF of the GQPs of the reference and current images, representing realizations of normal white noise, on the probability P_0 of the zero GQP samples formation.

Two variants of the learning algorithm according to the described learning method were proposed. One algorithm is based on the calculation of the RCCF and requires small measurements of the performance of the GQP correlator. Another algorithm is simpler to implement and is based on counting of the number of single samples of the current image GQP. A definition of the algorithm's estimate, which is equal to the average modulus of the sample mean values 00 of the positive and negative differences of the current image, is proposed. The proposed method is characterized by a small number of calculations and ease of implementation. Thus, the obtained method can be used for training in the processing of sampled images and the influence of normal white noise, while increasing the recognition efficiency.

References

[1] Bochkarev A. M.: Correlation-Navigation Navigation Systems. Foreign radio electronics 9, 1981, 12–16.
[2] Dougherty E. R.: Digital Image Processing Methods. CRC Press, Boca Raton 2020) [http://doi.org/10.1201/9781003067054].
[3] Gan Woon Siong: Signal Processing and Image Processing for Acoustical Imaging. Springer Singapore, 2020 [http://doi.org/10.1007/978-981-10-5550-8].
[4] Kondratiuk S., Kruchynin K., Krak I., Kruchinin S.: Information technology for security system based on cross platform software, NATO Science for Peace and Security Series A: Chemistry and Biology, 2018, 331–339.
[5] Kondratiuk S., Krak I.: Dactyl Alphabet Modeling and Recognition Using Cross Platform Software. Proceedings of the 2018 IEEE 2nd International Conference on Data Stream Mining and Processing, 8478417, 2018, 420–423.
[6] Kozlovska T., Pavlov S.: Optoelectronic Means of Diagnosing Human Pathologies Associated with Peripheral Blood Circulation. Academic Publishing, Beau Bassin 71504, Mauritius 2019.
[7] Krak I. V., Kryvonos I. G., Kulias A. I.: Applied aspects of the synthesis and analysis of voice information. Cybernetics and Systems Analysis 49(4), 2013, 89–596.
[8] Kutaev Y. F.: Systemic correlation-extreme measurement of coordinates with generalized Q-preparation of images: Ph.D. thessis. Vinnitsa, 1989.
[9] Pogrebnoy V. A.: Airborne signal processing systems. Scientific thought, Kiev 1984.
[10] Pratt W.: Digital image processing. In 2 books. John Wiley & Sons, Inc., 1982.
[11] Sacerdoti F. M.: Digital Image Processing. In: Sacerdoti, F., Giordano, A., Cavaliere, C. (eds): Advanced Imaging Techniques in Clinical Pathology. Current Clinical Pathology. Humana Press, New York 2016 [http://doi.org/10.1007/978-1-4939-3469-0_2].
[12] Timchenko L. I., Kokriatskaia N. I., Nakonechna S., Poplavskaia A. A., Stepaniuk D. S., Gromaszek K. and Rakhmetullina S.: Analysis of computational processes of pyramidal and parallel-hierarchical processing of information, Proc. SPIE 10808, 2018, 1080822.
[13] Timchenko L. I., Kutaev Y. F., Chepornyuk S. V., Grudin M. A., Harvey D. M., Gertsiy A. A.: A Brain Like Approach to Multistage Hierarchial Image, Lecture Notes in Computer Sciense. Image Analysis and Processing 1311, 1997, 246–253.
[14] Trishch R., Nechuiviter O., Vasilevskyi O., Dyadyura K., Tsykhanovska I., Yakovlev M.: Qualimetric method of assessing risks of low quality products, MM Science Journal 4, 2021, 4769–4774.
[15] Tulbure A., Tulbure A.: The use of image recognition systems in manufacturing processes. IEEE International Conference on Automation, Quality and Testing, Robotics 2018.
[16] Wójcik W., Pavlov S., Kalimoldayev M.: Information Technology in Medical Diagnostics II. Taylor & Francis Group, CRC Press, Balkema book, London 2019.

Prof. Leonid Timchenko
e-mail: tumchenko_li@gsuite.duit.edu.ua

Doctor of Technical Science, professor.
State University of Infrastructure and Technology, Kyiv, Ukraine.
62 articles published in Scopus, 241 citations in 118 articles (h-index = 8).
Scientific direction: information technologies, image processing

http://orcid.org/0000-0001-5056-5913

Ph.D. Natalia Kokriatskaia
e-mail: nkokriatskaia@gmail.com

Ph.D., associate professor.
State University of Infrastructure and Technology, Kyiv, Ukraine.
41 articles published in Scopus, 130 citations in 88 articles (h-index = 7).
Scientific direction: information technologies, image processing

http://orcid.org/0000-0003-0090-3886

Ph.D. Volodymyr Tverdomed
e-mail: tverdomed@gsuite.duit.edu.ua

Ph.D., associate professor.
State University of Infrastructure and Technology, Kyiv, Ukraine.
21 articles published in Scopus, 13 citations in 16 articles (h-index 3).
Scientific direction: information technologies, image processing

http://orcid.org/0000-0002-0695-1304

Ph.D. Natalia Kalashnik
e-mail: ukraine@vnmu.edu.ua

Associate professor, National Pirogov Memorial Medical University.
Scientific direction: information technologies, pedagogy. Formation of intercultural communicative competence among foreign students in higher medical educational institutions of Ukraine.

http://orcid.org/0000-0001-5312-3280

Ph.D. Iryna Shvarts
e-mail: s.irinach502@gmail.com

Assistant professor of the Department of Entrepreneurship, Logistics and Management, Vinnitsia National Technical University, Vinnitsia.
Scientific direction: information technologies in economy.

http://orcid.org/0000-0003-4344-5213

Plisenko Vladyslav
e-mail: plisenko_vo@gsuite.duit.edu.ua

Post-graduate student at State University of Infrastructure and Technology.
Scientific direction: information technologies, image processing.

http://orcid.org/0000-0002-5970-2408

Dmytro Zhuk
e-mail: zhuk_do@ukr.net

Post-graduate student at State University of Infrastructure and Technology.
Scientific direction: information technologies, image processing.

http://orcid.org/0000-0001-8951-5542

Ph.D. Saule Kumargazhanova
e-mail: SKumargazhanova@gmail.com

She is currently the dean of the Department of Information Technologies and Intelligent Systems of D. Serikbayev East Kazakhstan Technical University. She is a co-author over 50 papers in journals and conference proceedings.
Her professional interests are software engineering, data processing and analysis.

http://orcid.org/0000-0002-6744-4023

http://doi.org/10.35784/iapgos.3394 *received: 29.12.2022 | revised: 28.03.2023 | accepted: 27.04.2023 | available online: 30.06.2023*

MODELING AND ANALYSIS OF THE CHARACTERISTICS OF MULTICHANNEL AND MULTI-NODE COMPUTER NETWORKS WITH PRIORITY SERVICE

Zakir Nasib Huseynov, Mahil Isa Mammadov, Togrul Atabay Ismayilov
Azerbaijan State Agricultural University, Ganja, Azerbaijan

Abstract. *The subject of the research is modeling and analysis of the characteristics of multichannel and multi-node computer networks with priority services. The work is devoted to the study of the qualitative indicators of the functioning of computer networks with priority service. In this work, mathematical models are developed that make it possible to assess the quality of functioning of modern computer networks, taking into account the number of channels, waiting places in network nodes and the number of network nodes. The proposed methods for calculating the probability of failures and the probability of timely delivery of a stream of requests make it possible to determine the real values of the qualitative indicators of the functioning of computer networks and are suitable for both designed and operating computer networks. The proposed technique makes it possible to determine the number of packets in the queue and the optimal amount of buffer memory in computer network nodes.*

Keywords: multichannel, multi-node, probability, priority, algorithm, buffer memory

MODELOWANIE I ANALIZA CHARAKTERYSTYK WIELOKANAŁOWYCH I WIELOWĘZŁOWYCH SIECI KOMPUTEROWYCH Z USŁUGĄ PRIORYTETOWĄ

Streszczenie. *Przedmiotem badań jest modelowanie i analiza charakterystyk wielokanałowych i wielowęzłowych sieci komputerowych z usługami priorytetowymi. Praca poświęcona jest badaniu jakościowych wskaźników funkcjonowania sieci komputerowych z usługami priorytetowymi. W pracy opracowano modele matematyczne umożliwiające ocenę jakości funkcjonowania nowoczesnych sieci komputerowych z uwzględnieniem liczby kanałów, miejsc oczekiwania w węzłach sieci oraz liczby węzłów sieci. Proponowane metody obliczania prawdopodobieństwa awarii i prawdopodobieństwa terminowego dostarczenia strumienia żądań umożliwiają określenie rzeczywistych wartości wskaźników jakościowych funkcjonowania sieci komputerowych i są odpowiednie zarówno dla projektowanych, jak i działających sieci komputerowych. Proponowana technika umożliwia określenie liczby pakietów w kolejce i optymalnej ilości pamięci buforowej w węzłach sieci komputerowej.*

Słowa kluczowe: wielokanałowy, wielowęzłowy, prawdopodobieństwo, priorytet, algorytm, pamięć buforowa

Introductıon

The article shows a mathematical model of a multi-channel, multi-node computer network with a limited queue and absolute priority, depending on the number of network nodes, waiting places in individual nodes and the probability of failure of requests of individual priorities. It is shown that in multichannel, multi-node computer networks, to ensure the required quality of functioning, it is necessary to choose the optimal number of channels (s), waiting places (k) in the network nodes and the load of individual priorities (ρ_1, ρ_2). It was revealed that with an increase in the number of network nodes (N), it becomes necessary to increase the number of channels (s) and waiting places (k) in the network nodes. The resulting tables and functional dependencies make it possible to design a computer network that functions with the required quality indicators. In [8] and [9] article, the calculation is performed in single-channel multi-node families, the probability of failure for requests of the first and second priorities with a limited service queue. In contrast to [8] and [9], the proposed calculation methods make it possible to determine the delivery time, the number of packets in the queue, the probability of request flow failures in multi-channel multi-node computer networks with a limited queue and absolute priority.

The operation of an analytical model of a computer corporate network is studied, the probabilities of loss and timely delivery of requests are determined. The work of the computer corporate network "SEÇKİLƏR" of the Republic of Azerbaijan has been studied [7].

1. Materials and methods

In computer networks based on modern technologies, voice and text information are exchanged digitally in the form of packets. Due to the limited network resources, there is a delay and loss of packets, which leads to an increase in the quality of service. In practice, computer networks with different architectural structures are used [1]. As shown in figure 1, there are cases when a network consists of dozens of nodes and one or more parallel communication channels connecting these nodes to each other in a certain order.

Computer networks and various types of information's are divided into packets and transported from one address to another for exchange between network operators. As a rule, at the first node of the network, the information is processed by dividing it into packets. The processed individual packets are transported from these nodes to the required address in different ways, depending on the addresses written on them. In the process of transportation, packets may be forced to pass through several nodes of the network, which is due to the limited and busy communication channels between nodes. When packets are processed at nodes, they may be delayed due to delays, and new routes and high priority may be established to service them. Let's consider the activity of a computer network with an arbitrary structure when prioritizing packages [3].

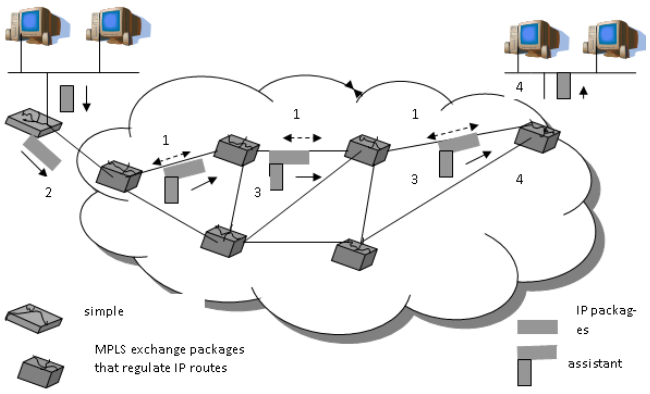

Fig. 1. The structure of using protocols and packages in prospective multi-channel, multi-node computer networks

In this paper, the characteristics of such a network are optimized in terms of QoS.

Let us consider a multichannel queuing system (QS) with waiting places. The system receives two streams of requirements with intensities and respectively [4] The distribution functions of

the service time for the first and second priority requirements are exponential with the parameter. In this case, the intensity of the incoming load of the first and second priorities will be respectively equal to and. The first thread has absolute priority over the second thread.

In multichannel single-node computer networks with a limited queue and absolute priority, the probability of failure for the first priority request flow due to the limited queue in service is determined by the following dependence [5]:

$$P_1 = \frac{\rho_1{}^{s+k}}{s^k s!}\left[\sum_{\nu=0}^{s}\frac{\rho_1{}^{\nu}}{\nu!} + \frac{\rho_1{}^{s}}{s!}\sum_{j=1}^{k}\left(\frac{\rho_1}{s}\right)^j\right]^{-1} \quad (1)$$

where: S – is the number of channels; k – number of waiting places; ρ_1 – load of the first priority.

With S = 1, it is possible to obtain a dependency for a single-channel network with a limited queue and absolute priority.

The probability of denial of service for requests of the second priority is equal to the probability that there are already requests of the first and / or second priority in the queue:

$$P_2 = \frac{(\rho_1+\rho_2)^{s+k}}{s^k s!}\left[\sum_{\nu=0}^{s}\frac{(\rho_1+\rho_2)^{\nu}}{\nu!} + \frac{(\rho_1+\rho_2)^{s}}{s!}\sum_{j=1}^{k}\left(\frac{\rho_1+\rho_2}{s}\right)^j\right]^{-1} \quad (2)$$

where: ρ_1 – is the load of the first priority; ρ_2 – load of the second priority.

An algorithm for solving the problem was developed for the calculation. In Fig. 2. an algorithm for calculating the probability of denial of service for requests of the first and/or second priorities in a multichannel single-node network is presented. The calculation according to this algorithm was performed using the Excel 2019 program.

Let's move on to obtaining a mathematical model for a multi-channel multi-node network. To obtain a mathematical model, you can use the position of probability theory and mathematical statistics. According to which, a sequence of random events is called monotonically increasing (non-decreasing) or monotonically decreasing (non-increasing), if for each The union of all events of such a sequence will be written as [2]:

$$\sum_{i=1}^{\infty} A_i = \lim_{i\to\infty} A_i \text{ or } \prod_{i=1}^{\infty} A_i = \lim_{i\to\infty} A_i \quad (3)$$

Since in multi-channel multi-node computer networks with a limited queue and absolute priority, the probability of failure increases with an increase in the number of switching nodes used, taking into account (3) from expressions (1) and (2) for single-priority and two-priority services, the following mathematical models can be obtained to calculate the probability failures in multichannel multi-node computer networks.

If we consider the probabilities of node failures to be the same, then the mathematical model for determining the probability of failure in multi-channel multi-node computer networks for first-priority requests due to a limited service queue has the following form:

$$P_{1m} = \sum_{i=1}^{N}\frac{\rho_{i_1}{}^{s_i+k_i}}{s_i{}^{k_i}s_i!}\left[\sum_{\nu=0}^{s_i}\frac{\rho_{i_1}{}^{\nu}}{\nu_i!} + \frac{\rho_{i_1}{}^{s}}{s_i!}\sum_{j=1}^{k_i}\left(\frac{\rho_{i_1}}{s_i}\right)^j\right]^{-1} \quad (4)$$

where: N – is the number of network nodes; ρ_i – the load of the first priority, s_i – the number of channels, k_i – the number of waiting places; i – the th network node.

If we consider the probabilities of node failures to be the same, the mathematical model of the probability of failures in multi-channel multi-node computer networks for second-priority requests due to a limited-service queue will have the following form:

$$P_{2m} = \sum_{i=1}^{N}\frac{(\rho_{i1}+\rho_{i2})^{s_i+k_i}}{s_i{}^{k_i}s_i!}\left[\sum_{\nu=0}^{s_i}\frac{(\rho_{i1}+\rho_{i2})^{\nu}}{\nu!} + \frac{(\rho_{i1}+\rho_{i2})^{s_i}}{s_i!}\sum_{j=1}^{k_i}\left(\frac{\rho_{i1}+\rho_{i2}}{s_i}\right)^j\right]^{-1} \quad (5)$$

where: ρ_{i2} – is the load of the second priority i-the network node.

2. Results and discussions

When designing a specific communication network, it is necessary to take into account the real probability of failures of the designed network nodes [6]. The calculation was performed according to the algorithm shown in Fig. 2.

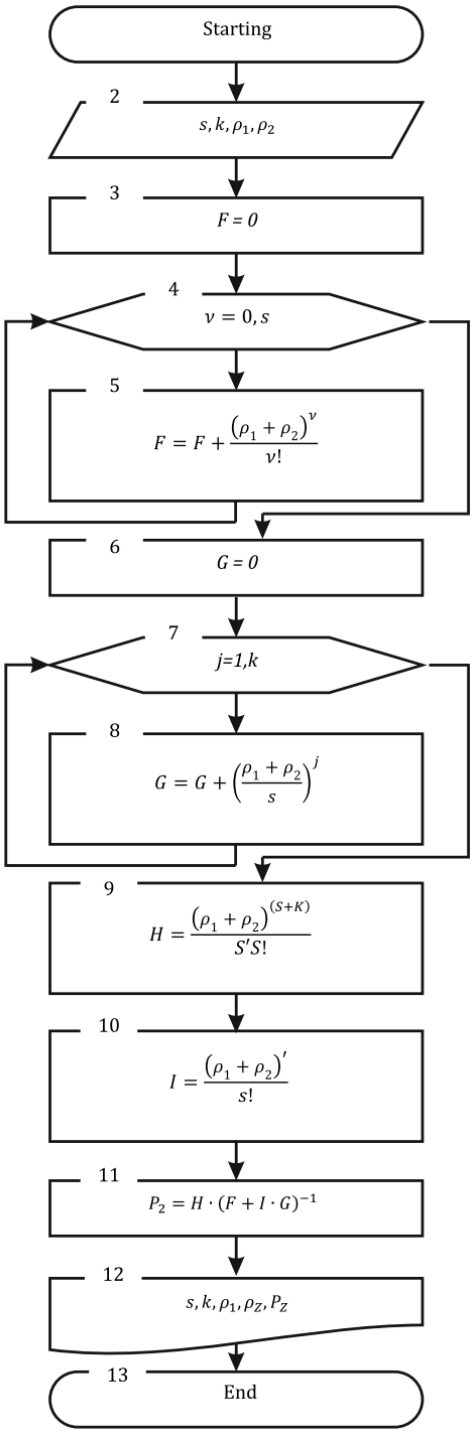

Fig. 2. Algorithm for calculating the probability of denial of service for requests of the first and / or second priority

Calculations based on the obtained models were performed for a different number of network nodes (N), the number of waiting places (k) and parallel channels (S). When obtaining numerical calculations and plotting, the Excel 2019 program was used.

Table 1. The results of calculating the probability of denial of service for requests of the second priority with a different number of N; k; ($s = 2; \rho_2 = 0.8$)

	P2m								
	N = 1			N = 2			N = 3		
	k = 14	k = 18	k = 20	k = 20	k = 24	k = 26	k = 24	k = 26	k = 28
0.2	1.02E-05	6.4E-07	1.59E-07	3.2E-07	1.99E-08	4.97E-09	2.98E-08	7.45E-09	7.45E-09
0.4	0.000141	1.8E-05	6.58E-06	1.3E-05	1.71E-06	6.14E-07	2.56E-06	9.21E-07	9.21E-07
0.6	0.001176	0.00028	0.000138	0.00028	6.63E-05	3.25E-05	9.94E-05	4.87E-05	4.87E-05
0.8	0.006416	0.00259	0.001651	0.0033	0.001347	0.000861	0.00202	0.001292	0.001291
1	0.023659	0.01446	0.011433	0.02287	0.014489	0.011593	0.021734	0.017389	0.017218
1.2	0.060606	0.04878	0.044444	0.08889	0.075472	0.070175	0.113208	0.105263	0.098361
1.4	0.114746	0.10594	0.102985	0.20597	0.197648	0.194706	0.296472	0.292059	0.28851
1.6	0.175361	0.17075	0.169481	0.33896	0.336024	0.335197	0.504036	0.502796	0.501938
1.8	0.233878	0.23185	0.231407	0.46281	0.461984	0.461802	0.692976	0.692703	0.692542
2	0.286843	0.28601	0.285864	0.57173	0.571506	0.571468	0.857259	0.857202	0.857173

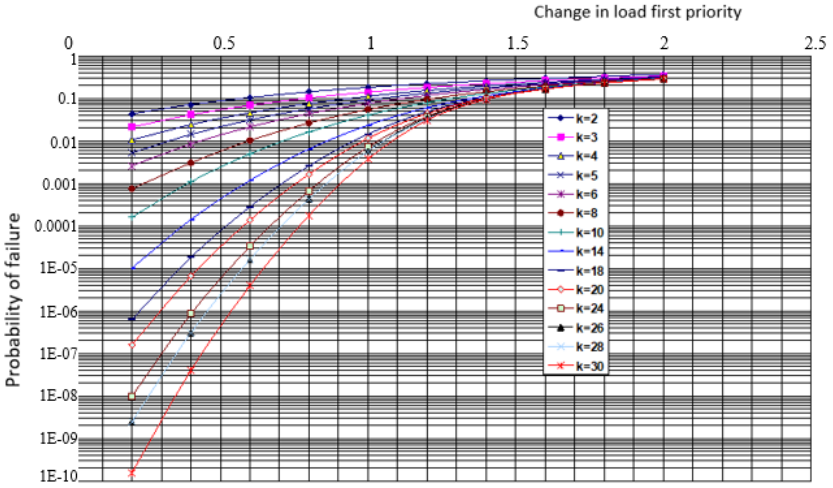

Fig. 3. Probability of denial of service for requests second priority ($N = 1; s = 2;\ \rho_2 = 0.8$)

Table 2. The results of calculating the probability of denial of service for requests of the second priority with different numbers of N, s and k ($\rho_2 = 0.8$)

	Probability of denial – P2m								
	N = 1			N = 2			N = 3		
	s = 2	s = 3	s = 4	s = 2	s = 3	s = 4	s = 2	s = 3	s = 4
	k = 20	k = 6	k = 3	k = 24	k = 8	k = 5	k = 26	k = 10	k = 5
0.2	1.59E-07	8.31E-05	0.000239	1.99E-08	0.00002	2.99E-05	7.45E-09	3.08E-06	4.48E-05
0.4	6.58E-06	3.50E-04	0.0007	1.71E-06	0.00011	1.26E-04	9.21E-07	2.66E-05	1.89E-04
0.6	0.000138	1.11E-03	0.001682	6.63E-05	0.00048	4.12E-04	4.87E-05	1.58E-04	6.18E-04
0.8	0.001651	2.95E-03	0.003491	0.001347	0.00168	1.11E-03	0.001292	7.20E-04	1.67E-03
1	0.011433	6.68E-03	0.006476	0.014489	0.00478	2.61E-03	0.017389	2.58E-03	3.92E-03
1.2	0.044444	1.33E-02	0.010989	0.075472	0.0117	5.45E-03	0.105263	7.74E-03	8.17E-03
1.4	0.102985	2.40E-02	0.01734	0.197648	0.025	1.03E-02	0.292059	1.99E-02	1.55E-02
1.6	0.169481	3.93E-02	0.025759	0.336024	0.0476	1.81E-02	0.502796	4.41E-02	2.71E-02
1.8	0.231407	5.94E-02	0.036367	0.461984	0.0815	2.96E-02	0.692703	8.61E-02	4.44E-02
1.9	0.285864	8.41E-02	0.049169	0.571506	0.127	4.55E-02	0.857202	1.49E-01	6.83E-02

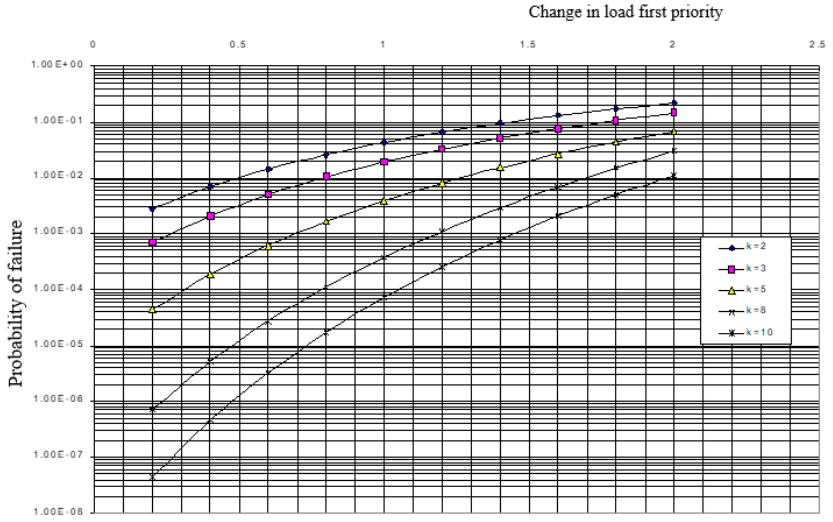

Fig. 4. Denial of service probability for second priority requests ($N = 3; s = 4; \rho_2 = 0.8$)

Table 1 shows the results of calculating the probability of denial of service for requests of the second priority (P2m) with a different number of waiting places (k). Number of nodes – N = 1. $-\rho_2 = 0.8$ second priority load, $-s = 2$ number of parallel channels. Table 1 shows the results of calculating the probability of denial of service for the requirements of the second priority (P_{2m}) with a different number of switching nodes (N) and waiting places (k). -ρ_2 = 0.8 is the load of the second priority, –S = *4* is the number of parallel channels.

In Fig. 3. the results of calculations of the probability of denial of service for requests of the second priority (P_{2m}) with a different number of waiting places (k) are given. The number of nodes –N = 3, –ρ_2 = 0.8 the load of the second priority and –S = *4* the number of parallel channels.

Table 2 shows the results of calculating the probability of denial of service for requests of the first and second priorities with a different number of switching nodes (N), parallel channels (s) and waiting places (k). Second priority load –ρ_2 = 0.8. The results of calculating the probability of denial of service for requests of the second priority (–ρ_2 = 0.8) in a multi-channel multi-node computer network with a different number of waiting places and different load of the first priority (= 0.1–2).

3. Conclusion

An algorithm has been developed for determining the probability of failure in multichannel and multinode networks for requests of the first and second priority due to a limited queue in service. Numerical calculations of the probability of denial of service for requests of the first and second priorities are given. It can be seen from the obtained characteristics and tables that in order to ensure the required QoS value, it is necessary to provide the required number of parallel serving channels between specific network nodes, as well as to determine the optimal number of waiting places (accumulator capacity) in its corresponding switching nodes.

References

[1] Amato V.: Fundamentals of network organization Cisco. 2, 2018.
[2] Baklanov I.G. NGN: Principles of construction and organization. Eco-Trendz, Moscow 2008.
[3] Black U. D.: Computer networks: Protocols, standards and interfaces. Moscow 2019.
[4] Bondarik Andreev D. V., Tarasov D. V., Kucheryavyy A. E.: Model networks for testing technical means of communication networks of the next generation. Recommendation MCE-T Q.3900, 2013.
[5] Bulgakov N. N., Miroshnikov V. I., Shibanov V. S.: Multi-channel system with limited queue and absolute priority, 2022.
[6] Guseynov Z. N.: Optimization of characteristics of computer networks. Proceedings of AzTU, Baku, 3, 2006, 29–32.
[7] Huseynov Z. N, Mammadov M. I, Ismayilov T. A.: Modeling and optimization of a computer corporate network with priority service “Seçkilər”. II international scientific conference “Challenge and problems of modern science”, London 2022, 138–142.
[8] Huseynov Z. N: Optimization of the Characteristics of single-chanel and multi-node computer networks providing priority services. German International Journal of Modern Science 30, 2022, 51–57.
[9] Vishnevsky V. M.: Theoretical foundations of designing computer networks. Technosfera, Moscow 2003.

Ph.D. Zakir Nasib Huseynov
e-mail: huseynov.z.n@mail.ru

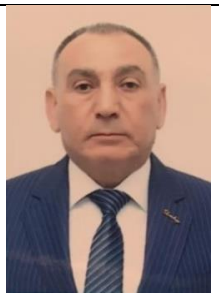

Zakir Huseynov was born 2 July 1955. In 1980 graduated from Kirovabad State Pedagogical Institute after named H. Zardabi, Mathematic Faculty. By the decree of the President of the Republic of Azerbaijan dated 03.10.2006, he was awarded the honorary title "Honored Teacher of the Republic". In 2012 he defended his dissertation on "Research of performance indicators of priority service telecommunication networks" and received the degree of Doctor of Philosophy in Technique. From november 2020 he is the head of the Information Technologies department of Azerbaijan State Agricultural University.

http://orcid.org/0000-0003-3828-091X

Ph.D. Mahil Isa Mammadov
e-mail: mahilmi@mail.ru

Mahil Mammadov was born 1 May 1966. In 1990 graduated from the Azerbaijan Polytechnic Institute (now ATU), Electronic Computing Machines. On September 20, 2013, he defended dissertation on "Improvement of technology for the preparation of feed grains with information-software" for the Ph.D. degree in Engineering in the specialty "3102.01-Agroengineering"

http://orcid.org/0000-0002-9384-2746

M.Sc. Togrul Atabay Ismayilov
e-mail: ismayilovtogrul26@gmail.com

Togrul Ismayilov was born 16 March 1992. In 2015 graduated from Ganja State University. In 2019 graduated from the Azerbaijan State Oil and Industrial University, Information Technologies. From 2020 is working at the Azerbaijan State Agricultural University, Information Technologies department. In 2022 he started Ph.D. degree on Telecommunication Technologies at the Azerbaijan University of Technology. His research area is “Study of the effectiveness of telecommunication systems based on the architectural concept of next-generation communication networks”.

http://orcid.org/0000-0002-2440-6385

http://doi.org/10.35784/iapgos.3504 *received: 16.02.2023 | revised: 13.03.2023 | accepted: 29.04.2023 | available online: 30.06.2023*

STATISTICAL METHODS FOR EVALUATING EXPERIMENTAL DATA ON THE USE OF MATHEMATICAL COMPETENCIES IN STUDY FOR A RESILIENT ECONOMY

Vira Petruk[1], Olena Prozor[1], Yuliia Sabadosh[1], Iryna Baranovska[2], Maksim Palii[3], Yevheniia Moroz[4], Saule Kumargazhanova[5], Dinara Mussayeva[6]

[1]Vinnytsia National Technical University, Vinnytsia, Ukraine, [2]Vinnytsia State Pedagogical University named after Mykhailo Kotsiubynsky, Vinnytsia, Ukraine, [3]Vasyl Stus Donetsk National University, Vinnytsia, Ukraine, [4]Taras Shevchenko National University, Kyiv, Ukraine, [5]D. Serikbayev East Kazakhstan Technical University, Ust-Kamenogorsk, Kazakhstan, [6]Al-Farabi Kazakh National University, Almaty, Kazakhstan

Abstract*. The description of the problems, solved within the statistics evaluation of the results of educational (pedagogical) experiment in resilient economy is given. Comparison of the two average samplings and hypothesis verification relative to dispersions of the two samplings are considered. It is shown the hypothesis that teaching and methodical training system of subjects of higher mathematics in technical universities, suggested on the base of the modern interactive technologies, significantly improves the quality of the base level of professional competence of future engineers. The methods for statistical processing of the obtained results, which very thoroughly research all the indexes which compose the suggested learning and methodical system for teaching higher mathematics in technical universities are used.*

Keywords: statistical methods, statistical analysis, abstract essence, elements of interaction, pedagogical experiment

STATYSTYCZNE METODY OCENY DANYCH EKSPERYMENTALNYCH DOTYCZĄCYCH WYKORZYSTANIA KOMPETENCJI MATEMATYCZNYCH W BADANIACH NA RZECZ ODPORNEJ GOSPODARKI

Streszczenie. *Podano opis problemów rozwiązywanych w ramach statystycznej oceny wyników eksperymentu edukacyjnego (pedagogicznego) w gospodarce odpornej. Rozważa się porównanie dwóch średnich prób i weryfikację hipotezy w odniesieniu do dyspersji dwóch prób. Wykazano hipotezę, że system nauczania i szkolenia metodycznego przedmiotów matematyki wyższej na uczelniach technicznych, zaproponowany w oparciu o nowoczesne technologie interaktywne, znacząco poprawia jakość podstawowego poziomu kompetencji zawodowych przyszłych inżynierów. Zastosowano metody statystycznego przetwarzania uzyskanych wyników, które bardzo dokładnie badają wszystkie wskaźniki składające się na proponowany system nauczania i metodycznego nauczania matematyki wyższej w uczelniach technicznych.*

Słowa kluczowe: metody statystyczne, analiza statystyczna, istota abstrakcyjna, elementy interakcji, eksperyment pedagogiczny

Introduction

Sustainable development and a resilient economy are impossible without the training of relevant personnel, because the quality of managerial decision-making depends on the professional training of specialists. Pedagogical experiments using elements of mathematical statistics are traditionally conducted in resilient economy. Mathematical statistics has a great variety of criteria, designed to verify the statistic hypothesis. The evaluation of manufacturing, medical, pedagogical and the like managerial decisions usually uses the hypothesis on numerical characteristics
of the received figures. The most fully developed theory is the one for hypothesis verification relative to numerical characteristics of the normal law of distribution [1, 2, 10].

Let's consider an algorithm for verification of statistical hypothesis.

1. The first stage forms the matrix of the received figures:

$$X = \begin{pmatrix} X_{11} & \dots & X_{1m} \\ \dots & \dots & \dots \\ X_{n1} & \dots & X_{nm} \end{pmatrix}; \quad i = \overline{1,n}; \quad j = \overline{1,m} \tag{1}$$

2. For each parameter of X_j the hypothesis shall be tested for normality. If parameter X_j has distribution, different from the normal one, it then reconstructs into the parameter V_j with the normal law of distribution. The reconstruction shall be done as follows. The elements of the *j-th* matrix column (1) shall be arranged in ascending order:

$$X_1 \le X_2 \le \dots \le X_n, \tag{2}$$

frequencies m_k which correspond to the values X_K, are calculated for the statistical series with the further calculation of the accumulated frequencies

$$M_K = M_{K-1} + m_K, \quad K = \overline{2,l}, \tag{3}$$

$M_1 = m_1$ and the value of the distribution function

$$F\left(X_K\right) = \frac{M_K}{n} \tag{4}$$

The value Z_{kj} of the normally distributed random variable $Z_j = V_j - m_{vj}$ with the zero mathematical expectation and unit variance, which correspond to the values of X_{kj} of the random variable X_j with the random distribution law, shall be found from the correlation

$$F\left(X_{kj}\right) = \mathrm{P}\left(X_j < X_{kj}\right) = \mathrm{P}\left(Z_j < Z_{kj}\right) = F_0\left(Z_{kj}\right) = \frac{1}{\sqrt{2\pi}} \int_{-\infty}^{Z_{kj}} e^{\frac{Z^2}{2}} dZ \tag{5}$$

from which Z_{kj} shall be found as a function, inverse to the error function integral

$$Z_{kj} = F_0^{-1}\left(Z_{kj}\right). \tag{6}$$

Equation (4.6) with the set accuracy may be solved by many methods. The approximate values of Z_{kj} with different stages of accuracy are found by the corresponding formulas. One of them:

$$Z_{kj} = \sqrt{\sum_{i=1}^{\infty} a_i \left(-\ln\left(1-4\left(F\left(X_K\right)-\frac{1}{2}\right)\right)^2\right)^i}. \tag{7}$$

The section of the series with the first four members provides for the necessary accuracy within the interval $0.03 < F(X_k) \le 0.97$, coefficients a_j equal: $a_1 = \frac{\pi}{2}$; $a_2 = 0.37068870 \times 10^{-1}$; $a_3 = 0.8320945 \times 10^{-2}$; $a_4 = -02323240 \times 10^{-3}$.

The second and more accurate formula:

$$Z_{kj} = t - \frac{\sum_{i=0}^{2} C_i \cdot t^i}{\sum_{i=0}^{3} d_i t^i} + \varepsilon\left(F\left(X_K\right)\right), \quad (8)$$

where $t = \sqrt{-2\ln\left(1-F\left(X_k\right)\right)}$; $0.5 \le F\left(X_K\right) < 1$;

$|\varepsilon| < 4.5\times10^{-4}$; $C_0 = 2.515517$; $C_1 = 0.802853$; $C_2 = 0.010328$

With $0 \le F\left(X_K\right) < 0.5$ there shall be used the property of the function, inverse to the error function integral, $Z\left(F\left(Z\right)\right) + Z\left(1-F\left(Z\right)\right) = 0$, from which

$$Z_{kj}\left(F\left(X_k\right)\right) = Z_{kj}\left(1-F\left(X_k\right)\right) \quad (9)$$

The value of Z_{kj}, calculated by the close formulas (7) and (8), may also be used as the initial during the solution of the equation (5). Evaluations of the mathematical expectations $\overline{V_j}$, dispersion S_{vj}, random variable V_j with the normal law of distribution may be found by solving the systems of the equations.

$$\begin{cases} Z_{kj} = \dfrac{V_{kj} - \overline{V_j}}{S_{vj}} \\ Z_{mj} = \dfrac{V_{mj} - \overline{V_j}}{S_{vj}} \end{cases} \quad (10)$$

in which

$$V_{kj} = X_{kj};\ V_{mj} = X_{mj};\ k \ne m;\ S_{vj} = \frac{X_{kj} - X_{mj}}{Z_{kj} - Z_{mj}};$$

$$\overline{V_j} = X_{kj} - S_{vj} Z_{kj}. \quad (11)$$

3. There shall be formed the hypothesis H_0 and an alternative hypothesis H_1. If hypothesis H_0 is simple, for example H_0: $\overline{x} = a$, it always may be reduced to H_0: $\overline{x} - a = 0$.

4. There shall be chosen the criteria K_n (critical statistics), which is a function of the observational results, $K_n = K\left(X_1, \ldots X_n\right)$. Criteria K_n, on condition of H_0 hypothesis validity, is a random quantity with the very well learned distribution law, which is set by the table in the kind of approximate formulas or programs for using a computer. Critical statistics, based upon the principle of correlation with the use of the Neumann-Pirson theorem is the most powerful.

5. There shall be set the level of significance by the table of critical quintiles; or using the approximation formula we find the critical quintiles $K_{1-\frac{a}{2}}$, $K_{\frac{a}{2}}$.

In cases, when the hypothesis H_0 relates only to one-way deviation of the criteria K_n, that is, when we are interested in "extremely large" or "extremely small" values of the criteria K_n, there shall be found from K_a or K_{1-a} critical fractal.

6. Following the observational data $\{X_1, \ldots X_n\}$ there shall be calculated the values of the criteria K_n. If this value gets into the critical area, the hypothesis H_0 then deviates to an alternative hypothesis H_0. If the value K_n gets into the legitimate range, the hypothesis H_0 may then be considered as the one, which does not contradict to the research data. Test of hypothesis in production control, pedagogic, medicine etc. allows to solve the tasks for comparing the selected numeric characteristics (average, dispersion) with the corresponding desired values; numeric characteristics of two or some samplings between each other (test of hypothesis on belonging of these samplings to one set).

Comparison problems lie behind the efficiency evaluation of managerial decisions in many spheres. The most universal are the problems for checking hypothesis on correspondence with the empirical distribution with certain theoretical model or hypothesis on significance of deviation between the empirical laws of distribution. If the parameters under investigation with the random law of distribution are transferred into parameters which are distributed against the normal law of distribution during the solution of the specific problems, then there is no need to test the hypothesis in the form of law of distribution, since the normal law may totally be determined by its mathematical expectation and dispersion. Among various approaches to the evaluation of the efficiency of managerial decisions obtained wide development the evaluation of the importance of change in mathematical expectations of the parameters under research, which reflect the trajectories of the centers of their grouping. However, even nowadays the potential of the given approach is not fully implemented.

1. Literature review

The definition of resilience has received considerable attention in the economics literature, for instance in publication: [3] a basis for policy discussions of resilience at the local level is presented. Resilient economy is not a very widely used concept. More often, scientists use the concept of resilience. For instance, Mustonen T., Shadrin V., Mustonen K., Vasiliev V. attempted a synthesis framework for analyzing resilience from an economics viewpoint [6, 9, 11]. Generally, resilience can be defined as the ability of an economy, society, organization or individual to recover effectively from an unexpected shock. This rough definition of resilience raises two related questions: what it means to "recover" and what we mean by an effective recovery [4]. Perrings C. gives a definition of resilience as "the ability of the system to withstand either market or environmental shocks without losing the capacity to allocate resources efficiently or to deliver essential services" leaves the term of analysis indeterminate [8]. Walker B., Holling C., Carpenter S., Kinzig A. have defined resilience as "the capacity of a system to absorb disturbance and reorganize while undergoing change, so as to retain essentially the same function, structure, identity and feedbacks". Hence, this definition encompasses the stability of a structure, rather than focus purely on the performance outcomes of that structure [7, 10].

It is in the conditions of a resilient economy that personnel who improve its results are especially valuable. The effectiveness of the system of educational and methodical training of personnel involved in the country's economy in institutions of higher education can be evaluated using various mathematical models and pedagogical experiments. The experience of pedagogical science research draws attention to the monotony of the application of mathematical statistics methods for analyzing the results of a pedagogical experiment. Also, quite often there are cases of only a percentage assessment of the data obtained in a pedagogical experiment without accompanying statistical analysis, which would scientifically confirm or refute the significance of the obtained positive changes. Works justifying the use of statistical criteria for processing and quality assessment of data for various types of pedagogical experiments are particularly relevant. Mathematical statistics includes a significant number of criteria designed to test various statistical hypotheses. As a rule, hypotheses concern either the law of distribution of data in the sample (normal, binomial, etc.) or the numerical characteristics of the sample (mean, variance, correlation, etc.) manual, which describes the use of criteria for the normal distribution law [5, 6].

As Gogol K., Brunner M., Martin R., Preckel F., Goetz T. [2] and Arens K. [1] truly state, that careful consideration is needed when selecting a specific model. Other core constructs in education research (e.g., academic anxiety, academic interest) have theoretical underpinnings that are similar to ASC as they can also be conceptualized as multidimensional and hierarchical in nature.

2. Material and methods

The aim of the research is the solution of problems of the statistics evaluation of the results of pedagogical experiment.

Objectives of the research:

1. Formulate and briefly describe the problems, solved by means of mathematical statistics for the assessing the efficiency of managerial decisions.
2. According to the suggested method and the presented algorithm check the efficiency of the teaching and methodical training system of subjects of higher mathematics in technical universities.

2.1. Comparison of the two average samplings

One of the main tasks during the evaluation of the efficiency of managerial decisions the evaluation of the importance of change in mathematical expectations of the parameters under research, which reflect the trajectories of the centers of their grouping. In the simplest case there shall be done the comparison of the averages in the two samplings, which correspond to the two types of managerial decisions. The task for comparing is formed as follows. There shall be researched the random quantities X_1, X_2, which have normal distributions $X_1 \in N(m_1\sigma_1),\ X_2 \in N(m_2\sigma_2)$.

Upon the results of the researches we receive the independent samplings $(X_{11},\dots X_{1n1})^T$, $(X_{21},\dots X_{2n2})^T$. For these data on formulas:

$$\overline{X} = \frac{1}{n}\sum_{i=1}^{n} X_i \tag{12}$$

$$S^2 = \frac{N}{N-1}\left(\overline{X^2} - (\overline{X})^2\right) \tag{13}$$

where $\overline{X^2} = \frac{1}{n}\sum_{i=1}^{n} X_i^2$, $i = \overline{1,n}$, there shall be calculated the point estimation $\overline{X}_1(n_1)$, $S_1(n_1)$ for the first sampling and $\overline{X}_2(n_2)$, $S_2(n_2)$ – for the second. It is necessary to check the hypothesis about the equity of mathematical expectations $m_1 = m_2$ of the random quantities X_1, X_2 against the alternative $m_1 \neq m_2$. There is a task to compare the mathematical expectation with the set value. To do this, we consider the random value $Y = X_1 - X_2$. It equals the difference of the two independent random values, which have the normal distribution, mathematical expectations m_1, m_2 and dispersions σ^2_1, σ^2_2. According to the theorem of adding the numerical characteristics of independent random values we receive $m_y = m_{X_1} - m_{X_2}$; $\sigma_y^2 = \sigma_1^2 + \sigma_2^2$.

The evaluation of the mathematical expectation of the random value *Y* is an average

$$\overline{Y} = \overline{X_1} - \overline{X_2} = \frac{1}{n_1}\sum_{i=1}^{n_1} X_{i_1} - \frac{1}{n_2}\sum_{i=1}^{n_2} X_{i_2} \tag{14}$$

and the evaluation of the dispersion of this statistic is the sampling dispersion

$$S_{\bar{y}}^2 = \left(\frac{1}{n_1} + \frac{1}{n_2}\right)\frac{1}{n_1 + n_2 - 2}\left((n_1 - 1)S_1^2 + (n_{2-1})S_2^2\right) \tag{15}$$

So the task of comparing the averages of the two samplings may be formed as follows.

Characteristics of the output data:

$Y \in N(0,\sigma_y)$, $Y = X_1 - X_2$, $X_1(n) = (X_{11},\dots X_{1n1})^T$, $X_2(n) = (X_{21},\dots X_{2n2})^T$; the known valuations $\overline{X_1}$, S_1^2, $\overline{X_2}$, S_2^2, $\overline{Y} = \overline{X_1} - \overline{X_2}$, $S_y^2 = \left(\frac{S_1^2}{n_1} + \frac{S_2^2}{n_2}\right)\frac{n_1 + n_2}{n_1 + n_2 - 2}$.

Hypothesis H_0: $m_y = 0$. Alternative hypothesis H_1: $m_y \neq 0$. Level of significance α. Criteria (critical statistics):

$$t = \frac{|\overline{Y} - 0|}{S_{\bar{y}}} = \frac{|\overline{X_1} - \overline{X_2}|}{S_{\bar{y}}} \tag{16}$$

where $\overline{X_1}$, $\overline{X_2}$, S_1, S_2 shall be determined on the formulas (13), (14), and – $S_{\bar{y}}$ – on (15).

Solution. If the dispersions of the samplings to be compared are the same

$$\sigma_1^2 = \sigma_2^2 \text{ i } |t| \geq t_{\frac{a}{2},(n_1+n_2-2)} \tag{17}$$

Then the zero hypothesis H_0 deviates to the alternative one, in the other case H_0 shall be coordinated with the experimental data. For the realization of the algorithm for comparing the averages of the two samplings, received on the base of manufacturing researches, the critical statistics $t_{\left(1-\frac{a}{2},(n_1+n_2-2)\right)}$ of Student's distribution is appropriate to calculate on the approximation formulas:

$$t_{\beta',n} \approx \sum_{i=0}^{4} q_i\left(Z_{\beta'}\right)/v^i \tag{18}$$

where $\beta' = 1 - \frac{a}{2}$; $n = n_1 + n_2 - 2$;

$q_0(Z_{\beta'}) = Z_{\beta'} \approx \sum a_i\left(-\ln\left(1-2(1-a)\right)^2\right)^i$; $a_1 = \frac{\pi}{2}$;

$a_2 = 0.37068870 \times 10^{-1}$; $a_3 = 0.8320945 \times 10^{-2}$;
$a_4 = -0.2323240 \times 10^{-3}$;

$q_1(Z_{\beta'}) = \frac{1}{4}\left(Z_{\beta'}^3 + Z_{\beta'}\right)$;

$q_2(Z_{\beta'}) = \frac{1}{96}\left(5Z_{\beta'}^5 + 16Z_{\beta'}^3 + 3Z_{\beta'}\right)$;

$q_3(Z_{\beta'}) = \frac{1}{384}\left(3Z_{\beta'}^7 + 19Z_{\beta'}^5 + 17Z_{\beta'}^3 - 15Z_{\beta'}\right)$;

$q_4(Z_{\beta'}) = \frac{1}{92160}\left(79Z_{\beta'}^9 + 776Z_{\beta'}^7 + 1482Z_{\beta'}^5 - 1920Z_{\beta'}^3 - 945Z_{\beta'}\right)$;

$v = n - 1$ – number of degrees of freedom.

If H_0 deviates,one must be extremely careful in case of «extremely large» criteria value $t(n_1 + n_2 - 2)$, which cause the equation gain (17). The causes for this may be either the wide disagreements of the averages, that is, hypothesis H_0 non-execution, or big disagreements between the dispersions of the under research samplings.

That is why the research of the causes of heterogeneity of the manufacturing data samplings under consideration requires to verify the hypothesis of equality of dispersions H_0: $\sigma_1^2 = \sigma_2^2$ against an alternative H_1: $\sigma_1^2 \neq \sigma_2^2$. If during the verification of the hypothesis H_0 of the equality of the averages there appears the significant disagreement between the dispersions, the statistics shall be used as a criterion:

$$t = \frac{\left|\overline{X}_1 - \overline{X}_2\right|}{\sqrt{\frac{S_1^2}{n_1} + \frac{S_2^2}{n_2}}} \tag{19}$$

The values of the critical statistics $\tilde{t}_{\frac{a}{2}}(v_1, v_2, c)$ are presented by the table of supplements in the textbooks [1]. These tables present $\tilde{t}_{\frac{a}{2}}(v_1, v_2, c)$ as $V(v_1,v_2,C,Q)$, where $v_j = n_j - 1$, J=1.2; $Q = \alpha / 2$; α = 2.5 %, 5%,

$$C = \frac{S_1^2 / n_1}{S_1^2 / n_1 + S_2^2 / n_2} \tag{20}$$

In is known that the statistics (19) has distribution which is close to t – Student's distribution with the number of degrees of freedom

$$\tilde{v} = \frac{\left(S_1^2 / n_1 + S_2^2 / n_2\right)^2}{\frac{\left(S_1^2 / n_1\right)^2}{n_1 - 1} + \frac{\left(S_2^2 / n_2\right)^2}{n_2 - 1}} \tag{21}$$

Value $\tilde{v}$ lies between the smallest from $(n_1 - 1)$ and $(n_2 - 1)$ and their sum $(n_1 + n_2 - 2)$. So, the decision on the equality of the averages shall be made depending upon the results of hypothesis verification of the dispersion equality in the under research samplings. During the equality of the dispersions there shall be applied the rule, based on the inequality (18). If dispersions to be compared turn to be equal $\sigma_1^2 \neq \sigma_2^2$, the zero hypothesis then H_0: $m_1 = m_2$ deviates to the alternative one H_1: $m_1 \neq m_2$, if the inequalities come true

$$\left|\tilde{t}\right| > t_{\frac{a}{2}}(\tilde{v}) \text{ or } \left|\tilde{t}\right| > \tilde{t}_{\frac{a}{2}}(v_1, v_2, C) \tag{22}$$

The closest value of the critical fractile $t_{\frac{a}{2}}(v)$ may be received by expanding into series by negative exponent v as in (19).

2.2. Hypothesis verification relative to dispersions of the two samplings

Dispersion characterizes the stability of any process, including the learning one. Any managerial decisions are directed to the decreases in dispersion. Hence, the test of the hypothesis about the dispersion change significance is an important task which is formulated as follows: there are two normally distributed random values $X_j \in N(m_j, \sigma_j)$, $j = 1,2$ for which the sampling dispersions $S_1^2 \neq S_2^2$ as well as samples size n_1, n_2 are known. It is necessary to make a decision on the significance of disagreements between the dispersions σ_1^2 and σ_2^2. This decision may be made upon the verification results of the zero hypothesis H_0: $\sigma_1^2 = \sigma_2^2$ against an alternative H_1: $\sigma_1^2 \neq \sigma_2^2$. Hypothesis H_0 is verified by the schema. The characteristics of the output data: $X_j \in N(m_j, \sigma_j)$, $j = 1,2$, the known sample dispersions σ_j^2, sample size n_j.

1. Hypothesis H_0: $\sigma_1^2 = \sigma_2^2$.
2. Alternative hypothesis H_1: $\sigma_1^2 \neq \sigma_2^2$.
3. Significance level α.
4. Criteria (critical statistics): $F = \frac{S_A^2}{S_B^2}$, where S_A^2, S_B^2 – correspondingly the bigger and the smaller of the dispersions to be compared S_j^2.

This statistics has *F*- Fisher's distribution with the density:

$$P(F) = \begin{cases} \dfrac{\Gamma\left(\frac{V_A + V_B}{2}\right)}{\Gamma\left(\frac{V_A}{2}\right)\Gamma\left(\frac{V_B}{2}\right)} \left(\dfrac{V_A}{V_B}\right)^{\frac{V_A}{2}} \dfrac{F^{\frac{V_A}{2}-1}}{\left(1 + \frac{V_A}{V_B} F\right)^{\frac{V_A + V_B}{2}}} & \text{for } F \geq 0 \\ 0 \quad \text{for } F < 0 \end{cases} \tag{23}$$

where $V_A = n_A - 1$ – numerator degree of freedom; $V_B = n_B - 1$ – denominator degree of freedom.

$$\text{If } F_{(v_A, v_B), 1-\frac{a}{2}} \leq F \leq F_{(v_A, v_B), \frac{a}{2}} \tag{24}$$

the hypothesis H_0 of the equality of the dispersions does not deviate, in the opposite case – deviates. Criteria *F* (24) is the most powerful one.

During the realization of the algorithm for hypothesis verification H_0 with the use of computer for the calculation of the critical statistics $F_{v_A, v_B, \frac{a}{2}}$ it is possible to use an approximation formula [11]:

$$F_{(v_A, v_B), \frac{a}{2}} \approx e^{2W} \tag{25}$$

where:

$$W = \frac{Z_p (h + \lambda)^{\frac{1}{2}}}{n} - \left(\frac{1}{2b-1} - \frac{1}{2a-1}\right)\left(\lambda + \frac{5}{6} - \frac{2}{3h}\right)$$

$$h = 2\left(\frac{1}{2a-1} - \frac{1}{2b-1}\right); \lambda = \frac{Z_p^2 - 3}{6}; b = \frac{v_A}{2}; a = \frac{v_B}{2}$$

Z_p shall be determined by one of the formulas (17), (18) when $P = 1 - \frac{\alpha}{2} = F(X_K)$ for double sided, $P = 1 - \alpha = F(X_K)$ – for one sided reliance area. The tables present the values $F_{(v_A, v_B), \frac{a}{2}}$. The second critical area region boundary shall be determined by correlation

$$F_{(v_A, v_B), 1-\frac{a}{2}} = \left(F_{(v_A, v_B), \frac{a}{2}}\right)^{-1} \tag{26}$$

and is used for the determination of reliable boundaries of root-mean-square deviation.

According to the suggested method [10] and the presented algorithm we set up a hypothesis and test it H_0: teaching and methodical training system of subjects of higher mathematics in technical universities, suggested on the base of the modern interactive technologies, *significantly* improves the quality of the base level of professional competence of future engineers [10]. For pedagogical experiment we select a screening group – $K(\bar{Z}, S_z^2)$, group for adjustable experiment $E(\bar{Y}, S_y^2)$

and a group for the formative experiment $\Phi\left(\bar{X}, S_x^2\right)$, which are homogeneous in structure, which is proved by statistical methods. Let's present the reliable probability $P = 1 - \alpha = 0.95$ and determine the formation of components (motivational, cognitive and creative, self-educational, communicative competence) of the basic level of professional competence.

2.3. Formation of motivational competence

For the statistical analysis of the indexes of the level of awareness of motivational competence we have composed a table of significance of their disagreements the students experience when they study parts of higher mathematics.

The results obtained allow to make a decision that the index of attitude to the chosen speciality remains stable. That is, the deviation percentage of the index of the respond to the question: "If you had to enter the university again, would you choose: *a*) same university, same speciality; *b*) same university, but the other speciality; *c*) other university?" in table 1 are insignificant.

The other indexes in the screening group – $K\left(\bar{Z}, S_z^2\right)$, where the training process followed the traditional methods and the experimental groups of adjustable – $E\left(\bar{Y}, S_y^2\right)$ and formative – $\Phi\left(\bar{X}, S_x^2\right)$ experiments, in which training followed the suggested methodical system (an adjusting experiment disclosed the drawbacks, which were corrected prior to the formative experiment) are significant This allows to state, that the suggested teaching and methodical training system of subjects of higher mathematics in technical universities significantly increases the level of students' motivational competence during the first training year.

The improvement of teaching methods caused positive changes in indexes of conceptions as for the application of the knowledge obtained in writing course and bachelor papers. The difference in statistical averages of the formative and adjusting experiments is significant (column 1), but in dispersions (column 4) – it is not. It means that the index remains stable and its deviation from the statistical variable is insignificant.

Table 1. Significance of disagreements in indexes of numerical characteristics of development of motivational competence ("1" – significant deviation, "0" – insignificant deviation)

No	Indexes	1	2	3	4	5	6
		$\bar{X}$	$\bar{X}$	$\bar{Y}$	S_x^2	S_x^2	S_y^2
	Self-estimation (adequacy factor considered)	$\bar{Y}$	$\bar{Z}$	$\bar{Z}$	S_y^2	S_z^2	S_z^2
1	Conceptions as for the chosen speciality	0	1	1	0	1	1
2	Attitude to speciality choice	0	0	0	0	0	0
3	Conceptions as for the application of the knowledge obtained in:						
3.1	learning special subjects	0	1	1	0	1	1
3.2	writing course papers	1	1	1	0	1	1
3.3	work on speciality	1	1	1	0	1	1
4	Ability to apply the knowledge obtained in:						
4.1	learning special subjects	0	1	1	0	1	1
4.2	writing course papers	0	1	1	0	1	1
4.3	work on speciality	0	1	1	0	1	1

2.4. Improvement of the formation level of components of cognitive and creative competence – level of the knowledge and skills obtained in higher mathematics

Results of comparison of the theoretical knowledge and skills in solution of usual and applied tasks, making decisions on all the topics following the results of the test papers and exams are presented in table 2.

Analysis of the results of statistical research of significances of differences in average and dispersions between the groups show that the suggested system for learning mathematical subjects in technical universities greatly increases the level of application of the obtained knowledge and skills for the solution of tasks of any content. This is shown by the data in columns 2 and 5.

Index "1" points to the significant difference in students' knowledge of all the topics towards the favor of the suggested teaching and methodical system. Really, the statistical average from all the topics is higher in the experimental group of the formative experiment. After the statistical processing of the results of the adjustable stage of an experiment we see that despite the higher test results and better examination answers in the experimental group "E" in comparison with the screening group "K", the difference of indexes was not that significantly stable (columns 3 and 6).

This means that the suggested part of the teaching system does not influence the results we would like to obtain. The methods of lecture-wise and practical classes in vector algebra, analytical geometry, multiple integral, theory of series, function of complex variety and operational calculus had been improved.

The results of statistical analysis after the formational experiment proved the positive shift in the results of knowledge obtained after the correction of the teaching methods, which is proved by data in columns 1 and 4 as well as 2 and 6.

This may be explained by the fact that the study of these sections following the curricula requires more hours. To change the situation, we issued study books aimed at organization of independent learning some sections of higher mathematics.

Table 2. Significance of differences in indexes of numerical characteristics of development of components of cognitive and creative competences ("1" – significant deviation, "0" – insignificant deviation)

No	Indexes	1	2	3	4	5	6
		$\overline{X}$	$\overline{X}$	$\overline{Y}$	S_x^2	S_x^2	S_y^2
	Section	$\overline{Y}$	$\overline{Z}$	$\overline{Z}$	S_y^2	S_z^2	S_z^2
1	Linear Algebra	0	1	1	0	1	1
2	Vektor Algebra	1	1	1	0	1	0
3	Analytik geometry	0	1	1	0	1	0
4	Indirect differentiation	0	1	1	0	1	1
5	Definition integral	1	1	0	1	1	0
6	Multiple integral	1	1	1	0	1	1
7	Differential equations	0	1	1	0	1	1
8	Theory of numerical and functional series	1	1	1	1	1	0
9	Function of complex variable	1	1	0	1	0	0
10	Operational calculus	0	1	0	0	1	0
11	Probability theory and mathematical statistics	0	1	1	1	1	1
Levels of residual knowledge of higher mathematics (4-th year)							
high		1	1	1	1	1	1
sufficient		0	1	1	0	1	1
satisfactory		1	1	1	0	1	1
Low		1	1	1	1	1	1

2.5. Formed components of self-education and communicative competence learning higher mathematics

The results of analysis of statistical indexes of self-instruction skills levels, strivings to an advanced learning of the subject, self-education, gaining skills of public speaking, research work are presented in table 3.

Results of comparing the indexes of acquiring skills for self-dependent work and strivings to self-education prove our hypothesis on the reliability level of 0.95, this means that the suggested learning and methodical system significantly increases the level of self-dependent work (rows 1–6), striving to self–education in comparison with traditional training methods. This is shown in columns 2 and 5, as well as 3 and 6. Throughout the indexes the difference of the statistical average and dispersions of the coefficient of availability of the knowledge of self–dependent work, strivings to an advanced learning of material, to self–education is significant.

The data of the columns 1 and 4 show that the correction of the methods for giving lectures and the additional developments of interactive methods for practical classes aimed at improvement of the research indexes after the adjusting experiment was a success. The Indicators of differences of the statistical averages and dispersions of parameters, which determine the skills for pedagogical and research activities show that the suggested learning methods for higher mathematics significantly increases the level of skills in the experimental groups Φ and E in comparison with the screening group K (columns 2 and 5, 3 and 6). Improvement of methods after the adjusting experiment made great positive changes in indicators of public speech skills, research activities and partially – abilities in self–education work with textbooks and independent solution of applied tasks in experimental groups of formative and adjusting experiments (columns 1 and 4).

For the statistical analysis of the indexes of level of formation of communicative competence we have considered the questionnaire data as well as quantitive evaluation of levels of awareness of this competence. The results of comparing indexes of levels of awareness of communicative competence are presented in item 11 of table 3 and item 3 of table 4.

Analyses of the results of significance in differences of the indexes of numerical characteristics of awareness show that there is a significant difference between the suggested teaching and methodical system and a traditional one. Differences between the values in the screening group of the formative (Φ) and adjusting (E) experiments show that the decision to test it by the adjusting experiment with further formative one was correct.

So, the results of statistical analysis of comparison of the averages and dispersions proved our hypothesis H_0: the suggested teaching and methodical system increases the formation of the basic level of professional competence of future specialists with technical education.

To process the obtained results in pedagogical experiment we used some methods for analysis. The quantitative assessment of the level of knowledge was the known index of progress. For obviousness and convenience of numerical indexes there had been built the bar graphs and diagrams, but the percentage analysis may not always answer the questions of efficiency of the suggested methods, therefore we used the methods for statistical processing of the obtained results, which very thoroughly researches all the indexes which compose the suggested learning and methodical system for teaching higher mathematics in technical Universities.

Table 3. Significance of differences in indexes of numerical characteristics of development of components of self-educational and communicative competence ("1" - significant deviation, "0" – insignificant deviation)

No	Indexes	1	2	3	4	5	6
		$\overline{X}$	$\overline{X}$	$\overline{Y}$	S_x^2	S_x^2	S_y^2
	Components of self-educational and communicative competence	$\overline{Y}$	$\overline{Z}$	$\overline{Z}$	S_y^2	S_z^2	S_z^2
1	Independent work with textbook and manuals (electronic resource)	1	1	1	0	1	1
2	Independent work on composing reference outlines for practical classes	0	1	1	0	1	1
3	Independent solution of problems per sample	0	1	1	0	1	1
4	Making algorithm for solving problems on speciality	0	1	1	0	1	1
5	Independent solution of applied tasks	1	1	1	0	1	1
6	Making decisions from professional point of view	0	1	1	0	1	1
7	Striving for advanced learning	0	1	1	0	1	1
8	Striving for self-education	0	1	1	0	1	1
9	Public speech skills	1	1	1	1	1	1
10	Skills for research work	1	1	1	1	1	1
11	First year students adaptation	1	1	1	1	1	1

Table 4. Significance of differences in indexes of numerical characteristics of development of basic professional competences for future specialists with technical education

No	Indicators	1	2	3	4	5	6
		$\overline{X}$	$\overline{X}$	$\overline{Y}$	S_x^2	S_x^2	S_y^2
		$\overline{Y}$	$\overline{Z}$	$\overline{Z}$	S_y^2	S_z^2	S_z^2
Levels							
1	Levels of formation of motivational competence						
1.1	IV (high)	1	1	1	0	1	1
1.2	III (sufficient)	0	1	1	0	1	1
1.3	II (satisfactory)	1	1	1	1	1	1
1.4	I (low)	1	1	1	1	1	1
2	Levels of formation of cognitive and creative competence						
2.1	High	0	1	1	0	1	1
2.2	Sufficient	1	1	1	0	1	1
2.3	Satisfactory	0	1	1	0	1	1
2.4	Low	0	1	1	1	1	1
	Levels of formation of communicational competence						
3.1	High	0	1	1	1	1	0
3.2	Sufficient	1	1	1	1	1	1
3.3	Satisfactory	1	1	1	0	1	1
3.4	Low	1	1	1	1	1	1

3. Conclusions

In the conditions of a resilient economy that personnel who improve its results are especially valuable. The effectiveness of the system of educational and methodical training of personnel involved in the country's economy in institutions of higher education can be evaluated using various mathematical models and pedagogical experiments. The experience shows that students of technical universities find it difficult to learn mathematical subjects. Academic course of parts and some subjects of higher mathematics is not always useful for future engineers. The development and the introduction of the new interactive training methods which rest on tasks with technical content considering the speciality, in particular RPG's and business games, project method, simulation, «brain storming colloquium», «scientific and technical seminar», «scientific and technical conference», «optimal project» etc. is a complex process for the fundamental subjects in technical universities, which requires interdisciplinary approach and teachers' wish to give students knowledge and form the basic level of professional competence. However, future graduates of environmental specialties must possess mathematical apparatus, in particular comparative analysis of the obtained statistical data, which is the basis for evaluating the effectiveness of management decisions. In our opinion, the gaps in the knowledge of the use of mathematical apparatus are due to the uniformity of the application of teaching methods to sections of higher mathematics and the filling of mathematical textbooks with general examples. As our long–term experience shows, the application of modern innovative teaching methods and the use of textbooks for sections of higher mathematics with tasks of applied content significantly increase not only knowledge from them, but also the ability of future ecologists to make the right management decisions.

The advantage of the suggested algorithm for the statistical analysis of the results of pedagogical experiment lies in the fact that after receiving the differences between the parameters under

research it is possible to make a decision on significance of difference of numerical characteristics of formation of the indexes received. The difference in percentage does not always respond to the efficient results. Correlation analysis, Pierson's criteria and other methods for the evaluation of the results of pedagogical experiment do not present such a strict, significant difference as the correlation of the statistical average and dispersion of the two samplings.

References

[1] Arens K.: The Structure of Academic Self–Concept: A Methodological Review and Empirical Illustration of Central Models. The Review of Educational Research 91(1), 2020, 34–72 [http://doi.org/10.3102/0034654320972186].

[2] Gogol K. et al.: Affect and motivation within and between school subjects: Development and validation of an integrative structural model of academic self–concept, interest, and anxiety. Contemporary Educational Psychology 49, 2017, 46–65 [http://doi.org/10.1016/j.cedpsych.2016.11.003].

[3] Grechanovska O., Petruk V.: Methods of formation of intercultural competence by means of art in students of technical universities. Scientific Bulletin of Kremenets Regional Humanitarian and Pedagogical Institute 2, 2013, 36–40.

[4] Kovtun V., Kovtun O., Semenov A.: Entropy–Argumentative Concept of Computational Phonetic Analysis of Speech Taking into Account Dialect and Individuality of Phonation. Entropy 24(7), 2022, 1006 [http://doi.org/10.3390/e24071006].

[5] Lytvynenko V. et al.: International Scientific and Technical Conference on Computer Sciences and Information Technologies 1, 2020, 36–39.

[6] Mustonen T. et al.: Songs of the Kolyma tundra co–production and perpetuation of knowledge concerning ecology and weather in the indigenous communities of Nizhnikolyma, Republic of Sakha (Yakutia), Mimeo, University of Essex Perrings C Resilience and sustainable development. Environment and Development Economics 11, 2006, 417–427.

[7] Petruk V., Kashkanova G.: Possible and statistical models and statistical evaluation of the decision, 2–nd edition. 2006.

[8] Petruk V., Sabadosh Y.: Development of self–educational competence of students of technical universities during foreign language teaching. Modern information technologies and innovative teaching methods in training: methodology, theory, experience, problems 50, 2018, 57–63.

[9] Régibeau P., Rockett K.: Economic analysis of resilience: a framework for local policy response based on new case studies. Journal of Innovation Economics & Management 2013 [http://www.cairn.info/revue–journal–of–innovation–economics–2013–1–page–107.htm].

[10] Walker B. et al.: Resilience, adaptability and transformability in social–ecological systems. Ecology and Society 9(2), 2004, 5.

[11] Zabolotna N. et al.: Diagnostics of pathologically changed birefringent networks by means of phase Mueller matrix tomography. Proc SPIE 8698, 2013, 86980E.

D.Sc. Vira Petruk
e–mail: petruk-va@ukr.net

Doctor of Pedagogical Sciences, professor, Department of Higher Mathematics, Vinnytsia National Technical University. Research Interests: formation of the basic level of professional competence in future specialists of technical specialties by means of interactive technologies, digitization of mathematics education in technical institutions, methods of statistical analysis of experimental data.

http://orcid.org/0000-0001-7588-6721

Ph.D. Olena Prozor
e–mail: prozor@vntu.edu.ua

Candidate of Pedagogical Sciences, associate professor, Department of Higher Mathematics, Vinnytsia National Technical University. Research Interests: professional pedagogy, theoretical foundations of technical education, mathematical modeling and computational methods.

http://orcid.org/0000-0003-1454-8352

Ph.D. Yuliia Sabadosh
e–mail: avataric87@gmail.com

Candidate of Science (Pedagogy), senior lecturer of the Department of Foreign Languages Vinnytsia National Technical University. Research interests are humanitarian integrated knowledge of future information technology specialists, the use of interactive technologies in the educational process.

http://orcid.org/0000-0002-2850-1224

Ph.D. Iryna Baranovska
e–mail: bdn993@gmail.com

Ph.D., associate professor. Vinnytsia State Pedagogical University named after Mykhailo Kotsiubynsky.
Research Interests: formation of the basic level of professional competence in future specialists of technical specialties by means of interactive technologies, digitization of mathematics education in technical institutions, methods of statistical analysis of experimental data.

http://orcid.org/0000-0003-0033-4425

Ph.D. Maksim Palii
e–mail: paliymv@ukr.net

Candidate of Legal Sciences, associate professor. Department of Constitutional, International and Criminal Law, Vasyl Stus Donetsk National University. Research Interests: criminal law, criminology, criminology of religion, crime prevention, statistical analysis of experimental data.

http://orcid.org/0000-0002-1113-6355

Ph.D. Yevheniia Moroz
e–mail: morozeo@knu.ua

Ph.D. associate professor. Department of Theory and History of Sociology, Taras Shevchenko National University of Kyiv. Scientific interests: history of sociology, modern sociological theories, theories of cultural capital, post–structuralist approach, urban studies, data analysis.

http://orcid.org/0000-0002-2618-3541

Ph.D. Saule Kumargazhanova
e–mail: SKumargazhanova@gmail.com

She is currently the dean of the Department of Information Technologies and Intelligent Systems of D. Serikbayev East Kazakhstan Technical University. She is a co–author over 50 papers in journals and conference proceedings.
Her professional interests are software engineering, data processing and analysis.

http://orcid.org/0000-0002-6744-4023

M.Sc. Dinara Mussayeva
e–mail: d_i_n_mus@mail.ru

Scientific Secretary and Research Associate of the IE. Institute of Economics CS MES RK, Almaty, Kazakhstan.
She is a master of Al–Farabi Kazakh National University, Ph.D. student of the Institute of Economics of the CS MES RK, specialty– "World Economy". She started her career at the Institute of Economics as a junior researcher. As a responsible executive, she actively participates in conducting fundamental and applied research in priority areas for the state, such as digitalization of the economy, knowledge–based economy, etc.

http://orcid.org/0000-0002-8349-213X

http://doi.org/10.35784/iapgos.3470 *received: 29.01.2023 | revised: 24.05.2023 | accepted: 24.05.2023 | available online: 30.06.2023*

SIMULATION OF THE INFLUENCE OF INVESTMENT AND INNOVATION ACTIVITIES ON ENSURING THE INTERNATIONAL COMPETITIVENESS OF COUNTRIES

Olena Liutak[1], Olena Baula[1], Anatolii Tkachuk[2]
[1]Lutsk National Technical University, Faculty of Business and Law, Department of International Economic Relations, Lutsk, Ukraine, [2]Lutsk National Technical University, Faculty of Computer and Information Technologies, Department of Electronics and Telecommunications, Lutsk, Ukraine

Abstract. *The purpose of this work is to study the quality of the innovation-investment component of the international competitiveness of EU countries and Ukraine, to reveal the potential of innovation-investment activity in ensuring the effectiveness of the national economy, as well as to substantiate the priority vectors of leveling external shocks and promoting economic growth in Ukraine. The work evaluates the quality of the innovation and investment component of the international competitiveness of Ukraine and its close neighbors – the countries of the Visegrad Group (Poland, the Czech Republic, Hungary and Slovakia) using econometric analysis; a multifactor economic-mathematical model was built, which determines the strength of the connection between indicators of innovation and investment activity in Ukraine and the main macroeconomic indicator – GDP; the European practice of developing strategic programs to increase the competitiveness of the country's economy was studied; strategic innovation and investment initiatives of Ukraine are substantiated. In addition, the article made a significant theoretical and practical contribution to solving the outlined problems. The results of the study revealed the main problems of the innovation-investment component of Ukraine's international competitiveness, as well as highlighted the potential prospects for its improvement, taking into account advanced European practices.*

Keywords: international competitiveness, innovation and investment activity, globalization, institutional environment

SYMULACJA WPŁYWU DZIAŁAŃ INWESTYCYJNYCH I INNOWACYJNYCH NA ZAPEWNIENIE MIĘDZYNARODOWEJ KONKURENCYJNOŚCI KRAJÓW

Streszczenie. *Celem pracy jest zbadanie jakości komponentu innowacyjno-inwestycyjnego konkurencyjności międzynarodowej krajów UE i Ukrainy, ujawnienie potencjału działalności innowacyjno-inwestycyjnej w zapewnieniu efektywności gospodarki narodowej, a także uzasadnienie priorytetowe wektorów niwelowania wstrząsów zewnętrznych i promowania wzrostu gospodarczego na Ukrainie. W pracy dokonano oceny jakości komponentu innowacyjno-inwestycyjnego międzynarodowej konkurencyjności Ukrainy i jej bliskich sąsiadów – krajów Grupy Wyszehradzkiej (Polska, Czechy, Węgry i Słowacja) za pomocą analizy ekonometrycznej; zbudowano wieloczynnikowy model ekonomiczno-matematyczny, który określa siłę związku między wskaźnikami aktywności innowacyjnej i inwestycyjnej na Ukrainie a głównym wskaźnikiem makroekonomicznym – PKB; zbadano europejską praktykę opracowywania strategicznych programów zwiększania konkurencyjności gospodarki kraju; strategiczne inicjatywy innowacyjne i inwestycyjne Ukrainy są uzasadnione. Ponadto artykuł wniósł znaczący wkład teoretyczny i praktyczny w rozwiązanie przedstawionych problemów. Wyniki badania ujawniły główne problemy komponentu innowacyjno-inwestycyjnego międzynarodowej konkurencyjności Ukrainy, a także zwróciły uwagę na potencjalne perspektywy jego poprawy, biorąc pod uwagę zaawansowane praktyki europejskie.*

Słowa kluczowe: konkurencyjność międzynarodowa, działalność innowacyjna i inwestycyjna, globalizacja, otoczenie instytucjonalne

Introduction and literature review

The basis of the economic growth of any country is the formation of a highly competitive environment, which is aimed at creating goods and services with high added value. The production of such goods is impossible without the activation of innovative research and appropriate investment support. The mechanism of the relationship between the country's international competitiveness and the pace of innovation and investment activity is that the intensity of accumulation of all types of capital by the country correlates with the growth of labor productivity, which, in turn, is determined by the quality of technological support for production. The intensity of the development of technological support, in turn, depends on the level of competitiveness of the operating conditions of economic entities and the effectiveness of motives for carrying out innovative and investment activities.

The intensity of implementation of all innovation and investment transformations depends on the incentives, tools and levers that will be determined as priorities in the country's policy, which, in turn, form the institutional environment for strategic changes in the country's economic system.

The innovative and investment component of competitiveness growth is being studied by many international organizations. Based on the methodology developed by them, basic indicators and criteria were formed, which make it possible to compare different countries. Key among them are the Index of Economic Freedom [1], the Global Innovation Index (GII) [2], the Corruption Perception Index [3] compiled by Transparency International since 1995, and the Global Competitiveness Index [4]. Accordingly, the presence of an analytical base actualizes the issue of modeling the impact of basic indicators on economic growth, which is manifested in the gross domestic product. The basis of this work is the study of the dynamics of indicators that reflect the innovation-investment component of the international competitiveness of the countries of the Visegrad Group and Ukraine, the use of economic and mathematical modeling to substantiate their impact on the international competitiveness of the outlined countries. These findings will make it possible to develop recommendations based on the European practice of forming strategic programs to increase the competitiveness of the country's economy.

1. Materials and methods

To achieve the goal of the research, the following scientific tasks were defined:

1) to assess the quality of the innovation and investment component of the international competitiveness of Ukraine and its close neighbors – the countries of the Visegrad Group (Poland, the Czech Republic, Hungary and Slovakia) using econometric analysis;
2) build a multi-factor economic and mathematical model that determines the strength of the connection between indicators of innovation and investment activity in Ukraine and the main macroeconomic indicator – GDP;
3) to investigate the European practice of developing strategic programs to increase the competitiveness of the country's economy;
4) the strategic innovation and investment initiatives of Ukraine are substantiated in order to ensure the optimal level of its international competitiveness.

Methods of abstraction, dialectics, economic-mathematical and correlational analysis, system-structural and comparative analysis, as well as quantitative and qualitative analysis form the methodological basis of the research.

The main data for the analysis were statistical data from the State Statistics Service of Ukraine, the Ministry of Finance of Ukraine, analytical materials from the Wall Street Journal and the Heritage Foundation, the World Intellectual Property Organization, Transparency International, and the World Economic Forum.

After the collection and processing of statistical data, a qualitative analysis of the relevant indicators was conducted. The collected and processed statistical material of the analysis made it possible to describe the state, structure, and dynamics of the relevant indicators of innovation and investment activity of Ukraine and the countries of the Visegrad Group, as well as to diagnose the level of correlation with the factors of determining international competitiveness.

The results of the economic-mathematical analysis made it possible to identify problematic points, positive aspects and shortcomings for the outline of strategic innovation and investment initiatives of Ukraine in order to ensure the optimal level of its international competitiveness.

2. Results and discussion

Prospective priorities of the country's development in the system of the world economy are determined by the factors that determine its competitiveness.

The rapid spread of globalization processes, the deepening of transformations, the transformation of competitive advantages leads to the emergence of new challenges for state policy regarding the formation of conditions for ensuring the international competitiveness of subjects of various levels. Globalization, like any profound process taking place in society, carries both new opportunities and risks. As a rule, opportunities are not available to all economic entities, and risks threaten both micro and macro entities. Among the most significant challenges of our time are economic instability, social inequality, economic discrimination and global problems of various directions.

The permanent task of modernity is to find the driving forces of rationalization of economic activity through the practical exhaustion of extensive factors of economic growth. Negative trends in the economic system of Ukraine are evidence of the lack of systematicity in the management of innovation and investment processes in the country. This state of affairs requires the development of a system of effective measures at all levels of management regarding the formation of an optimal innovation environment in order to increase the overall level of the country's international competitiveness under the conditions of global socio-economic transformations.

In world practice, in the vast majority of cases, the following approaches are used to quantify the level of international competitiveness of countries:

- a comparison of costs and prices, which gives an approximate value of specific remuneration, which is a function of, for example, productivity, wages or exchange rates;
- analysis of the results of the country's foreign trade activity, changes in the share of domestic goods in the domestic turnover, volumes and structure of exports;
- comparison of a group of weighted indicators of the functioning of the country's national economy.

In our opinion, the last of the mentioned approaches is the most optimal not only from the point of view of greater systematicity and multifacetedness, but also best suited if the assessment is carried out by comparing the level of international competitiveness of a group of countries.

Taking into account the European integration vector of the development of Ukraine's economy, we consider it expedient to assess the quality of the innovation and investment component of the international competitiveness of Ukraine and its close neighbors – the countries of the Visegrad Group (Poland, the Czech Republic, Hungary and Slovakia). To do this, we will apply econometric analysis, which involves establishing such a type of linear function that would most accurately describe the development of the economic process. The economic analysis is conducted on the basis of four institutional indices that reflect the quality of the investment and innovation component of the international competitiveness of countries for the period from 2013 to 2022 – the Index of Economic Freedom, the Global Innovation Index, the Corruption Perception Index, and the Global Competitiveness Index (table 1).

Table 1. Comparative values of international ratings reflecting the innovation and investment component of the international competitiveness of the Visegrad Group countries and Ukraine, 2013–2022

Indicator	Country	Years									
		2013	2014	2015	2016	2017	2018	2019	2020	2021	2022
Index of economic freedom	Poland	66	67	68.6	69.3	68.3	68.5	67.8	69.1	69.7	68.7
	Czech Republic	70.9	72.2	72.5	73.2	73.3	74.2	73.7	74.8	73.8	74.4
	Hungary	67.3	67	66.8	66	65.8	66.7	65.5	66.4	67.2	66.9
	Slovakia	68.7	66.4	67.2	66.6	65.7	65.3	65	66.8	66.3	69.7
	Ukraine	46.3	49.3	46.9	46.8	48.1	51.9	52.3	54.9	56.2	54.1
Global Innovation Index	Poland	40.12	40.64	40.16	40.22	41.99	41.67	41.31	39.95	39.9	37.5
	Czech Republic	48.36	50.22	51.32	49.4	50.98	48.75	49.43	48.34	49	42.8
	Hungary	46.93	44.61	43	44.77	41.74	44.94	44.51	41.53	42.7	39.8
	Slovakia	47.32	41.89	42.99	41.7	43.43	42.88	42.05	39.7	40.2	34.3
	Ukraine	35.78	36.26	36.45	35.72	37.62	38.52	37.4	36.32	35.6	31
Index of perception of corruption	Poland	60	61	63	62	60	60	58	56	56	–
	Czech Republic	48	51	56	55	57	59	56	54	54	–
	Hungary	54	54	51	48	45	46	44	44	43	–
	Slovakia	47	50	51	51	50	50	50	49	52	–
	Ukraine	25	26	27	29	30	32	30	33	32	–
Index global competitive capabilities	Poland	–	4.48	4.49	4.56	4.59	68.2	68.9	68.8	68.6	68.9
	Czech Republic	–	4.53	4.69	4.72	4.77	71.2	70.9	70.9	71	71.1
	Hungary	–	4.28	4.25	4.2	4.33	64.3	65.1	65.3	65.1	65.7
	Slovakia	–	4.15	4.22	4.28	4.33	66.8	66.8	66.9	66.9	67.2
	Ukraine	–	4.14	4.03	4	4.11	57	57	56.8	56	54.8

Note:

The index of economic freedom is based on 10 indices, which are evaluated on a scale from 0 to 100, and the indicator 100 corresponds to maximum freedom.

The Global Innovation Index (GII) provides detailed indicators of the innovation performance of 131 countries and economies around the world, on a scale from 0 to 100.

The Corruption Perceptions Index (CPI) is an annual ranking of the countries of the world compiled by Transparency International since 1995. The countries in the rating are ordered according to the level of corruption, which is based on the assessments of entrepreneurs and analysts. The rating reproduces the perception of corruption on a scale from 100 (no corruption) to 0 (extreme corruption).

The Global Competitiveness Index ranks a different number of countries each year on indicators grouped into 12 main components.

Compiled by the authors based on: [1, 2, 3, 4]

The reason for focusing on these metrics is that:

- firstly: they can significantly affect the uncertainty in the sphere of investment and innovation activities in the conditions of ensuring the international competitiveness of the countries' economies;
- secondly: these indices determine the importance of uncertainty factors regarding changes in economic policy in general and the transformation of innovation and investment policy in particular;
- thirdly: on the basis of the search for interrelationships using Excel Microsoft Office, the indicated indices are singled out as indicators characterized by a high level of correlation.

Microsoft Office Excel was used to calculate the economic-mathematical model. The econometric analysis of the innovation-investment component of the country's international competitiveness is based, first of all, on the construction of an econometric model of the following type:

$$Y = a_1X_1 + a_2X_2 + a_3X_3 + a_4X_4 + u \quad (1)$$

where Y – is the vector of the innovation-investment component of international competitiveness (the sum of innovation costs and direct investments in the country's economy); X_1 – vector of the index of economic freedom; X_2 – global innovation index vector; X_3 – corruption perception index vector; X_4 – global competitiveness index vector; u – is a vector of the stochastic component that accumulates the influence of all random factors on the innovation-investment component of international competitiveness.

The results of the calculations are given in table 2.

Table 2. Regression equation of the innovation-investment component of the international competitiveness of the Visegrad Group countries and Ukraine

Country	The equation of the multivariate model
Czech Republic	$Y = 59.5 \cdot X_1 + 34.0 \cdot X_2 - 1.9 \cdot X_3 + 23.0 \cdot X_4 - 16645.4$
Hungary	$Y = 20.2784 \cdot X_1 + 0.4575 \cdot X_2 - 7.6204 \cdot X_3 + 12.3347 \cdot X_4 + 11.64$
Slovakia	$Y = 10.926 \cdot X_1 + 20.044 \cdot X_2 - 4.302 \cdot X_3 + 11.821 \cdot X_4 - 753.142$
Poland	$Y = 6.2397 \cdot X_1 + 39.9805 \cdot X_2 - 3.6569 \cdot X_3 + 0.8132 \cdot X_4 - 5.6544$
Ukraine	$Y = 2.267 \cdot X_1 + 0.2479 \cdot X_2 - 1.4837 \cdot X_3 + 0.1525 \cdot X_4 + 1.2782$

As we can see from the table, the economic freedom index (X_1) has the most positive effect on the significant indicator (sum of innovation costs and direct investments in the country's economy), in all regression equations it has a positive value and is greater than 1. The opposite factor is the corruption perception index, as it reduces the total amount of innovation costs and direct investments in the country's economy due to a negative value.

When checking the reliability of models on the basis of multiple correlation coefficients, in the theory of statistics such basic indicators as multiple correlation coefficients – R are distinguished (the closer R is to unity, the closer the relationship between the dependent variable Y and factors X_1, X_2,..., X_n) and determinations – R^2 (the closer R^2 is to unity, the better the regression approximates the empirical data), Fisher's test (the tabular value of Fisher's test is searched for the given probability p (p = 0.95) and the number of degrees of equality $k1=m$ and $k2=n-m-1$; for the statistical data collected by us, the number of observations is n=10, therefore the number of degrees of freedom $k1$=1 and $k2$=8. The tabular value of the Fisher criterion: F_{tab}=5.32. If the inequality $F_{dis} > F_{tab}$ is satisfied, then with a probability of p=0.95, it can be stated that the built model is adequate to the statistical data and is suitable for further analysis and forecasting. A summary analysis of multiple correlation coefficients is given in table 3.

Table 3. Validation of models based on multiple correlation coefficients

No	Country	Multiple correlation coefficient (R)	Determination coefficient (R^2)	Fisher's test
1	Czech Republic	0.82745	0.68467	90.4150
2	Hungary	0.99757	0.99515	352.0821
3	Slovakia	0.98551	0.97122	47.5163
4	Poland	0.98295	0.96620	58.4282
5	Ukraine	0.97273	0.94620	35.1772

The analysis of the data in the table shows that all the coefficients correspond to the normative values. This gives us reason to say that the models are reliable and can be used for further forecasting.

A number of indicators are used to assess the effectiveness of innovative capital investments in promoting the country's international competitiveness, in particular: the volume of scientific production as the total number or average number of publications per researcher, completed and defended dissertations, completed topics or submitted reports; the value expression of the savings of live and tangible labor in social production from the use of the results of scientific and research activities and their comparison with the costs of conducting research; the number of introduced scientific and technical products and the term of introduction of scientific development into production; indicators of the effectiveness of applied scientific research: the level of diffusion of results in the spheres of the country's economy; indicator of the ratio of the beneficial effect of research and the costs of conducting it, etc.

Only a comprehensive assessment of these indicators can demonstrate a complete picture of the validity of innovative capital investments. In addition, they should be evaluated from the standpoint of obtaining both quantitative and qualitative results.

Among the quantitative parameters of innovation activity in the country, it is worth noting innovation costs for the purchase of machines, equipment and software; innovation costs for another; the number of organizations that implemented the NDR; the number of employees involved in the implementation of the NDR; number of innovatively active industrial enterprises; direct foreign investments in Ukraine; the number of industrial enterprises that introduced innovations; specific weight of the volume of scientific and scientific and technical works performed in GDP, %.

3. Experiment

The next step in our research will be the construction of a multifactor economic-mathematical model that will determine the strength of the connection between indicators of innovation and investment activity in Ukraine and the main macroeconomic indicator – GDP. The initial data for building this model are presented in table 4.

The use of software products (package extension "Data Analysis" Microsoft Excel) made it possible to determine the equation of the multifactor model of the dependence of GDP (Y) on indicators of the effectiveness of innovation and investment activity in Ukraine.

Equation of multifactor dependence of GDP in million hryvnias. looks like:

$$Y = 4820.3237 \cdot X_1 + 5961.334 \cdot X_2 - 4887.1648 \cdot X_3 - 4.2859 \cdot X_4 - 5877.817 \cdot X_5 + 8212.7868 \cdot X_6 + 458.3506 \cdot X_7 + 6285.4X_8 + 3895647.46$$

Checking the reliability of the model based on the multiple coefficients of correlation (R=0.8887) and determination (R^2=0.9773) shows that they are close to 1. This result of the calculation confirms the adequacy of the proposed model, its suitability for use.

Commenting on the weight coefficients in the equation of the multifactor model of the dependence of GDP (Y) on the performance indicators of innovation and investment activity in Ukraine, it is possible to state a significant positive influence of such performance indicators as:

- innovation costs for the purchase of machines, equipment and software;
- innovation costs for other;
- direct foreign investments in Ukraine;
- the number of industrial enterprises that introduced innovations;
- specific weight of the volume of performed scientific and scientific and technical works in GDP.

Taking into account the conducted analysis, significant indicators of the effectiveness of innovation and investment activities in Ukraine, which have a positive impact on the country's GDP, were singled out. In order to develop more thorough recommendations regarding the use of innovation and investment potential to increase the growth of the country's GDP, it is advisable to identify these indicators in more detail and their contribution to the overall economic development of the state. For this purpose, it is possible to build models of direct connection between GDP and selected indicators. Let's build appropriate paired regression models. A summary analysis of all indicators by defined functions describing the interdependence of indicators of innovation and investment activity and GDP is given in table 5.

The data in Table 5 show that almost all the equations that most accurately determine the influence of the resulting indicator and the factors affecting it testify to the hyperbolic nature of the relationship. The wave-like development of the world economy in general and the economy of Ukraine in particular, under the influence of various factors, is reflected by the mathematical function of a quadratic equation.

The most significant coefficient in the models of interdependence from macroeconomic indicators belongs to the factor "Expenditure on innovations and other" (R^2=0.97505), but in the multifactorial equation the coefficient of influence for this indicator is not the highest, therefore, for an in-depth correlation and regression analysis, it is advisable to use the factor "The specific weight of the volume of scientific and scientific and technical works performed in GDP, %" for which R^2=0.96251.

Let's analyze the suitability of this model:

$$y = 4495414.61848x^2 - 11770222.87901x + 7889269.68666$$

To do this, we will check its adequacy with statistical data, using Fisher's test. Let's calculate the value of this criterion using the formula:

$$F_{calculated} = \frac{R^2}{1-R^2} \cdot \frac{n-m-1}{m}$$

$$F_{calculated} = \frac{(0.96251)^2}{1-(0.96251)^2} \cdot \frac{15-1-1}{1} = 163.6916536$$

The tabular value of Fisher's test is calculated with the specified probability p (p=0.95) and the number of degrees of equality: $k1=m$ and $k2=n-m-1$. For the statistical data collected by us, the number of observations is n=15, so the number f degrees of freedom $k1$=1 and $k2$=13. The tabular value of Fisher's test: F_{table} = 4.67.

Table 4. Initial data for building a multifactor regression of the influence of quantitative indicators of the effectiveness of innovation and investment activities in Ukraine on GDP

Year	GDP, million hryvnias	Innovation costs for the purchase of machines, equipment and software, UAH million	Innovation costs for other, million hryvnias	The number of organizations that carried out the NDR, units	The number of employees involved in the implementation of the NDR, persons	Number of innovatively active industrial enterprises, units	Direct foreign investments in Ukraine, million US dollars	The number of industrial enterprises that introduced innovations, units	The specific weight of the volume of scientific and scientific and technical works performed in GDP, %
	Y	X_1	X_2	X_3	X_4	X_5	X_6	X_7	X_8
2007	751100	7441.3	2064.9	1404	155549	1472	9891	1186	0.93
2008	990800	7664.8	2664	1378	147275	1397	10913	1160	0.9
2009	947000	4974.7	2012.6	1340	139760	1411	4816	1180	0.95
2010	1120600	5051.7	1855.8	1303	182484	1462	6495	1217	0.9
2011	1349200	10489.1	2440.2	1255	175330	1679	7207	1327	0.79
2012	1459100	8051.8	2185.5	1208	164340	1758	8401	1371	0.8
2013	1522700	5546.3	2290.9	1143	155386	1715	4499	1312	0.8
2014	1586900	5115.3	778.8	999	136123	1609	410	1208	0.69
2015	1988500	11141.3	548	978	122504	824	-458	723	0.64
2016	2383200	19829.0	878.4	972	97912	834	3810	735	0.61
2017	2983882	5898.8	1027.1	963	94274	759	3692	672	0.56
2018	3558706	8291.3	633.9	950	88128	777	4455	739	0.51
2019	3974564	10185.1	4035.8	950	79262	782	5860	687	0.52
2020	4194102	8788.2	5618.7	769	78860	809	-868	718	0.52
2021	5459574	9325.4	4289.6	789	74256	784	6687	683	0.54

Source: compiled according to [5, 6, 7, 8]

Table 5. Equations describing the dependence of the influence of innovation and investment factors on GDP and the corresponding coefficients of determination

Linear equation	Logarithmic equation	Polynomial equation	Power equation	Exponential equation
Innovation costs for the purchase of machines, equipment and software				
y = 22.24565x + 622817.76518 R^2 = 0.19849	y = 147017.88160ln(x) – 62456.04346 R^2 = 0.45933	y = -0.00310x^2 + 135.78126x + 357449.52816 R^2 = 0.58652	**y = 161503.07611$x^{0.20369}$ R^2 = 0.73693**	y = 363466.70874$e^{0.00004x}$ R^2 = 0.47428
Spending on innovation for another				
y = 144488.22910x – 296994.73203 R^2 = 0.91460	y = 827187.78107ln(x) – 596904.75349 R^2 = 0.67625	y = 7895.10939x^2 – 5518.84933x + 203028.86275 R^2 = 0.97286	y = 93456.08140$x^{1.05039}$ R^2 = 0.91137	**y = 165849.34724$e^{0.16319x}$ R^2 = 0.97505**
Direct foreign investments in Ukraine				
y = -2953729.45015x + 3620773.65399 R^2 = 0.90268	y = -2409176.39474ln(x) + 602668.34181 R^2 = 0.94679	**y = 3450890.80678x^2 – 8797205.21121x + 5874349.74320 R^2 = 0.95128**	y = 476437.95994$x^{-2.52142}$ R^2 = 0.86676	y = 12598844.82770$e^{-3.22632x}$ R^2 = 0.90013
The number of industrial enterprises that introduced innovations				
y = 735.98698x – 219857.19806 R^2 = 0.26347	y = 1446154.84809ln(x) – 673776.47848 R^2 = 0.25357	y = -0.00483x^2 + 757.38751x – 241126.65197 R^2 = 0.26348	y = 3.19377$x^{1.66928}$ R^2 = 0.28237	y = 186429.64859$e^{0.00081x}$ R^2 = 0.26954
The specific weight of the volume of scientific and scientific and technical works performed in GDP, %				
y = -3674314.16534x + 4431662.85491 R^2 = 0.91247	y = -3241222.07886ln(x) + 695395.84735 R^2 = 0.94986	**y = 4495414.61848x^2 – 11770222.87901x + 7889269.68666 R^2 = 0.96251**	y = 524795.30684$x^{-3.39544}$ R^2 = 0.87122	y = 29979358.87863$e^{-3.99280x}$ R^2 = 0.90057

Source: calculated by the authors.

Inequality $F_{calc} > F_{tab}$ (163.692 > 4.49) is fulfilled, so with a probability of 95% it can be stated that the proposed model is adequate to the statistical data.

It is necessary to evaluate the indicators of the closeness and direction of the relationship between *X* and *Y*, using the correlation coefficient, which is calculated according to the following formula:

$$K_{correl}[X,Y] = \frac{\sum_{uu=1}^{n}(Xi - \overline{X}) * (Yi - \overline{Y})}{\sqrt{\sum_{i=1}^{n}(Xi - \overline{X})^2 * \sum_{i=n}^{n}(Yi - \overline{Y})^2}}$$

The value of the correlation coefficient is calculated using the built-in function of the Microsoft Excel program, in particular the function of the CORELL category.

The coefficient and correlation r [x; y] = 0.93258 were obtained.

Based on the obtained value, we conclude: since r [x; y] < 0, then the relationship between *X* and *Y* is direct; since $0.7 < |r[x; y]| < 1$, then the relationship between *X* and *Y* is strong.

Therefore, the indicator of the specific weight of the volume of performed scientific and scientific and technical works in GDP exerts the greatest influence on the volume of GDP. Negative trends are observed in the field of innovative development in Ukraine, in particular, problems associated with low volumes of financing of scientific and scientific and technical works. These problems increase in conditions of economic recession, as the opportunities to invest in innovative development are narrowing.

Investment and innovation activity in terms of ensuring the international competitiveness of countries is directly determined by the strategic initiatives of the state. Some countries emphasize the implementation of programs aimed at developing the technological factor of competitiveness, others direct resources to increase the country's innovation capital. A number of states prefer to develop resource conservation in order to restore the natural capital of the country, and some of them increase the use of non-renewable resources. The variety of these strategies is explained by the different degree of economic development of countries, the availability of production factors and many other reasons.

The countries with a fairly high international assessment of competitiveness are the countries of the European Union, which traditionally have a consistently high level of innovative development, quality of education, technological equipment and infrastructure. Framework programs for the development of scientific research and technology are one of the instruments for the development of innovations in the region.

Examples of such programs include "HORIZON-2020", which was a tool for the development of high-tech competitiveness in the context of the "Europe 2020" strategy [9]. The purpose of this program was to develop Europe's competitiveness through the implementation of large-scale research and the introduction of innovations aimed at solving modern problems. In particular, during the implementation of the project, about 78 billion euros were invested, and about 900 new innovative products were created.

There are a number of other strategic programs and initiatives of the European region aimed at increasing the competitiveness of European countries through the expansion of innovative cooperation. For example, the ERA-NET project [10] is aimed at coordinating national and regional research programs, holding joint events, and discussing international cooperation. The initiative "European Technology Platforms" [11] is aimed at technology transfer and international cooperation in the industrial sector.

Getting acquainted with the European experience of developing strategic programs to increase the competitiveness of countries, it can be concluded that the countries of this region have managed to build a chain of effective interaction "education – research and development – high-tech business". This system of ensuring competitiveness and growth in Europe performs the functions depicted in Fig. 1.

The purpose of joint technology initiatives in the European Union is the strategic development of areas in which research and innovation are important for competitiveness, for example bio-industry, "clean sky", electronic components and systems, as well as innovative medicines. These initiatives are implemented through special legal entities – joint ventures – created in accordance with the Treaty on the Functioning of the European Union (TFEU). Currently, several projects are being implemented in the region, aimed at creating coordination platforms, within which it is expected to combine the efforts of representatives of political circles, the scientific community, business and third countries to determine the priority areas of research (Fig. 2).

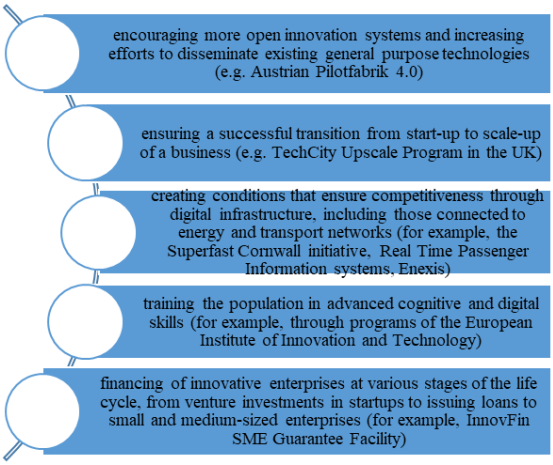

Fig. 1. Functions of the system for ensuring competitiveness and growth in EU countries Source: constructed by the authors

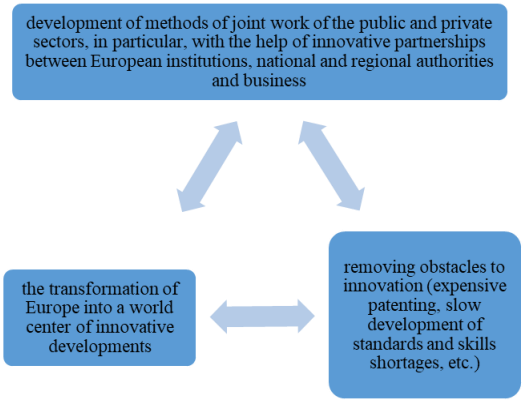

Fig. 2. Strategic goals of the system for ensuring competitiveness and growth in EU countries Source: constructed by the authors

It is worth noting that European countries not only develop and implement strategic initiatives at the national level, but also actively work with private business and the population. For example, in environmental issues, which are determinants of the development of international competitiveness in the long term, consumer preferences are being changed towards conscious consumption and businesses are being supported in the transition to low-carbon practices [12].

In general, the strategic policy of the EU in matters of increasing the competitiveness of the region is aimed at the development of innovations, education and high-tech industry. This statement is confirmed by the regression equations of the innovation-investment component of international competitiveness compiled by us and the equations describing the dependence of the influence of innovation-investment factors on GDP.

The conducted monitoring of Ukraine's place in international ratings reflecting the innovation and investment component of the country's international competitiveness in 2013–2022 shows relatively low rating positions. However, the built multifactorial regression of the influence of quantitative indicators of the effectiveness of innovation and investment activity in Ukraine on GDP indicates its weight of influence on the macroeconomic situation in the country and its international competitiveness.

The dynamics of the transformation of investment and innovation factors of international competitiveness prove that there is a global trend for the development of high-tech production, innovative capital and the environmental factor [13, 14, 15]. At the same time, the instability of the financial market and the strengthening of the protection of national producers often hinder the development of the country's competitiveness. Most developed economies are developing strategic programs aimed at developing the three aforementioned factors and mitigating the destructive effects of the other two.

In Ukraine, the government has already taken a number of strategic decisions regarding the technological modernization of the economy, but the effectiveness of many of them would be better. Of course, there are endogenous circumstances (armed aggression of the Russian Federation against Ukraine) that reduce the effectiveness of the country's innovation and investment activities. In addition to military operations on the territory of our country, Ukraine has socio-economic problems typical of developing countries (social inequality, economic instability, etc.). At the same time, Ukraine already needs to respond to the challenges of post-industrial development, which arise under the influence of global transformations of the world economy, and to promote the transition from a resource-dependent to a high-tech economy.

Ukraine's strategic innovation and investment initiatives should outline sources of investment in new infrastructure and modernization of outdated technological capacities. It is also necessary to work out the mechanism of their insurance in order to increase the confidence of domestic and foreign investors. It is also necessary to clearly define the organization of vocational training and retraining programs for employees who may lose their jobs due to increased innovation in the economy. A strategic approach to product diversification, development of raw materials industries with a high degree of processing and the use of high-tech developments is necessary to create the stability of raw materials enterprises under conditions of changing economic conditions.

These points should be taken into account during the development of relevant programs for the development of the competitiveness of the economy. When implementing strategies aimed at the development of innovations in the country, it is necessary to pay attention to high-tech industries with a significant multiplier effect, which stimulates innovative activity in related areas. Additional investments will be needed for the implementation of projects related to the creation of energy-efficient technologies. Their use will allow to reduce the price of products, which means it will increase its price competitive advantages. To solve the problems caused by the transformation of investment and innovation activities, Ukraine needs to develop a scientific and technological program aimed at the implementation of complex target programs through the creation of specialized technological clusters, which include technology parks, industrial parks, technology transfer centers and engineering centers.

It is also advisable to develop a comprehensive program to support small and medium-sized businesses, including through the activation of specialized innovative institutions. Small and medium-sized enterprises are more open to innovation than large ones, but the inherent high risks of innovative projects restrain their development. World practice proves that the high-tech sector needs state protection, especially at the initial stages of development. With the successful implementation of innovations, they can make a significant contribution to the development of the competitiveness of the Ukrainian economy. The country's government should pay special attention to the development of strategic programs to increase market competition, which will contribute to the rational use of resources for the production of products and the optimal activity of entities at all stages of production.

In order to update education, it is necessary to intensify the implementation of scientific and practical programs aimed at developing cooperation between relevant educational institutions and business, increasing public awareness of scientific and technological trends, new opportunities for training and retraining, as well as the development of international dialogue on joint research. Increasing the competitiveness of strategically important industries requires the organization of a modern system of technical regulation, which contributes to the acceleration of the processes of technological and organizational modernization of production. It is also critically necessary for the inclusion of Ukrainian companies in technological and production and sales chains in the world.

4. Conclusions

The conducted research shows the threatening indicators of the corruption perception index in Ukraine. That is why it is advisable to improve the monitoring procedure and methods of detecting fraudulent activities.

Reducing the dependence of the Ukrainian economy on energy resources can significantly contribute to technological development and increase the country's innovation and investment potential. For this, programs for attracting foreign and domestic investments in R&D and education are necessary. This should be accompanied by the improvement of the business climate and legal regulation, the development of investment insurance programs, the organization of a modern system of technical regulation, and an increase in the level of competition on the national market. Thus, it is impossible to ensure the international competitiveness of the Ukrainian economy without using the innovation and investment potential. Increasing the effectiveness of the practical implementation of programs in this area, first of all, it is necessary to improve the interaction of society and business, the formation of institutions of parallel control, which can potentially help solve the problem of corruption and irrational use of state budget funds. The high effectiveness of the implementation of existing and future programs can help the country cope with the uncertainty caused by the current global economic situation, level external shocks and, ultimately, increase the level of the country's international competitiveness.

References

[1] Index of Economic Freedom 2013–2022, https://www.heritage.org/ (available: 28.01.2023).
[2] The Global Innovation Index 2013–2022, https://www.wipo.int/ (available: 28.01.2023).
[3] Corruption Perceptions Index 2013–2021, https://www.transparency.org/ (available: 28.01.2023).
[4] The Global Competitiveness Report 2013–2022, https://www3.weforum.org/ (available: 28.01.2023).
[5] Scientific and innovation activities of Ukraine. 2019, https://ukrstat.gov.ua/druk/publicat/kat_u/2020/zb/09/zb_nauka_2019.pdf (available: 28.01.2023).
[6] Direct foreign investment. Ministry of Finance of Ukraine, https://index.minfin.com.ua/ua/economy/fdi/2021/ (available: 28.01.2023).
[7] Scientific and innovation activities of Ukraine. 2020, https://ukrstat.gov.ua/druk/publicat/kat_u/2021/zb/10/zb_Nauka_2020.pdf (available: 28.01.2023).
[8] Scientific, technical and innovative activities in 2021: priorities and their implementation, problems and possible solution tools, https://mon.gov.ua/ua/news/naukovo-tehnichna-ta-innovacijna-diyalnist-u-2021-roci-prioriteti-ta-yihnya-realizaciya-problemi-ta-mozhlivi-instrumenti-virishennya (available: 28.01.2023).
[9] Horizon 2020, https://research-and-innovation.ec.europa.eu/funding/funding-opportunities/funding-programmes-and-open-calls/horizon-2020_en (available: 28.01.2023).
[10] ERA-NET, https://www.era-learn.eu/partnerships-in-a-nutshell/type-of-networks/era-net-scheme (available: 28.01.2023).
[11] OLD EN: European Technology Platforms, https://www.ffg.at/en/european-technology-platforms (available: 28.01.2023).
[12] EU Bank launches ambitious new climate strategy and Energy Lending Policy, https://www.eib.org/en/press/all/2019-313-eu-bank-launches-ambitious-new-climate-strategy-and-energy-lending-policy (available: 28.01.2023).
[13] Liutak O. et al.: The Development of Renewable Energy in the Context of Formation of Innovative Economy and Energy Independence as the Geopolitical Priorities of the State. IOP Conference Series: Earth and Environmental Science 628, 2021 (https://iopscience.iop.org/article/10.1088/1755-1315/628/1/012012/pdf).
[14] Liutak O. M.: Problems of information support for transborder indices calculation. Actual Problems of Economics 124(10), 2011, 276–283.
[15] Kostiuchko S. et al.: The Auxiliary Parametric Sensitivity Method as a Means of Improving Project Management Analysis and Synthesis of Executive Elements. Miraz M. H., Southall G., Ali M., Ware A., Soomro S. (eds) Emerging Technologies in Computing. iCETiC 2021. Lecture Notes of the Institute for Computer Sciences, Social Informatics and Telecommunications Engineering 395, 2021, 174–184.

Prof. Olena Liutak
e-mail: olenalutak@gmail.com

Scientific direction: global institutionalization of the service sector, international competitiveness, international tourism, regulation of the development of global food and non-food markets; innovation and investment potential.

http://orcid.org/0000-0002-4293-0586

Prof. Olena Baula
e-mail: o.baula@lntu.edu.ua

Scientific direction: structural modernization of international innovation and investment activity, development of international economic integration, impact of globalization processes on the development of national economies, digital transformation of the financial sector of the world economy, organizational and financial determinants of the innovative component of the country's competitiveness.

http://orcid.org/0000-0003-2609-0211

Ph.D. Anatolii Tkachuk
e-mail: a.tkachuk@lntu.edu.ua

Vice-dean for R&D Faculty of Computer and Information Technologies, Lutsk National Technical University.
Member of European Alliance for Innovation (EAI), International Association for Technological Development & Innovations (IATDI).

http://orcid.org/0000-0001-9085-7777